ISBN 978-82-471-1021-8 (printed ver.)
ISBN 978-82-471-1022-5 (electronic ver.)
ISSN 1503-8181

Torjus Åkre
Doctoral Thesis

Doctoral Theses at NTNU, 2008:172

Torjus Åkre

Electrowinning of Cobalt from Chloride Solutions: Anodic Deposition of Cobalt Oxide on DSA®

NTNU
Norwegian University of
Science and Technology
Thesis for the degree of
doktor ingeniør
Faculty of Natural Sciences and Technology
Department of Materials Science and Engineering

NTNU
Norwegian University of
Science and Technology

Theses at NTNU, 2008:172

NTNU

Torjus Åkre

Electrowinning of Cobalt from Chloride Solutions: Anodic Deposition of Cobalt Oxide on DSA®

Thesis for the degree of doktor ingeniør

Trondheim, April 2008

Norwegian University of
Science and Technology
Faculty of Natural Sciences and Technology
Department of Materials Science and Engineering

NTNU
Norwegian University of
Science and Technology

NTNU
Norwegian University of Science and Technology

Thesis for the degree of doktor ingeniør

Faculty of Natural Sciences and Technology
Department of Materials Science and Engineering

ISBN 978-82-471-1021-8 (printed ver.)
ISBN 978-82-471-1022-5 (electronic ver.)
ISSN 1503-8181

IMT-Report 2008:101

Theses at NTNU, 2008:172

Printed by Tapir Uttrykk

ACKNOWLEDGEMENTS

The present work was carried out at Department of Materials Science and Engineering, NTNU and at Xstrata Nikkelverk AS, Kristiansand, from January 2002 to April 2008. It was part of Eureka project *2440 Depolarised Anodes for Electrowinning of Metals (DEANEW)*, and the Research Council of Norway (NFR) and Xstrata Nikkelverk are acknowledged for financial support. Thanks are due to Permascand AB, Ljungaverk, Sweden for supply of DSA® electrodes.

I would like to thank my main supervisor Prof. Geir Martin Haarberg for all help and support during these years. Thank you for giving me the opportunity to participate in several international conferences around the world – our tour in the 5100 feet deep Xstrata Craig mine outside Sudbury, Canada is something that I will never forget. My co-supervisor Dr. Sarbjyot Haarberg is acknowledged for valuable guidance and for motivating me to carry on. A special thank to Prof. emeritus Jomar Thonstad for providing relevant literature and for giving me useful feedback after reading the entire manuscript of this thesis. I would like to thank the rest of the staff at the Electrochemistry group, particularly Dr. Ole Edvard Kongstein for showing me how to perform electrochemical experiments and Dr. Sten Egil Johnsen for fruitful discussions and assistance during SEM examinations. Thanks are also due to IAESTE trainee Ana Rita Moura and Ingar Jacobsen for their contributions in the project.

Above all I want to thank Nils Roll-Lund at Xstrata Nikkelverk for preparing the pilot cell and for his invaluable help in the pilot experiments. I am grateful to my boss Øivind Stenstad for encouraging me to embark on this project and for allowing me to spend most of my working time to complete this thesis. Dr. Ole Morten Dotterud is thanked for representing Nikkelverk in the DEANEW collaboration and for preparing status reports to NFR. The very useful and inspiring discussions with electrowinning experts Jostein P. Sætre and Ernst Rosseland are highly appreciated. I would also like to thank the staff at the Nikkelverk analytical laboratory for analysing a huge number of samples from the pilot work, Tone Josephsen and the rest of "Ni-service" for bagging more than 200 anodes for the pilot cell and all my colleagues in the R&D group and elsewhere at Nikkelverk.

I am indebted to members of the DEANEW project for valuable discussions at our biannual project meetings. I want to express my sincere gratitude to the late Dr. Bo Håkansson for initiating the DEANEW project and for his enthusiasm and great interest in my work. After Bo's tragic death, Fredrik Herlitz, Permascand became a key member of the project, and his advice and support have been of great importance.

Finally, I would like to thank my parents Ingrid and Bjug, my sister Gunnhild and her Bjørn for always being there and for "feeding" me when I didn't have the time to cook myself. Playing with my little nephew Fredrik made me think of other things than this thesis. I also want to thank my friends – the weekly running trips with Børge and Christian were essential breaks, especially during the last hectic weeks before finishing this work.

Kristiansand S, April 2008

Torjus Åkre

SUMMARY

Cobalt oxide is deposited on dimensionally stable anodes (DSA®) during electrowinning of cobalt from acidic chloride solutions. This anode scale formation is undesirable for industrial operations, since it has a negative effect on productivity, energy consumption, working conditions and anode service life. The objective of the present work was to obtain a deeper understanding of the cobalt oxide deposition reaction, and to develop alternative methods to suppress or eliminate anode scaling.

Electrowinning of cobalt from industrial cobalt chloride electrolyte was investigated. Galvanostatic electrolysis experiments were carried out in a three-electrode electrochemical cell, and in a pilot cell at Xstrata Nikkelverk AS, Kristiansand, Norway. Each of the six anodes in the pilot cell, of same size and design as used in commercial cells, was surrounded by a diaphragm bag to collect the produced chlorine gas. Anode materials were supplied by Permascand AB, Ljungaverk, Sweden. Cobalt oxide deposits and DSA®-type anodes were characterized using scanning electron microscopy, x-ray diffraction analysis and electrochemical techniques. To support the interpretation of the experimental results, ionic activity and chloro complex formation were estimated theoretically for concentrated cobalt chloride solutions.

Black cobalt oxide deposit collected from anodes in the Xstrata Nikkelverk cobalt tankhouse was identified as alpha cobalt oxyhydroxide (α-CoOOH, heterogenite 3R). The cobalt content was about 60 %, and smaller amounts of manganese, silicon, chloride and sulphate were also detected. Sulphate ions were incorporated preferentially over chloride ions. Fresh cobalt oxide films prepared in the laboratory showed similar but less crystalline structure. The deposit covered the entire DSA® surface.

The extent of anodic formation of cobalt oxide was found to be highly dependent on several key electrowinning parameters. No anode scaling was observed at pH levels below 0.7, while at pH levels above 2, cobalt oxide precipitated in the bulk solution as well as on the DSA®. The anode potential stabilized at relatively low levels after the electrode was covered by cobalt oxide, indicating good electrocatalytic activity and high electrical conductivity of freshly prepared films. In the pilot cell, the anode gas

typically contained 98 % chlorine, 1 % oxygen and 1 % nitrogen, the latter due to dilution by air.

The rate of cobalt oxide deposition increased with increasing cobalt chloride concentration. Although the anode potential was lowered when sodium chloride was added to the electrolyte, anode scaling was not suppressed. This was explained by a higher cobalt activity. Introduction of sulphate ions to the chloride electrolyte inhibited cobalt oxide growth, while higher growth rates were observed in all-sulphate electrolyte. Accelerated rates of anode scaling with increasing current density and temperature along with no significant influence of the degree of convection indicated that the cobalt oxide deposition reaction was activation controlled. The anodic current efficiency for cobalt oxide deposition was reduced when increasing the current density at higher pH.

Ruthenium-iridium-titanium and iridium-tantalum mixed oxide electrodes of constant nominal composition were prepared by thermal decomposition at temperatures ranging from 350 to 500°C. When the temperature was lowered, the coatings became less crystalline and the electrochemically active surface area increased. The low-temperature electrodes showed higher activity for chlorine evolution, and the deposition of cobalt oxide was extensively suppressed. Build-up of cobalt oxide films on graphite and pure titanium electrodes resulted in depolarization of the chlorine evolution, and the nature of the deposited cobalt oxide seemed to protect titanium from passivation.

Hydrogen peroxide added to the electrolyte was consumed both at the cathode and by reaction with dissolved chlorine, resulting in reduced current efficiencies for cobalt and chlorine. However, the electrolyte acidity increased, and less anode scale was generated. Cobalt oxide deposits were not completely stable at open circuit potential, and the accumulation of anode deposit was reduced by operating with periodically interrupted current at low frequency. Periodically reversed current was more effective, but the deposited cobalt metal was bent due to internal stresses. Short-circuiting of the pilot cell resulted in only partial dissolution of cobalt oxide, owing to preferential reduction of dissolved chlorine.

In most of the pilot experiments, pH in the anode compartments was higher than in the cathode compartment. This difference in pH was explained by low rates of anodic oxygen evolution combined with hydrogen ions taking

part in the current transport across the diaphragm, thus migrating out of the anode bags towards the cathodes. This view was supported by estimating the anolyte pH from the proton balance for an anode compartment, showing excellent agreement with the experimental results. Consequently, the anolyte pH was decreased by increasing the rate of anolyte flow, suppressing the formation of cobalt oxide. When hydrochloric acid was added inside the anode bags, a large difference in pH was obtained between the anolyte and the catholyte. The cobalt current yield was then improved by increasing the pH of the feed electrolyte, with simultaneous inhibition of anode scaling.

The experimental results clearly demonstrated that several of the possible methods to suppress anode scaling had detrimental effects on other important parameters of the cobalt electrowinning process. Lower electrolyte pH, lower cobalt chloride concentration and lower temperature resulted in reduced cathodic current efficiency for cobalt and increased cell voltage, with adverse effect on productivity and energy consumption. The DSA® coatings prepared at reduced temperatures were also shown to be less stable than the commercial coatings.

LIST OF PAPERS

Parts of this thesis have been presented at four conferences and published in three proceedings volumes:

1. Torjus Åkre, Geir Martin Haarberg, Jomar Thonstad, Ole Morten Dotterud, *"Scaling of DSA Anodes in Cobalt Electrowinning"*, 42nd Conference of Metallurgists, The Metallurgical Society of CIM, Vancouver, British Columbia, Canada, August 24-27, 2003, poster.

2. Torjus Åkre, Geir Martin Haarberg, Sarbjyot Haarberg, Jomar Thonstad, Ole Morten Dotterud, *"Anodic Precipitation of Cobaltic Oxide in Cobalt Electrowinning"*, 4th Kurt Schwabe Corrosion Symposium, Helsinki, Finland, June 13-17, 2004, proc. p. 348-356.

3. Torjus Åkre, Geir Martin Haarberg, Sarbjyot Haarberg, Jomar Thonstad, Ole Morten Dotterud, *"The Anode Process in Cobalt Electrowinning"*, 206th Meeting of the Electrochemical Society, Honolulu, Hawaii, USA, October 3-8, 2004, Electrode Processes VII, PV 2004-18, The Electrochemical Society, Pennington, NJ, USA, 2005, 276-287.

4. Torjus Åkre, Geir Martin Haarberg, Sarbjyot Haarberg, Jomar Thonstad, Ole Morten Dotterud, *"Electrowinning of Cobalt from Chloride Solution – A Pilot Plant Study"*, 44th Conference of Metallurgists, The Metallurgical Society of CIM, Calgary, Alberta, Canada, August 21-24, 2005, Nickel and Cobalt 2005: Challenges in Extraction and Production, 359-374.

TABLE OF CONTENTS

Chapter 1

INTRODUCTION

1.1 Cobalt in general

Cobalt is a relatively common element in nature, and the earth's crust contains 0.002 %, which ranks it no. 33 in abundance [1]. It is an essential element for all animal life and is the central constituent of vitamin B_{12}, which catalyses the regeneration of red blood cells. The metabolism of vitamin B_{12} and the daily ingestion of cobalt-containing foodstuffs provide the most significant source of cobalt in the human body. An adult human body contains around 3 mg of cobalt, and malabsorption of vitamin B_{12} or diet deficiency can lead to anaemia. On the other hand, the ingestion of relatively high levels of cobalt may pose health risks to humans. Cobalt salts (1-2 ppm) were added to beer as a foam stabilizer in the 1960's, and heart disease with subsequent death was reported among heavy beer drinkers.

The name cobalt is derived from the German term "kobold" applied in the 14th century to the gnomes living in the silver mines of Schneeberg. Certain ores were difficult to smelt and produced toxic arsenic vapours when roasted, and these problems were blamed on the "kobolds". The name nickel has a similar origin ("Old Nick").

Commercially, cobalt has been used to colour pottery and glass from at least 2000 B.C. Metallic cobalt was isolated in 1735 by the Swedish scientist G. Brandt, and electroplating of cobalt was performed for the first time in 1842. Colouring from oxides and silicates was the main use up to the 20th century, and even in 1916 the global cobalt output was only 554 metric tonnes (mt), of which 400 mt was in the form of oxide. The development of the stellite cobalt chrome alloys by E. Haynes in the early 1900's caused a great leap in

the use of cobalt, and other new applications resulted in a steady increase in demand through the 20th century. The total refined cobalt production in 2007 was close to 54 000 mt [2].

Due to its ability to impart strength and corrosion resistance at high temperatures, cobalt is favoured in alloys used in high temperature applications, e.g. gas turbines, jet engines and high speed tools. Cobalt is a ferromagnetic material, and it retains its magnetism up to 1121°C, the highest Curie temperature known. Hence, cobalt is vital in the magnet industry. Other applications include its use as a drying agent in paint, a catalyst in the petroleum industry and in the medical field, in prosthetics and radiology. The use of cobalt in electronics has grown enormously during the last years, in magnetic recording and especially in the battery sector. Cobalt is an important component in nickel-cadmium, nickel-metal hydride and lithium-ion rechargeable batteries, and in 2007 the manufacture of batteries represented about 22 % of the total cobalt consumption [3]. As a result of the economic growth in China combined with constrained availability of raw materials from Central Africa, the cobalt price is presently all time high at around 50 US$/lb (April 2008).

1.2 Cobalt production

Cobalt is mainly recovered as a byproduct from copper and nickel production. The raw materials are sulphide, oxide and arsenide ores together with slags and recycled materials. Polymetallic deep sea nodules are a large potential source of cobalt, but they have not yet been exploited commercially due to high processing costs [4].

Until recently, most of the cobalt was supplied from the Copper Belt located along the border between the Democratic Republic of Congo (DRC) and Zambia, where copper and cobalt are produced by a roast-leach-electrowinning process. However, during the last years this situation has changed, since the African production has declined, while the global nickel output has increased. Furthermore, an increasing portion of the nickel production is now based on lateritic ores found in tropical and subtropical regions, having higher cobalt to nickel ratios than the traditional sulphide deposits mined in Canada, Australia and Russia. Pyrometallurgy and hydrometallurgy are employed to upgrade nickel and cobalt, and the two

elements are usually separated at a late stage in the process. It is interesting to note that until the end of World War II, cobalt was not separated and ended up in the nickel product. When nuclear power reactors were introduced, only stainless steel based on pure nickel was tolerated, since cobalt would have been converted to the Co-60 isotope, a hard gamma ray emitter with a half-life of over five years [5]. In addition, high purity cobalt was needed for the newly developed aircraft jet engine. To meet these two new demands, the main nickel producers decided to modify their refining processes so that both nickel and cobalt could be extracted into pure metals.

Cobalt metal is produced either by electrowinning or by hydrogen reduction. In the latter method, a key part of the Sherritt-Gordon process [6], aqueous cobalt ammine complexes are reduced by hydrogen to metallic powder in autoclaves operated at high pressure and high temperature (35 atm, 175°C):

$$Co(NH_3)_2^{2+} + H_2 = Co + 2\ NH_4^+ \qquad (1.1)$$

The reduction technique is a semi-continuous operation. Cobalt is produced in a cycle comprising one initial "nucleation" reduction with Na_2S-NaCN catalyst and 30-50 "densification" reductions, in which cobalt is deposited on the produced cobalt particles. At the end of the cycle, the cobalt product is discharged, washed and dried. It is sold directly as cobalt powder or it is pressed into briquettes. In addition to cathodes, powders and briquettes, cobalt is marketed in the form of granules and as different types of oxides and salts.

1.3 Electrowinning of cobalt

1.3.1 General principles

Cobalt cathodes are electrowon from aqueous sulphate and chloride solutions. The main electrode reactions with standard electrode potentials vs. the standard hydrogen electrode (SHE) are as follows:

Cathode reactions:

$$Co^{2+} + 2\ e^- \rightarrow Co \qquad E° = -0.28\ V_{SHE} \qquad (1.2)$$

$$2\ H^+ + 2\ e^- \rightarrow H_2 \qquad E° = 0\ V_{SHE} \tag{1.3}$$

Anode reactions:

$$H_2O \rightarrow ½\ O_2 + 2\ H^+ + 2\ e^- \qquad E° = 1.23\ V_{SHE} \tag{1.4}$$

$$2\ Cl^- \rightarrow Cl_2 + 2\ e^- \qquad E° = 1.36\ V_{SHE} \tag{1.5}$$

$$Co^{2+} + 2\ H_2O \rightarrow CoOOH + 3\ H^+ + e^- \qquad E° = 1.6\ V_{SHE}\ [7] \tag{1.6}$$

Since cobalt is less noble than hydrogen, the cathodic deposition of cobalt (reaction 1.2) is accompanied by simultaneous hydrogen evolution (reaction 1.3). However, when operating in solutions of low acidity, cobalt current efficiencies close to 100 % can be achieved. In sulphate media the main anode reaction is oxygen evolution (reaction 1.4), but if chloride ions are present, chlorine evolution is kinetically favoured (reaction 1.5). Furthermore, Co^{2+} ions may be oxidized up to the trivalent state in both types of electrolyte and form a cobalt oxyhydroxide anode scale by hydrolytic precipitation (reaction 1.6). More details about this anode scaling reaction are presented in section 1.5.3.

Cobalt exists in two allotropic modifications; the hexagonal closed-packed α phase and the face-centered cubic β phase [8]. Although the β phase is stable only at temperatures above 417°C, cobalt electrodeposits often contain both phases, especially when deposited at low pH and low temperature. Other important structural features of the electrodeposits are their fibrous texture and the large differences in surface morphology at various electrolysis conditions. A shift in the cobalt deposition mechanism from a simple two electron transfer in acidic solutions to a pH dependent mechanism at pH levels higher than ~3 has been observed in both sulphate and chloride solutions [9-12]. Owing to hydrogen evolution, pH at the cathode surface is higher than in the bulk solution, and $Co(OH)_2$ may precipitate on the cathode when pH is high.

Several studies of the influence of the electrolysis conditions on the current efficiency for cobalt have been reported [8-16]. It is a general trend that current efficiency is enhanced by increasing the cobalt concentration, the pH and the temperature. In chloride solutions the current efficiency increases steadily with increasing current density, while in some of the studies

involving sulphate solutions the current efficiency was observed to deteriorate at high current densities [13, 15, 16]. The cell voltage is usually lowered when the cobalt concentration and the temperature are increased, due to higher electrolyte conductivity and depolarization of the electrode reactions.

Electrowinning of cobalt from chloride solutions has several advantages over sulphate, like higher electrolyte conductivity, lower electrolyte viscosity, lower anodic and cathodic overpotentials, more uniform and ductile metal deposition at high current densities and higher activity of the cobalt ion, resulting in less sensitivity towards fluctuations in electrolyte pH. Higher solubility also makes it possible to operate with more concentrated solutions. However, more advanced cell designs are needed for the safe handling of toxic chlorine liberated at the anodes, and chloride solutions are more corrosive than sulphate solutions. The fact that smooth and coherent cobalt cathodes can be produced from pure chloride electrolytes without additives is quite unique. Except for nickel, other metals like copper, zinc and lead tend to form powders when electrodeposited from chloride solutions due to low polarization [17].

1.3.2 Cobalt production at Xstrata Nikkelverk

Electrorefining of nickel anodes by the Hybinette process started in Kristiansand, Norway in 1910, based on domestic ore [18]. After takeover of the refinery by Falconbridge Nickel Mines Ltd. in 1929, the main feed material has been converter matte from the Sudbury district, Ontario, Canada. Falconbridge Ltd. was acquired by Xstrata plc in 2006. Originally, cobalt in the feed ended up in the nickel cathodes, but the conversion in 1952 to a mixed chloride-sulphate electrolyte made the separation of cobalt possible. As part of the nickel anolyte purification circuit, cobalt was oxidized by chlorine for precipitation as cobaltic hydroxide, which was further upgraded to cobalt metal.

Today, nickel and cobalt are leached from the raw materials using chlorine, and later separated by solvent extraction in the chlorine leach process [19]. Extracted cobalt is stripped from the organic phase with cobalt anolyte and water, giving a cobalt chloride electrolyte that is subjected to solution purification before entering the cobalt tankhouse. Here cobalt is deposited on titanium mother blanks or cobalt starting sheets, for one and seven days

respectively. Chlorine gas is produced on DSA®-type anodes, and each anode is encapsulated in bags of permeable synthetic cloth to collect the chlorine (Fig. 1.1). Catholyte is sucked into the bags and leaves the cells via hoods as anolyte along with the anode gas. The anolyte is dechlorinated and returned to the electrowinning tanks or the stripping section, while the chlorine gas is sent to the leaching department to dissolve more matte.

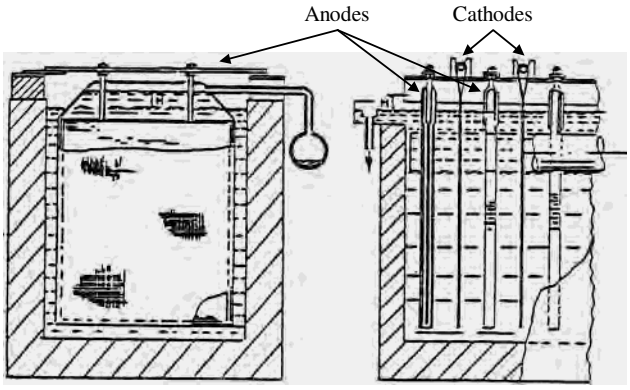

Inlet electrolyte composition:

Co 55 g/l, Cl 70 g/l , pH 1, 60°C

Electrowinning operating data:

- Cathodic CD 220 A/m^2
- Cobalt current efficiency 90 %
- Cell voltage 3.7 V
- Inlet flow 3.5 m^3/h,tank
- Anolyte flow 3 m^3/h,tank
- 48 cathodes/49 anodes per tank
- Anode spacing 140 mm

Figure 1.1 *End view (left) and side view (middle) of the Xstrata electrowinning cell [20]. Xstrata Nikkelverk cobalt tankhouse operating data to the right.*

1.3.3 Industrial practice

A major portion of global cobalt production is in the form of cathodes electrowon from sulphate or chloride solutions. Operating conditions for 7 cobalt tankhouses are summarized in Table 1.1.

Industrial electrowinning of cobalt is carried out in rectangular open cells with alternate anode and cathode vertical plate electrodes connected in parallel within each cell, while the cells are connected in series. In sulphate solutions permanent stainless steel cathodes are mostly used, while in chloride solutions cobalt starting sheets are produced on titanium blanks. Lead alloyed with antimony (~6 %) is the dominating anode material in sulphate solutions, although inert cobalt alloy anodes (Co 82 %, Si 14 %, Mn 4 %) have been used by some African cobalt producers [21]. Lead contamination of the cobalt product is thus avoided, but these expensive

anodes are affected by higher electrical resistivity and brittleness [22]. Graphite anodes were used in chloride media [23], but they have now been replaced by DSA® anodes.

Table 1.1 Electrowinning operating conditions for selected cobalt refineries.

Refinery / Media	pH	Co (g/l)	ΔCo [1] (g/l)	Temp. (°C)	CD [2] (A/m^2)	CE_{Co} [3] (%)	U [4] (V)	Cycle (days)
Shituru SO_4^{2-} [24]	6.2-6.4	30-40	-	-	300	55-60	-	-
Luilu SO_4^{2-} [21]	-	45	6	70	350-400	80	-	4
Chambishi SO_4^{2-} [25]	1.9	30-40	4	70-75	280-400	65-70	4.8	4 or 5
Port Colborne SO_4^{2-} [26]	3.7	45	7	50	200	93	3.7	5
Sumitomo Cl^- [27]	1.2-1.5	55-65	9	55-60	233	90	3.1	8
Jinchuan Cl^- [28]	2	65-80	35-60	55-60	300-350	-	3.5	4
Nikkelverk Cl^-	1	55	5	60	220	90	3.7	7

[1] ΔCo = Drop in cobalt concentration across the cell.
[2] CD = Cathodic current density.
[3] CE_{Co} = Cathodic current efficiency for cobalt.
[4] U = Cell voltage.

When operating in sulphate media, anodic production of oxygen results in increased acidity of the electrolyte, which has a negative effect on cobalt current efficiency. To counteract this, pH of the feed electrolyte is adjusted to high levels combined with a high circulation rate. The Gecamines Shituru plant in the DRC is operated with in-pulp electrolysis, where cobalt is added as $Co(OH)_2$ particles suspended by air sparging, neutralizing the acid in the electrowinning cells as it is produced. However, extensive dendritic growth occurs, and the cathodes must be lifted frequently to break electric shorts. At the Vale Inco Port Colborne cobalt refinery, high current efficiency is achieved in divided cells where the anodes are bagged. This also results in lower levels of aerosols in the tankhouse atmosphere. Since cobalt cathodes are difficult to shear due to brittleness, cobalt rounds are produced by Vale Inco on 1 inch diameter areas not masked by dielectric heat-cured epoxy paint.

Cobalt cathodes are currently being produced from chloride solutions at three locations. Sumitomo in Japan operates with a technology very similar to Xstrata Nikkelverk, while Jinchuan in China has reported the use of cathode bags, ventilation hoods on the upper part of each anode and shorter cells with smaller electrode size. Cobalt electrowinning in chloride media was also practiced at a plant in Plombières, France [29], but it is now closed. Cathodes produced at the chloride plants and at Port Colborne contain only small amounts of impurities, while most of the African plants utilize thermal refining to upgrade the cobalt product. Cathodes are sometimes annealed at ~800°C to remove hydrogen.

1.4 Dimensionally stable anodes

The dimensionally stable anode (DSA®) is a key component in several electrochemical processes, e.g. chlor-alkali electrolysis, chlorate production, electrowinning of metals, electroplating, copper-foil production, cathodic protection, electrosynthesis and waste water purification [30]. The name reflects the fact that this electrode retains its shape during operation, as opposed to graphite anodes, which are consumed over time. The DSA® consists of a substrate of a valve metal coated with noble metal oxides formed by thermal decomposition. When polarized in the cathodic direction, valve metals like titanium, tantalum, zirconium and niobium are able to conduct current. On the other hand, when polarized anodically, a non-conducting oxide film is formed, which makes these metals extremely stable in many aggressive media.

1.4.1 History

Traditionally, graphite electrodes were employed for electrolytic chlorine production [31]. However, their use was associated with a range of operational problems. The graphite material was consumed over time, increasing the inter-electrode distance and causing slime formation. Hence, in order to reduce the frequency of electrode replacement, bulky electrodes were applied, occupying much cell space. Furthermore, the overpotential for chlorine evolution on graphite is relatively high, and the cell voltage was further increased by adhering gas bubbles and low electrical conductivity.

Chlorinated organic compounds harmful to the environment were also generated. An improved type of anode was highly demanded.

When titanium metal became commercially available in the 1950's, the Belgian scientist Henri Beer wanted to make an aqueous solution of titanium ions by anodic dissolution of the metal. Contrary to what was expected, no titanium seemed to go into solution, and the applied voltage increased. From the observed passivation and stability of titanium, Beer soon realized the potential of this metal as an electrode substrate. Electrodeposited metallic coatings on titanium were developed, and the platinized titanium electrode showed quite promising results in chlor-alkali cells. However, these anodes were very expensive, the anode potential tended to increase with time and the wear rate of the platinum coating was high, especially when short-circuits occurred. The stability of the platinized titanium electrodes was later improved by alloying with 30 % iridium.

The real breakthrough came in 1964 when Beer discovered a way to make metallic oxide coatings of high catalytic activity and high stability [32, 33]. A solution containing the coating components was applied on the titanium substrate, which was then thermally treated in the presence of oxygen to convert the coating components into oxides. This classic DSA®, still widely used in the chlor-alkali industry, consisted of a solid solution of 30 mole-% ruthenium oxide and 70 mole-% titanium oxide, representing the active/conducting component and the dispersing/stabilizing component respectively. The benefits of mixed oxide coatings, consisting of both a conducting and an inert film-forming component, were clearly demonstrated.

Due to the excellent properties of the DSA® anode, e.g. very low overpotential for chlorine evolution, low levels of oxygen in the anode gas and dimensional stability, it soon became a great success in the chlor-alkali industry. The invention was commercialized by the Italian De Nora company, and it was introduced to the industry before the fundamental research of these electrodes had started at the universities. Rising energy prices during the 1970's accelerated the conversion from graphite to DSA®, and at the end of the decade most of the chlorine plants were operating with DSA® anodes. The use of more efficient and environmentally friendly membrane cells also became feasible in combination with the DSA®.

In the time after Beer's discovery, ranked among the most important in electrochemistry during the last 50 years, a large number of different oxides

have been tested, and the DSA® anode has found new applications. Much effort has been put into the development of less expensive oxide coatings without noble metals, however, such electrodes still suffer from a lack of performance when compared with the original DSA®'s.

1.4.2 Preparation and its influence on electrode properties

The preparation of dimensionally stable anodes involves a series of steps, all influencing the properties of the final product, although some steps are more critical than others. The key steps in the method of DSA® preparation are illustrated in Fig. 1.2, and each step is then discussed separately in the following paragraphs.

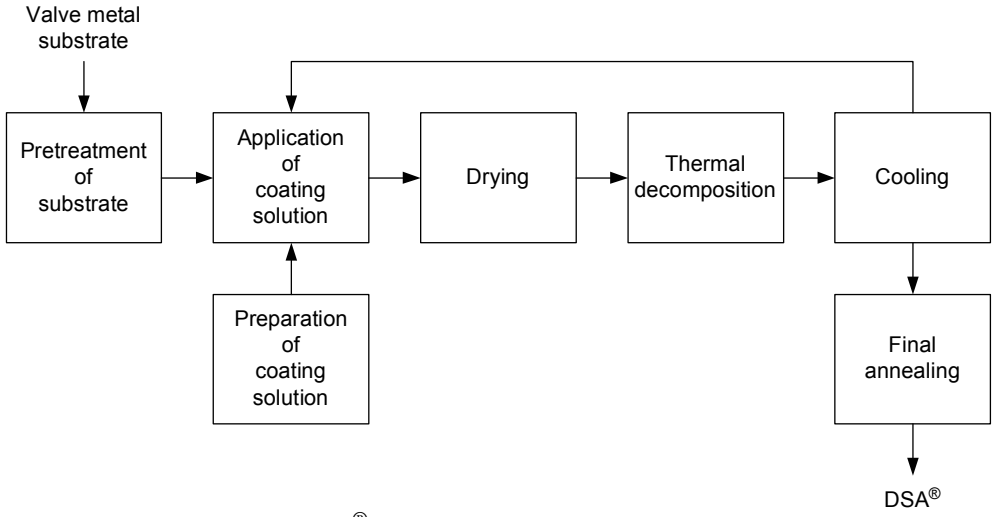

Figure 1.2 *Method of DSA® preparation.*

1.4.2.1 Pretreatment of substrate

Titanium is usually the preferred substrate material, due to its low density and lower cost compared to tantalum [34]. The critical temperature at which an insulating oxide film is formed is also higher for titanium than the other valve metals. A high critical temperature means fewer restrictions in thermal decomposition.

The substrate is roughened by sandblasting followed by etching in boiling hydrochloric acid or hot oxalic acid. A rough surface is essential for proper adhesion of the coating to the support. Thick oxide films that may interfere with the current distribution are also removed during pretreatment. Remaining catalytic coating may also be removed from recycled electrodes by sandblasting and etching before recoating.

Pretreatment is very important for anode service life. If the surface roughness is too low, the catalytic coating may peel off during operation. On the other hand, if the surface is too rough, a brittle coating may be obtained [35]. Since the oxide coatings are porous, the electrolyte will reach the underlying support. It is therefore important that the support is corrosion-resistant. Tantalum is more corrosion-resistant than titanium, and a tantalum interlayer between the substrate and the coating is sometimes used to improve anode lifetime during oxygen evolution.

1.4.2.2 Preparation of coating solution

The coating solution is prepared by dissolving suitable precursors in aqueous or organic solvent. To avoid extensive hydrolytic precipitation, acid is added to the aqueous based solutions. Despite this acidification, hydrated oxides are being formed, and the interactions between these clusters and other dissolved ions play an important role for the structure of the final coating [36].

Metal chloride salts are mostly employed as precursors, and the coatings normally contain a few percent of residual chlorine. Different precursors decompose at different temperatures, e.g. nitrate salts are converted to oxides at lower temperatures than chlorides [37]. The valence state of the precursors may also have an effect. It has been shown that $Ir(III)Cl_3$ and $H_2Ir(IV)Cl_6$ give rise to different oxide structures, since they form different chloride complexes in the coating solution [36]. Whether solid solutions or separate oxide phases are formed is also dependent on the choice of precursors. Finally, the concentration of the coating solution affects the amount of solvent that is evaporated in the drying step, and the coating solution may age over time.

1.4.2.3 Application of coating solution

Various techniques are used for the application of coating solution on the substrate, like brushing, spraying, dipping or rolling. The amount of coating solution applied will depend on the technique used.

1.4.2.4 Drying

In the drying step, the electrode is treated at temperatures around 100°C for 5-10 minutes in order to evaporate the solvent. The rate of evaporation is usually higher for organic solvents than for aqueous solvents, and this may affect the coating porosity. In addition, certain types of precursors like $SnCl_4$ and H_2PtCl_6 are volatile, and high losses of these components have been observed [38]. Consequently, the ratio between the components in the final coating can differ significantly from the ratio in the coating solution.

1.4.2.5 Thermal decomposition

After drying, the electrode enters the thermal decomposition step, where the precursors are converted to oxides by heat treatment in air at temperatures in the normal range of 400-550°C typically for 10 minutes.

The thermal decomposition temperature and the nature of the precursors are regarded as primary factors influencing the properties of oxide coatings. A low temperature results in small oxide crystallites with high surface area, whereas a high temperature results in crystallization and sintering, giving larger particles. It is well known that oxide electrodes prepared at reduced temperatures have a higher electrocatalytic activity, but unfortunately these electrodes are less stable. If the firing temperature is too low, the conversion of the precursors into oxides will be incomplete. On the other hand, at very high temperatures the underlying substrate may be covered by an insulating film, causing passivation or coating exfoliation [34]. The time of thermal treatment and the atmosphere in the furnace are two other important factors.

1.4.2.6 Cooling

When the thermal decomposition is finished, the electrode is removed from the furnace and cooled at room temperature. Cracks may form in the coating due to the rapid drop in temperature, and it has been demonstrated that more compact oxide films are produced at controlled cooling rates [39].

The cooled electrode is then returned to the coating application step, and the sequence is repeated until the desired catalyst loading is reached. Commercial electrodes may consist of up to 30 layers. The electrode activity is improved as the number of layers is increased, but this effect is levelling off since the first layers become less accessible for the reacting species. The effect of catalyst loading is also dependent on the type of reaction. For instance, the facile chlorine evolution reaction is less influenced by the coating thickness than the more demanding oxygen evolution reaction. It should be mentioned that the real electrode surface area can be more than 1000 times larger than the geometric surface area, reflecting the 3-dimensional structure of DSA® anodes.

1.4.2.7 Final annealing

The final step in the preparation of DSA® electrodes is usually a ~1 hour thermal treatment at temperatures similar to that of thermal decomposition in order to stabilize the oxide coating. Lodi et al. [40] showed that the final annealing process had less effect on iridium based electrodes compared to ruthenium based electrodes.

1.4.3 Chlorine and oxygen evolution

1.4.3.1 Electrocatalytic activity

The rate of the chlorine and oxygen evolution reactions is dependent on the electrode material, and it is governed by both electronic factors coupled to the chemical composition of the electrode and surface area effects [41]. Intermediates are formed, and the bond strength between these intermediates and the metal oxide surface is important with respect to reaction rate. The highest electrocatalytic activity is obtained for those oxides at which the intermediates are adsorbed not too weakly and not too strongly. The degree

of adsorption is related to the oxidation and reduction of active sites, and the catalytic activity is favoured by a match in oxidation potentials between the electrode reaction and the active component in the coating. Oxides like SnO_2 and PbO_2 are in their highest oxidation states, and they are therefore poor electrocatalysts for chlorine and oxygen evolution [42].

In acidic chloride solutions, the oxidation of chloride ions to chlorine gas proceeds at a higher rate than the splitting of water molecules to oxygen gas and acid. Chlorine evolution is known to be a facile reaction less dependent on the active surface area than the more demanding oxygen evolution reaction. Ruthenium oxide is the most active oxide for both reactions, and when mixed with titanium oxide the activity becomes even higher. Such synergetic effects may be obtained for intimately mixed oxide structures [42]. Titanium oxide is non-conducting and has zero activity, so that a certain amount of ruthenium oxide is needed.

1.4.3.2 Reaction mechanisms

Chlorine evolution

The chlorine evolution reaction at oxide electrodes was reviewed by Trasatti [43]. Three proposed reaction mechanisms are given below.

Bianchi 1971:

$$Cl^- = Cl_{ads} + e^- \quad (1.7)$$

$$2\ Cl_{ads} \rightarrow Cl_2 \quad (1.8)$$

Krishtalik 1975:

$$Cl^- = Cl_{ads} + e^- \quad (1.7)$$

$$Cl_{ads} \rightarrow (Cl_{ads})^+ + e^- \quad (1.9)$$

$$(Cl_{ads})^+ + Cl^- = Cl_2 \quad (1.10)$$

Erenburg 1981: $H_2O = OH_{ads} + H^+ + e^-$ (1.11)

$$OH_{ads} + Cl^- \rightarrow HOCl + e^- \quad (1.12)$$

$$HOCl + HCl = Cl_2 + H_2O \quad (1.13)$$

Bianchi was the first to mention a possible mechanism for chlorine evolution. The proposed electrochemical-chemical path had a Tafel slope of 30 mV/decade at 25°C, and the reaction rate was controlled by the surface recombination of chlorine atoms, or the removal of produced Cl_2 from the electrode. Krishtalik observed a reaction order of 1 with respect to Cl^- and suggested a mechanism giving a Tafel slope of 40 mV/decade. In 1981, Erenburg published a pH dependent mechanism, where the retarding effect of H^+ was taken into account.

Oxygen evolution

In acidic solution, oxygen evolution shows Tafel slopes of typically 40 and 60 mV/decade on RuO_2 and IrO_2 respectively [44]. When the current density is increased, a break in the Tafel curve is sometimes observed, due to oxide dissolution or a change in the reaction mechanism. If the primary water discharge is the rate determining step, the Tafel slope becomes 120 mV/decade at 25°C.

Three mechanisms for oxygen evolution in acidic solution are given below, where S denotes a surface active site [44]. Note the different oxygenated species adsorbed on the electrode surface, and that the first and last steps are identical in all mechanisms.

El. chem. oxide path: $S + H_2O = S\text{-}OH + H^+ + e^-$ (1.14)

$$S\text{-}OH = S\text{-}O + H^+ + e^- \quad (1.15)$$

$$2\ S\text{-}O \rightarrow 2\ S + O_2 \quad (1.16)$$

Oxide path: $S + H_2O = S\text{-}OH + H^+ + e^-$ (1.14)

$2\ S\text{-}OH = S\text{-}O + S + H_2O$ (1.17)

$2\ S\text{-}O \rightarrow 2\ S + O_2$ (1.16)

Krasil'shchikov path: $S + H_2O = S\text{-}OH + H^+ + e^-$ (1.14)

$S\text{-}OH = S\text{-}O^- + H^+$ (1.18)

$S\text{-}O^- = S\text{-}O + e^-$ (1.19)

$2\ S\text{-}O \rightarrow 2\ S + O_2$ (1.16)

1.4.3.3 Selectivity

As pointed out earlier, chlorine evolution proceeds faster than oxygen evolution in acidic solutions. Hence, chlorine current efficiencies (CE_{Cl2}) close to 100 % are often observed in chloride solutions. Improved CE_{Cl2} has been reported at increasing electrolyte acidity, chloride concentration, temperature and current density [44]. Due to specific adsorption, sulphate ions may reduce CE_{Cl2}.

The selectivity is also dependent on the anode material. DSA®-type anodes exhibit excellent CE_{Cl2}, and the mixed RuO_2-TiO_2 electrode is better than the pure RuO_2 electrode [35]. Cl_2 evolution is also favoured on compact coatings. Doping with Sn, Sb or Bi oxides results in higher overpotential for oxygen, improving CE_{Cl2} even more [35]. On the other hand, if oxygen is the preferred anode product from chloride solution, few anode materials are suitable. Anodically deposited MnO_2 has been shown to generate almost pure oxygen from sea water and saturated brine [44]. This effect was explained by high overpotential for Cl_2 evolution on amorphous MnO_2.

1.4.3.4 DSA® stability

The wear rate of the ruthenium based DSA® electrodes employed in chlorine production is very low, and the lifetime of thick coatings (10-20 μm) can be more than 10 years before the electrodes must be recoated. Coating degradation in chloride solutions is linked to current density and oxygen evolution, and operating conditions favouring the latter reaction accelerate wear [45]. RuO_2 is not stable during oxygen evolution, as it may then be oxidized up to volatile RuO_4 species. Increased rates of coating dissolution in the case of current interruption have also been observed [44, 45]. Mixed oxide coatings are used industrially since they are much more stable than pure oxides.

Due to higher anode potentials, more stable coatings are needed for oxygen-evolving DSA®'s. The IrO_2-Ta_2O_5 electrode with 70 mole-% iridium appears to be the preferred choice for oxygen evolution. Other deactivation mechanisms dominate in sulphate media, and passivation is one of them. The acidified solution penetrates the porous coating, and over time an insulating film of TiO_2 is formed between the coating and the substrate. Large portions of the original coating may still be present on the surface of passivated electrodes [34]. At very high current densities, extensive gas bubble formation can cause coating detachment in the form of powder [45].

Certain electrolyte impurities can induce premature anode failure in both chloride and sulphate solutions. Deposits like MnO_2, SiO_2 and organic material may block parts of the anode surface [35], increasing the corrosion at unblocked parts due to higher local current density. Complexing agents like thiourea may dissolve noble metal oxides [46], and fluorides can attack titanium [47].

1.4.4 DSA® in metal electrowinning

Nickel and cobalt are produced by electrowinning from chloride solutions at 6 different locations, all using DSA® anodes. Other metals like zinc and copper are electrowon from sulphate solutions using lead anodes. Introduction of DSA® would result in lower energy consumption and reduced lead contamination of the cathode product, but the cost of the expensive oxygen-evolving coatings has been too high so far. Owing to the relatively low current densities employed in metal electrowinning, the value

of product produced per square metre anode area is low compared to the chlor-alkali industry [48].

Zinc electrolytes normally contain several grams per litre of manganese, which is oxidized at the anodes and precipitates as MnO_2 slime. Increasing anode potential is observed for DSA®'s covered by MnO_2 [49], and parts of the catalytic coating may detach when MnO_2 flakes off. A new type of coating has been developed having a topcoat of valve metal oxide, and it is claimed that manganese deposition is considerably reduced due to diffusion limitations of Mn^{2+} compared to water [50]. Traces of fluorides in the electrolyte is another potential problem in the zinc electrowinning process.

In order to reduce anode manufacturing costs, hybrid anodes have been developed for copper electrowinning, consisting of coated titanium sponge or mesh attached to regular lead anodes [51]. Power savings of 12 – 17 % and enhanced current efficiency were reported. In addition, the lead base was stabilized without cobalt addition so that the cathode quality was improved. Cobalt is usually added to copper electrolytes to stabilize the lead anodes (see section 1.5.5), representing a significant operating cost.

1.5 Formation of higher cobalt oxides

1.5.1 Electrochemical formation of cobalt oxide in neutral/alkaline solutions

When cobalt metal is polarized anodically in alkaline aqueous solution, passivating cobalt oxide films with oxidation states II, III and IV can form on the surface [52-54]. Since the reduced $Co(OH)_2$ form is slightly soluble, thick hydrous oxide films can be grown by potential cycling. The behaviour changes from irreversible oxide formation and reduction to the development of a largely reversible redox oxide film, where only the outer regions participate in the redox reactions.

Similar behaviour is observed when cobalt oxides are deposited anodically on foreign substrates from neutral solutions, where cobalt is present at low concentrations in the form of soluble complexes or solid $Co(OH)_2$ particles. Tench and Warren [55] prepared cobalt oxide films on platinum by anodic deposition from cobalt sulphate-sodium acetate solution at constant potential (0.1 M Co, pH 7.5, 1 V vs. the saturated calomel electrode (SCE)). In this

way 1 μm thick films were obtained, showing high electrical conductivity, while deposits formed at lower potentials appeared to be much less conducting. Chen and Noufi [56] deposited cobalt oxide on platinum and graphite from cobalt acetate solution by both potential cycling and potentiostatic electrolysis (0.05 M Co). The anodic current efficiency for cobalt oxide deposition was found to decrease when the potential was increased. Spataru et al. [57] reported the formation of discontinuous films of cobalt oxide on boron-doped diamond by anodic voltammetry in nitrate solution (< 0.002 M Co, pH 8.4). Pauporté et al. [58] prepared cobalt oxide films on nickel by potentiostatic electrolysis from nitrate solution (0.09 M Co, pH 7.4, 0.5 V_{SCE}). The current efficiency for cobalt oxide deposition increased at elevated temperatures, and crystalline films were obtained for temperatures above 60°C. Finally, Hu and Hsu [59] studied the effect of complex agents (acetate, citrate, EDTA) on anodic deposition of cobalt oxide on graphite (0.01 M Co, pH 6.3). The oxidation potential of divalent cobalt ions was found to differ significantly between the complexing agents, but the deposition rate was also dependent on the rate of adsorption and chemical conversion of oxidized species into cobalt oxide deposits.

1.5.2 Chlorine and oxygen evolution on cobalt oxide

Titanium-supported cobalt oxide anodes prepared by thermal decomposition have been evaluated as anode material for chlorine production. Co_3O_4 layers were prepared by Boggio et al. [60], using thermal decomposition of $Co(NO)_3$ on titanium between 200 and 500°C. A retarding effect of acidity on the anodic chlorine reaction was observed, along with a Tafel slope of 40 mV/decade. Hence, a pH-dependent mechanism was proposed, similar to the one first suggested by Erenburg (see section 1.4.3.2).

Contrary to Boggio et al. [60], da Silva et al. [61] did not observe any effect of pH on the rate of chlorine evolution on thermally prepared cobalt oxide electrodes (470°C). They measured a Tafel slope of about 33 mV/decade, and with a transfer coefficient of ~0.8, the experimental data corresponded to Krishtalik's mechanism (see section 1.4.3.2). However, the electrode was not stable in the acidic solution, and ruthenium oxide was introduced in the coating for stabilization.

Cobalt oxide electrodes are much more stable in alkaline solutions, where high electrocatalytic activity for oxygen evolution is observed, for both

anodically deposited [62, 63] and for thermally prepared [64] cobalt oxides. Various reaction mechanisms have been suggested, most of them involving tetravalent cobalt.

1.5.3 Anodic deposition of cobalt oxide during electrolysis of cobalt from acidic solutions

In the Xstrata Nikkelverk cobalt tankhouse, cobalt oxide deposits are formed on the DSA® anodes at a rate of approximately 3 kg Co/anode,year. The anode scaling is detrimental, because the electrocatalytically active noble metal oxides then become less accessible to the chloride ions. Consequently, the cell voltage is increasing with time, and the current distribution between the electrodes is adversely affected. To control scale formation, the cobalt electrowinning process is operated at a low pH, reducing cobalt current efficiency. Aggressive corrosion attacks on the DSA® catalytic coating caused by the cobalt oxide have also been observed.

Due to the unwanted scaling, the anodes are removed from the cells every three months for cleaning, which is a labour-intensive operation with poor working conditions. If not removed, some scale will grow through the diaphragm bags, resulting in chlorine evolution in the catholyte. Chlorine outside the anode bags will either be decomposed at the cathodes, reducing the cobalt current efficiency, or end up in the tankhouse atmosphere giving an unacceptable working environment. As a consequence, the consumption of bag cloth is high. Furthermore, some scale flakes off the anodes during operation. Most of this material is collected at the bottom of the anode bags, but some is withdrawn from the anode compartments along with the anolyte and accumulates in the anolyte handling system. Over time this may lead to clogging of piping, causing stop in production for cleaning.

Kongstein [65] studied the electrolysis of cobalt from chloride solutions. He found that α-CoOOH was formed on DSA® anode by electrochemical deposition. The deposition reaction could be suppressed by lowering the pH, by applying cathodic pulses or by addition of hydrogen peroxide to the electrolyte. Grøntoft [20] pointed out that the pH should be kept below about 1.7 during electrowinning from cobalt chloride solution when using bagged graphite anodes. At higher pH the anode bags were filled with cobaltic hydroxide precipitate, which could penetrate the diaphragms and result in chlorine evolution on the outside of the bags. Some information about the

use of DSA® in cobalt chloride media has been published in the Russian literature [66, 67]. Cobalt slime formation was avoided by operating with high acidity in the electrolyte (> 10 g/l HCl).

Cobalt oxide slimes are also formed on lead anodes used in electrowinning from cobalt sulphate solutions. Bagged lead anodes are used in the Vale Inco Port Colborne cobalt refinery, and the slime produced, which contains typically 4 % Pb and 2 % Mn, is equivalent to ~10 kg Co/anode,year [68, 69]. Since acid is generated on the anodes inside the bags, it has been demonstrated that the accumulation of slime can be reduced by decreasing the anolyte flow [70]. Formation of cobalt oxide on lead anodes during cobalt electrowinning was also observed by Das and Subbaiah [15] and Lenthall and Bryson [14]. Anodically formed β-CoOOH has also been detected in the cathode product [71].

Lakshminarayanan et al. [72] carried out cobalt plating from sulphate bath using a platinum anode. They found that the undesirable anodic deposition of cobalt oxide was suppressed by addition of vanadium pentoxide to the electrolyte. Oxidized cobalt was then reduced by vanadium ions of lower oxidation state generated at the cathode. The vanadium ions were not incorporated in the cobalt metal. Titanium or molybdenum could be used instead of vanadium [73]. Matsumoto et al. [74] showed that anodic cobalt oxide deposition on platinum was suppressed when lanthanide ions were present in the electrolyte. The lanthanide ions were incorporated in the CoOOH structure, thus restricting growth of cobalt deposit. In another paper by Matsumoto et al. [75], determination of the hydration number in CoOOH films using a quartz crystal microbalance was described. When CoOOH was deposited from chloride or sulphate solution, the hydration number was found to be very high during the initial stage of electrolysis before it stabilized at around 1.

1.5.4 Chemical precipitation of cobalt oxide

Separation of cobalt from nickel by chemical oxidation and hydrolytic precipitation is widely applied in the nickel industry [76, 77]. Different types of oxidation agents can be used, e.g. chlorine, hypochlorite, nickelic hydroxide ($Ni(OH)_3$), ozone, Caro's acid (H_2SO_5) or ammonium persulphate ($(NH_4)_2S_2O_8$). pH is controlled in the range of 2 – 5 by addition of base. Low pH results in almost pure $Co(OH)_3$ and some remaining cobalt in solution,

while high pH results in extensive coprecipitation of nickel. Mobbs and Mounsey [78] found that no cobalt oxide was precipitated at pH levels below 2, using Caro's acid in sulphate solution. In the case of ozone as oxidizer, Nikolic et al. [79] did not observe any cobalt oxide formation when the pH was lower than 3.

The mixed $Co(OH)_3$-$Ni(OH)_3$ precipitates formed are leached with sulphuric acid to dissolve most of the nickel, before cobalt is dissolved using a reduction agent in acid media. Various reductants may be utilized, like sulphur dioxide, sodium sulphite, methanol, formalin or hydrogen peroxide.

1.5.5 The role of cobalt as an additive in copper electrowinning

Addition of small amounts of cobalt (~100 mg/l) to acidic copper sulphate electrolytes for electrowinning has become common practice in the copper industry [80]. The presence of cobalt in copper electrolyte results in depolarization of oxygen evolution on lead anodes, in the range of 0.1 – 0.2 V depending on concentration [81]. In addition to reduced energy consumption, the corrosion rate of the lead anodes is reduced, increasing their lifetime and improving product quality through lower levels of lead contamination of copper cathodes.

Gendron et al. [81] found that the scale formed on the lead anode surface contained no significant amounts of cobalt. They explained the catalytic effect of cobalt by electrochemical oxidation of Co^{2+} to Co^{3+} at the anode, followed by reduction of generated Co^{3+} ions with simultaneous oxidation of water to oxygen gas. Hyvärinen [82] investigated the oxygen evolution reaction on lead from sulphuric acid solutions with different concentrations of cobalt. Deposited cobalt oxide was detected on the lead surface, and a mechanism for oxygen evolution involving tetravalent CoO_2 was proposed. It was further assumed that Co^{2+} ions reacted with OH species adsorbed on the anode surface.

1.6 Scope of the present work

This work is a continuation of the studies on electrowinning of cobalt carried out by Kongstein [12, 65, 83]. Since the cathode process was examined in

great detail by Kongstein, focus was put on the anode process in chloride media, with emphasis on the undesirable deposition of cobalt oxide scale on dimensionally stable anodes. Influence of key operating parameters should be investigated, along with alternative methods to suppress or eliminate anode scaling. Larger scale testing in a new pilot plant at Xstrata Nikkelverk should also be a key part of the study.

The present work is part of Eureka project 2440 Depolarised Anodes for Electrowinning of Metals (DEANEW). Helsinki University of Technology, The Royal Institute of Technology (Stockholm), Norwegian University of Science and Technology, Outotec Oyj, Permascand AB and Xstrata Nikkelverk AS participated in this project.

Chapter 2

THERMODYNAMICS OF COBALT CHLORIDE SOLUTIONS

The majority of electrolyte solutions in hydrometallurgical processing have a high ionic strength. Concentrated electrolytes may show large deviations from ideal behaviour, which is the case for many metal chloride solutions. The ionic activity in concentrated chloride solutions of non-associated salts can be extremely high, and many transition metals form chloro complexes, which have a profound effect on its chemistry, such as solubility and reduction potential. Since cobalt chloride is influenced by both these effects in aqueous solution, it was found beneficial to put some effort into understanding its solution chemistry. A thorough knowledge of the degree of non-ideal behaviour is essential when interpreting many phenomena taking place in solutions of high ionic strength.

In this chapter the Pourbaix diagram, also known as the potential – pH diagram, of the cobalt – chlorine – water system is presented and discussed, following an introduction to cation hydrolysis in general. This diagram gives an idea of the thermodynamic stability of species as a function of potential and pH. A review of some important properties of the cobalt-containing species in the Pourbaix diagram is also included. The chapter then continues with an overview of ionic activity, and single-ion activities of cobalt and chloride are estimated from the Stokes-Robinson hydration theory. pH measurement is also discussed here. The last section of the chapter focuses on complexation in cobalt chloride solutions.

2.1 Stability of the cobalt – chlorine – water system

2.1.1 Cation hydrolysis

Hydrolysis reactions are common to most cations in aqueous solution, due to their coulombic attraction to the dipolar water molecules [84]. They can be represented either by the reaction between a free metal ion Me^{z+} and H_2O molecules from bulk solution (equation 2.1), or by the direct acid dissociation of an aquo complex (equation 2.2):

$$Me^{z+} + n\ H_2O = Me(OH)_n^{z-n} + n\ H^+ \qquad (2.1)$$

$$Me(H_2O)_6^{z+} = Me(H_2O)_{6-n}(OH)_n^{z-n} + n\ H^+ \qquad (2.2)$$

A strong attraction between the cation and the oxygen atom of water makes the water O – H bonds weaker, facilitating the release of protons. Hydrolysis is, therefore, more extensive for cations of high charge and small size, i.e. high charge density, and several high valency cations exist in solution as oxyions. Since most anions are larger than the cations, they show only moderate association with water.

When increasing the pH of metal ion solutions, successive deprotonation of solvated cations will occur. The neutral hydroxy species, e.g. $Me(OH)_2$ (aq) for Me^{2+}, is the least soluble in the polar water solvent, and may precipitate as solid metal hydroxide. The higher the cation charge density the lower is the pH at which precipitation starts, so oxidation of a cation thus often reduces its solubility in water. High valency cations also tend to form oxide compounds instead of hydroxides. If pH is further increased, the metal hydroxides may redissolve as negatively charged hydroxy complexes.

Hydrolysis is usually favoured at high metal ion activity and high temperature. High Me^{z+} activity may also lead to polymerization into polynuclear hydroxide species; the tendency of OH^- to coordinate more than one cation to form bridges is almost unique among the simple ligands [84]. Kong et al. [85] showed that various transition metal salts in aqueous solutions that are stable at room temperature, were partially precipitated when the temperature was increased to 200 – 300°C in an autoclave. In addition, high temperatures promote metal oxide formation at the expense of hydroxides [86], and the precipitates are more crystalline [87]. Presence of

certain ligands may, on the other hand, stabilize the cations in solution through strong complex formation, thus suppressing hydrolytic precipitation [84, 85].

The solubility of hydrous metal oxides increases with decreasing particle size, related to the relatively high surface energy of the interface between solid and aqueous phase [84]. This means that large nuclei must form before crystal growth can proceed spontaneously, requiring a high degree of supersaturation. Metastable phases may then be formed first, which over time are converted to more stable modifications by ageing. Amorphous metastable phases are actually formed preferentially due to their smaller critical nucleus size.

2.1.2 Pourbaix diagram

The Pourbaix diagram of the cobalt – chlorine – water system at 25°C and unit activities is shown in Fig. 2.1. The stability domains of cobalt and chlorine species are indicated by red and blue lines respectively, and the stability of water is represented by black dotted lines. The diagram is based on thermodynamic data given by Pourbaix [88], except the standard Gibbs energy of formation for the species CoOOH and Co_3O_4, taken from Hem et al. [89] (-386 kJ/mole) and Wagman et al. [90] (-774 kJ/mole) respectively. Values of $\Delta G°_f$ between -394 kJ/mole [91] and -357 kJ/mole [92] were found for CoOOH in the literature, and for Co_3O_4 the difference in the reported Gibbs energy data was even larger (-795 kJ/mole [93] to -702 kJ/mole [88]). As a result, many versions of the Pourbaix diagram for cobalt can be found in the literature, especially when it comes to the stability domains of CoOOH and Co_3O_4, and whether CoO_2 is included or not. Metastable oxide phases may form, and the thermodynamics will be influenced by nonstoichiometry and hydration effects.

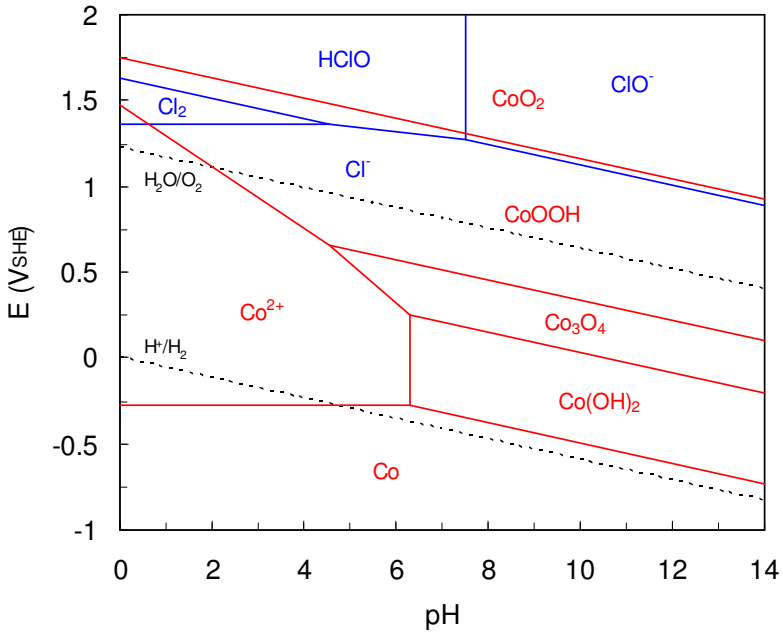

Figure 2.1 *Pourbaix diagram of the Co-Cl-H_2O system at 25°C (activities are unity).*

It is clear from Fig. 2.1 that, according to thermodynamics, electrolysis from an aqueous cobalt chloride solution of pH 1 should result in only the splitting of water into hydrogen gas on the cathode and release of oxygen gas on the anode. However, for kinetic reasons, cobalt metal can be electrowon from acidic chloride solutions at high current efficiency, and the main anode product will be chlorine gas on most electrode materials. The cathodic current efficiency for cobalt is increased at higher pH, but the catholyte pH must be kept below 6.3 in order to avoid the precipitation of $Co(OH)_2$. As H_2 evolution causes a pH increase close to the cathode surface, the catholyte pH value is usually operated much below this level so that $Co(OH)_2$ particles are not included in the product. Fig. 2.1 also shows that cobalt corrodes in acidic solution under hydrogen evolution. The corrosion rate is very low though in non-oxidizing acids, due to the large hydrogen overpotential of cobalt [88]. In neutral solutions, cobaltous ions can in fact be reduced to cobalt metal by hydrogen, which is done industrially in the Sherritt-Gordon process (see section 1.2). Dissolved oxygen and chlorine formed on the anode will be reduced by contact with the cathode, thus lowering the cobalt current efficiency. This is one of the reasons why separate catholyte and anolyte is

employed in the industrial electrowinning of cobalt from chloride electrolytes.

If chlorine is the preferred anode product, pH should be kept low in order to suppress oxygen formation and chlorine hydrolysis. The chlorine evolution reaction is independent of pH from a thermodynamic point of view, whereas oxygen generation is promoted in less acidic solutions. At higher pH levels dissolved chlorine reacts with water to form the hypochlorites (HClO and ClO^-). Perchlorate is actually the thermodynamically most stable chlorine species at high electrode potentials, but conversion from the metastable hypochlorite and chlorate forms to perchlorate is normally very slow [88]. The stability domains of Cl_2, HClO and ClO^- are outside the stability domain of water, but they are all stable due to the sluggish oxidation of water to oxygen and acid.

When polarized anodically in alkaline solutions, the surface of cobalt metal is converted to various solid cobalt oxide compounds, viz. $Co(OH)_2$, Co_3O_4, CoOOH and CoO_2. According to Fig. 2.1, cobalt oxides may form on an inert anode in cobalt chloride media as well, by anodic oxidation of Co^{2+} ions. Based on thermodynamics, oxidation and precipitation of cobalt oxides will be the main anode reaction in neutral solutions. However, the potential needed for this reaction to proceed, increases steeply with decreasing pH, and oxygen and chlorine evolution are more favourable in acidic solutions.

When discussing Pourbaix diagrams it should be emphasized that they are valid at equilibrium conditions only – they give no information about how fast equilibrium will be attained, e.g. reaction kinetics. The stability domains are also shifted if the temperature or ionic activities are altered. Huang et al. [94] presented Pourbaix diagrams of the Co – H_2O system at 20 – 80°C developed using the Outotec HSC Chemistry software. The diagrams show that temperature has a substantial influence on the thermodynamic stability of the cobalt oxides. An increase in the temperature reduces the stability domains for $Co(OH)_2$ and $Co(OH)_3$, whereas Co_3O_4 becomes more favoured. In fact, $Co(OH)_3$ is not included in the diagrams at 60 and 80°C. The temperature effect on the stability of the Co^{2+} ion is insignificant though. This trend is in contrast to the diagrams at 25 and 80°C reported by Mansour et al. [95], where CoOOH is present at both temperatures along with a somewhat decreased stability domain for Co^{2+} at 80°C compared to 25°C. Increased Co^{2+} activity results in a decrease of its stability domain. On the other hand, the presence of certain ligands may stabilize Co^{2+} in solution as a

complex, even in neutral and alkaline media. Co^{2+} forms complexes with chloride (see section 2.3), but they are not strong enough to be part of the Pourbaix diagram in Fig. 2.1 where the activities of all species are unity.

2.1.3 Cobalt species in the Co-H_2O system

The divalent cobaltous ion Co^{2+} is the stable form of dissolved cobalt in aqueous solutions. In acidic solutions it exists as the octahedrally coordinated $Co(H_2O)_6^{2+}$ ion, giving a red colour. When pH is increased, hydrolysis is taking place, and the mononuclear species $CoOH^+$, $Co(OH)_2$ (aq), $Co(OH)_3^-$ and $Co(OH)_4^{2-}$ have been reported [84]. The concentration of these species is very low though due to the precipitation of $Co(OH)_2$, except for $Co(OH)_4^{2-}$ in alkaline solutions. This species is sometimes referred to as the dicobaltite ion $HCoO_2^-$, and the colour of its solution is blue [88]. Polynuclear species like Co_2OH^{3+} and $Co_4(OH)_4^{4+}$ have also been detected in concentrated Co^{2+} solutions, although their exact formula is uncertain.

The trivalent cobaltic ion Co^{3+} is not shown in the Pourbaix diagram in Fig. 2.1, as it is stable only in very acidic solutions at high redox potentials in aqueous solutions free from complexing agents. There has been a controversy in the literature on the Co^{2+}/Co^{3+} standard potential, and Rotinjan et al. [96] claim 1.45 V_{SHE} to be the correct value based on experimental measurements. However, Bard et al. [97] point out that uncertainties in liquid junction potentials explain the low potential obtained by Rotinjan, and it is now believed that the correct value should lie between 1.8 and 1.9 V (1.81 V as reported by Pourbaix [88] was used when deriving Fig. 2.1). According to Davies and Warnqvist [98], hexa-coordinated $Co(H_2O)_6^{3+}$ can be generated chemically by using ozone or electrochemically by anodic oxidation from acidic Co^{2+} solutions at low temperature. Co^{3+} is a very strong oxidizing agent, and it decomposes water under the evolution of oxygen. Dilute Co(III) solutions containing 3 M $HClO_4$ are, on the other hand, moderately stable at 0°C ($t_{1/2}$ ~ 30 days [98]). Like divalent cobalt ions, Co^{3+} undergoes hydrolysis to form $CoOH^{2+}$ ($K \sim 2 \cdot 10^{-3}$ at 25°C and ionic strength = 1 [98], or 0.33 at 25°C and ionic strength = 3 [99]), and polymerization may result in polynuclear hydroxy complexes. The hydrolysis reactions are promoted at higher temperatures. Furthermore, Co^{3+} ions show a slow exchange of ligands and a slow attainment of

equilibrium [84], and several organic and inorganic ligands can make the Co^{3+} complexes even more stable than Co^{2+} (see section 2.3.5).

Cobalt metal *Co* exists in two allotropic modifications, α (hexagonal closed packed) and β (face centered cubic) [65]. The α form is the most stable at ambient temperature, and the transition temperature is 417°C. The Gibbs energy difference between the two forms is, however, rather small, and both phases are usually present in cobalt metal electrodeposited from aqueous solutions.

Cobaltous hydroxide *$Co(OH)_2$* precipitates from neutral cobalt solutions to form at least two different modifications; blue α-$Co(OH)_2$ and red β-$Co(OH)_2$, the latter being thermodynamically more stable [88]. Thermodynamic data for active and inactive pink $Co(OH)_2$ are given in [90], and it is indicated that the active form is converted to the inactive form by ageing. The crystal structure of β-$Co(OH)_2$ has been determined [100], while the structure of the blue form is dependent on the method of preparation. The hydroxide is more stable than the nonhydrated cubic CoO, which is unstable in air at ambient temperature and is therefore oxidized to Co_3O_4.

Cobalto-cobaltic oxide *Co_3O_4* ('$Co(II)O \cdot CO(III)_2O_3$') can be formed by oxidation of $Co(OH)_2$ or Co^{2+} from slightly acidic solutions, but it is not stable in stronger acidic solutions at 25°C (Fig. 2.1). This black coloured cobalt oxide has the normal spinel structure with Co^{2+} ions occupying the tetrahedral sites and the Co^{3+} ions the octahedral sites [100]. Specific conductivities ranging from less than 10^{-11} [101] to 2 $\Omega^{-1}cm^{-1}$ [102] have been reported for Co_3O_4, depending on the degree of oxide nonstoichiometry. Rasiyah and Tseung [103] increased the conductivity of Co_3O_4 from $2.5 \cdot 10^{-4}$ to 1 $\Omega^{-1}cm^{-1}$ by doping with 7 at-% Li^+ ions, and the improved conductivity was attributed to an electron hopping process between Co^{2+} and Co^{3+} ions in the tetrahedral sites of the lattice. The dissolution rate of Co_3O_4 is very slow in both ammonia and acid H_2SO_4 solutions, probably due to the extremely strong Co – O bonds of the spinel structure [104].

Cobalt oxyhydroxide *CoOOH* of trivalent cobalt, also referred to as $HCoO_2$, $CoHO_2$, $Co(OH)_3$ or $Co_2O_3 \cdot x\ H_2O$ in the literature, can be produced by oxidation and precipitation from acidic cobalt solutions, and by oxidation of $Co(OH)_2$. The colour of CoOOH depends on preparation and film thickness,

varying from orange [53, 56] and yellow [55, 88] to brown and black, the latter two being the most common.

Benson [105] prepared two different types of CoOOH from $Co(OH)_2$ using either chemical or electrochemical oxidation. Brown $CoHO_2$, later denoted as α-CoOOH by Simmons [100], was formed when either α- or β-$Co(OH)_2$ was allowed to stand in 1 M KOH at room temperature (oxidized by dissolved oxygen from air). The conductivity of this product was very low in dry form (10^{-6} $\Omega^{-1}cm^{-1}$), and it did not retain any K^+ ions. A different modification of CoOOH was produced when blue α-$Co(OH)_2$ was polarized anodically in aqueous KOH. Two different forms of black β-CoOOH, termed I and II by Benson, were generated, where CoOOH(II) was a stacking variant of CoOOH(I). The structure of β-CoOOH resembled that of α-$Co(OH)_2$ very closely with a hexagonal-rhombohedral unit cell, although the symmetry of the CoOOH(II) structure was unsufficiently determined. The conductivity of dry β-CoOOH powder was as high as 5 $\Omega^{-1}cm^{-1}$, and it contained 3 – 5 wt. % K^+. The electrochemical behaviour of the various cobalt oxyhydroxides was published in a part II article by Benson et al. [7], and it was shown that α-CoOOH was electrochemically less reactive than β-CoOOH.

α-CoOOH prepared by Benson has the same structure as the black material obtained by Kondrashev and Fedorova [106] when $Co(OH)_2$ was boiled in water for 50 hours. According to Amatucci et al. [107] this compound, traditionally referred to as heterogenite 3R, is of a rhombohedral space group R3m, commonly indexed on a hexagonal lattice (a = 2.86 Å, c = 13.16 Å). The structure consists of edge sharing CoO_6 octahedra connected to form CoO_2 sheets, joined together by strong hydrogen bonds parallel to the c-axis [100]. There is a three-layer repeat in the structure. Furthermore, α-CoOOH (or $HCoO_2$) is isostructural with $LiCoO_2$, which is used as the positive electrode material in Li-ion batteries. In this respect, Amatucci et al. [107] indeed synthesized $LiCoO_2$ powders by mixing α-CoOOH particles and an excess of aqueous LiOH at 100°C. An ion exchange process took place between H^+ in CoOOH and Li^+ ions in solution, and after two days the CoOOH particles were completely converted to $LiCoO_2$. The structure of β-NiOOH used as cathode in Ni-Cd and Ni-metal hydride batteries is also similar to α-CoOOH [107].

Preparation of CoOOH by anodic oxidation of either cobalt metal [52], $Co(OH)_2$ [7] or an aqueous Co^{2+} solution using an inert substrate [56], is a

quite irreversible process, since the reduction of CoOOH is very slow. Therefore, CoOOH has proved unsuitable for use in alkaline secondary batteries, except when added in small amounts to NiOOH positive plates [7]. The dissolution of CoOOH separated from nickel solutions by chemical precipitation is sluggish even in acidic media, and reductants are usually added to speed up the reaction (see section 1.5.4).

Cobalt peroxide CoO_2 containing tetravalent cobalt, formed when cobalt metal or cobalt oxide is polarized anodically at high potentials in alkaline solution, is highly unstable and decomposes water with the formation of lower cobalt oxides and the evolution of oxygen [88]. Simmons et al. [108] demonstrated using emission Mössbauer spectroscopy that α-$Co(OH)_2$ on a platinum substrate yielded a mixture of β-CoOOH and CoO_2 at 600 mV_{SCE}, and CoO_2 only at 900 mV_{SCE}, in a borate buffer of pH 8.5. On the other hand, when cobalt metal was polarized in the same solution at 900 mV_{SCE} the oxide film was not completely transformed into CoO_2 but contained also β-CoOOH. After storing in air for three months, CoO_2 was decomposed to nonstoichiometric Co_3O_4. CoO_2 in the mixture formed at 600 mV_{SCE} was indeed stable enough to obtain a spectrum in air without appreciable decomposition within 24 hours. CoO_2 has also been generated by Amatucci et al. [109], starting with $LiCoO_2$, which was converted to CoO_2 on complete lithium deintercalation at high potentials. In situ x-ray diffraction showed that CoO_2 had a hexagonal single-layered structure similar to β-$Co(OH)_2$, and it was transformed back into the regular three-layer Li_xCoO_2 phase on Li reinsertion. Unlike Simmons et al. [108], CoO_2 produced by Amatucci et al. [109] was reduced to α-CoOOH when exposed to air for three days, probably by intercalation of protons resulting from the parallel decomposition of atmospheric moisture to oxygen.

2.2 Ionic activity

2.2.1 Introduction to ionic activity

The ionic activity, a, is related to concentration m (molality, mole/kg H_2O) through the activity coefficient γ:

$$a = \gamma \cdot m \tag{2.3}$$

Strictly speaking, electrolyte solutions are ideal, i.e. a = m or $\gamma = 1$, only at infinite dilution. In real electrolytes, interactions between individual ions of the solutes and between dissolved ions and the solvent (water) result in deviations from ideality. This is shown in Fig. 2.2 a), where mean activity coefficients $\gamma_{\pm}$ for some simple aqueous electrolytes are presented. When small amounts of a salt is added to pure water, the activity coefficient of the salt decreases due to long-range electrostatic interactions between individual ions of the solute, which tend to decrease its Gibbs energy [110]. As the salt concentration is further increased, short-range interactions between dissolved ions and the dipolar water molecules become increasingly important. For non-associated electrolytes like $MgCl_2$ solutions, this leads to a sharp rise in ion activity, which is a result of the change in the activity of water itself.

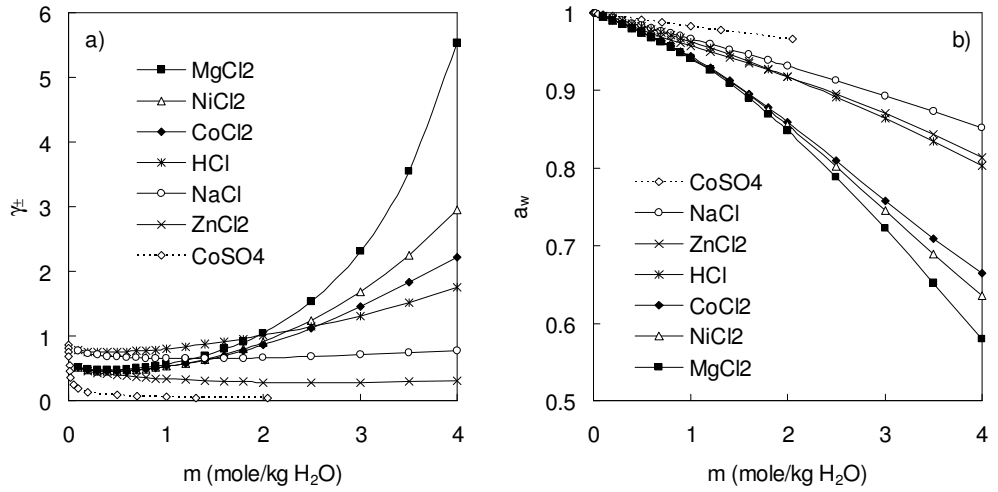

Figure 2.2 *a) Mean activity coefficients and b) water activities in single electrolytes at 25°C. Data from Robinson and Stokes [110], except for $CoSO_4$, which was taken from Lobo [112] (a_w in $CoSO_4$ solution was calculated according to Jansz [113]).*

The water activity a_w is determined by the solute's ability to attract water molecules, i.e. the degree of hydration. Therefore, the drop in water activity is most pronounced in non-associated electrolytes containing ions with large charge densities. This is shown in Fig. 2.2 b), where the divalent metal chlorides cause a larger reduction in water activity compared to monovalent NaCl. By comparing Figs. 2.2 a) and b), it is evident that a large drop in

water activity results in a large increase in the activity of the solute, in accordance with the Gibbs-Duhem relation, which states that the chemical potential of a component in a mixture cannot be changed independently [111].

The difference in activity between the four divalent metal chlorides in Fig. 2.2 a) can be explained by the extent of chloride complexation. $MgCl_2$ shows no evidence of chloride complex formation [110], while $ZnCl_2$ forms quite strong chloro complexes. The extremely low activity of $CoSO_4$, which is typical for divalent metal sulphates, is due to extensive ion-pairing. Actually, neutral $Me \cdot SO_4$ ion-pairs are the predominant species in most practical metal sulphate solutions [114]. Ion-pairing is defined as purely electrostatic attraction between oppositely charged ions. Ion-pairs are less structured than complexes, and they retain their water of solvation. Since the ion-pairs are neutral, they do no take part in the current transport during electrolysis.

2.2.2 Activity measurement

Chemical potentials of the components of an electrolyte solution are determined either by measuring the activity of the solvent (water), or the activity of the solute [110]. Various vapour pressure methods are the most important in the first category, while the latter is dominated by electromotive force (emf) measurements of suitable cells. When the activity of the solvent has been determined, the activity of the solute can readily be calculated by use of the Gibbs-Duhem equation, or vice versa.

The vapour pressure methods are based on the fact that the water activity is equivalent to the ratio of the vapour pressure of water over the electrolyte solution to that of pure water at the same temperature. In the emf method, the activity of e.g. $CoCl_2$ can be calculated from the measured reversible potential E^{rev} between a cobalt metal electrode in a $CoCl_2$ solution of known concentration and a Ag/AgCl reference electrode, using the Nernst equation:

$$E^{rev} = E^{\circ} - \frac{RT}{2F} \ln\left(a_{Co^{2+}} a_{Cl^-}^2\right) \tag{2.4}$$

where E° is the standard potential of the cobalt electrode.

The mean activity coefficient of cobalt chloride is then defined by the following relation:

$$a_{Co^{2+}} a_{Cl^-}^2 = a_{\pm}^3 = (\gamma_{\pm} m_{\pm})^3 = \gamma_{\pm}^3 \cdot m_{Co^{2+}} m_{Cl^-}^2 = \gamma_{\pm}^3 \cdot 4m_{CoCl_2}^3 \qquad (2.5)$$

As pointed out by Muir and Senanayake [115], the activities obtained by the emf method rely on accurate values of the reference electrode potential and also on the liquid junction potential E_J between the reference electrode and the test solution to be known. In aqueous solutions E_J values can be as large as 30 mV, which for a divalent metal chloride like $CoCl_2$ corresponds to more than a twofold change in $\gamma_{\pm}$ at 25°C. The effect of liquid junction potential is accounted for by proper choice of a salt bridge and the use of the Henderson equation for estimation of E_J (see section 2.2.7). It should also be emphasized that direct measurements of single-ion activities are not possible, since the concentration of a particular ion cannot be changed independently due to electrical neutrality.

2.2.3 Calculation of mean activity coefficients at elevated temperatures

Measurement of activity is a tedious work that must be carried out accurately for the results to be reliable, as outlined in the previous section. Most of the activity data available in the literature relates to pure electrolytes at 25°C, while in the real life in the hydrometallurgical industry mixed electrolytes at higher temperatures are commonly used. As a consequence, empirical activity equations are sought in order to be able to describe such complicated systems.

Physical chemists have been working for many years in establishing equations for predicting activity coefficients. Modeling of the behaviour of electrolyte solutions is a formidable task when all types of interactions between ions, solvent effects, Brownian motion etc. should be taken into account. Reasonable assumptions and simplifications are, therefore, necessary for the equations to become useful. Debye and Hückel derived the following expression for the mean activity coefficient in a simple electrolyte [110]:

$$\log \gamma_{\pm} = -\frac{A|z_+ z_-|\sqrt{I}}{1 + B\mathring{a}\sqrt{I}} \qquad (2.6)$$

where A and B are constants, z_+ and z_- the charge number of cations and anions respectively, I the ionic strength and å is an ion-size related parameter. From equation 2.6 it can be seen that the mean activity coefficient approaches linearity in the square root of the concentration at high dilutions, known as the Debye-Hückel limiting law. Short-range ion-ion and ion-solvent interactions are not accounted for in equation 2.6, a fact that restricts its validity to $I < 0.1$. By adding to equation 2.6 a term $b \cdot I$, representing the short-range interactions and b being a constant, the equation can be used up to at least $I = 1$.

Stokes and Robinson extended the Debye-Hückel equation by introducing the theory of ionic hydration [110], correlating the ionic activity coefficient with the water activity and the hydration number h, regarded as the number of moles of water molecules bound to one mole of solute:

$$\log \gamma_{\pm} = -\frac{A|z_+ z_-|\sqrt{I}}{1 + B\mathring{a}\sqrt{I}} - \frac{h}{\nu}\log a_w - \log\left[1 + 0.018(\nu - h)m\right] \qquad (2.7)$$

where ν is the stoichiometric coefficient, i.e. the number of moles of ions for each mole of solute. Equation 2.7, derived by assuming that water bound to ionic species is no longer part of the bulk solvent, has been reported to be remarkably successful with non-associated aqueous electrolytes [110].

During the early 1970's, more extensive and accurate semi-empirical equations for activity coefficients were developed by Pitzer and Meissner, see [115]. Pitzer's equations have the most fundamental basis based on statistical mechanical theories of electrolyte solutions [116], and they are considered to give the best fit to experimental data up to $I = 6$. Furthermore, the Pitzer model has been extended to moderately associated and mixed electrolytes, including the temperature dependence, and the database of parameter values for several metals like cobalt is fairly extensive (see [116] and references therein). However, the large number of adjustable parameters needed makes the model complicated, especially for non-symmetrical mixing like $CoCl_2$ + NaCl.

In the present work, Meissner's method, as outlined by Jansz [113], was adopted for the estimation of mean activity coefficients in aqueous cobalt chloride and $CoCl_2$-NaCl mixtures at elevated temperatures. The method utilizes experimentally determined mean activity coefficients for the pure components at 25°C, it is easy and practical to use and it was claimed to be quite successful in chloride media [117]. Meissner's equations are based on the observation that the data for most strong electrolytes fall into a common family of curves when the reduced activity coefficient $\Gamma = \gamma_{\pm}^{1/|z+\cdot z-|}$ is plotted versus the ionic strength, with very little crossover. This applies at any temperature T, and the effect of T (°C) on Γ at a given ionic strength can be estimated from the relationship:

$$\log \Gamma_T = (1.125 - 0.005 \cdot T) \log \Gamma_{25^\circ C} - (0.125 - 0.005 \cdot T) \log \Gamma_{ref} \quad (2.8)$$

where Γ_{ref} can be obtained from the equation:

$$\log \Gamma_{ref} = -\frac{0.41\sqrt{I}}{1+\sqrt{I}} + 0.039\, I^{0.92} \quad (2.9)$$

Equations 2.8 and 2.9 were used to calculate mean activity coefficients for pure $CoCl_2$ solutions at 60 and 100°C. Data for $\gamma_{\pm}$ at 25°C were taken from [110], and concentrations were converted from the molality to the molarity scale using density data from Herrington et al. [118]. The results illustrated in Fig. 2.3 show that for $CoCl_2$ concentrations lower than 0.5 M there is a small increase in $CoCl_2$ activity with temperature (too small to be noticeable in the figure), whereas for concentrations > 0.5 M the effect of temperature is opposite, as the activity decreases at elevated temperatures. The influence of temperature on $\gamma_{\pm}$ is more pronounced as the concentration is increased from 0.5 M. According to Peters [119], solutions generally approach ideality with increasing temperature: Activity coefficients that are larger than unity decrease, while those being lower than unity tend to increase.

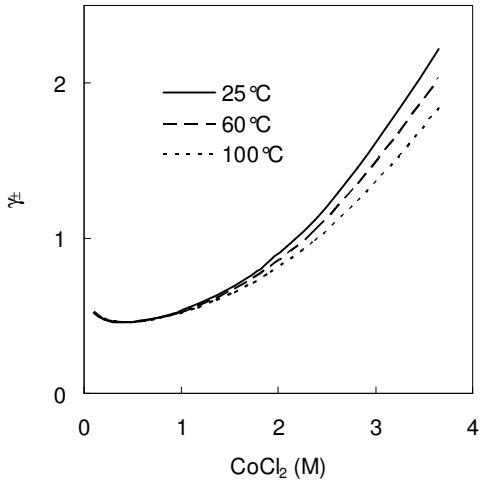

Figure 2.3 *Mean activity coefficients of $CoCl_2$ solution at 25, 60 and 100°C.*

Ji [117] used an alternative version of Meissner's theory on the nickel chloride system, showing good agreement with experimental data. Here, a single parameter for each solute is sufficient to predict activity coefficients and water activities in pure and mixed electrolytes at different temperatures. No experimental data is needed as long as this parameter is known. Parameter values for selected electrolytes are tabulated in [120], and for $CoCl_2$ it is reported to be valid up to a maximum ionic strength of 4.5 – 6.

2.2.4 Calculation of mean activity coefficients in mixed solutions

The activity of a component in a mixture can be very different from that in the pure electrolyte, and the equations for activity coefficients become more complicated as the number of dissolved species increases. As mentioned earlier, data for mixed solutions are scarce, particularly at elevated temperatures. Hence, correlations are needed to provide the necessary data.

Harned and co-workers have measured activities in several binary mixtures [121]. They found that under the condition of constant total ionic strength I_{tot}, $\log \gamma_{\pm}$ of a salt is directly proportional to the ionic strength fraction of the other component, which has later become known as Harned's rule [110].

However, the slope of the log $\gamma_{\pm}$ – I curve changes with I_{tot}, which means that if reliable calculations are to be made, a total set of slope values is required.

Meissner and Kusik [122] developed an alternative method for approximating activities in multi-component electrolytes, involving reduced activity coefficients. For a mixture of two components (1 and 2) with a common anion, like $CoCl_2$ + NaCl, their equations reduce to:

$$\log \Gamma_1 = \log \Gamma_1^{\circ} + 0.5\, X_2 \log\left(\frac{\Gamma_2^{\circ}}{\Gamma_1^{\circ}}\right) \tag{2.10}$$

$$\log \Gamma_2 = \log \Gamma_2^{\circ} - 0.5\, X_1 \log\left(\frac{\Gamma_2^{\circ}}{\Gamma_1^{\circ}}\right) \tag{2.11}$$

where Γ° is the reduced activity coefficient in pure solution with the same ionic strength as I_{tot}, and X is the ionic strength fraction of the cation. The similarities to Harned's rule are evident.

Mean activity coefficients for cobalt chloride in mixtures of $CoCl_2$ and NaCl at 25°C were calculated using equation 2.10. Data for $\gamma_{\pm}$ NaCl were taken from [123], and values for supersaturated solutions were estimated from the nomographs given in [122]. Linear interpolation between known values for $\gamma_{\pm}$ was used whenever necessary. Densities of the mixtures, needed for the conversion from molality to molarity scale, were found simply by adding to the density of a pure $CoCl_2$ solution of actual concentration, the density difference between a pure NaCl solution of actual concentration and pure water. This gives precise density values for binary chloride systems [124]. The results presented in Fig. 2.4 show that the mean activity coefficient for $CoCl_2$ increases when NaCl is added, and the effect of NaCl is larger at high $CoCl_2$ concentration. The role of added salt is to solvate free water, which causes the activity of the solvated Co^{2+} and Cl^- ions to rise. Note that the mixtures of 2 M $CoCl_2$ and > 2 M NaCl are supersaturated [125].

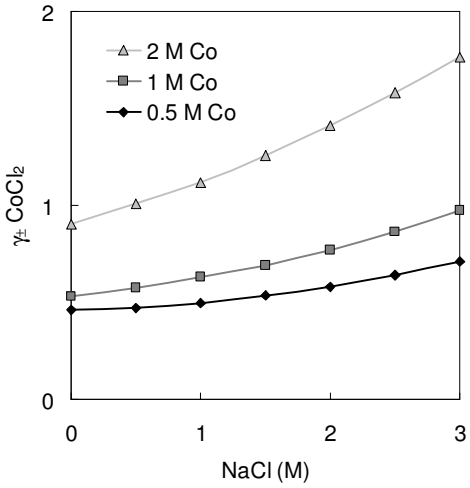

Figure 2.4 *Calculated mean activity coefficients of $CoCl_2$ in $CoCl_2$-NaCl mixtures at 25°C.*

In Fig. 2.5, calculated results obtained by using equations 2.10 and 2.11 are compared with experimental data for mixtures of $CoCl_2$ and NaCl reported by Downes [126]. There is a reasonable agreement for NaCl (Fig. 2.5 b)), but for $CoCl_2$ the experimental activity coefficients are larger than the calculated ones (Fig 2.5 a)). Furthermore, the difference between experimental and calculated data increases as cobalt chloride is replaced by sodium chloride. The equations derived by Meissner and Kusik are thermodynamically rigorous only if all dissolved ions have identical absolute values of charge. Nevertheless, good agreement has been obtained for the HCl-$MgCl_2$ system at $I_{tot} = 5$ [113]. However, Meissner's theory is based on strong electrolytes, while cobalt forms week complexes with chloride, which may explain the deviations in Fig. 2.5 a). Muir [127] claims that trace amounts of $NiCl_2$ in solutions of NaCl has the same activity coefficient as pure solutions of $NiCl_2$ at similar ionic strength, which is equivalent to horizontal lines in a graphical presentation like Fig. 2.5. The results by Downes [126] for the $CoCl_2$-$CaCl_2$ system show this kind of behaviour, whereas the $CoCl_2$-NaCl system follows a trend deviating from a horizontal curve for $\gamma_{\pm}$ $CoCl_2$. This difference is mentioned in Downes' paper, but no explanation is given. It should be commented that certain mixed electrolytes, like HCl-$MgCl_2$, show large deviations from Muir's "rule of thumb", but still the formulas derived by Meissner and Kusik give reasonable results.

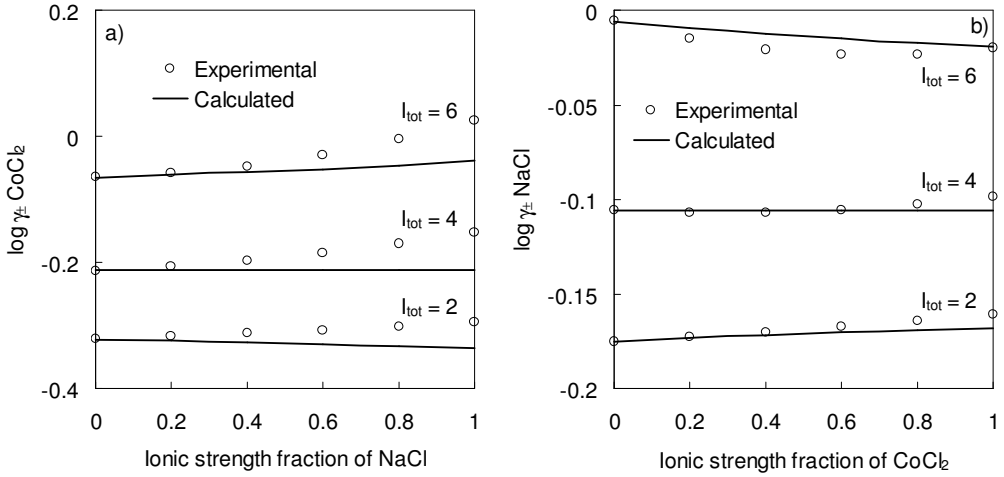

Figure 2.5 *A comparison of experimental and calculated mean activity coefficients of a) $CoCl_2$ and b) NaCl in $CoCl_2$-NaCl mixtures at 25°C. Experimental data are taken from [126].*

In order to elucidate the effect of background salt on the activity of hydrochloric acid, Peters [119] made some calculations using equations 2.10 and 2.11. His results are reproduced in Table 2.1. The estimated data show that strong chloride salts enhance the activity of HCl, and completely ionized divalent salts should be more effective than monovalent salts. 2 M HCl in 3 M $CaCl_2$ or $MgCl_2$ will have a strength equivalent to ~7 M HCl by itself, and 6 M NaCl would enhance the strength of a 2 M HCl solution to the equivalent of a 5 M pure HCl solution (though the solubility of NaCl in 2 M HCl is only ~3.5 M). A similar behaviour is expected for $CoCl_2$, which means that $MgCl_2$ will have a larger effect on the activity of cobalt than NaCl. The power of background salts can be understood by considering the influence of water activity, as will be discussed in the following section.

Table 2.1 Mean activity coefficients of HCl in mixtures of 2 M HCl with several salts at 25°C [119].

Salt conc.	NaCl	$CaCl_2$	$MgCl_2$
0	1.01	1.01	1.01
2 N	1.42	1.73	1.85
4 N	2.10	3.48	3.86
6 N	(3.11) *	6.89	7.65

* Supersaturated with respect to NaCl.

2.2.5 Calculation of water activity

When activity coefficients for all dissolved species in a system are known, the water activity can be calculated from the Gibbs-Duhem relationship. After substituting the osmotic coefficient ϕ for a_w and rearranging, Jansz [113] deduced the following expression for a single electrolyte:

$$\phi = 1 + \ln \gamma_{\pm} - \frac{1}{m} \int_0^m \ln \gamma_{\pm} \, dm \qquad (2.12)$$

Osmotic coefficients are readily obtained at any temperature from equation 2.12 when the activity coefficients at the prevailing temperature have been calculated according to the procedure described earlier. In Fig. 2.6 are shown calculated osmotic coefficients for pure cobalt chloride and pure sodium chloride solution at 25°C, compared with experimental data. The integral in equation 2.12 was solved by a simple Simpson-type graphical integration method. While the calculated values for NaCl in Fig. 2.6 b) are showing excellent agreement, a certain discrepancy exists for $CoCl_2$ in Fig. 2.6 a). The low ϕ values calculated for $CoCl_2$ at low concentrations are due to the lack of activity data for $m < 0.1$, resulting in a rough graphical integration.

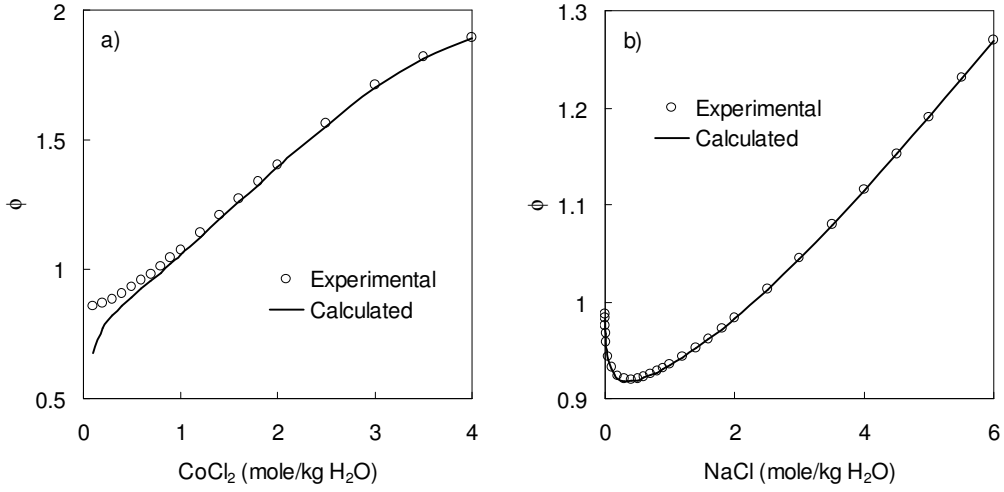

Figure 2.6 *Osmotic coefficients for pure electrolytes of a) $CoCl_2$ and b) NaCl at 25°C. Experimental data taken from [110] and [123] respectively.*

The water activity is related to the osmotic coefficient via:

$$\ln a_w = -\frac{18\,\phi \sum_i \nu_i\, m_i}{1000} \tag{2.13}$$

The summation is made over all solutes in solution.

Calculated water activities in $CoCl_2$ electrolyte at 25, 60 and 100°C are shown in Fig. 2.7. A small increase in a_w with temperature is observed, as the system then shifts towards ideality.

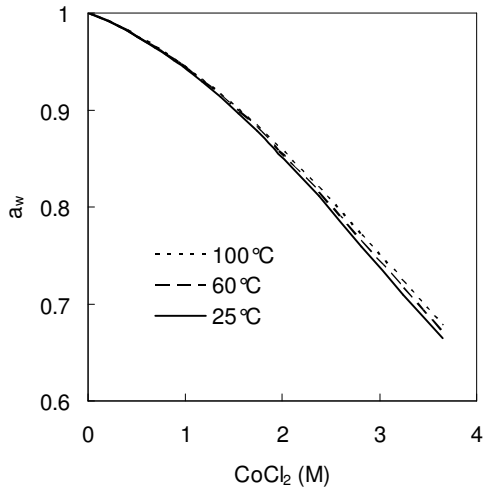

Figure 2.7 *Calculated water activity in $CoCl_2$ solution at 25, 60 and 100°C.*

For the estimation of water activity in mixed solutions, the equation proposed by Kusik and Meissner [120] was selected. $a_{w,mix}$ can simply be calculated from the pure solution activities of water a_w° at the total ionic strength and temperature of the mixed solution. a_w° values for each component are obtained using equations 2.12 and 2.13. For the three-ion system $CoCl_2$-NaCl the water activity becomes:

$$a_{w,\,mix} = \left(a^\circ_{w,\,CoCl_2}\right)^{W_{CoCl_2}} \cdot \left(a^\circ_{w,\,NaCl}\right)^{W_{NaCl}} \tag{2.14}$$

In equation 2.14, W_{CoCl2} and W_{NaCl} are defined as:

$$W_{CoCl_2} = \frac{I_{Co^{2+}} I_{Cl^-} \left(z_{Co^{2+}} + \left| z_{Cl^-} \right| \right)^2}{\left| z_{Co^{2+}} z_{Cl^-} \right| I_{tot}^{\ 2}} = \frac{4.5\, I_{Co^{2+}} I_{Cl^-}}{I_{tot}^{\ 2}} \tag{2.15}$$

and

$$W_{NaCl} = \frac{I_{Na^+} I_{Cl^-} \left(z_{Na^+} + \left| z_{Cl^-} \right| \right)^2}{\left| z_{Na^+} z_{Cl^-} \right| I_{tot}^{\ 2}} = \frac{4\, I_{Na^+} I_{Cl^-}}{I_{tot}^{\ 2}} \tag{2.16}$$

Results from the use of equations 2.14 – 2.16 are illustrated in Fig. 2.8. It can be seen that the water activity drops when NaCl is added to $CoCl_2$ electrolytes, but at high ionic strength this effect is counteracted to some extent by increasing the temperature.

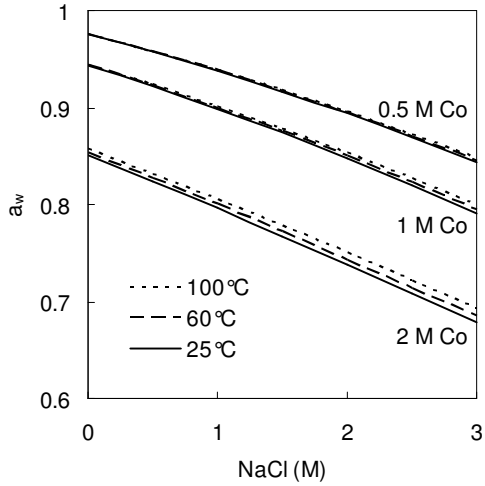

Figure 2.8 *Water activity in $CoCl_2$-NaCl mixed solutions at 25, 60 and 100°C.*

In Fig. 2.9, the calculated water activities at 25°C are compared with experimental data from Downes [126]. The calculated values were somewhat higher than the results reported by Downes, which makes sense in view of the lower calculated salt activities (Fig. 2.5).

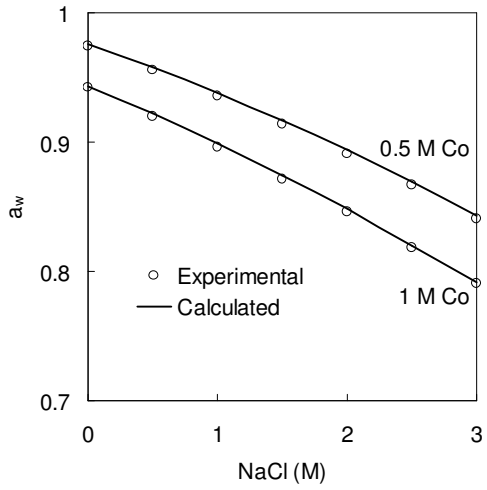

Figure 2.9 *Calculated water activity in $CoCl_2$-NaCl mixtures at 25°C, compared with experimental data taken from [126].*

2.2.6 Calculation of single-ion activity coefficients

When evaluating the effects of process parameters on chemical and electrochemical reactions taking place in an aqueous system, attention should be paid to the individual free ions, as they are mostly involved. However, thermodynamics does not allow direct calculation of single-ion activity coefficients, but estimated values may be obtained from a non-thermodynamic but physically acceptable assumption, as outlined by Jansz [113]. For chloride solutions, separation of mean ionic activities into individual activities of cations and chlorides is especially important, due to the difference in hydration. Most of the hydration is attributed to the positive ions, from strong Lewis-Acid interaction with water dipoles [110]. On the other hand, negative ions like chloride are larger (ionic radius 1.81 Å vs. 0.72 Å for Co^{2+} [110]) with a low surface charge, and their H-bonding with water is relatively weak. Consequently, the extent of hydration of chloride ions is fairly low. A decrease in the availability of free water molecules at higher ionic strength will, therefore, lead to a rise in activity of the solvated cations, whereas the activity of the poorly solvated chloride ions remains almost the same. Thus, considering the cation or anion activity coefficient as equivalent to the mean activity coefficient can be very misleading. As will be shown later, the cationic activities govern the overall activity of a metal

salt, and addition of a background salt may have a similar effect on the metal ion activity as increasing the concentration of the metal salt itself.

The hydration number h, i.e. the number of water molecules associated to an ion, depends on the valency and the radius of the bare ion. Both the bare radii and the mobility of the alkali metal ions increase in the order $Li^+ < Na^+ < K^+$ [128], which seems peculiar. However, when their hydration numbers are taken into account, 14, 8 and 5 respectively, the order of real ion sizes becomes opposite, and it is the real ion size that governs ion mobility. Note that the h number as discussed here is not equal to the real primary hydration number. For instance, $CoCl_2$ has six coordinated water molecules in dilute chloride solutions [76], while its h number is as high as 13 [110]. The latter is a result of curve-fitting to experimental data using the Stokes-Robinson equation (equation 2.7), and it can be looked upon as representing a kinetic unit of one Co^{2+} (and one Cl^-) ion surrounded by 13 relatively firmly attached water molecules.

In the original ionic hydration theory, a fixed hydration number, independent of concentration, is assigned. However, in concentrated solutions, h numbers should begin to fall, owing to the effects of the competition for water molecules between neighbouring cations [110], see also Table 1 in [115]. Jansz [113] allowed for this by introducing a decreasing hydration number at low water activities. An expression was derived for estimation of the hydration number from the water activity at very high concentrations, using Henry's law, after neglecting electrostatic effects and assuming that the activity coefficient for water is unity:

$$h = \frac{55.51}{m} + \nu\left(1 - \frac{1}{1 - a_w}\right) \tag{2.17}$$

The hydration numbers calculated from equation 2.17, for water activities between 0.4 and 0.9 where the assumptions should hold, can then be fitted to the following empirical equation:

$$\log h = \log h_\circ + \beta \log a_w \tag{2.18}$$

where the hydration number at infinite dilution, $h_\circ$, is determined by extrapolation to $a_w = 1$ in a log h – log a_w plot. For verification, the data by

Jansz for HCl are reproduced in Fig. 2.10 a), and the results for $CoCl_2$ are presented in Fig. 2.10 b).

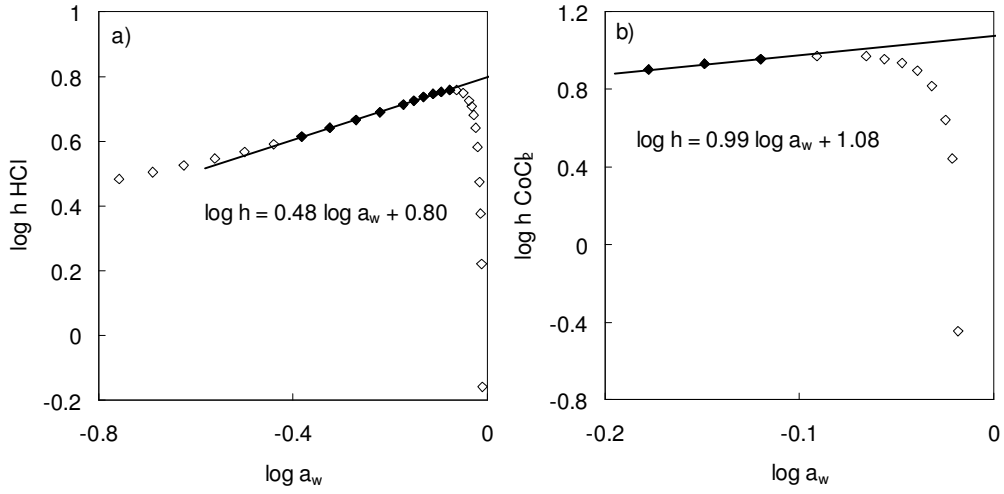

Figure 2.10 *Calculated hydration number of a) HCl and b) $CoCl_2$ vs. water activity at 25°C. Ionic activity data for HCl were taken from [123].*

The $h_\circ$ value and slope β for HCl from Fig. 2.10 a) of 6.3 and 0.48 respectively are in perfect agreement with $h_\circ = 6.4$ and $\beta = 0.51$ given by Jansz [113]. Furthermore, a hydration number at infinite dilution of 12 for $CoCl_2$, as obtained from Fig. 2.10 b), compares well with the fixed h number of 13 used by Robinson and Stokes [110]. Even though the estimated variable hydration number for $CoCl_2$ is based on a limited set of experimental data, it is believed that its use will result in more reliable ionic activities to be predicted than if a constant hydration number had been employed for highly concentrated solutions.

The hydration theory for electrolyte solutions has been extended, in order to separate mean salt activities into the contributions of individual ionic species [113, 115, 117]. For a non-associated divalent metal chloride MCl_2, it was derived that:

$$\log \gamma_{M^{2+}} = 2 \log \gamma_{\pm} + 0.00782\, h\, m\, \phi + \log\left[1 + 0.018\,(3 - h)\, m\right] \quad (2.19)$$

$$2\log\gamma_{Cl^-} = \log\gamma_{\pm} - 0.00782\,h\,m\,\phi - \log\left[1 + 0.018\,(3-h)\,m\right] \quad (2.20)$$

where γ_{M2+} and γ_{Cl-} are single-ion activity coefficients for the divalent cations and chloride anions respectively. In the development of equations 2.19 and 2.20, it was assumed that Cl^- is not hydrated. According to Jansz [113], there is considerable evidence to support this, while Senanayake [129] refers to a hydration number of 1 – 2 for the chloride ion, based on theoretical and experimental studies.

Despite the controversy about the degree of chloride hydration, and the fact that a pure cobalt chloride solution undergoes weak complexation at high ionic strength, single-ion activity coefficients have been postulated, using equations 2.19 and 2.20 with a variable hydration number, to indicate, at least qualitatively, the influence of concentration and temperature on γ_{Co2+} and γ_{Cl-}. From the results illustrated in Fig. 2.11, it can be seen that there may be a considerable difference between γ_{Co2+} and γ_{Cl-}, both deviating from the mean activity coefficient shown in Fig. 2.3. Whereas γ_{Co2+} is highly dominated by concentration and temperature, γ_{Cl-} is, on the other hand, almost unaffected. This is in line with to what extent metal ions and chloride ions are solvated, as described previously.

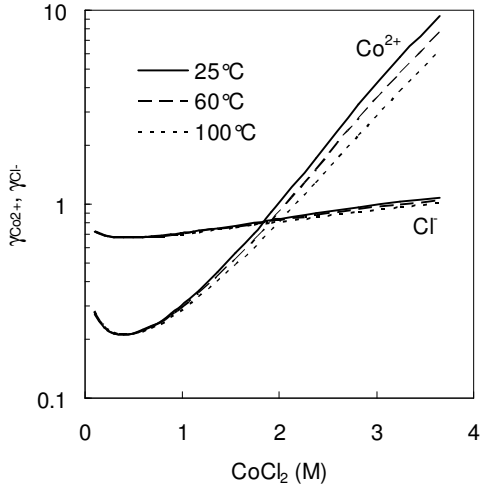

Figure 2.11 *Calculated single-ion activity coefficients for pure $CoCl_2$ electrolyte at 25, 60 and 100°C.*

Expressions for single-ion activity coefficients have been derived also for mixed solutions of metal chloride salts. Jansz [113] was the first to develop individual activity equations for binary mixtures of a univalent and a bivalent chloride, and later Ji [117] ended up with identical equations. Again, chloride ions were supposed to be unhydrated, resulting in the following equation for the activity coefficient of Cl^-:

$$\begin{aligned}(Y_A + 2\,Y_B)\log\gamma_{Cl^-} &= Y_A \log\gamma_A^{\pm} + Y_B \log\gamma_B^{\pm} \\ &- 0.00782\,\phi\left(Y_A\frac{h_A}{2} + Y_B\frac{h_B}{3}\right)(2m_A + 3m_B) \\ - Y_A \log\left[1 + 0.018\,(2 - h_A)\,m_A\right] &- 2\,Y_B \log\left[1 + 0.018\,(3 - h_B)\,m_B\right] \\ &+ \log\left\{1 + 0.018\left[(2 - h_A)\,m_A + (3 - h_B)\,m_B\right]\right\} \end{aligned} \qquad (2.21)$$

where A and B denotes MCl and MCl_2 respectively, $m = m_A + m_B$, $Y_A = m_A/m$ and $Y_B = m_B/m$. When γ_{Cl^-} has been calculated using equation 2.21, γ_{M2+} is easily obtained from the mean activity coefficient of MCl_2:

$$\log\gamma_{M^{2+}} = 3\log\gamma_{MCl_2}^{\pm} - 2\log\gamma_{Cl^-} \qquad (2.22)$$

Equations 2.21 and 2.22 were applied to the $CoCl_2$-NaCl aqueous system, and the results from the calculations are shown in Fig. 2.12. A variable hydration number was used for $CoCl_2$, while a fixed h number of 3.5 was used for NaCl [110], since its dependence on water activity will be small. Note that ionic activities are now presented and not activity coefficients. As seen in Fig. 2.12, the increase in cobalt ion activity by the addition of common salt to cobalt chloride electrolytes is dramatic, particularly at high $CoCl_2$ concentrations and low temperatures. The chloride activity is again less affected. Finally, it must be emphasized that similar shortcomings as mentioned earlier are still relevant, i.e. neglecting chloride complexation and supersaturation at 25°C.

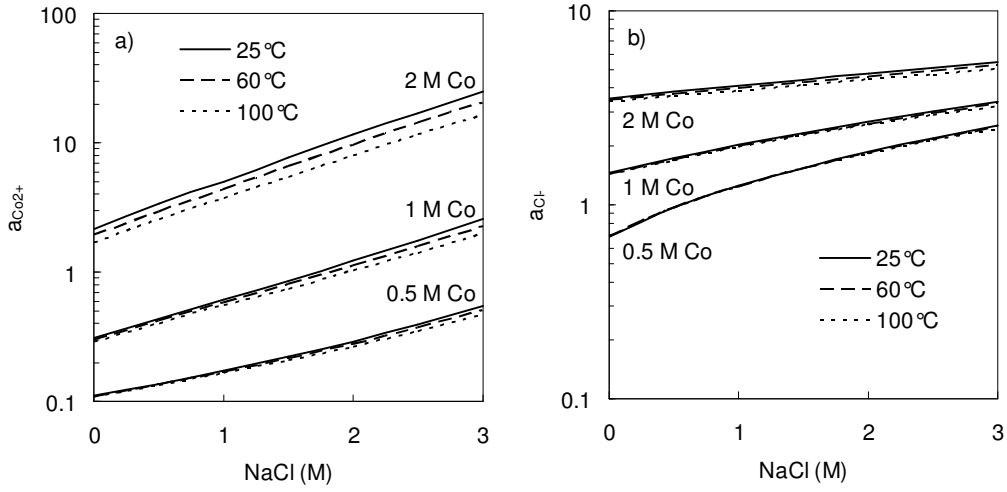

Figure 2.12 *Calculated single-ion activities of a) Co^{2+} and b) Cl^- in $CoCl_2$-NaCl mixed solutions at 25, 60 and 100°C.*

2.2.7 Hydrogen ion activity and pH measurement

The activity of the hydrogen ion, or pH as it is usually represented, is one of the most important parameters in hydrometallurgy and aqueous electrometallurgy. Hydrochloric acid may be considered as a non-associated electrolyte except at extreme concentrations, and its hydration number is reported to be 8 [110]. It is therefore expected that the HCl activity will increase as the water activity falls at high concentrations, which is actually observed (Fig. 2.2). A decrease in water activity, obtained by the addition of a background salt, will also increase the HCl activity, as seen in Table 2.1 and Fig. 2.13 below. Fig. 2.13 shows that when $CaCl_2$ is added to 0.1 M HCl up to 5 M, the pH of the solution drops by more than two units, from 1.02 to -1.19. Since the system studied in the present work shows a marked pH dependence, it was found useful to clarify how to make correct pH measurements.

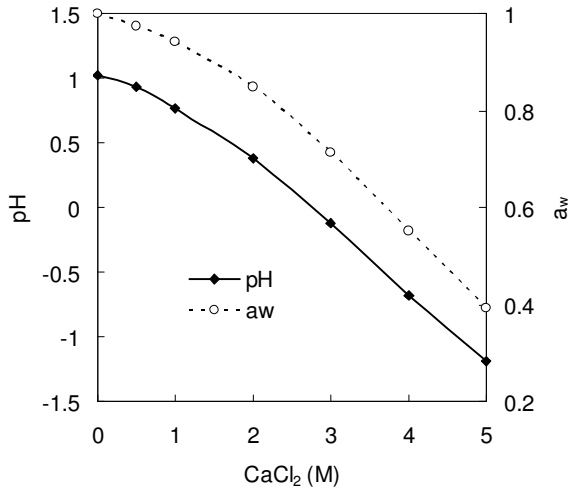

Figure 2.13 *pH of 0.1 M HCl when $CaCl_2$ is added at 25°C. Water activities are shown for comparison. Data taken from [129].*

Ji [117] developed a practical method for evaluating the pH response of nickel chloride electrolytes. By adding strong HCl successively to the electrolyte while measuring the pH, starting at pH 4, a linear relationship was found between the hydrogen ion activity and its concentration. This means that the activity coefficient of the hydrogen ion in the solutions, γ_{H+}, was constant over the pH range studied, and it could be extracted from the slope of the straight line in a $a_{H+} - C_{H+}$ plot.

$$a_{H^+} = 10^{-pH} = \gamma_{H^+} \cdot m_{H^+} \approx \gamma_{H^+} \cdot C_{H^+} \tag{2.23}$$

This procedure was applied on industrial $CoCl_2$ electrolytes at two different concentrations, from pH 1.6 to 1.0 at room temperature. The results in Fig. 2.14 show that linear relationships were obtained, and both activity coefficients were above unity. It can be seen that for a 1.44 M $CoCl_2$ solution, the amount of HCl needed to change the pH from 1.6 ($a_{H+} = 0.025$) to 1.0 ($a_{H+} = 0.1$) was only half compared to at 0.92 M $CoCl_2$.

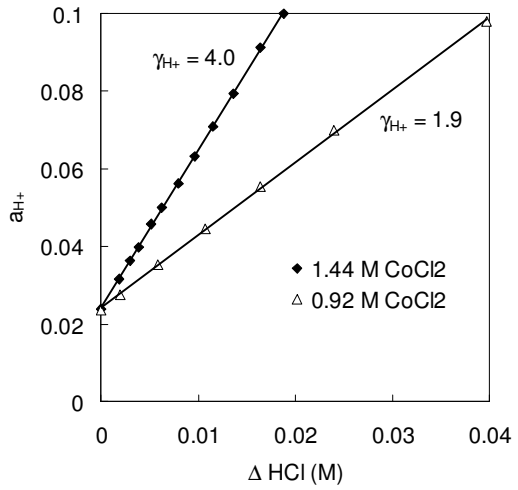

Figure 2.14 *Proton activity vs. change in HCl concentration for $CoCl_2$ electrolytes at two different concentrations (room temperature).*

Ji [117] performed several pH titrations on various nickel electrolytes. He found that γ_{H+} increased with increasing $NiCl_2$ concentration, and when NaCl was added. For 3.92 M $NiCl_2$ at 25°C, γ_{H+} as high as 96.4 was obtained, compared to 2.7 for 0.94 M $NiCl_2$. Furthermore, γ_{H+} decreased with increasing temperature, and when sulphate ions were introduced. The buffering effect of sulphate is due to the formation of bisulphate:

$$SO_4^{2-} + H^+ = HSO_4^- \tag{2.24}$$

Kongstein [65] studied the influence of different parameters on the measured pH of acidic cobalt electrolytes. The pH decreased as the $CoCl_2$ concentration was increased at constant HCl concentration, and it increased at elevated temperatures. The temperature effect on pH was stronger in concentrated electrolytes. The temperature dependence can be explained by changes in the water activity, which in turn affects the proton activity. Kongstein also observed a larger increase in pH with temperature in cobalt sulphate solution, due to a shift to the right in equation 2.24.

Several different techniques exist for pH measurement in aqueous solutions, from pH sensitive papers to various pH electrodes. In the last category, the convenient and versatile glass electrode has become very popular. It utilizes

the phase boundary potential which arises when protons in solution are exchanged with Li^+ ions in the outer hydrated gel layer of the glass membrane [130]. This potential is determined by calibration with standard buffers of assigned pH.

The following equation has been derived for the potential difference E measured between the two Ag/AgCl electrodes in a combination glass pH electrode [65, 117]:

$$E = \text{Const.} - \frac{R \cdot \ln 10 \cdot T}{F} pH_{\text{Test Solution}} + E_J \tag{2.25}$$

where E_J is the liquid junction potential between the test solution and the saturated KCl solution in the reference electrode. Since the regular buffer solutions used for calibration have E_J values close to zero, the liquid junction potential may lead to a considerable error in the measured pH in electrolytes of high ionic strength. As mentioned earlier, corrections due to E_J should be made when using any potentiometric method if accurate measured values are needed. The pH shift ΔpH and E_J are linked by:

$$\Delta pH = \frac{F}{R \cdot \ln 10 \cdot T} E_J \tag{2.26}$$

which, combined with equation 2.25, gives an expression for the relationship between the true pH and the measured pH:

$$pH_{\text{True}} = pH_{\text{Measured}} + \Delta pH \tag{2.27}$$

Equations 2.26 and 2.27 show that, if E_J or ΔpH is positive, the true pH is higher than the measured pH.

The liquid junction potential, or diffusion potential as it is sometimes called, can be calculated using the Henderson equation [65, 117]:

$$E_J = -\frac{RT}{F} \frac{\left(U^I - U^{II}\right)}{\left(V^I - V^{II}\right)} \ln \frac{V^I}{V^{II}} \tag{2.28}$$

where the parameters U and V are defined by

$$U = \sum_i C_i \lambda_i \tag{2.29}$$

$$V = \sum_i C_i z_i \lambda_i \tag{2.30}$$

I and II denote the test solution and the saturated KCl solution (4.16 M) respectively, and C_i is the molar concentration, and λ_i the equivalent conductivity of component i. Negative values for λ_i must be used for the anions in equations 2.29 and 2.30. The activity coefficients have been ignored in equation 2.28.

Equation 2.28 was used to estimate pH shifts due to E_J for several solutions at 25°C. All electrolytes were assumed to be completely dissociated, and equivalent conductivities at infinite dilution from [110] were used. The results presented in Fig. 2.15 show that the absolute value of the pH shift increases as the concentration of the test solution is increased. HCl solutions are accompanied by a large negative pH shift, whereas $CoCl_2$ and NaCl solutions have a smaller positive ΔpH. The pH shifts of pure divalent $CoCl_2$ and monovalent NaCl at 4 M are 0.20 and 0.07 pH units respectively. Furthermore, the calculations indicate that the addition of NaCl to 1 M $CoCl_2$ has only a marginal effect on ΔpH.

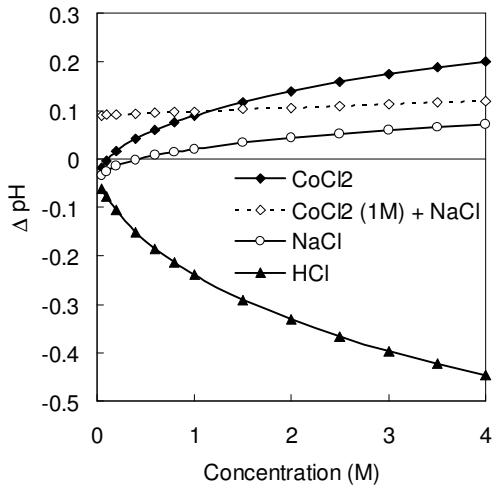

Figure 2.15 *Calculated error in pH measurement due to the liquid junction potential for various electrolytes at 25°C.*

Ji [117] also made ΔpH calculations for $NiCl_2$ solutions, using real conductivities in concentrated solutions in equation 2.28. When using conductivities at infinite dilution, his results were similar to those obtained for the $CoCl_2$ system. However, when real conductivities were applied, all pH shifts were reduced to less than 0.1 pH units. Based on these calculations, both Ji [117] and Kongstein [65] neglected the effect of liquid junction potential on measured pH values. Such pH shifts were also neglected in the present work.

Modern pH meters have temperature compensation to correct for the temperature variation in the electrode response. The temperature compensation is based on the following equation [131]:

$$E = E'\cdot T - s\cdot\frac{R\cdot\ln 10\cdot T}{F}\,pH \qquad (2.31)$$

where the constant in equation 2.25 has been replaced by a temperature function E'·T, and the theoretical slope of the E – pH curve is adjusted by a sensitivity parameter s. The parameters E' and s are determined by calibration using two or more standard buffers, and both parameters are treated as temperature independent constants by the pH meter.

In order to evaluate the accuracy of the pH temperature compensation, pH was measured in industrial cobalt chloride electrolytes between room temperature and 80°C by two alternative methods: 1) calibration at each specific temperature using heated buffer solutions and the pH vs. temperature data printed on the buffer solution bottles, and 2) calibration at room temperature only and use of temperature compensation. As can be seen in Fig. 2.16 a), the use of temperature compensation resulted in a too large increase in pH at elevated temperatures, which tells that E' and s are not true constants. At 60°C, the pH indicated by method 2) was 0.1 pH units higher than the value from method 1). Hence, it is necessary to calibrate the pH electrode at the measuring temperature to obtain accurate data, and this procedure was therefore adopted in the present laboratory work.

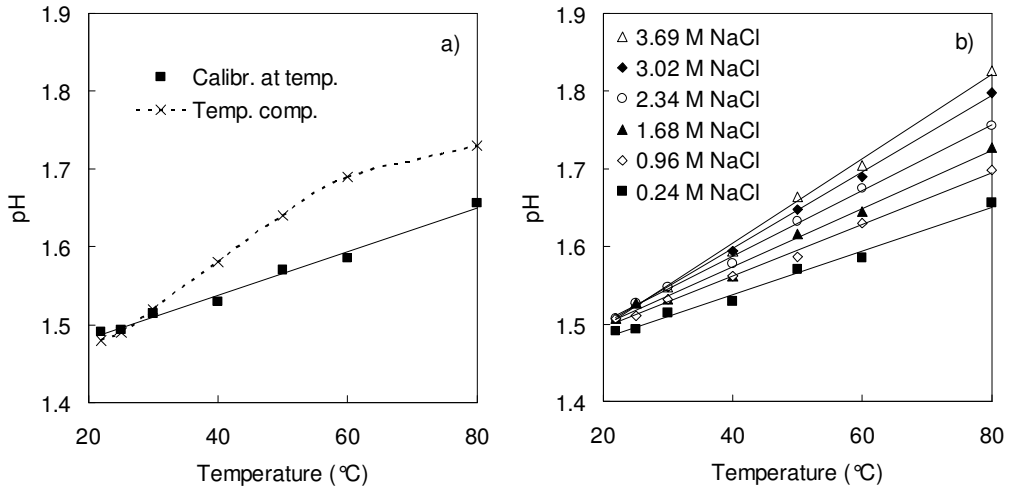

Figure 2.16 *Effect of temperature on pH of a) 0.93 M $CoCl_2$ + 0.24 M NaCl mixed solution measured after calibration at temperature or using the temperature compensation, and b) 0.93 M $CoCl_2$ electrolytes with different NaCl content.*

In Fig. 2.16 b), the influence of temperature on pH in $CoCl_2$ electrolytes containing different amounts of NaCl is illustrated (calibration according to method 1). It is clearly seen that a high ionic strength results in a larger rise in pH with temperature. If the same hydrogen ion activity is preferred in all solutions, it is thus important to carry out the pH adjustments at the relevant temperature.

2.3 Complexation

2.3.1 Introduction to chloride complexation

Transition metal ions can form complexes with a wide variety of inorganic and organic ligands in aqueous media [132]. The ligands are anions or neutral compounds able to donate at least one electron to the central metal ion. The transition metals possess electrons in their d orbitals as the outer electron configuration, and hence are also called d block elements. When a complex is formed, the energies of the metal ion d orbitals change, and this generally leads to lowered energies, and hence a greater overall stability. A

range of oxidation states typical for transition metals may form complexes, and the charge of the complexes can be positive, neutral or negative. The octahedral geometry is by far the most common for transition metal complexes, but tetrahedral, square planar and linear geometries are also reported. Solutions of transition metal complexes often have bright colours, and the complex formation may affect the properties of these solutions, like solubility, reduction potential and activity.

The chloride ion has an extra electron in its outer electron configuration, and this, in combination with its relatively small size, makes it a versatile ligand able to complex many metals and compounds. The extent of chloro complexation is largely dependent on the free chloride ion activity, and it tends toward higher substitution by Cl^- at higher activity. The maximum coordination number of chloride complexes is often taken to be four [133]. Mononuclear complexes are most common, but the existence of polynuclear species like $Cu_2Cl_4^{2-}$, $Cu_3Cl_6^{3-}$ and $Cu_2Cl_3^-$ has also been suggested [132]. Ions of the first row transition metals are strongly complexed with water and form only weak chloro complexes [127], whereas the heavier elements of the next rows show larger formation constants. Furthermore, the stability of the transition metal chloride complexes increases toward the end of each transition group. Hence, Hg^{2+} forms the strongest chloro complex, but strong complexes are also formed by the precious metals, which are characterized by several oxidation states and their very slow ligand exchange [115]. On the other hand, high valency metal ions, such as Ti(IV), V(V) and Mo(VI), are extensively hydrolysed and form only weak chloro complexes with their oxide species, i.e. TiO^{2+}, VO_2^+ and MoO_2^{2+}.

2.3.2 Cobalt(II) chloro complex formation

In dilute aqueous solutions, cobalt chloride behaves as a typical strong electrolyte (see the comparison of ionic activities in Fig. 2.2), while complexes are formed in concentrated solutions. For concentrations below 2.5 molal, the water activity in $CoCl_2$ solutions is slightly lower than in $CaCl_2$ solutions, but for higher concentrations, a_w in $CoCl_2$ falls progressively less than a_w in $CaCl_2$ [126]. The less rapid decrease in a_w in $CoCl_2$ at high concentrations is due to chloride complexing and dehydration of Co^{2+}. However, since the divalent cobalt ions are strongly complexed by water molecules and extensively solvated with a hydration number of 12, they form only weak chloro complexes. Fig. 2.17 illustrates the effect of

electrolyte concentration on the cation transport number, i.e. the fraction of the total current carried by the cations, of $CoCl_2$ and $ZnCl_2$ solutions. While the cobalt transport number shows only a moderate reduction with concentration, the transport number of zinc drops markedly and becomes negative at concentrations above 2 molal. This behaviour is explained by differences in the degree of chloro complexation, and the negative zinc transport number is caused by the presence of anionic complex species with higher mobilities than the normal hydrated metal ion [110].

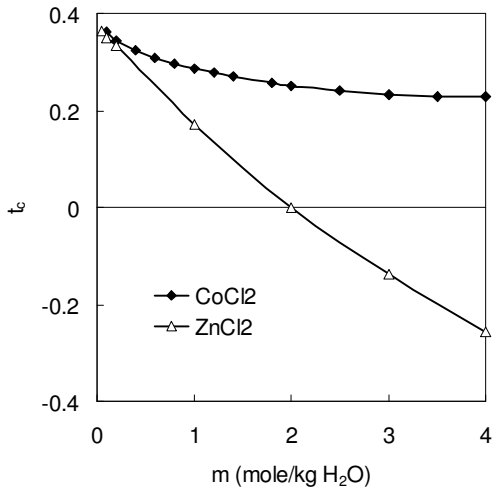

Figure 2.17 *Cation transport number vs. the concentration of $CoCl_2$ and $ZnCl_2$ solutions at 25°C. Data taken from [112] and [110] respectively.*

Although cobalt exists preferentially as divalent hexahydrated ions with an octahedral geometry in dilute aqueous solutions, it shows a tendency to form a tetrahedral configuration under more concentrated electrolyte conditions [76]. The cobalt complex formation takes place by successive addition of chloride ligands and loss of bound water [134]:

$$Co(H_2O)_6^{2+} + Cl^- = CoCl(H_2O)_5^+ + H_2O \qquad (2.32)$$

$$CoCl(H_2O)_5^+ + Cl^- = CoCl_2(H_2O)_2 + 3H_2O \qquad (2.33)$$

$$CoCl_2(H_2O)_2 + Cl^- = CoCl_3(H_2O)^- + H_2O \qquad (2.34)$$

$$CoCl_3(H_2O)^- + Cl^- = CoCl_4^{2-} + H_2O \qquad (2.35)$$

From equations 2.32 – 2.35 it is evident that chloride complexation is favoured by high activity of free chlorides and low water activity. In addition, the complex equilibria are shifted in the forward direction at elevated temperatures [134, 135], and formation of the tetrahedral $CoCl_4^{2-}$ complex results in a colour change of cobalt chloride solutions from red to blue. The degree of complex formation can be represented by stepwise stability constants K_n and cumulative stability constants β_n defined as:

$$K_n = \frac{[CoCl_n^{2-n}]}{[CoCl_{n-1}^{3-n}][Cl^-]} \qquad n = 1, 2, 3, 4 \qquad (2.36)$$

and

$$\beta_n = \frac{[CoCl_n^{2-n}]}{[Co^{2+}][Cl^-]^n} = K_1 K_2 \cdots K_n \qquad (2.37)$$

where the square brackets denote molar concentrations. The water molecules are usually omitted in these equations.

A large scatter exists among the experimentally determined stability constants reported in the literature, especially for those species forming weak complexes like cobalt chloride [136, 137]. The reason for this variation is a combination of the different ionic strengths used, the different experimental techniques applied and the large number of electrolyte systems involved. The stability constants are true constants independent of concentration if activities are used, but single-ion activities are not known. As a consequence, the stability constants based on concentrations are highly dependent on the electrolyte ionic strength, and also on the temperature, due to changes in activity coefficients. Therefore, their practical applicability remains restricted to closely related solutions, having the same ionic strength.

Reported stability constants for the cobalt chloride system are compared in Table 2.2. As can be seen, a large discrepancy exists between the values. The constants given by Bjerrum et al. [135] and Zeltmann et al. [134] are so-called effective stability constants, obtained by curve-fitting to experimental measurements, and by introducing an activity term for the free chloride ion,

so that the constants can be used at different ionic strengths. A constant ratio of the activity coefficients for the cobalt chloride complexes was also assumed. Bjerrum et al. [135] studied the complexation of $CoCl_2$ in concentrated LiCl, HCl and $CaCl_2$ aqueous solutions by spectrophotometric measurements, and the chloride activity was estimated using a one-parameter expression based on Harned's rule (log γ_{Cl^-} proportional to C_{Cl^-} at high ionic strength). Zeltmann et al. [134] carried out their experiments in HCl solution containing small amounts of $CoCl_2$, and the complex species distribution was determined by NMR. Activity corrections were made by setting the mean activity of HCl as the free chloride activity, and by also including the water activity. The temperature dependence of the stability constants was included as well.

Table 2.2 Comparison of stability constants for the $CoCl_2$ system.

Reference	log K_1	log K_2	log K_3	log K_4	log β_4
Bjerrum et al. [135]	-1.05	-2.69	-1.54	-1.34	-6.62
Zeltmann et al. [134]	-0.77	-2.77	-2.51	-2.06	-8.11
Belousov et al. [138]	0.82	0.44	0.35	-0.17	1.43
Skibsted & Bjerrum [139]	1.34				2.57

In contrast to the aforementioned effective stability constants, Belousov et al. [138] and Skibsted and Bjerrum [139] determined by spectrophotometry the concentration constants for the cobalt chloro complexes in 10 M $HClO_4$. These stability constants are much larger, as they include the high chloride ion activity coefficients and the low water activities in concentrated perchloric acid. From Table 2.2 it can be seen that, except for the results by Belousov et al., the dichloro and trichloro complexes have a negligible small range of existence.

By combining the stability constants and the total mass balances of cobalt and chloride, given in equations 2.38 and 2.39 respectively, the complex species distribution at a certain concentration can be estimated.

$$[Co_{tot}] = [Co^{2+}] + [CoCl^{+}] + [CoCl_2] + [CoCl_3^{-}] + [CoCl_4^{2-}] \quad (2.38)$$

$$[Cl_{tot}] = [Cl^{-}] + [CoCl^{+}] + 2[CoCl_2] + 3[CoCl_3^{-}] + 4[CoCl_4^{2-}] \quad (2.39)$$

In solutions containing a large excess of chlorides, the total chloride concentration can be used as the free chloride concentration. However, if the

total cobalt content is considerable, the cobalt ions will bind chlorides to such an extent that a lower concentration of free chloride ions is obtained, which should be accounted for in the calculations. Jansz [133] developed an iterative procedure to calculate the distribution of complex species, including the effects of both ionic strength and temperature on the stability constants. Here, recalculations are needed because the species distribution alters the ionic strength, which again alters the stability constants. In order to establish the stability constant – ionic strength relationships for each complex at different temperatures, a range of experimentally determined K values at different concentrations must be known. Sufficient data exist for the $ZnCl_2$ and $PbCl_2$ solutions studied by Jansz, but this is not the case for $CoCl_2$ solutions. Therefore, the stability constants and chloride activity function given by Bjerrum et al. [135] were used in the present work. Their data are of the latest date of those available, the stability constants reported by Zeltmann et al. [134] and Belousov [138] are evaluated in this paper, and their chloride activity function is easier to use than the one employed by Zeltmann et al.

When using effective stability constants to calculate the distribution of complex species, the activity of the free chloride ions should be estimated by means of the same type of activity function as used to fit the stability constants to experimental data. β_4, representing the stability of the tetrachloro complex, is a function of the fourth power of the chloride activity, so the calculated species distribution is very dependent on the activity function. Bjerrum et al. [135] introduced the following expression for the chloride ion activity in solutions containing more than 5 M chlorides:

$$a_{Cl^-} = [Cl^-] \cdot 10^{B[Cl^-]-0.5} \qquad (2.40)$$

where B is a constant specific to the type of background chloride salt involved (B = 0.170 for LiCl, 0.185 for HCl and 0.132 for $CaCl_2$). Bjerrum's stability constants given in Table 2.2 were used together with equations 2.37 – 2.40 to calculate the degree of formation of each cobalt chloride complex, as a function of the total chloride concentration, in mixed solutions of 0.001 M $CoCl_2$ and varying concentrations of LiCl at 25°C (B = 0.170). To find the free chloride activity, the equations were solved using a trial and error routine. The resulting species distribution is displayed in Fig. 2.18. Even though the results are only approximate for chloride concentrations below 5 M, they indicate that a significant portion of the cobalt ions exists in the

form of $CoCl^+$ at intermediate chloride concentrations. The low stability of $CoCl_2$ and $CoCl_3^-$ is also evident from the figure, and in very concentrated solutions $CoCl_4^{2-}$ is the predominant cobalt species (> 8.5 M Cl^-).

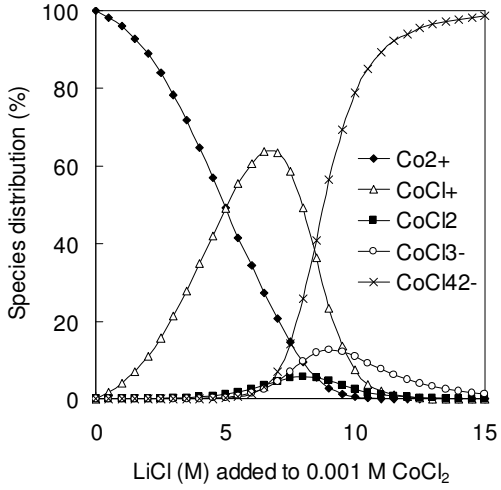

Figure 2.18 *Calculated distribution of cobalt chloride complexes vs. the concentration of LiCl added to 0.001 M $CoCl_2$ solution at 25°C.*

To get an idea of the extent of chloro complex formation in solutions containing appreciable amounts of cobalt, similar calculations were made for pure cobalt chloride solution and mixed solutions of $CoCl_2$ and NaCl. Since the B value in equation 2.40 was not known for neither $CoCl_2$ nor NaCl, the LiCl value was used throughout. The effect of temperature was also included, by using the change in enthalpy accompanying the formation of the complexes, as reported by Zeltmann et al. [134], ΔH (kJ/mole): 12.1 for K_1, 8.8 for K_2, 47.3 for K_3 and 3.3 for K_4. If ΔH is regarded as independent of temperature within the range of interest, the stability constants may be adjusted from the reference temperature T_{ref} to the relevant temperature T according to [133]:

$$\log \beta_T = \log \beta_{T_{ref}} - \frac{\Delta H}{2.303 \cdot R}\left[\frac{1}{T} - \frac{1}{T_{ref}}\right] \qquad (2.41)$$

The calculated complex species distributions for pure cobalt chloride solutions at 25 and 100°C are shown in Figs. 2.19 a) and b) respectively. In

dilute solutions, the free Co^{2+} ion predominates, but as the concentration is raised, an increasing portion is converted to $CoCl^+$. For concentrations above 3.4 M, $CoCl^+$ is the most abundant cobalt species at 25°C. Furthermore, the extent of chloro complexation is increased at elevated temperatures, and the more highly coordinated complexes become noticeable at high ionic strength, especially $CoCl_3^-$, which has the highest ΔH value. However, the formation of these complexes is restricted in pure $CoCl_2$ solutions due to the limited availability of free chloride.

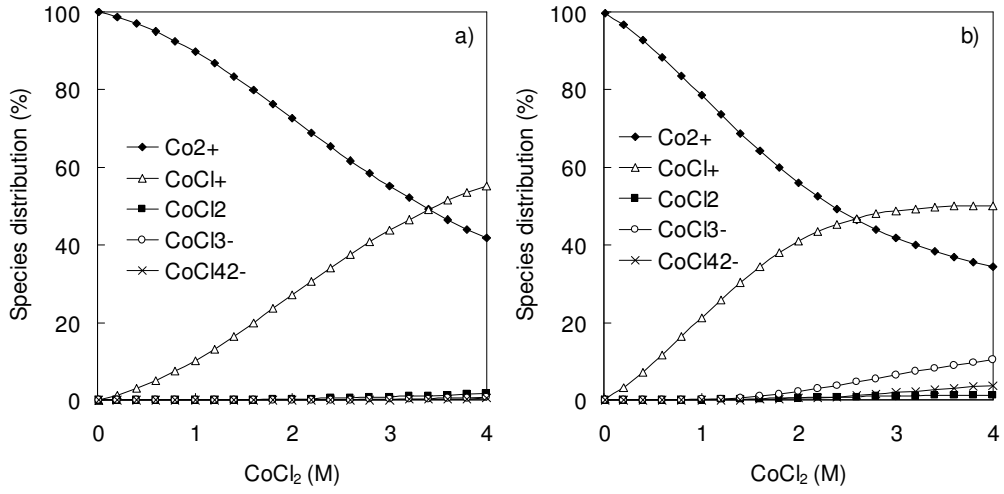

Figure 2.19 *Calculated distribution of cobalt ions and chloride complexes vs. $CoCl_2$ concentration at a) 25°C and b) 100°C.*

Fig. 2.20 shows how the distribution of cobalt species may change when sodium chloride is added to a 1 M $CoCl_2$ solution. Na^+ ions do not form chloro complexes, so NaCl can be regarded as a chloride ligand donor [140]. Hence, addition of NaCl results in an increase in the free chloride concentration, leading to more extensive cobalt chloro complex formation. As for pure $CoCl_2$ solutions, higher temperatures are associated with a higher degree of complexation.

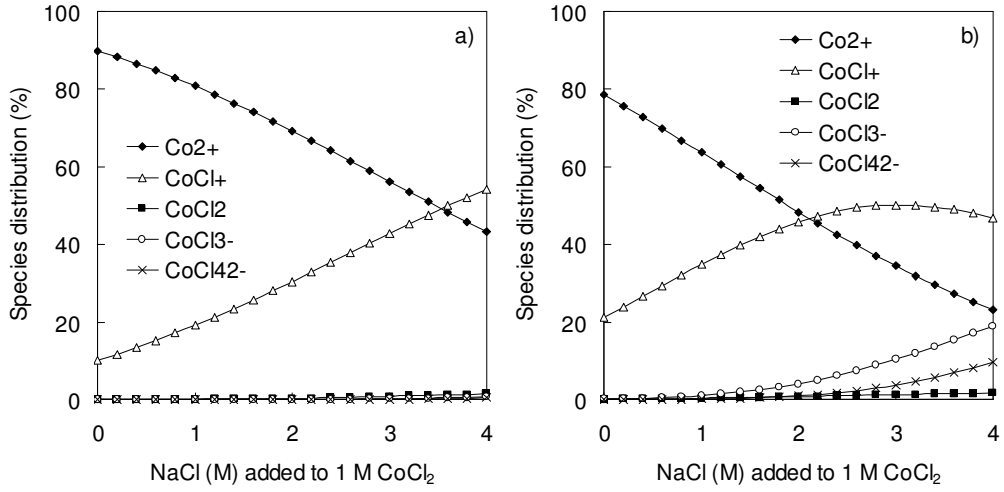

Figure 2.20 *Calculated distribution of cobalt ions and chloride complexes in mixed solutions of $CoCl_2$ (1 M) and NaCl at a) 25°C and b) 100°C.*

2.3.3 Reduction potentials in chloride media

Electrode potentials for many species are altered in chloride solutions as a result of chloride complex formation. The formation of strong metal complexes lowers the potential at which the metal species is reduced to its metallic state [115]. As a consequence, the selectivity of the metal deposition process may change, resulting in codeposition of impurity elements, causing a deterioration of product quality. Complexation may also lead to higher electrowinning energy consumption, from an increase in cell voltage, and from reduced current efficiency due to more intense hydrogen evolution. By introducing the cumulative stability constant (see equation 2.37) in the Nernst equation and assuming that only free Co^{2+} ions are electroactive, the following equation was derived for the reversible reduction potential of cobalt chloride complexes to cobalt metal:

$$E^{rev}_{CoCl_n^{2-n}/Co} = E^{\circ}_{Co^{2+}/Co} - \frac{2.303 \cdot RT}{2F}\left(\log \beta_n + n \log [Cl^-] - \log [CoCl_n^{2-n}]\right) \quad (2.42)$$

where $E°_{Co2+/Co}$ is the standard reduction potential of free Co^{2+} ions to cobalt metal. Equation 2.42 was used to predict the change in reduction potential at 25°C when the free chloride ion activity is increased. The results, based on the stability constants given by Bjerrum et al. [135], are presented in Fig. 2.21, in the form of a E-log a_{Cl^-} diagram. It can be seen that the reduction potential is lowered at high chloride activities, where the predominant cobalt species is either $CoCl^+$ or $CoCl_4^{2-}$. The effect of chloride activity is more pronounced for the reduction potential of the highly coordinated tetrachloro complex; however, very high a_{Cl^-} is needed to stabilize this compound. It should be noted that the complex species $CoCl_2$ and $CoCl_3^-$ are not included in Fig. 2.21, since neither of them is the most stable cobalt species for any chloride concentration (see Fig. 2.18).

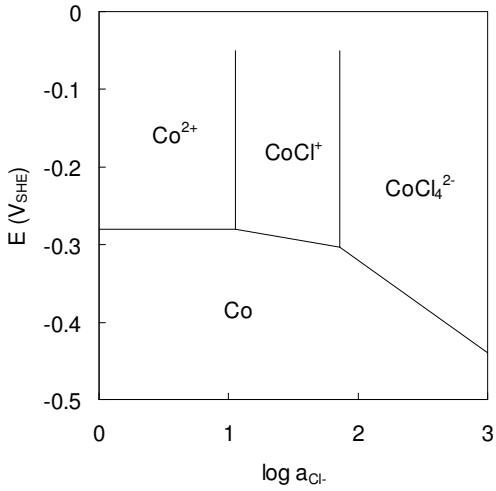

Figure 2.21 *Calculated E-log a_{Cl^-} relationships for $CoCl_2$ solution at 25°C. All cobalt species have unit activity.*

2.3.4 Cobalt solvent extraction from concentrated chloride solutions

One way of separating cobalt from nickel ions is by the use of solvent extraction [76]. In chloride aqueous solutions, amines serve as the organic extractant. The separation is based on the fact that, while cobalt is forming stable anionic tetrahedral chloro complexes in strong chloride solutions, nickel does not. The cobalt extraction process by anion exchange, highly dependent on the activity of free chloride ions, may be described as [141]:

$$CoCl_{4\,(aq)}^{2-} + 2\,R_3NH_{(org)}^{+} = (R_3NH)_2CoCl_{4\,(org)} \qquad (2.43)$$

Equation 2.43 shows that it is the tetrachloro cobalt complex which is being extracted, in this case by a protonated tertiary amine. Industrially, triisooctylamine (TIOA) is the most common extractant used to separate cobalt from strong nickel electrolytes of varying acidity. In the Falconbridge Matte Leach Process [141], cobalt (2 g/l) is extracted from a very acidic solution containing 120 g/l Ni and 160 g/l HCl (8.6 M Cl^-), whereas in the Falconbridge Chlorine Leach Process [19], the cobalt solvent extraction process is carried out in a high chloride low free acid solution (g/l: Co 10, Ni 230, HCl 4; 7 M Cl^-). From the cobalt complex species distribution in Fig. 2.18, it can be seen that an appreciable portion of the cobalt exists as $CoCl_4^{2-}$ at these high chloride concentrations. However, the species distribution will probably be somewhat different in $NiCl_2$ solutions. It should also be mentioned that a much stronger complex formation is found in non-aqueous solvents, since they have a lower solvating power toward Co^{2+} [139]. Muir and Senanayake [115] explain the more extensive complexation observed when adding water soluble organic solvents by an enhanced chloride activity, caused by the disruption of hydrogen bonding to water. The ease of solvent extraction will be influenced by the stability of the complex in the organic phase as well [142].

2.3.5 Stability constants for various metal chloride and cobalt complexes

Stability constants for selected metal chloride complexes are listed in Table 2.3. In concentrated aqueous solutions, divalent nickel ions are converted to the monochloro complex $NiCl^+$ to a significant degree, but there is no evidence of $NiCl_3^-$ or $NiCl_4^{2-}$ species [127]. Ferric ions are known to form quite strong chloro complexes, and it is interesting to see that trivalent cobalt ions may form an even stronger $CoCl^{2+}$ complex, which decomposes to Co^{2+} and Cl_2 [98]. Furthermore, monovalent copper is stabilized in chloride solutions, which makes it possible to reduce the energy consumption in copper electrowinning considerably compared to traditional copper sulphate electrowinning [140]. Finally, the very high stability of the mercuric chloride complexes is evident.

Table 2.3 Stability constants for different metal chloride complexes at 25°C. Data taken from Martell and Smith [99].

Metal ion	log β_1	log β_2	log β_3	log β_4
Ni^{2+}	0.00 [a]			
Fe^{3+}	0.63 [a]	0.75 [a]	-0.7 [a]	
Co^{3+}	1.42 [b]			
Zn^{2+}	0.43 [c]	0.61 [c]	0.5 [c]	0.2 [c]
Pb^{2+}	1.59 [c]	1.8 [c]	1.7 [c]	1.4 [c]
Cu^{+}	2.70 [d]	6.00 [d]	6.0 [d]	
Hg^{2+}	6.74 [e]	13.22 [e]	14.1 [e]	15.1 [e]

[a] Ligand ionic strength I = 1, [b] I = 3, [c] I = 0 (corrected), [d] I = 5, [e] I = 0.5.

In Table 2.4, stability constants for several cobalt complexes in aqueous solution are shown. While cobalt ions form relatively weak complexes with most inorganic ligands, very strong complexes are formed with many organic ligands. Hence, an excess of these organic ligands may solubilize cobalt ions in neutral or alkaline solution. The degree of complexation is often strongly pH dependent, since for the majority of organic ligands, the deprotonated form has the greatest affinity for metal ions. The data in Table 2.4 also illustrate that the trivalent cobaltic ions may be stabilized to a higher degree than the divalent cobaltous ions, which may cause a considerable decrease in the $Co^{3+} - Co^{2+}$ reduction potential [143].

Table 2.4 Stability constants for selected cobalt complexes [99].

Cobalt valency	Ligand	log β_1	log β_2	log β_3	log β_4	log β_5	log β_6
+2	Fluoride [a]	0.4					
"	Bromide [b]	-0.13	-0.4				
"	Ammonia [c]	1.99	3.50	4.43	5.07	5.13	4.39
+3	" [d]						35.21
+2	Glycine [e]	5.07	9.04	11.63			
"	Acetate [e]	1.46					
"	Tartrate [e]	3.05	4.0				
"	Citrate [f]	5.00					
"	Ethylenediamine [g]	5.6	10.5	13.8			
+3	" [h]			48.69			

[a] 25°C I = 1, [b] 20°C I = 0.7, [c] 20°C I = 0, [d] 30°C I = 2, [e] 25°C I = 0, [f] 20°C I = 0.1,
[g] 25°C I = 0.1, [h] data taken from [143] (temp. and I not specified).

Chapter 3

EXPERIMENTAL

The cobalt electrowinning process from aqueous chloride solutions was studied in a laboratory scale electrochemical cell and in a pilot plant at Xstrata Nikkelverk AS, Kristiansand, Norway. In both experimental setups, focus has been put on the anode process and the deposition of cobalt oxide scale in particular, which takes place on dimensionally stable anodes parallel to chlorine evolution. The intention of the preliminary testing on a laboratory scale was to examine the effects of key parameters on the electrowinning process, and to develop alternative methods to suppress or eliminate anode scaling. The results obtained in the laboratory should then form the basis for the pilot testing. Cobalt oxide precipitates and various anode materials were also characterized by scanning electron microscopy and x-ray diffraction analysis.

3.1 Laboratory scale experiments

3.1.1 Electrochemical cell

All electrochemical experiments on a laboratory scale were carried out using the setup shown in Fig. 3.1. The single-compartment electrochemical cell was made of glass, it had a cylindrical cross-section and the volume of electrolyte was 3 litres. The cell was immersed in a water bath for temperature control (± 1°C), and gentle electrolyte mixing was provided by a magnet stirrer placed underneath the water bath. A lid covering the cell to minimize electrolyte evaporation had separate holes for electrodes, salt bridge, thermometer and a glass sinter for nitrogen sparging.

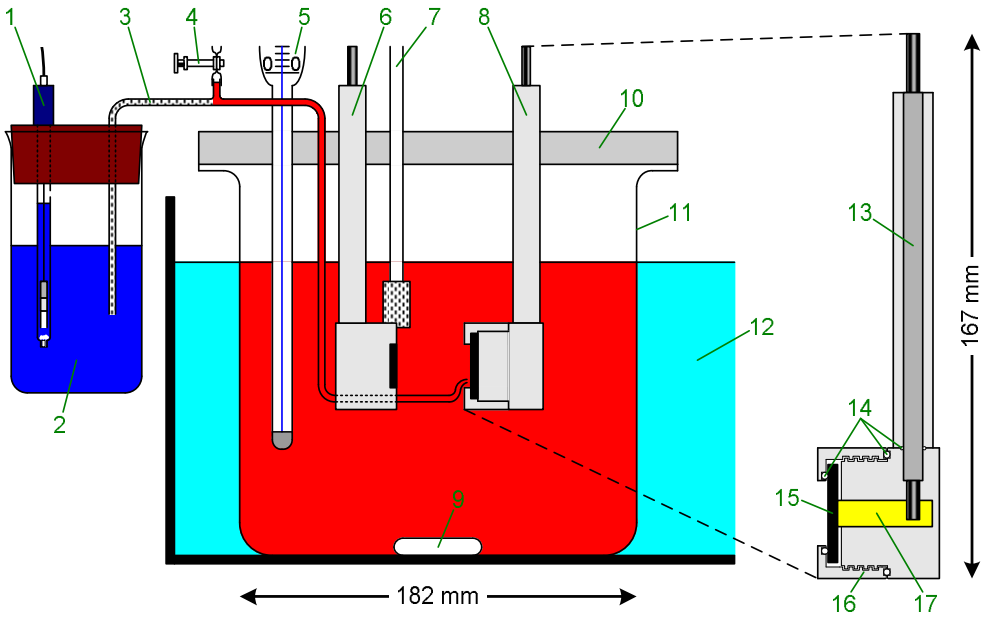

1) Reference electrode (calomel)
2) KCl solution (saturated)
3) Salt bridge (Bacto Agar/electrolyte)
4) Clamp
5) Thermometer
6) Counter electrode (Ti/PVDF)
7) Glass sinter for N_2 sparging
8) Working electrode (DSA®/PVDF)
9) Magnet for stirring
10) Cell cover (PVDF)
11) Electrochemical cell (glass)
12) Water bath
13) Current conductor (Ni)
14) O-rings (EPDM/Viton)
15) DSA® disk
16) Threads
17) Current conductor (Cu)

Figure 3.1 *Laboratory electrochemical cell with magnified cross-sectional view of the working electrode.*

The geometric surface area of the stationary working electrode that was exposed to the electrolyte was 3.1 cm^2 and circular in shape. The disk-shaped electrode, usually a DSA® (see section 3.1.3), was mounted in a holder of PVDF designed for easy disk replacement. A Luggin capillary, in ionic contact with a calomel reference electrode (Radiometer REF401 in saturated KCl) through a salt bridge of KCl-saturated Bacto Agar gel (Merck), was placed close to the electrode surface for measuring the electrode potential. The counter electrode consisted of a 3.1 cm^2 titanium bolt embedded in PVDF. Electrochemical measurements were performed with either a PAR 173/175 potentiostat/universal programmer or a VoltaLab DEA332/IMT102 potentiostat. A Keithley 2000 multimeter connected to a PC served as current and electrode potential logger when using the PAR equipment, which was equipped with a PAR 179 digital coulometer for measuring the total electric charge applied during electrolysis.

3.1.2 Cobalt electrolytes

Industrial electrolyte from the Xstrata Nikkelverk cobalt tankhouse was used in all experiments. Large quantities were acquired twice, in January 2002 and March 2004, from the inlet to the electrowinning tanks. The chemical compositions of the two electrolyte batches, as assayed by the Xstrata Nikkelverk analytical laboratory, are given in Table 3.1.

Table 3.1 Cobalt electrolyte compositions.

Date	Co (g/l)	Na (g/l)	Cl (g/l)	SO_4 (g/l)	Ni (mg/l)	Si (mg/l)	Cu (mg/l)	Fe (mg/l)	Pb (mg/l)	Mn (mg/l)	Zn (mg/l)
Jan. 02	55	5.6	75	0.24	80	3	0.02	< 0.5	0.02	< 0.5	0.5
Mar. 04	54	1.8	69	0.58	41	2	0.07	< 0.5	0.02	< 0.5	< 0.2

From Table 3.1 it can be seen that the electrolyte was an almost all-chloride solution containing some sodium in addition to cobalt. The concentrations of other impurity elements were low. The electrolyte pH was 1.15 and 1.05 at room temperature, and the concentration of HCl was 1.2 and 1.6 g/l respectively for the Jan. 02 and Mar. 04 samples.

The pH of the electrolyte was adjusted by adding hydrochloric acid or sodium hydroxide (both p.a., from SDS). pH measurement was carried out after the electrolyte was heated to the prevailing experimental temperature,

since the change in pH with temperature was found to depend on the electrolyte composition (see section 2.2.7). In each experiment, the pH equipment (Radiometer PHC2001-8 electrode connected to a Radiometer PHM210 pH-meter) was calibrated at the experimental temperature by using heated buffer solutions (pH 1.68 (Radiometer) and pH 1.00 (Merck), 25°C).

The regular cobalt electrolyte was modified in the following ways for use in separate sets of experiments:

- The cobalt chloride concentration was decreased by dilution with deionized water and increased by evaporation.
- The chloride concentration was increased by adding NaCl (p.a., SDS).
- Cobalt sulphate electrolyte was prepared by electrolytic dissolution of Xstrata cobalt metal in sulphuric acid (p.a., SDS) to the same cobalt concentration as the industrial electrolyte. It was then mixed with regular electrolyte to different $Cl : SO_4$ ratios.

All modified electrolytes were analysed at the Xstrata Nikkelverk analytical laboratory.

3.1.3 Anode materials

The various anode materials studied in the laboratory are listed in Table 3.2. 12 different DSA®-type anodes, made of titanium coated with noble metal oxides, were characterized and tested as anodes for electrowinning of cobalt. Pure titanium and graphite were also tested.

Table 3.2 Anode materials tested in the laboratory electrochemical cell.

Designation	Coating composition (molar ratio)	Catalyst loading (g noble metal/m^2)	Coating application
Reg	Ru:Ir ~2:1 + Ti		Electrostatic spray
Reg*	See text		
Ir-Ru-Ti	Ir:Ru ~1:1 + Ti		Electrostatic spray
Ru-Ti	Ru 30 % + Ti 70 %		Electrostatic spray
Ru-Ir-Ti 350°C	Ru:Ir ~2:1 + Ti	3.8	Brushing
Ru-Ir-Ti 400°C	Ru:Ir ~2:1 + Ti	3.5	Brushing
Ru-Ir-Ti 450°C	Ru:Ir ~2:1 + Ti	3.3	Brushing
Ru-Ir-Ti 500°C	Ru:Ir ~2:1 + Ti	2.8	Brushing
Ir-Ta 350°C	Ir 70 % + Ta 30 %	6.3	Brushing
Ir-Ta 400°C	Ir 70 % + Ta 30 %	4.7	Brushing
Ir-Ta 450°C	Ir 70 % + Ta 30 %	4.9	Brushing
Ir-Ta 500°C	Ir 70 % + Ta 30 %	4.6	Brushing
Ti			
Graphite			

3.1.3.1 Anode preparation

The DSA® anodes were prepared by Permascand AB by thermal decomposition of coating solution applied on pretreated titanium plate of thickness 2.5 or 3 mm. After coating, DSA® disks with diameter 30 mm were made by punching.

The first four electrodes in Table 3.2 were commercial coatings, and they consisted of many layers applied by electrostatic spray deposition. The Reg electrode was used in most experiments, while the Reg* electrode was used in only a few tests. Originally, these two electrodes had the same type of coating, but due to various testing carried out by Kongstein in a previous PhD study [65], the latter electrode was modified. The Ir-Ru-Ti electrode had a lower catalyst loading than the other commercial coatings, while the Ru-Ti electrode had a standard chlor-alkali coating.

Electrodes with the regular Ru-Ir-Ti oxide coating and an Ir-Ta oxide coating were prepared at different thermal decomposition temperatures in the Permascand laboratory. The substrates of ASTM grade 1 titanium were first degreased and then etched in a boiling solution of 6 M HCl until 1 % loss of

weight. Coating solution was painted on the pretreated substrates by brushing before the electrodes were dried at 80°C for 10 minutes and then fired at 350, 400, 450 or 500°C for 10 minutes. After baking the electrodes were cooled at room temperature. This coating procedure was repeated 5 times. The Ru-Ir-Ti and Ir-Ta coating solutions were made by dissolving metal chloride precursors in acidified water and an organic/water mixture respectively. To avoid variation in the oxide composition, the same two batches of coating solution were used for all temperatures. Contrary to the commercial coatings, the mixed oxide electrodes prepared at different decomposition temperatures were not subjected to any final annealing. The catalyst loading was calculated from the anode weight increase.

Titanium metal without catalytic coating was tested as anode without any pretreatment. When polarized anodically in aqueous solutions of NaCl or Na_2SO_4, this anode material was found to become passivated [144]. The graphite anode tested was of HLM quality supplied by SGL, and it was machined into disks of identical size and shape as the DSA®'s.

3.1.3.2 Characterization

Scanning electron microscopy (SEM), x-ray diffraction analysis (XRD) and cyclic voltammetry (CV) were performed on the DSA® anode materials to study surface morphology and coating composition, structure, crystallinity and electrochemically active surface area. A Hitachi S-4300 field emission scanning electron microscope, equipped with an Oxford energy dispersive spectroscopy (EDS) system for element distribution analysis, was used for SEM examination. XRD spectra of the anodes were recorded by a Philips PW 1050/25 x-ray diffractometer, with a step size of 0.02°, step time of 1 second, fixed slit opening and a Cu-Kα x-ray source (wave length 1.54 Å). Cyclic voltammetry was carried out in 0.5 M H_2SO_4 (25°C, p.a., Merck) between 0.4 and 1.4 V_{SHE} with a sweep rate of 20 mV/s. The cell in Fig. 3.1 was used, but this time with platinum mesh as counter electrode. Nitrogen gas was bubbled through the solution for removal of dissolved oxygen prior to electrochemical analysis. Nitrogen atmosphere was also maintained in the cell during measurements, as the nitrogen addition was continued above the electrolyte surface.

DSA® disks covered by various amounts of anode deposit were also subjected to SEM and XRD analysis. After cobalt electrolysis, the electrodes were washed with deionized water and dried in air at room temperature. X-ray diffractograms of anode deposit on DSA® were obtained by the same procedure as used for the deposit-free electrodes. Industrial scale collected from anodes in the Xstrata Nikkelverk cobalt tankhouse and precipitates formed in the bulk solution during cobalt electrolysis at high pH were washed with deionized water, dried at 60°C and ground to fine powder before their XRD spectra were recorded using a Siemens D5005 diffractometer. The settings were a step size of 0.1°, step time of 10 seconds, variable slit opening and a Cu-Kα x-ray source (1.54 Å).

3.1.4 Experimental procedures

The rate of anode scaling during cobalt electrolysis was determined by two alternative methods, shown schematically in Fig. 3.2. Both methods started with galvanostatic cobalt electrolysis, but there were differences in the subsequent determination of the amount of scale formed. In the electrochemical route, developed by Kongstein [65], the cobalt oxide was redissolved by sweeping the electrode potential in the cathodic direction, whereas in the chemical route the scale was dissolved chemically in etching solution. The electrochemical route was used in most experiments, but the chemical route was introduced since it was found that the anode scale was not completely stable in cobalt electrolyte at open circuit potential (see section 4.2.4.2).

When the electrolyte was heated to the desired temperature before electrolysis, nitrogen gas was introduced to remove dissolved oxygen and chlorine. Nitrogen sparging was continued during electrolysis, but with less intensity and just below the electrolyte surface. When the correct temperature was reached, the pH of the electrolyte was measured and adjusted if necessary, and the electrodes, rinsed carefully with deionized water, were then immersed in the electrolyte and left at open circuit potential for at least 30 minutes to stabilize the system. Shortly before electrolysis start-up, the ohmic drop in electric cables, connections and in the electrolyte between the tip of the Luggin capillary and the anode surface was measured by using the VoltaLab potentiostat. Its VoltaMaster 2 software has a separate function for the determination of ohmic drop at zero faradaic current, where

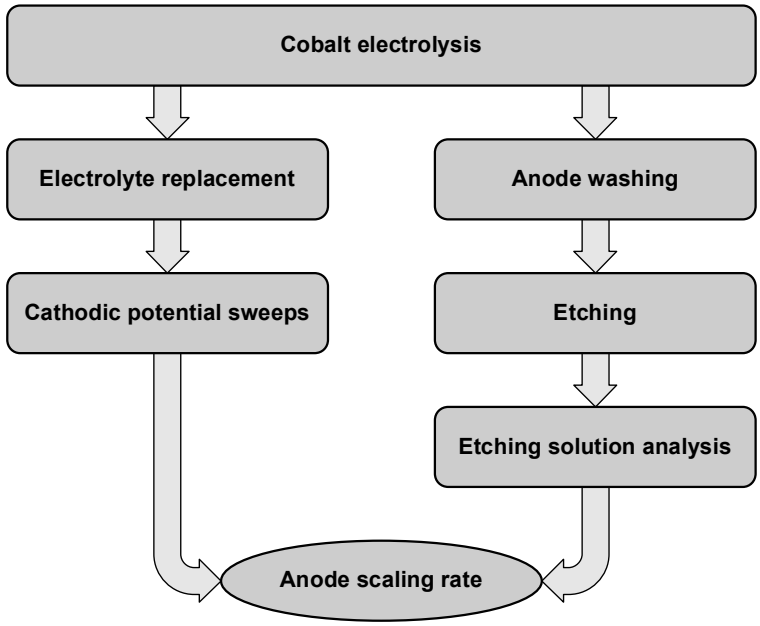

Figure 3.2 *Two alternative methods for determination of anode scaling rate.*

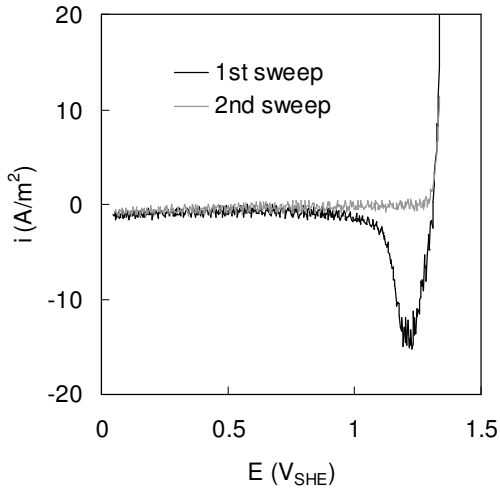

Figure 3.3 *Linear sweep voltammograms of DSA® with anode scale (1st sweep) and without anode scale (2nd sweep). The potential sweeps were performed in cobalt chloride solution from 1.34 to 0.04 V_{SHE} at sweep rate 1 mV/s.*

current pulses were applied for 35 μs, and the ohmic drop was then calculated automatically from the relationship between the measured potentials and the applied currents. After each experiment, the anode potentials measured during galvanostatic electrolysis were IR-compensated and converted to the standard hydrogen scale (SHE) according to the equation:

$$E_{SHE}\,(V) = E_{SCE} - I \cdot R + 0.241 \tag{3.1}$$

where E_{SCE} is the uncompensated potential measured relative to the saturated calomel electrode (V), I the constant current applied (A) and R the ohmic drop obtained as described above (Ω).

When following the electrochemical route, the cell cover containing the electrodes was moved to a separate cell immediately after the termination of electrolysis. This identical cell always contained 3 litres of regular N_2-sparged cobalt electrolyte at temperature 60°C and pH 1.6. The electrolyte was replaced to avoid the unwanted influence of dissolved chlorine during linear sweep voltammetry, which was started as soon as the equipment was reassembled. The potential of the working electrode was swept in the cathodic direction from 1.34 V_{SHE} (the approximate onset of chlorine evolution) to 0.04 V_{SHE} at 1 mV/s sweep rate, which resulted in the electrochemical reduction of the trivalent cobalt and subsequent redissolution of the anode scale, giving rise to a cathodic current, as shown in Fig. 3.3. The potential sweep was ended at 0.04 V_{SHE} in order to avoid hydrogen evolution and cobalt metal deposition on the DSA®. At the end of the first potential sweep the anode scale had dissolved, and a second sweep was then performed on the clean electrode after holding the potential at 1.34 V_{SHE} for 1 minute to reoxidize the noble metal oxides in the catalytic coating. The extent of anode scaling, expressed as the current efficiency for CoOOH deposition, was calculated from the charge difference between the two potential sweeps:

$$CE_{CoOOH}\,(\%) = \frac{\left(I_{sweep\,2} - I_{sweep\,1}\right) \cdot t \cdot 100}{Q_{EW}} \tag{3.2}$$

where $I_{sweep\,1}$ and $I_{sweep\,2}$ are the average currents during the first and the second sweeps respectively (A), t is the time per sweep (seconds) and Q_{EW} is the total electric charge applied during electrolysis (C). A few tests involving

cathodic potential steps instead of sweeps to dissolve anode scale were also conducted.

In the chemical route, the working electrode was washed with deionized water once the electrolysis current was switched off. The washing was carried out with care in order to avoid scale peeling off the electrode. After drying at 50°C, the electrode was dipped in 100 ml of aqueous etching solution (12 g/l H_2O_2, 18 g/l H_2SO_4, < 0.05 mg/l Co, 2 – 4 mg/l Cl) for 10 minutes to redissolve the anode scale. Then the etching solution was submitted to chemical analysis of its cobalt and chloride contents, conducted at the Xstrata Nikkelverk analytical laboratory by atomic absorption and potentiometric titration respectively. The anode scaling rate was calculated from the cobalt content in the etching solution, after it was adjusted for the cobalt present due to traces of electrolyte, estimated from the increase in chloride concentration during etching:

$$CE_{CoOOH}\ (\%) = \frac{\left(\left(C_{Co} - C_{Co,0}\right) - \left(C_{Cl} - C_{Cl,0}\right)\frac{C_{Co,el}}{C_{Cl,el}} \right) \cdot V \cdot F \cdot 100}{M_{Co} \cdot Q_{EW} \cdot 10^6} \qquad (3.3)$$

where $C_{Co,0}$ and $C_{Cl,0}$ are the concentrations of cobalt and chloride in the etching solution before use (mg/l), C_{Co} and C_{Cl} the concentrations after etching (mg/l), $C_{Co,el}$ and $C_{Cl,el}$ the cobalt and chloride concentrations in the electrolyte (g/l), V the volume of etching solution (ml), F the Faraday constant (96487 C/mole) and M_{Co} the atomic weight of cobalt (58.93 g/mole).

The current efficiency for cobalt metal deposition on the counter electrode was estimated by weighing the metal (± 0.0001 g) after it was stripped off the titanium surface, washed with water and dried in air at room temperature:

$$CE_{Co}\ (\%) = \frac{2 \cdot F \cdot W_{Co}}{M_{Co} \cdot Q_{EW}} \qquad (3.4)$$

where W_{Co} is the mass of cobalt metal deposited. In the case of the electrochemical route, where the cobalt metal acted as counter electrode during linear sweep voltammetry, its weight was corrected for the metal

dissolution, assuming that this reaction proceeded at 100 % current yield during potential sweeps.

The same electrolyte could be used in several experiments, since its volume was large compared to the electric charge applied, resulting in negligible changes in the cobalt and chloride concentrations. The electrolyte volume was checked between experiments, and deionized water was added if needed.

3.2 Pilot scale experiments

3.2.1 Description of the Xstrata Nikkelverk electrowinning pilot plant

In August 2000, a project group at Xstrata Nikkelverk started preliminary work on a new pilot plant for electrowinning of metals from aqueous solutions. Previously, most of the electrowinning process development work was carried out in full-size production tanks or bench scale setups, both accompanied with several shortcomings. It was, therefore, essential that the new equipment was to be based on the same technology as used in production (see section 1.3.2), and with large enough dimensions so that the tankhouse processes could be simulated properly. Making it mobile and suitable for operation as a separate unit was also regarded as important. Since commissioning at the end of 2003, the electrowinning pilot plant has, after some minor modifications, been operated successfully, producing both nickel and cobalt cathodes of high quality from chloride solutions. A flowsheet and a photograph of the plant, with a capital cost of more than NOK 2 million, are shown in Figs. 3.4 and 3.5 respectively.

The electrowinning pilot plant consists of three main units; an electrowinning cell, a dechlorination facility and a mixing tank. Feed electrolyte is introduced continuously at one end of the electrowinning cell, below the electrolyte surface. The open tank (length 1 m, width 0.8 m, depth 1.6 m), containing five parallel-plate cathodes and six anodes with 130 mm anode-anode spacing, is made of GRVE, and it has the same dimensions as the production tanks with the exception of a shorter length, thus fitting commercial electrodes. Each anode is surrounded by a permeable bag to collect the chlorine gas produced. Chlorine compressors in the chlorine leach department simultaneously provide suction in the electrowinning section for

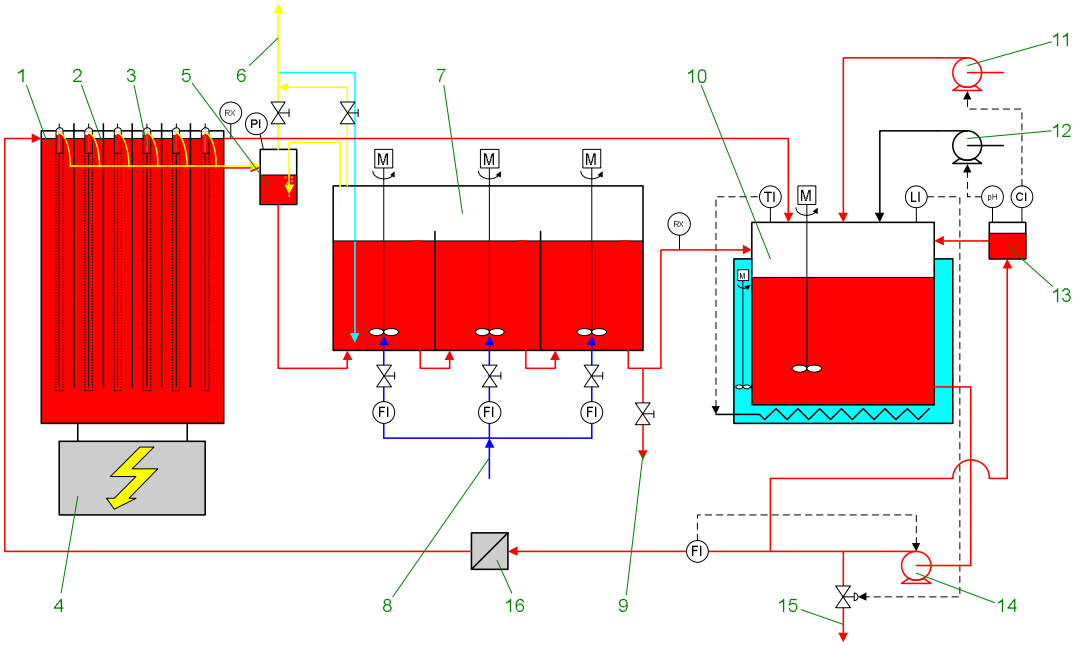

1) Electrowinning cell
2) Cathodes
3) Anodes
4) Power supply
5) Gas-liquid separator
6) Chlorine gas outlet
7) Dechlorination facility
8) Air for chlorine stripping
9) Sampling of anolyte
10) Mixing tank
11) Make-up solution pump
12) HCl pump
13) pH & cobalt analysis
14) Circulation pump
15) Electrolyte bleed
16) Electrolyte polishing filter

Figure 3.4 *Flowsheet of the Xstrata Nikkelverk electrowinning pilot plant.*

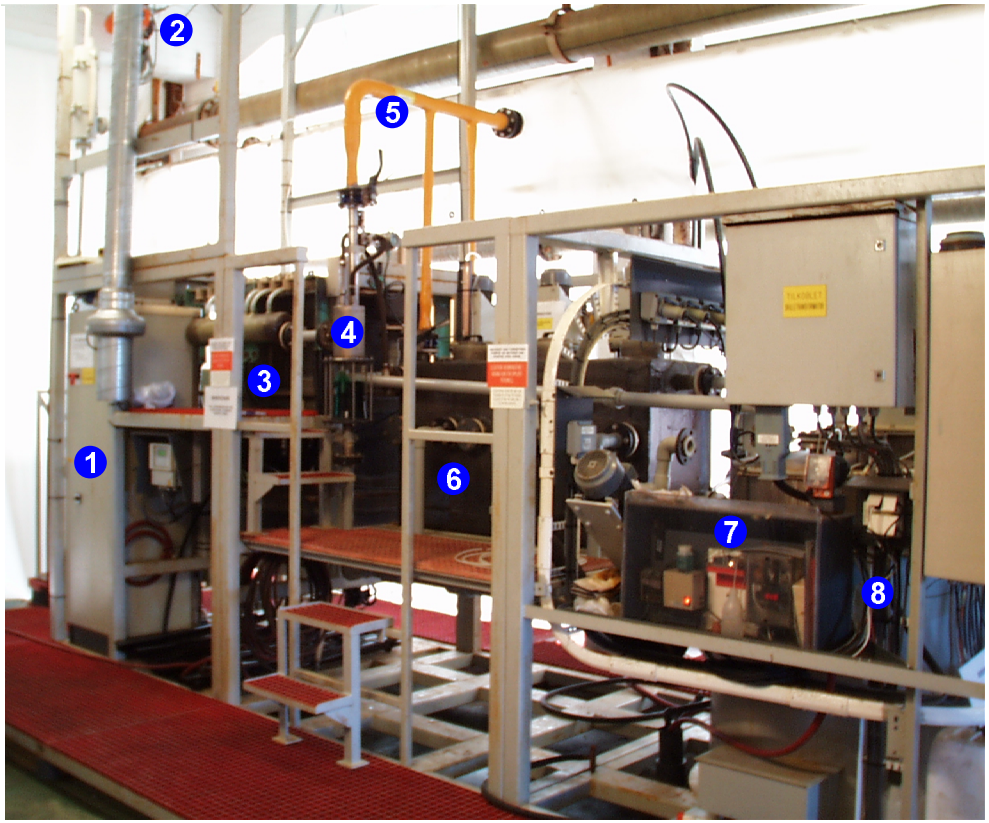

1. Power supply
2. Crane for electrodes
3. Electrowinning cell
4. Gas-liquid separator
5. Chlorine gas withdrawal
6. Dechlorination facility
7. Cobalt analyser
8. Mixing tank

Figure 3.5 *Photograph of the Xstrata Nikkelverk electrowinning pilot plant.*

withdrawal of the anode gas along with the anolyte, via anode hoods through overflow ducts connected to a manifold running alongside the electrowinning cell. Excess electrolyte is returned directly to the mixing tank by overflow at the opposite end to the inlet, thereby securing a constant catholyte level in the electrowinning cell. The catholyte surface is covered with styrofoam beads to suppress the extent of aerosols in the tankhouse atmosphere. A separate power supply with a capacity of 4000 A and 10 V, type pe5010-CT-W provided by Plating Electronic, generates the electrolysis current needed. It can deliver periodically interrupted current (PIC; on-time 1-1000 seconds, off-time 0.01-10 seconds) as well as constant direct current.

Anolyte from the anodes is saturated with chlorine, which must be removed before the electrolyte can be returned to the electrowinning cell after make-up with strong solution. First, the chlorine gas is separated from the anolyte in a gas-liquid separator, from where the gas is piped to the tankhouse chlorine suction system. The anode suction is adjusted manually with a valve and a moveable bubble tube connected to the freeboard of the dechlorination facility and submerged in a constant level liquid phase of the separator for fine-tuning, the negative pressure being metered by a digital manometer mounted on top of the separator. Anolyte from the separator is then directed to a container of GRVE divided into three compartments in series constituting the dechlorination facility, where dissolved chlorine is stripped out by air. In each compartment, holding 0.2 m^3 of electrolyte, air is introduced below a Rushton turbine impeller of titanium, rotating at up to 1000 rpm for efficient air dispersion. Stripped chlorine and air are vented to the same suction system as the anode gas, while condensed water is returned to the first compartment through a separate pipe. To control the dechlorination efficiency, the redox potential is measured in the anolyte leaving the last compartment. For safety reasons, the electrolysis current is stopped if the redox value exceeds a predetermined value.

The mixing tank, receiving anolyte from the dechlorination facility as well as overflow catholyte from the electrowinning cell, is made of titanium and contains 1 m^3 of electrolyte. It is heated by an outside water jacket of stainless steel. A portion of the electrolyte pumped to the electrowinning cell is returned back to the mixing tank, and in this loop the electrolyte pH is measured continuously, as is the cobalt concentration, using a photometer of Xstrata Nikkelverk design. pH and concentration are then controlled by adding HCl (concentrated, technical grade) and strong make-up solution from the cobalt refinery (typically 85 g/l Co, pH 1.6 at room temperature).

The volume balance of the system is taken care of by bleeding some electrolyte to the chlorine leach department, controlled by the electrolyte level in the mixing tank.

The electrowinning cell is mounted at a higher level than the dechlorination facility, which again is above the mixing tank. In this way only one centrifugal pump is needed for electrolyte circulation, transporting the electrolyte from the mixing tank to the electrowinning cell, while the remaining electrolyte streams are driven by gravity. Before being subjected to electrolysis, the feed electrolyte is polished in a Bofil 9000-M filtering unit equipped with filter cartridges containing active carbon for removal of organic impurities and solid material. A Siemens PLS is used for process control, to which a personal computer is connected for process data logging.

3.2.2 Electrodes

In all pilot scale experiments, the electrowinning cell was equipped with five cathodes and six anodes of the same size as used in the tankhouse production tanks. Cobalt starting sheets from the cobalt refinery served as cathodes (1.31 m × 0.72 m × ~0.5 mm, ~5 kg), placed in plastic frames to promote cathode verticality and to minimize edge build-up. The 7 different anode types tested, which were all of the DSA® type, are presented in Table 3.3. Sketches of the five anode substrate designs involved are shown in Fig. 3.6.

Table 3.3 Anodes tested in the electrowinning pilot plant.

Designation	Titanium substrate	Geometric coating surface area (m^2/anode)	Coating state
Reg	Rod (dia. 4 mm)	0.46	Recoated
Reg*	Rod (dia. 4 mm)	0.46	Worn
Ti	Rod (dia. 4 mm)	0.46	Sandblasted
1st cut	Rod (dia. 4 mm)	0.26	Worn
2nd cut	Rod (dia. 4 mm)	0.17	Worn
ESA	Rod (dia. 3 mm)	0.61	Recoated
Box	Mesh	2.06	New

The majority of the experiments were carried out using anodes consisting of grids of titanium rods, identical to those applied in the Xstrata Nikkelverk

cobalt tankhouse. In these experiments, one particular anode, which had been in operation in the nickel tankhouse for several years since being recoated (Reg* in Table 3.3), was always placed in the no. 3 anode position from the cell inlet, while the other five were picked out from a group of ten anodes recoated by Permascand. Titanium substrates, obtained by removing the original catalytic coating by sandblasting, were also tested as anodes. To study the effects of anode surface area, vertical rods were cut off and removed from six worn anodes in two steps as shown in Figs. 3.6 c) – e), and experiments involving larger area ESA (extended surface area) and box DSA®'s were carried out. For the ESA anode, the number of vertical rods was twice that of the regular type, which with a rod diameter of 3 mm instead of 4 mm resulted in a 35 % increase in anode surface area.

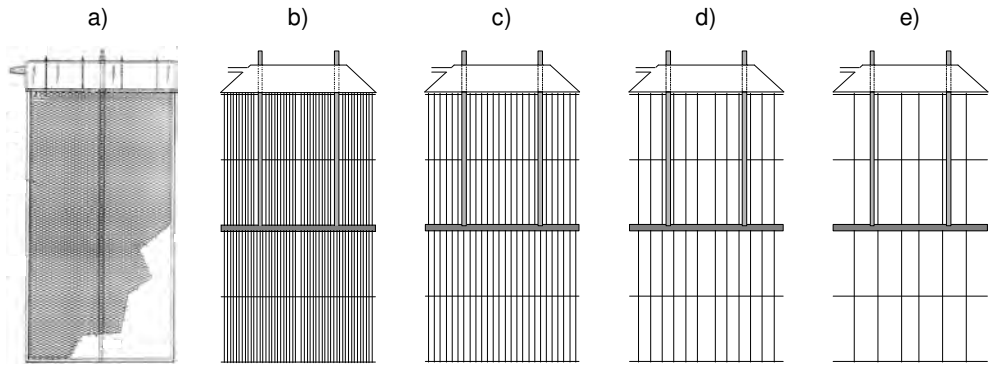

Figure 3.6 *Anode substrate designs tested in the electrowinning pilot plant. a) Box (Sjöberg et al. [145]), b) ESA, c) Regular rod, d) 1st cut, e) 2nd cut.*

In two separate series of experiments, either concentrated HCl (technical grade) or H_2O_2 (35 %) was added continuously into the anode compartments during electrowinning. A hole was drilled in each regular anode hood for rubber tubes laid towards the bottom of the bags, through which the additives were pumped using a displacement pump.

3.2.3 Experimental procedures

As mentioned in section 3.2.1, the levels of several key electrowinning parameters were logged continuously throughout each pilot scale

experiment. In addition, the following process data were collected at least twice per test during electrolysis:

- Cathodic and anodic current distribution. The current supplied to each electrode was measured with a hand-held digital clamp amperemeter (± 1 A).
- Temperature in the catholyte overflow (± 0.1°C).
- Anode gas composition. Concentrations of chlorine and oxygen in the anode gas sampled from the manifold were analysed using an Orsat setup, the two gases being absorbed consecutively in aqueous potassium iodide and pyrogallol respectively (± 0.1 %). The gas was not dried prior to analysis.
- Anolyte flow. The flow of anolyte was measured after dechlorination by collecting the volume leaving the third compartment for one minute, sampled by opening the valve 9) in Fig. 3.4 (± 0.1 ltr/min).
- Cell voltage. The voltage applied by the rectifier was read from its digital display (± 0.1 V).
- Electrolyte pH values. Samples of feed electrolyte, catholyte overflow and dechlorinated anolyte were cooled to room temperature for pH measurement (± 0.001 pH unit). For practical reasons, in the pilot work pH was measured at room temperature.

Furthermore, feed electrolyte sampled prior to termination of each experiment was submitted to the Xstrata Nikkelverk analytical laboratory for analysis of its content of cobalt and chloride. Cobalt was analysed by complex titration with EDTA, while the chloride content was determined by potentiometric titration.

Shortly after switching off the electrolysis current, the cobalt cathodes were harvested one at a time, using an electric crane, and then weighed (± 0.05 kg) for the determination of cobalt current efficiency. The Q_{EW} value in equation 3.4 was measured by the power supply (± 0.1 Ah). The cathodes were used over again until their single weight reached a maximum of 90 kg, whereafter they were all replaced by new starting sheets.

About 20 minutes after stop of electrolysis, at least one of the six anodes was removed from the cell for determination of the amount of anode scale formed, utilizing a method based on the same principles as the laboratory chemical route (see section 3.1.4). The applied suction was maintained on

the anodes after current interruption, thus withdrawing the bulk of the chlorine before anode removal. It was, however, found to be important not to wait too long, to avoid redissolution of scale. Once out of the electrowinning cell, the anode bags were filled with water for stabilizing and washing the scale. A separate container made of GRVE was constructed for anode cleaning. Its two compartments, 60 litres each, were filled with water and etching solution for additional washing and scale dissolution respectively. The anodes were cleaned one at a time after removing the anode bag, first in the water compartment and then in the etching solution. 10 minutes of etching was normally sufficient to dissolve all the scale from an anode. Some scale was flaking off the electroactive anode surface, accumulating at the bottom of the bag during electrowinning. This material was collected and added to the etching solution, followed by thorough mixing and sampling. Cobalt and chloride concentrations of the etching solution were used for the calculation of current efficiency for CoOOH formation according to equation 3.3, where Q_{EW} was the charge applied to the particular anode (C), obtained by multiplying the measured anode current (A) with the electrowinning time (seconds). The same etching solution was utilized in several experiments before being replaced. Subsequent to etching, the anodes were washed with water and equipped with new bags, after which they were ready for continued electrolysis.

Chapter 4

RESULTS AND DISCUSSION

This chapter consists of two major parts. In the first part, results obtained in the laboratory, using the three-electrode electrochemical test cell (section 3.1), are presented and discussed, including characterization of the anode deposit. Effects of key operating parameters on the cobalt electrowinning process are outlined, with emphasis on the anodic deposition of cobalt oxide, followed by evaluation of different anode materials, alternative methods to suppress anode scaling and the experimental techniques applied. The second part is devoted to the larger scale experiments carried out in the Xstrata Nikkelverk electrowinning pilot plant (section 3.2).

4.1 Characterization of anode deposit

4.1.1 X-ray diffraction analysis

An XRD diffractogram of the black flakes of scale formed on the anodes in the Xstrata Nikkelverk cobalt tankhouse is shown in Fig. 4.1, along with database patterns of various cobalt oxides. Several well defined peaks can be seen, indicating a crystalline structure, identified as heterogenite 3R, also known as alpha cobalt oxyhydroxide (α-CoOOH, see section 2.1.3). A close match was obtained for the 2θ peak positions, but there were some deviations in peak intensity from the database values. The diffractogram of α-CoOOH reported by Amatucci et al. [107] was similar to Fig. 4.1, although the peaks at high 2θ values were lower.

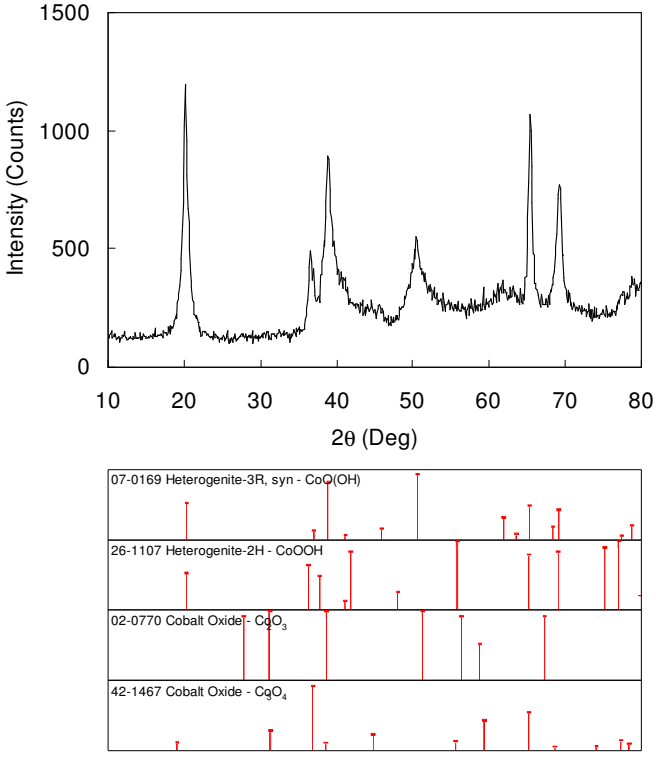

Figure 4.1 *XRD diagram of industrial cobalt anode scale. JCPDS database patterns of various cobalt oxides below.*

Cobalt oxide deposited anodically in the laboratory was also subjected to XRD analysis, without removing it from the DSA® surface. The electrolysis conditions were the same as in the cobalt tankhouse, except for a higher pH (1.6 vs. ~1.3). A charge of 5000 coulombs was applied, giving ~1 mg of Co in the deposit per cm^2 of geometric anode surface area. The diffractograms in Fig. 4.2 demonstrate that the underlying DSA® was still detectable when covered by cobalt oxide. The main peaks of α-CoOOH were also present in the diagram of cobalt oxide on DSA®, but they were much smaller and broader compared to Fig. 4.1. This can be due to a low thickness of the cobalt oxide layer, or a more amorphous precipitate. Ageing effects may have been involved, since the film on the laboratory electrode was deposited, washed and dried within a few hours time, while parts of the anode scale from the tankhouse were probably several months old when collected.

Transformation over time from an amorphous phase to a more defined crystalline structure is typical for hydrated metal oxides (see section 2.1.1).

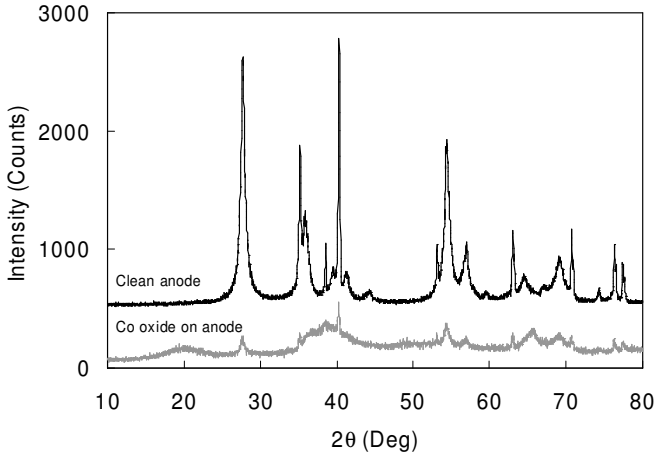

Figure 4.2 *XRD diagrams of clean regular DSA® (upper curve) and DSA® covered by anodically deposited cobalt oxide (lower curve).*

4.1.2 Chemical analysis

On three occasions, industrial anode scale was collected, crushed, washed with deionized water and dried overnight at 60°C before being submitted to the Xstrata Nikkelverk analytical laboratory for chemical analysis. The analysed compositions are given in Table 4.1.

Table 4.1 Chemical compositions of anode scale from Xstrata Nikkelverk cobalt tankhouse (wt %).

Date	Sampling point	Co	Mn	Na	Si	Cl	SO_4^{2-}
February 2004 *	Anode	61.9	0.57	< 0.1	0.32	1.3	0.87
October 2004	Manifold	63.0	< 0.1		0.14	0.16	0.23
February 2005	Anode	60.8	0.43		0.21	0.16	0.21

* Ni, Cu, Fe, Zn, Pb, Al, Cr, Mg, Ca, Ba, As, Te, Se, Bi, Sb, Sn, Ag < 0.5 wt % each

Cobalt was the main component in the deposit, accounting for more than 60 % of the dry total weight. The variation in cobalt content was low between the three samples, and it was very close to the theoretical cobalt content of 64 % in pure CoOOH, indicating a small degree of hydration after drying.

Using the quartz crystal microbalance technique, Matsumoto et al. [75] found a hydration number of 1 for CoOOH deposited anodically on platinum from a 0.01 M cobalt chloride solution of pH 6 and ambient temperature, corresponding to 54 % Co. The hydration number was very much higher during the initial stage of electrolysis before decreasing to a constant value. The hydration number was also found to be dependent on the type of anion in solution.

Even though Xstrata Nikkelverk cobalt electrolyte normally contains only traces of manganese (< 0.5 mg/l, see Table 3.1), it was accumulated in the anode deposit, most likely as MnO_2. However, in the material collected from the manifold, which receives anode gas and electrolyte from each anode, the Mn level was below the detection limit. It is believed that this deposit originated from the anodes, and since it had probably been in the manifold for many years, there was plenty of time for Mn to be leached out. Hem et al. [89] demonstrated that Mn(III)/Mn(IV) oxides at the rest potential are acting as electron transfer mediators for oxidation of Co^{2+} ions to Co_3O_4 and CoOOH precipitates. The Mn oxides are then reduced and dissolve as Mn^{2+}. According to Wei et al. [146], presence of Mn^{2+} ions in cobalt electrolyte results in an acceleration of the anodic deposition process, forming a film of mixed Co-Mn oxides. Bouchat and Saquet [147] claim that having a high level of Mn in solution is beneficial during cobalt electrowinning from sulphate media, as it suppresses the unwanted deposition of trivalent cobalt oxide on the lead anodes.

The low level of sodium in the deposit agrees with the marginal alkali content in α-CoOOH reported by Benson et al. [105], in deep contrast to β-CoOOH, which retained several percent of alkali (see section 2.1.3). Furthermore, it is not known whether the observed enrichment of silicon in the anode deposit came from inclusion of SiO_2 particles suspended in the electrolyte, or a precipitation reaction at the anodes. Anyway, particles that go through the diaphragm surrounding each anode must be very small in size.

Sulphate ions were incorporated preferentially to chloride ions in all samples, as the Cl : SO_4^{2-} weight ratio was around unity in the deposit compared to > 100 in the electrolyte. The anions may be specifically adsorbed on the surface of the oxide particles, and insufficient washing can explain the high levels of Cl and SO_4^{2-} in the first sample. Several transition

metals form oxychlorides or basic sulphates [115], which tend to precipitate at somewhat lower pH than the corresponding metal hydroxides [148], but the formation of such compounds does not seem to be typical for cobalt.

The first sample was also analysed for its noble metal content, which amounted to approximately 160 ppm for the elements present in the DSA® catalytic coating. With annual CoOOH formation of 3 kg per anode, approximately 0.5 g of noble metals will then be lost with the deposit every year, representing almost 10 % of a typical new DSA® coating.

The high purity of the anode scale from Xstrata Nikkelverk becomes evident when comparing its composition with that reported for the Vale Inco Port Colborne refinery (see section 1.5.3). It is interesting to see that if the high lead and manganese contents in the Inco deposit are subtracted as PbO_2 and MnO_2 respectively, the cobalt content becomes 58 %, which is relatively close to the Nikkelverk level.

4.2 Laboratory scale experiments

The effects of key operating parameters on the cobalt electrowinning process were studied in the cell described in section 3.1.1, by varying one parameter at the time in separate sets of experiments, keeping the rest constant at the standard conditions summarized in Table 4.2. Experiments were carried out in random order within each series, and some of them were repeated.

Table 4.2 Standard electrolysis conditions in the laboratory experiments.

Electric charge (C)	pH	Electrolyte comp.	Temp. (°C)	Current density (A/m^2)	Stirring rate (rpm)	Anode material
500	1.6	$CoCl_2$	60	800	150	Regular

Industrial cobalt chloride electrolyte, with composition as given in Table 3.1, was used as standard electrolyte. Its pH was, however, increased to 1.6 at 60°C in order to accelerate the deposition rate of anodically formed cobalt oxide. Galvanostatic electrolysis was conducted at identical anodic and cathodic current densities based on geometric surface areas. The standard anode material was titanium coated with the regular catalytic coating, consisting of RuO_2, IrO_2 and TiO_2 (see section 3.1.3). The rotation speed of

the magnet at the bottom of the cell was the same during both electrolysis and the subsequent linear sweep voltammetry in cathodic direction, carried out to redissolve the deposited anode film.

4.2.1 Influence of key electrowinning parameters

In this section, results are presented from experiments focusing on the effects of the general electrolysis conditions, including electrolyte composition. Electrolyte from January 2002 was used as basis in all these tests, and the extent of anode scale formation was measured by the electrochemical route (see section 3.1.4). Experiments involving anode materials other than the regular coating are described in a separate section (see section 4.2.2).

4.2.1.1 Effects of electric charge

In these experiments, the total electric charge applied during electrolysis, Q_{EW}, was varied from 100 to 3000 coulombs, equivalent to deposition times of 6.6 minutes and 3.3 hours respectively. The calculated anodic current efficiency for cobalt oxide formation (CE_{CoOOH}) and the average anode potential measured during electrolysis (E_{avg}) are shown in Fig. 4.3 a), while the cathodic current efficiency for cobalt metal deposition (CE_{Co}) is presented in Fig. 4.3 b).

As shown in Fig. 4.3 a), CE_{CoOOH} decreased from 0.16 to 0.13 % when the electric charge was increased from 100 to 3000 C, which corresponds to a surface coverage of 0.03 and 0.76 mg Co/cm^2 respectively. By using a density of 4.9 g/cm^3 for CoOOH (JCPDS XRD file card no. 07-0169), the CoOOH film thickness was estimated to 0.1 and 2.4 μm for the two cases. Nucleation and growth of a film on a foreign substrate usually require an extra initial energy, until the substrate has been covered by stable nuclei which can form a macroscopic deposit. Relatively long induction periods and high nucleation overpotentials have been demonstrated for anodic cobalt oxide deposition on several anode materials (see section 1.5.1). From Fig. 4.3 a) it is apparent that the deposition rate was more or less constant for all electrolysis times tested at standard conditions, i.e., there was no sign of any induction period. At lower supersaturation, the induction period will probably become more significant.

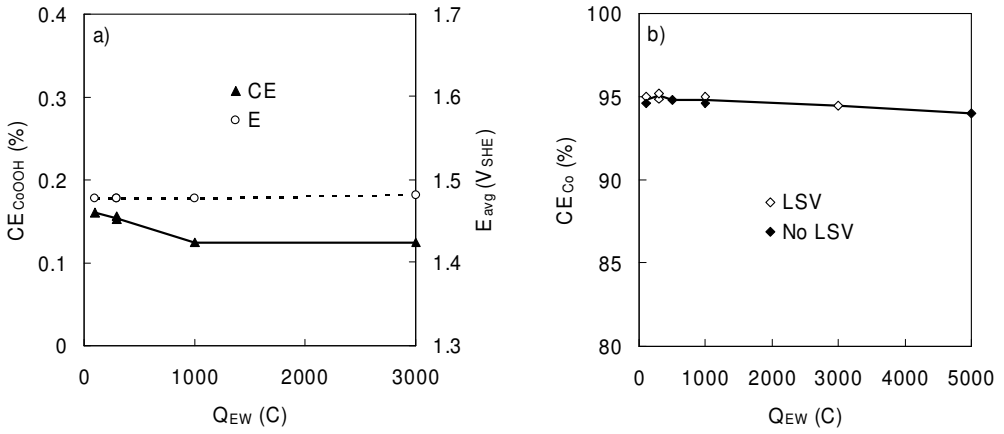

Figure 4.3 *Effects of electric charge on the cobalt electrowinning process. a) Anode scaling rate and anode potential, b) Cathodic cobalt current yield. CE_{Co} obtained in tests without linear sweep voltammetry are included (No LSV).*

According to Fig. 4.3 a), the average anode potential was stabilized after a relatively short time (~3 minutes), and it did not change further as the anode deposit was growing thicker on the DSA®. This indicates that the cobalt oxide layer had a high electrocatalytic activity for the gas evolution reactions taking place, in agreement with relevant literature, confirming the low overpotentials for both chlorine and oxygen evolution on cobalt oxides (see section 1.5.2). An increase in the active surface area of the electrode could also have been involved, as the anode was being covered by increasing amounts of electrochemically active cobalt oxide. The real active surface area of anodically deposited cobalt oxides can be very much higher than the geometric area, however, diffusion limitations of reactants and products in pores, cracks, grain boundaries etc. are restricting the utilization of inner layers of thick films (see section 1.5.1).

Since the anode potential did not increase over time during electrolysis, the electrical conductivity of the anode deposit must have been relatively high, as the electrode surface was completely covered by cobalt oxide shortly after electrolysis start-up (see SEM images in Fig. 4.5). However, Benson et al. [105] measured the specific conductivity of α-CoOOH to be only 10^{-6} $\Omega^{-1}cm^{-1}$, and a similar test carried out in our laboratory, on industrial anode deposit, confirmed the very low conductivity of dried material [149]. During

electrolysis at standard conditions, such a low conductivity would result in a voltage drop of 8 V across a film of 1 μm thickness. Ohmic drop measuments in cobalt electrolyte, using the current pulse technique described in section 3.1.4, were performed on DSA®'s covered with various amounts of cobalt oxide, but these tests did not show any noticeable effect of film thickness. On the other hand, when an anode covered by cobalt oxide was washed with deionized water and dried at room temperature, the conductivity became poor. However, once reintroduced to electrolyte, the ohmic drop was back on the same low level as before drying. These tests indicate that the conductivity properties of the anode deposit changed remarkably when the material was dry, which may have been caused by the removal of water molecules from the CoOOH crystal lattice. Charge transfer through the hydrous oxide film is probably taking place by electron hopping between cobalt ions of different oxidation states (+2, +3, +4), which is coupled with proton transfer events, i.e., water must be present [54]. It should be noted that cracks in the deposited material may have influenced on the ohmic drop measured in electrolyte.

In addition to the results from the regular experiments, Fig. 4.3 b) also shows cobalt current yields obtained in separate experiments performed for subsequent SEM and XRD analysis of anode deposits on DSA®. In these tests, no linear sweep voltammetry was carried out, and the cobalt metal was stripped off the titanium cathode immediately after electrolysis. CE_{Co} obtained in the two series corresponded well, decreasing from 95 % at low electric charge to 94 % at 5000 C. The lower CE_{Co} at high Q_{EW} was probably due to an increasing rate of chlorine reduction on the cathode with time, since each experiment started with chlorine-free electrolyte. The gentle nitrogen sparging during electrolysis was not very efficient in removing dissolved chlorine from the electrolyte.

After the experiments, black particles could be observed both on the anode holder and as a residue when the electrolyte was filtered, and the number of particles increased when several experiments were carried out in the same electrolyte without filtration. The particles were probably anode deposit, which had flaked off the anode surface during electrolysis, due to vigorous gas evolution and residual stresses in the deposited film. The fact that scale detached from the anode during operation was confirmed by SEM analysis (see Fig. 4.5 f)). It is believed that the extent of peeling of the cobalt oxide scale increased as the film became thicker, which can explain the decline in

the amount detected as the electrolysis duration increased (Fig. 4.3 a)). Therefore, it was regarded as important not to run the experiments for too long, in order to minimize the loss of deposit. However, a certain amount of electric charge was needed for the anode scaling rate to be determined with acceptable precision. Short deposition times resulted in very small differences between the first potential sweep with anode deposit and the second sweep without, thereby increasing the uncertainty in the measurements. It should also be noted that the separate electrolyte used for dissolution of cobalt oxide, by means of linear sweep voltammetry, was almost free of particles, indicating that the deposit adhered well to the anode surface during potential scans.

At 1000 and 3000 C, the anode surface was partly covered with a precipitate after cathodic potential sweeps. The colour of this precipitate was brown, as opposed to the regular black anode deposit. Furthermore, it was loosely attached to the DSA®, and could easily be washed off with water. Formation of this precipitate may have influenced the dissolution process during potential sweeps, resulting in less deposit being reduced and dissolved. Fig. 4.4 presents voltammograms of anodes initially covered with different amounts of cobalt oxide. It is clear that the dissolution of scale was a relatively slow process, and a low sweep rate was preferred (1 mV/s). On the other hand, it was also found that the fresh anode deposit was not completely stable in the electrolyte at open circuit potential (OCP), and some of it would, therefore, be lost in the time between electrolysis and voltammetry due to chemical dissolution. To minimize this loss of cobalt oxide, potential scans were started right after the electrolysis was finished. Both the brown precipitates and the stability of anode deposits are discussed in more detail in sections 4.2.4.2 and 4.2.5.

SEM images of DSA® surfaces covered with different amounts of cobalt oxide are shown in Fig. 4.5. The surface of the clean DSA®, free from any anode deposit, had a compact structure with unevenly distributed ruthenium-rich pyramidal crystals of typical size ~0.5 μm (Fig. 4.5 a)). After 100 C of charge applied under standard electrolysis conditions, the anode surface was almost completely covered by a thin film of cobalt oxide (Fig. 4.5 b)). According to EDS analysis, the film thickness was larger on the Ru-rich crystals than elsewhere, which can be explained by a higher local current density at these active sites. At this stage, circular cracks were also observed in the deposit, but it is not known whether they were formed during electro-

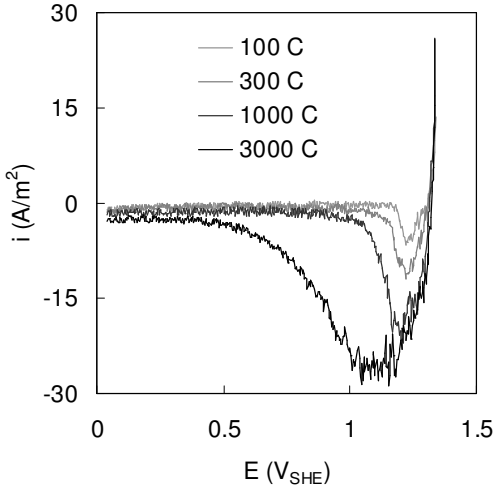

Figure 4.4 *Linear sweep voltammograms for the reduction of different quantities of cobalt oxide on DSA®. First potential sweeps from 1.34 to 0.04 V_{SHE} at 1 mV/s sweep rate, in standard cobalt electrolyte at pH 1.6 and 60°C.*

lysis, or in the subsequent drying process. As more charge was applied, the thickness of the film increased, and the electrode surface became more homogeneous, as the hemispherical grains growing on each crystal overlapped into larger agglomerates (Figs. 4.5 c) – e)). The width of the cracks, now more straight in shape, seemed to increase with increasing film thickness, and some of them followed the grain boundaries.

For 1000 C and 5000 C in particular, some deposit had been detached from the anode surface. The existence of thin layers of cobalt oxide in some of the pits caused by deposit exfoliation demonstrates that some cobalt oxide was lost from the anode surface during electrolysis (Fig. 4.5 f)).

Cross-sections of a DSA® covered with anode deposit were also examined by SEM, but, unfortunately, both the cobalt oxide film and the underlying catalytic coating had become partly broken during sample preparation.

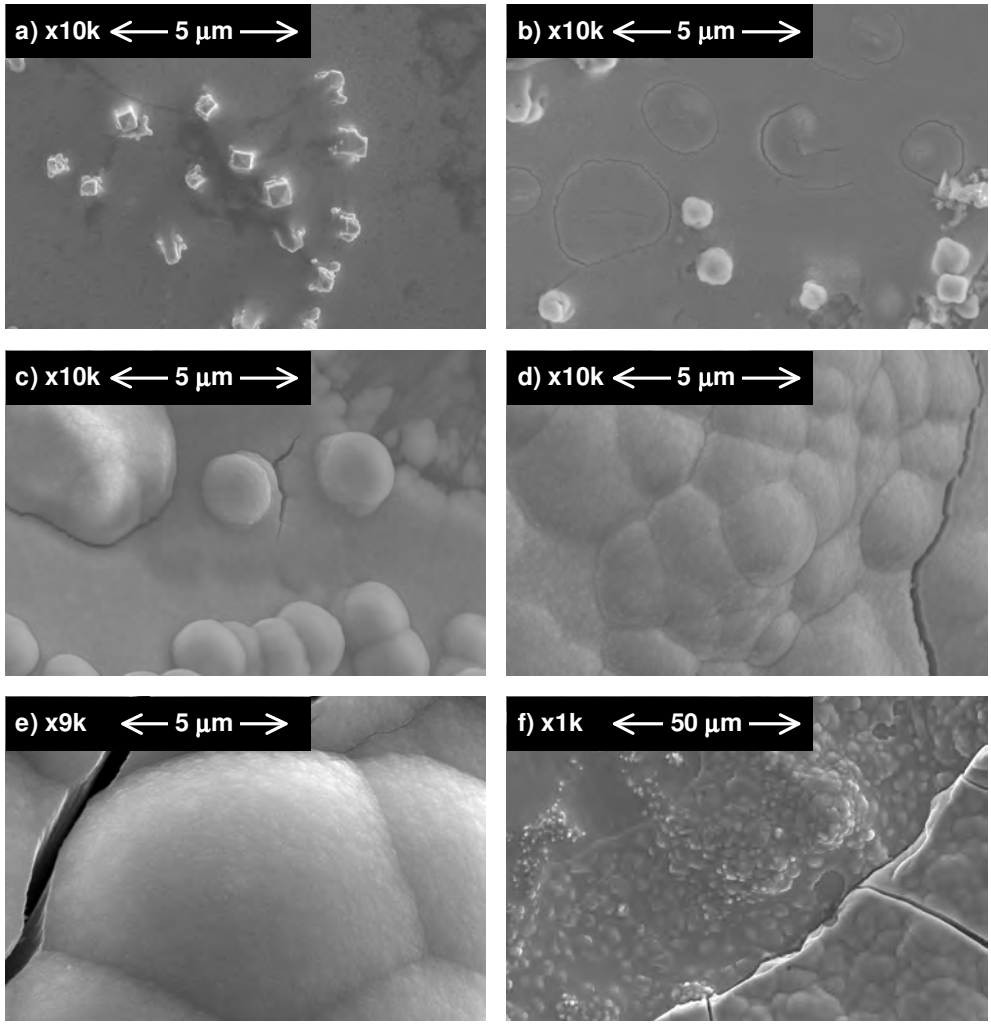

Figure 4.5 *SEM images of DSA® surface after applying different electric charges. a) 0 C (new electrode), b) 100 C, c) 500 C, d) 1000 C, e) and f) 5000 C.*

4.2.1.2 Effects of pH

From the Pourbaix diagram of the Co-Cl-H_2O system (see Fig. 2.1), a strong dependence on solution pH was expected for the anodic cobalt oxide deposition reaction. According to this diagram, CoOOH is the

thermodynamically most stable cobalt oxide at pH levels below 4.6, and the electrochemical potential required to form CoOOH from dissolved Co^{2+} ions increases by 18 mV for every 0.1 drop in pH. Furthermore, chlorine produced on the anode may oxidize Co^{2+} at pH levels above ~0.6. If parallel anodic deposition of CoOOH is unwanted during Cl_2 evolution, pH should be kept below this value.

The acidity of the standard cobalt chloride electrolyte was varied from pH 0.9 to pH 2.1 at 60°C, and the results from these experiments are shown in Fig. 4.6. In some of the tests, the anode potential recorded during electrolysis was not stable, probably due to contact problems, either in the salt bridge to the reference electrode, or between the back side of the DSA® disk and the copper conductor in the anode holder. However, more stable potentials were achieved in additional experiments performed in the pH range from 0.9 to 1.9, where the anode deposit was redissolved by the chemical route (see section 4.2.5.1). Since conditions were identical in the two sets of experiments except for the anode disk used, the anode potentials measured in the additional tests are presented in Figs. 4.6 a) and 4.7.

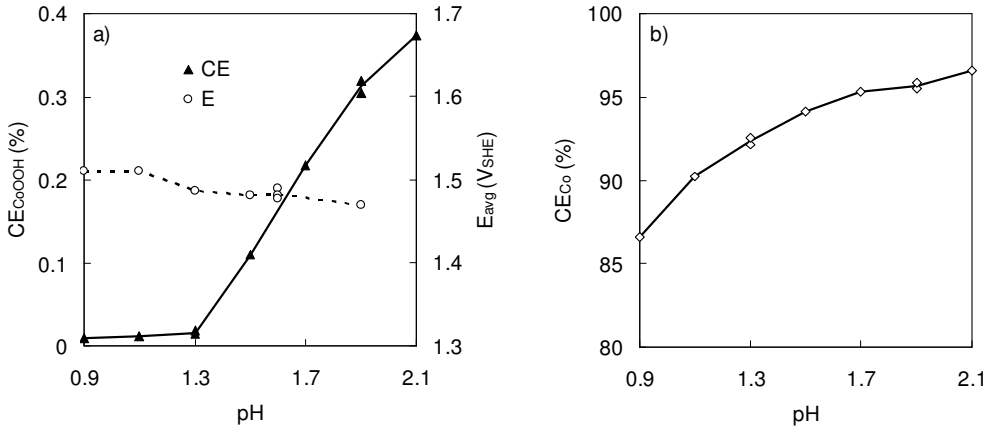

Figure 4.6 *Effects of electrolyte pH on the cobalt electrowinning process. a) Anode scaling rate and anode potential, and b) Cathodic cobalt current yield. Average anode potentials shown in a) were obtained in a separate set of experiments.*

In accordance with thermodynamics, the extent of anodic cobalt oxide deposition was highly dependent on the electrolyte acidity, CE_{CoOOH}

increasing from 0.01 % at pH 0.9 to 0.37 % at pH 2.1. At the lowest pH, no reduction wave appeared during the first potential scan after electrolysis, which indicates that the anode was free from precipitate. The reaction order with respect to H^+ deviated from the theoretical value of 3 given by the total reaction (equation 1.6), decreasing to less than 1 at high pH. This may be attributed to a lower local pH on the anode surface than in the bulk solution, as a result of increased current efficiency for oxygen evolution and the cobalt hydrolysis reaction itself. The reaction order of H^+ gives information about the reaction mechanism and its rate determining step. Deposit exfoliation and the formation of a brown precipitate during cathodic dissolution of cobalt oxide formed at pH 1.9 and pH 2.1 could also have been involved.

An additional factor is the lowering of the anode potential at galvanostatic electrolysis when pH was increased, from 1.51 V vs. SHE at pH 0.9 to 1.47 V at pH 1.9 (Fig. 4.6 a)). Such a depolarization may reduce the extent of cobalt oxidation and precipitation. Boggio et al. [60] studied the chlorine evolution reaction on thermally decomposed cobalt oxide electrodes from acidic solutions, and they found that H^+ had a retarding effect on Cl_2 evolution. To include this effect of pH, they proposed a reaction mechanism for Cl_2 evolution on cobalt oxide involving the adsorbed intermediate HClO (see section 1.5.2).

The apparent depolarizing effect of higher pH is illustrated in Fig. 4.7, showing the first half of potential-charge profiles recorded at six different acidity levels. In the pH 0.9 experiment (Fig. 4.7 a)), the anode potential increased gradually due to polarization effects, i.e., concentration gradients and blocking of pores of the DSA® by gas bubbles produced, reducing the available active surface area. The anode potential was not completely stabilized within the time frame of this experiment (33.2 minutes). At pH 1.1 (Fig. 4.7 b)), a maximum in the potential was reached after ~90 coulombs (~6 minutes), followed by depolarization, whose extent was increasing as electrolysis proceeded. When the electrolyte pH was raised further, the position of the potential peak shifted to lower values of electric charge applied, along with a decrease in peak potential (Figs. 4.7 c) – f)).

It is believed that the initial rise in potential was accelerated by the precipitation of cobalt oxide on the Ru-rich crystals, covering these active sites. The peak potential was probably representing the complete coverage of active sites by anode deposit (‘monolayer’), and the subsequent depolariza-

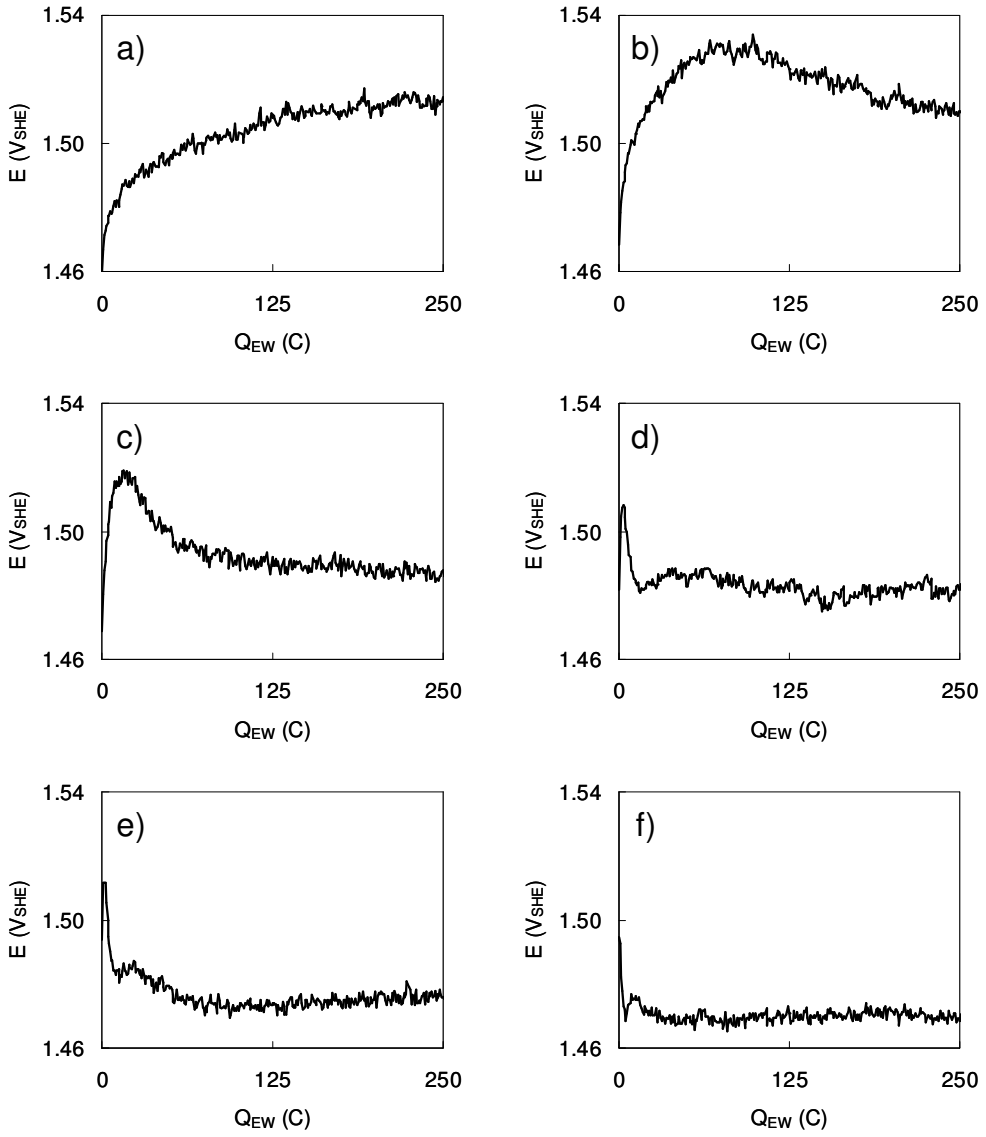

Figure 4.7 *Anode potential-charge profiles from electrolysis at different pH. a) pH 0.9, b) pH 1.1, c) pH 1.3, d) pH 1.5, e) pH 1.6, f) pH 1.9.*

tion obtained during continued electrolysis may be related to the formation of a thicker cobalt oxide film, increasing the surface area for chlorine evolution. Stabilization of the anode potential occurred when the film had reached a thickness where the diffusion of chloride ions and chlorine gas, in

cracks, pores, grain boundaries etc., restricted the effective utilization of the entire film. If the electric conductivity of the oxide film is lower than in the electrolyte, E_a will eventually start to increase.

The depolarization effect achieved at high pH may also be due to a more active modification of cobalt oxide formed at high supersaturation, or increased film porosity. It should be noted that the potential was already stabilized for the electrode depicted in Fig. 4.5 b), indicating that the change in morphology observed as additional charge was applied (Figs. 4.5 c) – f)) did not have any significant effect on the anode potential.

At pH 1.9 and above, a precipitate was formed in the bulk solution during cobalt electrolysis. The amount of precipitate increased with pH, and its colour changed from yellowish brown at pH 1.9 and pH 2.1 to dark brown at pH 3. In the test at pH 3, carried out in order to produce enough precipitate for further characterization, the pH had dropped to 1.6 after 5000 C of electric charge applied. The XRD pattern and a SEM image of this chemically formed precipitate are shown in Fig. 4.8, along with the diffractogram of industrial anode deposit. By comparing the XRD spectra, it becomes evident that the two deposits had almost identical structures. Several of the peaks were actually sharper for the bulk precipitate, indicating a higher degree of crystallinity, and the relative peak intensities were more similar to the database pattern for α-CoOOH (see Fig. 4.1). On the other hand, bulk precipitate formed at pH 2.1 was amorphous and could not be identified. Examination of the pH 3 precipitate by SEM revealed that it consisted of ~1 μm spherical particles made up of platelet-shaped crystals. Hexagonal platelet crystals are typical for CoOOH [105]. Such high surface area agglomerates were also observed along the edge of the exposed area of DSA® disks.

The formation of cobalt oxyhydroxide in the bulk solution during electrolysis can be described by the following equation:

$$Co^{2+} + ½\ Cl_2 + 2\ H_2O \rightarrow CoOOH + 3\ H^+ + Cl^- \qquad (4.1)$$

When pH was increased, dissolved chlorine produced on the anode then became a strong enough oxidant for the oxidation of Co^{2+} to Co^{3+}, and CoOOH was formed chemically in the bulk solution as well as electrochemically on the anode surface. The fact that a pH of 1.9 was needed

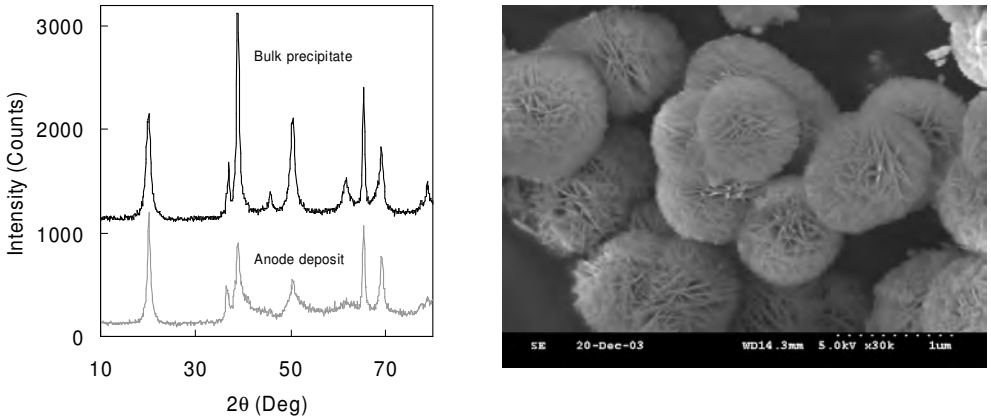

Figure 4.8 *XRD pattern and SEM image of bulk precipitate. The diffractogram of industrial anode deposit is included for comparison.*

for reaction 4.1 to proceed, considerably higher than pH 0.6 indicated by the potential-pH diagram in Fig. 2.1, demonstrates the high supersaturation needed for stable cobalt oxide particles to be formed by homogeneous nucleation. However, when a large number of nuclei were produced at pH 3, the subsequent growth of cobalt oxide resulted in a drop in bulk pH to 1.6. Furthermore, at this high supersaturation level, reactor walls, electrode holders etc. were covered by precipitate, a situation not observed in other experiments. This preferential deposition of cobaltic oxide on solid substrates (heterogeneous nucleation), by chemical oxidation and hydrolysis, is described in a patent held by Silver and Martin [150]. Another effect of increased pH is the possibility of forming HClO by hydrolysis of dissolved chlorine (see Fig. 2.1), HClO being a stronger oxidant than Cl_2. Finally, it should be noted that the chemically formed bulk precipitate was not included in the anodic deposition rate of cobalt oxide.

As illustrated in Fig. 4.6 b), the cathodic current efficiency for cobalt showed a strong pH dependency, increasing gradually from 87 to 97 % when the pH was raised from 0.9 to 2.1. At low pH, hydrogen evolution was the main side reaction on the cathode, but as pH was increased, the influence of the reduction of dissolved chlorine became increasingly important with respect to cobalt current yield. The colour of the cobalt metal became lighter grey when pH was increased. Marks from hydrogen bubbles, normally noticeable on the lower edge of the metal disk, were more pronounced at high pH,

because each bubble stayed on the cathode for a longer time when less gas was produced. Also, tiny holes were observed in the thin cobalt disk deposited at pH 0.9. However, severe pitting, as reported for pH 2.08 by Kongstein [65], was not observed, which may be explained by differences in the current density used (800 vs. 230 A/m^2) and electric charge applied (500 vs. 4162 C). Another difference was the absence of chlorine in Kongstein's experiments, since he was using a soluble cobalt metal anode. Dissolved chlorine may consume the adhering hydrogen bubbles responsible for the pit formation:

$$H_2 + Cl_2 \rightarrow 2\ HCl \tag{4.2}$$

The presence of NaClO [117] or H_2O_2 [151] in the electrolyte has been found to reduce the extent of pitting during nickel electrolysis. Finally, it should be emphasized that the colour of the cobalt metal reported in this work was probably modified during the potential scans after electrolysis.

4.2.1.3 Effects of cobalt chloride concentration

When the concentration of cobaltous ions in solution is increased, a higher rate of anodic cobalt oxide deposition would be expected. However, if cobalt exists as cobalt chloride, a change in concentration also affects the chlorine evolution reaction. From a thermodynamic point of view, the addition of $CoCl_2$ should actually have no effect on the extent of cobalt oxide formation on the anode, since the decrease of the reversible potential for this reaction and the parallel Cl_2 evolution will be identical, when using molar concentrations in the Nernst equation (a depolarization of 66 mV at 60°C for every tenfold increase in $CoCl_2$ concentration).

The influence of cobalt chloride concentration on the cobalt electrowinning process was examined by varying the $CoCl_2$ content between 18 and 181 g/l Co (0.3 – 3.1 M). From the results illustrated in Fig. 4.9 a), it is apparent that the cobalt oxide deposition reaction was highly dependent on $CoCl_2$ concentration, contrary to what was predicted above from simple thermodynamic calculations. The growth rate of cobalt oxide increased linearly with $CoCl_2$ concentration, from 0.04 % at 18 g/l Co to 0.33 % at 110 g/l Co, where a maximum was reached, as CE_{CoOOH} dropped by further increase of the $CoCl_2$ content. As expected, the anode potential decreased

with increasing $CoCl_2$ concentration up to 110 g/l Co (~4 M Cl^-), however, a further increase in concentration resulted in a small increase in potential. The current efficiency for cobalt metal deposition on the cathode increased continuously with $CoCl_2$ concentration, from 85 % at 18 g/l Co to 98 % at 181 g/l Co (Fig. 4.9 b)). It can be seen that the effect of $CoCl_2$ concentration on CE_{Co} was larger at low concentrations.

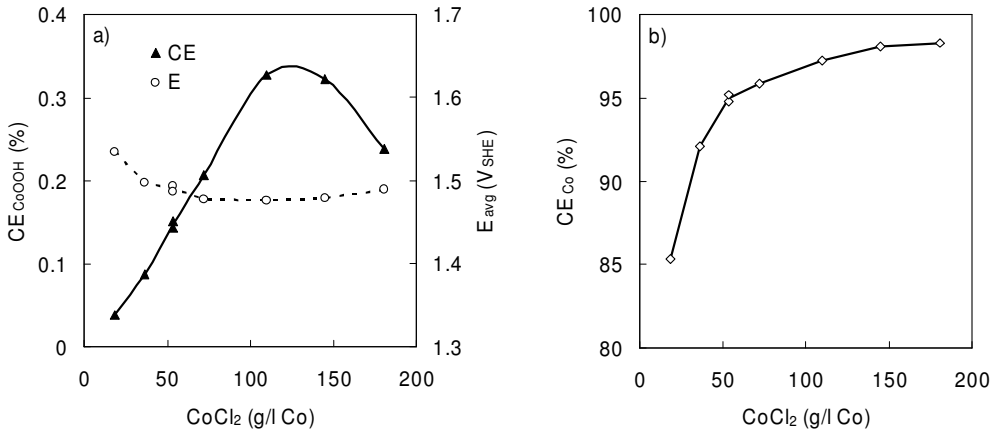

Figure 4.9 *Effects of cobalt chloride concentration on the cobalt electro-winning process. a) Anode scaling rate and anode potential, and b) Cathodic cobalt current yield.*

Increase in cobalt chloride concentration will have a huge impact on many solution properties, e.g., ionic activity coefficients, water activity, electrical conductivity and viscosity. According to the total reaction of the anodic cobalt oxide deposition process (equation 1.6), increased Co^{2+} activity, increased water activity and reduced H^+ activity (higher pH) should lead to more extensive anode scaling. The rate of chlorine evolution on cobalt oxide has been shown to follow a first order dependence on Cl^- concentration at constant ionic strength [60, 61].

Even though cobalt chloro complexes are formed when the $CoCl_2$ concentration is raised (see Fig. 2.19), the concentration of free Co^{2+} ions increases monotonically with increasing concentration, whereas the free Cl^- ion concentration increases asymptotically toward an upper limiting value. Upon heating, it was observed that the strongest cobalt electrolytes changed colour from red to purple, which indicates the formation of the blue $CoCl_4^{2-}$ complex (see section 2.3.2). On the other hand, due to the intense

colouration of some of the chloride complexes, visual observation may give a false impression of the extent of formation [126]. Enhanced stabilization of trivalent cobalt by chloride ions versus divalent cobalt will lower the $Co^{2+} \rightarrow Co^{3+}$ oxidation potential, but it is assumed that dehydrated cobalt ions shielded by chloride are less amenable to hydrolysis than cobalt ions surrounded by a sheath of water molecules.

In fact, when the $CoCl_2$ concentration is increased, the influence of complexation is counteracted by the strong hydration effects in this system, resulting in higher single-ion activity coefficients of Co^{2+} and Cl^- (Fig. 2.11). A larger gain in log a_{Co2+} than log a_{Cl-} with increasing concentration, related to the different degrees of hydration of the two types of ions, may explain the increasing rate of cobalt oxide deposition measured up to 110 g/l Co. As shown in Fig. 4.10, this difference in activity change results in a larger drop in the reversible potential for the anode scaling reaction compared to chlorine evolution, i.e., the change in overpotential will be less for the latter reaction when the $CoCl_2$ concentration is increased. The calculations indicate that the reversible potentials for CoOOH deposition and Cl_2 evolution drop by 133 and 78 mV respectively, when going from 18 to 181 g/l Co (as $CoCl_2$, pH 1.6, 60°C).

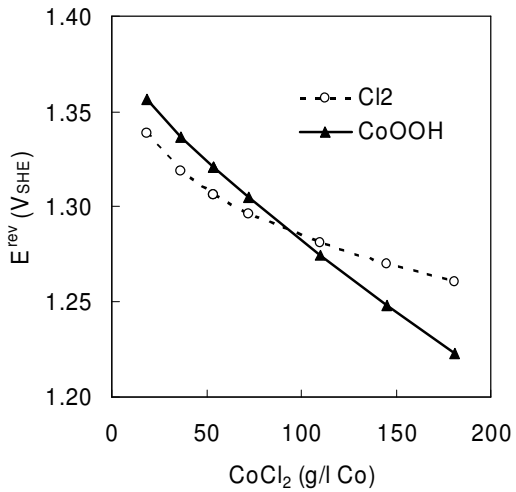

Figure 4.10 *Calculated reversible potentials for chlorine evolution and for anodic deposition of CoOOH vs. $CoCl_2$ concentration (pH 1.6, 60°C).*

Thermodynamic data for CoOOH given by Benson et al. [7], $\Delta G°_f$ = -372 kJ/mole and $\Delta H°_f$ = -454 kJ/mole at 25°C, were used to derive Fig. 4.10. Standard reduction potentials were estimated at 60°C, assuming no change in the enthalpy and entropy values from 25°C. This is an acceptable assumption for reactions having an absolute value of the enthalpy of reaction larger than 40 kJ/mole [61], justified for both reactions. The activity coefficients of Co^{2+} and Cl^- at 60°C, presented in Fig. 2.11, were used in the calculations. When using the data of which the Pourbaix diagram in Fig. 2.1 was based, the results indicated a more stable cobalt oxide than experienced from potential sweeps (the potential where the current became cathodic, see Fig. 4.4), which suggests that a less stable phase was formed in the present work. There may also be differences between the Gibbs energy of bulk oxides and that of thin oxide films [54, 152].

The activity of water is usually assumed to be unity in thermodynamic calculations. This is, however, not the case in concentrated chloride brines, as outlined in section 2.2.5. Fig. 2.7 shows that a_w is dropping to less than 0.7 in concentrated $CoCl_2$ solutions, shifting the reversible potential for CoOOH formation in the anodic direction. The effect of reduced a_w, which could explain the downward trend in anode scaling rate for $CoCl_2$ concentrations above 120 g/l Co, was included in Fig. 4.10, using the estimated a_w values presented in Fig. 2.7. Despite the drop in a_w, the reversible potential for CoOOH deposition decreases steadily with increasing concentration, due to the larger effect of the increasing Co^{2+} activity. It should be noted that the effect of water activity will be intensified if the more hydrous and metastable $Co(OH)_3$ species is the initial precipitation product, but it is still not large enough to support the results in Fig. 4.9 a).

During electrolysis from cobalt chloride solutions, the local pH on the anode surface will be lower than in the bulk solution, due to acid generation from oxygen evolution and CoOOH precipitation. In concentrated solutions, the activity coefficient of the hydrogen ion is much larger than in dilute solutions (see section 2.2.7), which means that if the anodic acid production remains unaltered, the anode surface pH will decrease when the $CoCl_2$ concentration is increased. Rough calculations, based on the adjustment of pH performed in each experiment prior to electrolysis, indicate γ_{H+} values at 60°C of ~1 and ~16 at 18 and 181 g/l Co respectively, i.e., the anodic H^+ formation at 18 g/l Co must be 16 times higher to give the same surface pH as 181 g/l Co. The rate of oxygen release will surely decline at higher $CoCl_2$

concentrations, but probably not to such an extent that the effect of increased γ_{H+} is completely offset. In addition, the higher viscosity of concentrated solutions will retard the transport of H^+ away from the anode. Thus, the decreased amount of anodically formed cobalt oxide measured above 120 g/l Co may be explained by a lower pH on the anode surface.

A systematic error in the measurement of pH in bulk solution, increasing in magnitude as the ionic strength is raised, will affect the measured rate of cobalt oxide deposition. However, all pH adjustments were performed at the electrolysis temperature. Furthermore, as seen in Fig. 2.15, the effect of increasing $CoCl_2$ concentration on the liquid junction potential should in fact result in a continuous rise of the true pH versus the measured pH, which suggests that the observed drop in CE_{CoOOH} was not linked to errors in pH induced by E_J.

Specific adsorption of Cl^- ions is another effect that may retard the electrodeposition of CoOOH at high $CoCl_2$ concentrations. A high coverage of Cl on the anode surface may restrict the number of active sites for Co^{2+} oxidation, it may complex with Co^{2+} ions to a higher degree than in the bulk solution and there will be less adsorbed OH species present, which can react with cobalt ions to form CoOOH (see section 1.5.5).

The increase of the anode potential for the most concentrated electrolytes is not completely understood. If the chlorine evolution on cobalt oxide is restricted by a fall in pH, as indicated by the trend in anode potential versus pH shown in Figs. 4.6 and 4.7, a low pH on the anode surface, related to a high γ_{H+} combined with hindered H^+ transport as discussed above, may have been involved. Furthermore, when the $CoCl_2$ concentration was increased, the difference in potential between the peak in potential usually observed in the first phase of electrolysis and the final stabilized potential was observed to shift from positive to negative, see Fig. 4.11. This may be related to a higher degree of blocking of pores etc. in the cobalt oxide deposit by gas bubbles when the electrolyte became more viscous, reducing the available electrode surface area. It can also be seen from Fig. 4.11 that the initial potential peak appeared earlier for the highest cobalt concentration. Similar to the experiments where the pH was varied, the amount of electric charge applied when this potential peak was reached was found to be a good indicator for the rate of anode scaling. The discussion continues in the next

section, where the present results are compared to those obtained when sodium chloride was added to standard cobalt chloride electrolyte.

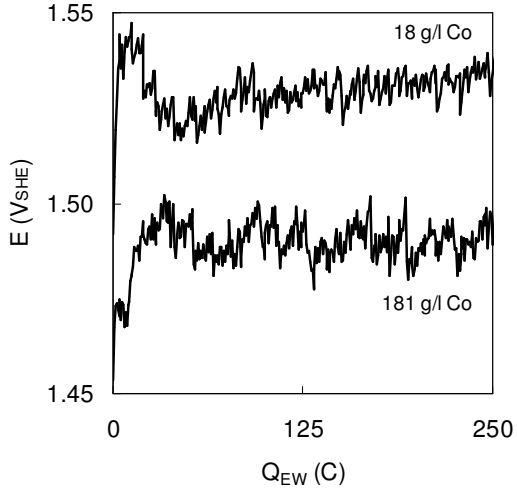

Figure 4.11 *Anode potential vs. charge applied during electrolysis from the lowest and the highest $CoCl_2$ concentration tested (18 and 181 g/l Co).*

The gradually improving cathodic current efficiency for cobalt with increasing $CoCl_2$ concentration, as shown in Fig. 4.9 b), indicates increasing Co^{2+} activity. It also suggests that the falling trend in CE_{CoOOH} obtained at high concentrations was probably not caused by a too low pH in the bulk solution, although a portion of the CE_{Co} gain is ascribed to reduced solubility of chlorine in concentrated aqueous metal chloride solutions [125]. Slower transport of H^+ in concentrated solutions will also improve CE_{Co}. The visual appearance of the deposited cobalt metal changed from dark to light grey when going from low concentration and up to 120 g/l Co. By further increase in concentration, it became somewhat darker again. At 181 g/l Co, the surface was covered by evenly distributed tiny pits, of which some had caused small holes in the metal.

4.2.1.4 Effects of sodium chloride addition

Anode depolarization is one possible way of suppressing the anodic cobalt oxidation and hydrolysis in cobalt electrowinning. By adding sodium

chloride to the cobalt chloride electrolyte, more free chloride ions will be available for chlorine evolution, and the anode potential will be lowered. If, at the same time, the cobalt concentration is kept constant and ideal calculations are used, the reversible potential for the anode scaling reaction remains unchanged. From the resulting reduced overpotential for this reaction, less cobalt oxide deposition on the anode would be expected.

Electrolysis experiments were conducted in standard cobalt chloride electrolyte, to which NaCl was added successively. Contrary to what could be expected from the ideal calculations mentioned above, additions of NaCl up to 69 g/l extra Cl^- (~4 M total Cl^-) caused a small increase in CE_{CoOOH} from 0.16 to 0.19 % (Fig. 4.12 a)), even though the anode potential dropped 20 mV. A further increase in the NaCl content resulted in a decrease in the rate of cobalt oxide deposition, to 0.14 % at 111 g/l extra Cl^-. As opposed to when the $CoCl_2$ concentration was varied, the lowest anode potential was recorded in the most concentrated solution. The cobalt concentration decreased gradually from 55 to 48 g/l due to liquid expansion, caused by the dissolved NaCl. Nevertheless, as seen in Fig. 4.12 b), CE_{Co} improved from 95 to 98 % when 111 g/l extra Cl^- was added.

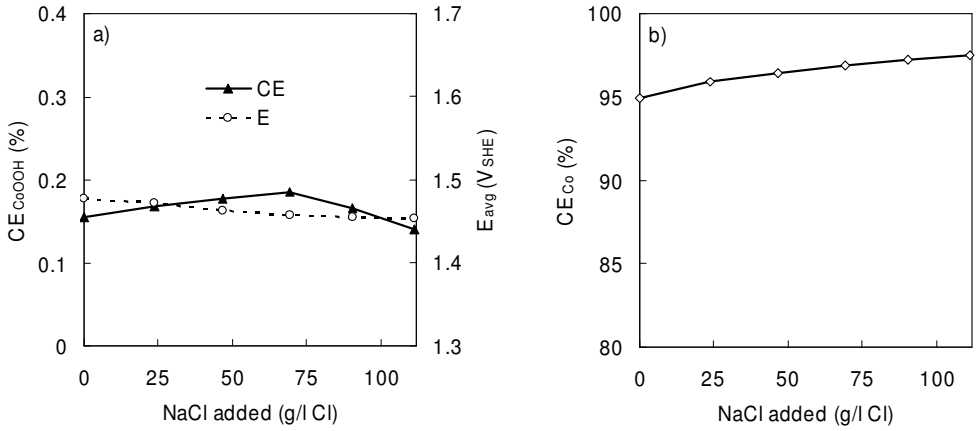

Figure 4.12 *Effects of NaCl addition to standard cobalt chloride electrolyte. a) Anode scaling rate and anode potential, and b) Cathodic cobalt current yield.*

The trends observed when adding NaCl can be attributed to the influence of the activity coefficients, parallel to the effect of varying the $CoCl_2$ concentration, as described in the previous section. According to Fig. 2.12

a), addition of NaCl to the $CoCl_2$ electrolyte has a remarkable effect on the activity of Co^{2+}. As an example, mixing in NaCl equivalent to 3 M in a 1 M $CoCl_2$ solution at 60°C will have the same effect on a_{Co2+} as if the pure $CoCl_2$ concentration had been doubled. Cobalt chloride complexes are formed when NaCl is added (see Fig. 2.20), but they are too weak to have a marked effect on a_{Co2+}, although the colour of the solution turned purple with increasing NaCl content.

Reversible potentials for chlorine evolution and for the anodic deposition of CoOOH were calculated for each of the $CoCl_2$-NaCl mixtures tested. Single-ion activities and water activities were estimated using the procedure outlined in chapter 2 and section 4.2.1.3. The results presented in Fig. 4.13 indicate that E^{rev} for CoOOH was lowered to a greater extent than E^{rev} for Cl_2 when NaCl was added, 46 and 25 mV respectively (111 g/l extra Cl^-). This may explain the initial rise in CE_{CoOOH} with increasing NaCl concentration (see Fig. 4.12 a)), in the same way as for the pure aqueous $CoCl_2$ system (Fig. 4.9 a)).

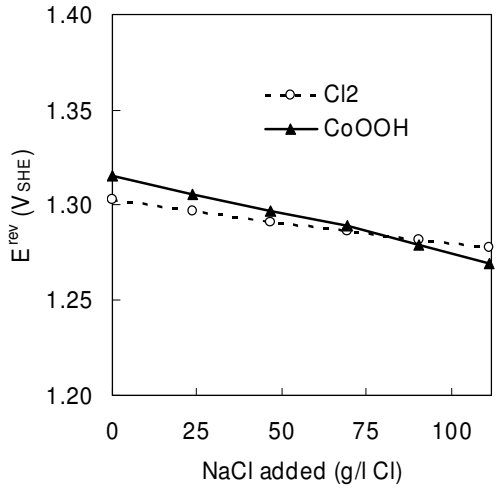

Figure 4.13 *Calculated reversible potentials for chlorine evolution and for anodic deposition of CoOOH vs. NaCl added to standard $CoCl_2$ electrolyte at pH 1.6 and 60°C.*

To support the discussion, the results obtained when adding NaCl to the standard electrolyte are compared graphically in Fig. 4.14 with the results from the variation of $CoCl_2$ concentration. The calculated cobalt ion activity

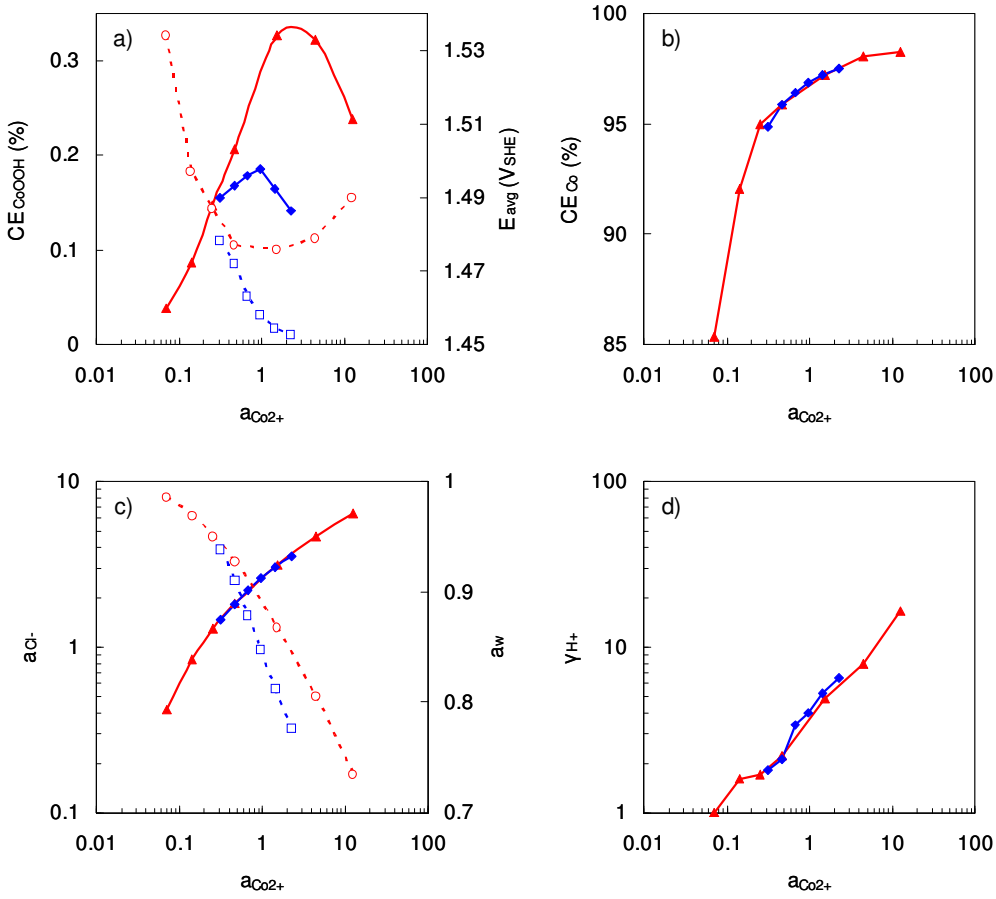

Figure 4.14 *Comparison between the variation of $CoCl_2$ concentration (red curves) and the addition of NaCl to standard $CoCl_2$ electrolyte (blue curves), vs. calculated cobalt ion activity. a) Anode scaling rate (full symbols) and anode potential (open symbols and dotted lines), b) cathodic cobalt current yield, c) calculated chloride activity (full symbols) and water activity (open symbols and dotted lines), d) activity coefficient of the hydrogen ion from pH adjustment of electrolytes.*

is shown along the abscissa in all four diagrams. Fig. 4.14 b) shows that, at a certain a_{Co2+}, CE_{Co} was almost identical in the two series of experiments, which should be expected, since other important parameters were the same. This indicates that the method used to estimate single-ion activity coefficients gives reasonable results, although the calculated data for the

$CoCl_2$-NaCl system deviated somewhat from the experimental data reported by Downes [126] (see Fig. 2.5). Furthermore, the calculated chloride ion activity (Fig. 4.14 c)) and the activity coefficient of H^+ estimated from the adjustment of pH carried out for each electrolyte (Fig. 4.14 d)) showed the same dependency on a_{Co2+}. A higher a_{Cl-}/a_{Co2+} ratio was expected when NaCl was added; however, the effect of increased chloride concentration was just offset by the lower γ_{Cl-} in NaCl solutions.

The rate of anode scaling reached a maximum for approximately the same a_{Co2+} in the two series (Fig. 4.14 a)). The decreased rates observed at higher activities are assumed to be associated with Cl adsorption and a lower local pH on the anode surface, related to the higher γ_{H+} values and inhibited H^+ transport in concentrated solutions (Fig. 4.14 d)). A reduced active surface area, from e.g., Cl adsorption or slower diffusion, means a higher local current density, which has been shown to reduce CE_{CoOOH} (see section 4.2.1.7).

No maximum in CE_{CoOOH} was obtained in a similar series with NaCl addition, where the pH was adjusted at room temperature (pH 1.5). From the different change in pH with temperature (see Fig. 2.16 b)), the bulk acidity of the most concentrated solution was, therefore, ~0.1 pH units higher at 60°C than in the pure $CoCl_2$ solution with no added NaCl, giving more anode scaling. This is a good example of the significance of pH with respect to anodic cobalt oxide deposition. In addition, in this series, a small amount of a very fine brown precipitate was separated from the electrolyte when it was filtered immediately after the last experiment was accomplished. The higher a_{Co2+} when NaCl is added, will favour the precipitation of CoOOH in the bulk solution, and the local pH will be approximately the same as in the bulk, since no oxygen is formed here.

The higher anode potentials at high a_{Co2+} may explain the more extensive cobalt oxide deposition observed in pure $CoCl_2$ solutions compared to $CoCl_2$-NaCl mixtures. The somewhat higher water activity would also favour anode scale formation to some extent (Fig. 4.14 c)). Furthermore, from Fig. 2.15 it is apparent that when NaCl is added to the $CoCl_2$ electrolyte, there is almost no increase in the true pH versus the measured pH. On the other hand, when the concentration of $CoCl_2$ is raised, the effect of the liquid junction potential of the pH electrode becomes more evident, increasing the pH error. A higher true pH in the bulk solution may have

contributed to the increased rate of anode scaling at intermediate $CoCl_2$ concentrations. However, it should be pointed out that the calculations of pH errors are based on ideal solutions, so that the results obtained are only rough estimates.

The reason for the difference in anode potential between the two series is not known. A similar trend in the potential difference between the initial peak and the stabilized potential, as described previously for pure $CoCl_2$ solutions of increasing concentration (see Fig. 4.11), was also observed when NaCl was added. This fact indicates that the electrode area available for chlorine evolution was reduced in concentrated electrolytes, as mentioned earlier.

If the electrode area and the electrochemical activity of cobalt oxide are unaffected, identical a_{Cl^-} should give the same rate of Cl_2 evolution, although the lower water activity in $CoCl_2$-NaCl mixtures may shift the O_2/Cl_2 ratio to less O_2 evolution. Less O_2 means less H^+ produced, which according to Boggio et al. [60] is beneficial for Cl_2 evolution on cobalt oxide.

Since all solutions of varying $CoCl_2$ content were prepared from industrial cobalt electrolyte, either by dilution with water or by boiling off water, the concentration of other ions present changed accordingly. Hence, the specific adsorption of sulphate ions, organic material etc., covering active sites on the cobalt oxide surface, may have induced the higher potentials observed in concentrated $CoCl_2$ solutions (for influence of SO_4^{2-}, see the next section). The SO_4^{2-} concentration was, however, low (< 1 g/l at 181 g/l Co).

The surface of the electrodeposited cobalt metal became lighter grey at higher NaCl concentrations, and the darker edge that was usually present was hardly visible. This darker edge is believed to be due to higher local current density, and the fact that it became less pronounced can be explained by a more even current distribution, induced by increased a_{Co2+} and improved electrical conductivity of the electrolyte in the presence of NaCl [65]. A few pits, but no holes, could be seen on the surface of the metal plated from the solution that contained the highest concentration of NaCl, in the series where the pH was adjusted at ambient temperature (higher bulk pH at 60°C).

4.2.1.5 Effects of chloride/sulphate ratio

Based on ideal thermodynamic calculations, the type of anion in solution, chloride or sulphate, should have no effect on the anode process in cobalt electrowinning, since oxygen evolution is the preferred reaction in both cases. However, when chloride is present, chlorine evolution predominates because the generation of O_2 is less reversible. Thus, an increase in anode potential is expected during galvanostatic electrolysis when the chloride concentration is lowered and Cl_2 evolution becomes diffusion controlled. The higher anode potentials in sulphate electrolytes should increase the rate of cobalt oxide electrodeposition, but O_2 evolution will result in a lower pH on the anode surface, suppressing anode scaling.

Electrolysis was performed in electrolytes with chloride/sulphate ratios in the range from the standard cobalt chloride electrolyte containing only traces of sulphate (0.24 g/l) to a cobalt sulphate electrolyte containing only traces of chloride (0.18 g/l). The cobalt content was kept constant at 55 g/l (it varied from 54.7 to 55.3 g/l Co in the various electrolytes tested). The results in Fig. 4.15 a) show that when a portion of the chloride content was replaced by sulphate, the amount of anodically formed cobalt oxide decreased. How-

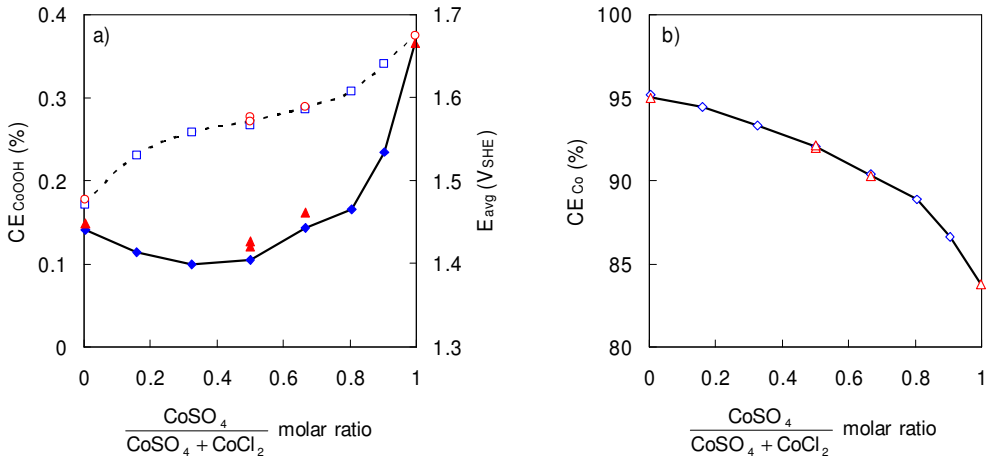

Figure 4.15 *Effects of chloride/sulphate ratio in the electrolyte at constant cobalt content. a) Anode scaling rate (full symbols) and anode potential (open symbols and dotted line). b) Cathodic cobalt current yield. Red and blue colours represent the two anode disks tested (both with regular coating).*

ever, in sulphate-rich electrolytes, anode scaling accelerated. The anode potential increased gradually with increasing sulphate concentration, though more pronounced at low and high chloride/sulphate ratios. E_a in $CoSO_4$ solution was approximately 200 mV higher than in the standard $CoCl_2$ electrolyte. As shown in Fig. 4.15 b), CE_{Co} dropped continuously with increasing sulphate content, from 95 to 84 % when going from $CoCl_2$ to $CoSO_4$ solution.

In view of the strong rise in anode potential when sulphate ions were introduced into $CoCl_2$ electrolyte, the suppressed rate of cobalt oxide precipitation at intermediate Cl^-/SO_4^{2-} ratios was quite surprising. At these sulphate levels, a positive step in E_a of ~40 mV appeared shortly after the initial potential peak, see Fig. 4.16. The peak and the step in potential were shifted to shorter electrolysis times with increasing sulphate content, and in sulphate-rich electrolytes both became less distinct. This indicates that the covering of DSA® active sites by cobalt oxide became gradually faster when chloride ions were replaced by sulphate, i.e., no inhibiting effect of sulphate was observed for the initial nucleation and growth of cobalt oxide. On the other hand, it is believed that the following step in potential was caused by SO_4^{2-} ions specifically adsorbed on the cobalt oxide, blocking active sites for Cl_2 evolution and CoOOH precipitation. As shown in Table 4.1, SO_4^{2-} was

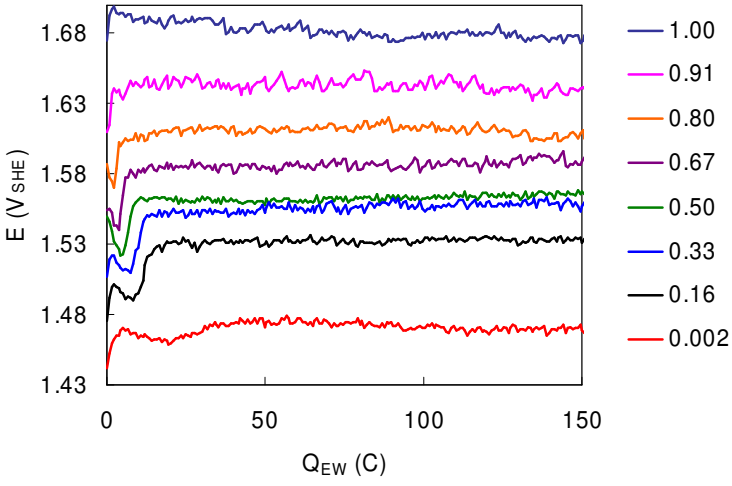

Figure 4.16 *Anode potential vs. charge applied during the first part of electrowinning, for the various Cl^-/SO_4^{2-} ratios tested.*

indeed accumulated in the washed industrial anode deposit, generated from a solution with only traces of sulphate, which indicates that sulphate may play an important role in the anode scaling process. Ishikawa et al. [154] have reported that adsorbed SO_4^{2-} ions impede the precipitation of β-FeOOH from $FeCl_2$ solutions, resulting in lower growth rate and less crystalline material. The retarding effect of sulphate on the Cl_2 evolution reaction on metal oxide electrodes is also well documented [44]. A reduced electrode surface area, due to the incorporation of sulphate, adhering gas bubbles or a more compact deposit, will also give a higher local current density, which may favour the 'facile' Cl_2 evolution versus cobalt oxide deposition (see section 4.2.1.7).

In addition to sulphate sorption, other factors may also have been involved in the suppression of CE_{CoOOH} in mixed $CoCl_2$-$CoSO_4$ solutions. A higher degree of oxygen evolution and a more viscous electrolyte will lead to lower pH on the anode surface, however, the buffering effect of sulphate when forming bisulphate will reduce this effect (equation 2.24). As a consequence, the measured activity coefficient of H^+ at 60°C (including the effect of the SO_4^{2-}/HSO_4^- equilibrium) dropped from 1.7 in the standard $CoCl_2$ electrolyte to 0.3 at a Cl^-/SO_4^{2-} molar ratio of 0.5.

According to Ji [117], the error in the measured pH, induced by the liquid junction potential, is somewhat lower in sulphate than in chloride media, but the difference is so small that the true pH of the bulk solution is assumed to have been approximately the same in the various electrolytes.

Owing to extensive ion-pairing, the activity of cobalt in sulphate solutions is very low compared to in chloride solutions (see Fig. 2.2). Mean activities in aqueous mixtures of $CoCl_2$ and $CoSO_4$ were calculated using the procedure described in chapter 2, and the results are displayed in Fig. 4.17. Single-ion activities could not be estimated because sulphate ions are highly hydrated (h ~10 [155]). From the figure it is evident that the cobalt activity decreases continuously when going from $CoCl_2$ to $CoSO_4$ solution at constant cobalt concentration, which explains the downward trend in CE_{Co} shown in Fig. 4.15 b). Such a decrease in Co^{2+} activity tends to reduce the amount of anodically formed CoOOH. The possible formation of complexes between Co^{3+} and SO_4^{2-}, which may stabilize oxidized Co^{3+} in solution, could have been contributing as well. Fig. 4.17 also shows that the cobalt activity increases with temperature in these mixtures, especially in sulphate-rich

solutions. The water activity is assumed to be too high to have any noticeable effect on the anode scaling reaction in these experiments.

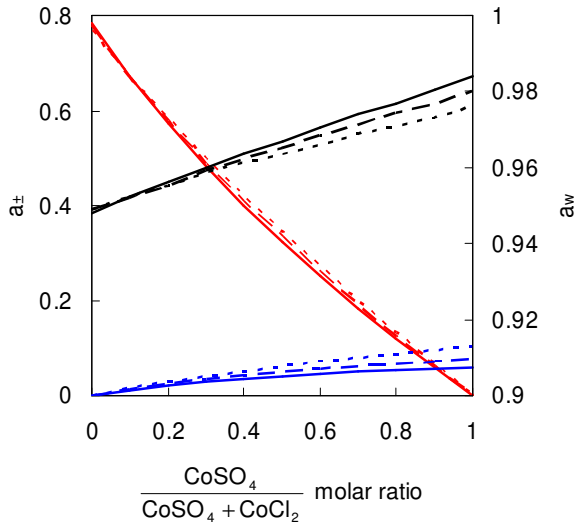

Figure 4.17 *Calculated mean activity vs. Cl^-/SO_4^{2-} ratio for $CoCl_2$ (red curves), $CoSO_4$ (blue curves) and water activity (black curves). Temperature 25°C (unbroken curves), 60°C (dashed curves) and 100°C (dotted curves). Constant Co content at 55 g/l.*

Two anode disks, both with the regular coating, were tested in this series, and the results are presented in Fig. 4.15 by red and blue symbols respectively. The first anode tested ('red') operated at a somewhat higher potential, and more cobalt oxide was formed. This indicates that there may be differences between individual anodes, even though they were produced simultaneously by the same procedure, as pointed out by Nylén and Cornell [156]. It should be noted that the characteristic step in potential appeared for both anodes at intermediate Cl^-/SO_4^{2-} ratios (the E vs. Q_{EW} profiles in Fig. 4.16 were recorded using the 'blue' anode, except for the $CoSO_4$ solution with molar ratio 1).

In sulphate-rich solutions, the Cl_2 evolution reaction was probably diffusion controlled, bringing about the additional increase in anode potential seen to the right in Fig. 4.15 a). The accelerated rate of anode scaling suggests that this increase in E_a was predominant compared to sulphate adsorption, reduced cobalt activity and a lower pH on the anode surface, which all tend

to lower the extent of scaling. The results obtained in the $CoSO_4$ solution containing only traces of chloride also indicate that a high surface concentration of intermediates in the Cl_2 evolution reaction, such as HClO or Cl radicals, was not a prerequisite for the formation of CoOOH at the prevailing conditions. However, oxygen is always formed, and cobalt ions may react preferentially with the O_2 reaction intermediates adsorbed on the anode surface (see section 1.5.5). This type of mechanism has been suggested for the electrodeposition of PbO_2 on platinum and gold from aqueous Pb^{2+} solutions [157].

Cobalt oxide electrodeposited from the electrolyte that contained almost no chloride was observed to dissolve more slowly during the cathodic potential sweep performed in standard electrolyte. After the sweeps, particles were partly covering the anode surface, which was typical when thick cobalt oxide films were dissolved electrochemically (see sections 4.2.4.2 and 4.2.5.2). In other experiments it was found that these particles did not have any retarding effect on the dissolution process. The higher stability of cobalt oxide deposited from sulphate solution may, therefore, be related to a different structure (e.g., higher levels of SO_4^{2-} ions), different crystallinity or a less porous morphology. The structure of FeOOH precipitated chemically from aqueous solution at ambient pressure and 80 – 90°C has been shown to depend on the nature of the anion, since the use of sulphate and chloride solutions resulted in the formation of α-FeOOH and β-FeOOH respectively [158].

The darkest cobalt metal was produced from the electrolyte having equal molar concentrations of $CoCl_2$ and $CoSO_4$. The sulphate-rich electrolytes (molar ratios ≥ 0.8) gave a light grey and very uniform appearance, the latter as a result of extensive hydrogen evolution. Furthermore, in these solutions the metal disks were partly detached from the titanium electrode, indicating internal stresses in the deposit. Cobalt metal plated from a pure $CoSO_4$ electrolyte by Kongstein [65] was actually bent, but the electrolysis conditions were not identical. As mentioned earlier, the poor CE_{Co} in sulphate solution was mainly caused by the low cobalt activity. Absence of dissolved chlorine must have been another contributing factor improving current efficiency (dissolved O_2 will also be reduced on the cathode during cobalt electrowinning, but its solubility is much lower than that of Cl_2). The buffering effect of sulphate ions will also lower the surface pH on the cathode, which will favour H_2 evolution [65]. Finally, it has been claimed

that chloride ions promote the electrolytic deposition of metals due to a catalytic effect on electron transfer [117].

4.2.1.6 Effects of temperature

Anodic evolution of chlorine gas and anodic deposition of CoOOH are both endothermic reactions, which means that the reactions are promoted at elevated temperatures. Another factor of great importance, reaction kinetics, is also enhanced by an increase in temperature. Since Cl_2 evolution is known to be a quite rapid reaction, as opposed to the sluggish reactions involving oxidized cobalt, it was expected that higher temperatures would lead to more extensive anode scaling.

The temperature of the standard $CoCl_2$ electrolyte was varied between 30 and 80°C. The pH of the electrolyte was adjusted to 1.6 at the prevailing temperature before galvanostatic electrolysis was started. Fig. 4.18 a) shows that CE_{CoOOH} increased by one order of magnitude, from 0.03 to 0.30 %, when the temperature was raised from 30 to 80°C. The exponential increase in the rate of anode scaling took place despite a decay in the average anode potential from 1.57 V at 30°C to 1.46 V at 80°C. As shown in Fig. 4.18 b), a maximum in CE_{Co} of 95 % was achieved at 60°C, somewhat higher than the results obtained at 30 and 80°C, being 93 and 94 % respectively.

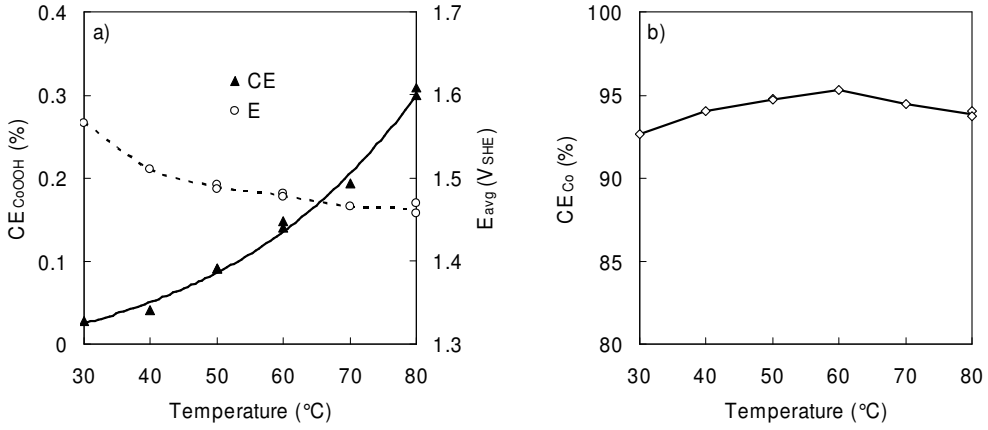

Figure 4.18 *Effects of temperature on the cobalt electrowinning process. a) Anode scaling rate and anode potential, and b) Cathodic cobalt current yield.*

According to the estimates outlined in chapter 2, there is only a small decrease in the activity of Co^{2+} and Cl^- with increasing temperature, in a $CoCl_2$ electrolyte containing 55 g/l Co (Fig. 2.11). Consequently, the increase in water activity at this concentration is almost non-existent (Fig. 2.7). The accelerated rates of cobalt oxide deposition obtained at high temperatures were, therefore, not a result of changes in ionic activities. In addition, Fig. 2.19 illustrates the higher degree of cobalt chloro complexation at elevated temperatures – it was actually observed that the colour of the electrolyte turned purple upon heating. The fact that the amount of cobalt scale increased with temperature demonstrates that the decrease in the concentration of free Co^{2+} ions, due to complexation, was of minor importance.

Reversible potentials for Cl_2 evolution and CoOOH deposition at the various temperatures tested, calculated using the same procedure as described in section 4.2.1.3, are displayed in Fig. 4.19. It can be seen that the drop in E^{rev} with temperature was similar for the two reactions; 64 and 72 mV respectively, when going from 30 to 80°C. This means that Cl_2 evolution was thermodynamically favoured at all temperatures. When the temperature was increased from 30 to 40°C, the overpotential for Cl_2 evolution (E_{avg} – E^{rev}) was lowered by 40 mV. However, a further rise in temperature had no

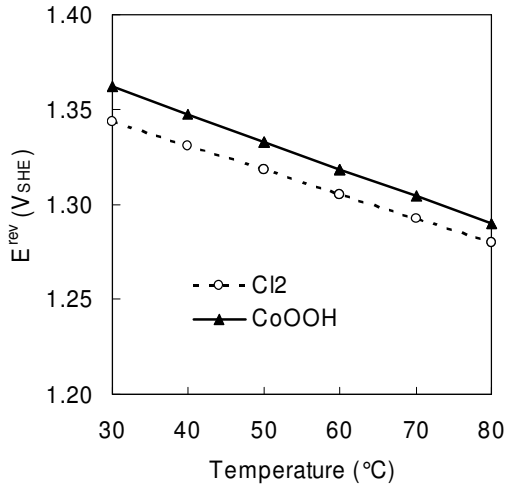

Figure 4.19 *Calculated reversible potentials for chlorine evolution and anodic deposition of CoOOH vs. temperature in standard $CoCl_2$ electrolyte of pH 1.6.*

noticeable effect on the measured overpotential.

When the reaction rate shows a strong temperature dependence, as seen for the deposition of cobalt oxide, the reaction is probably activation controlled. Pauporté et al. [58] prepared CoOOH films on nickel substrates by electrodeposition from aqueous $Co(OH)_2$ slurries (see section 1.5.1). They also observed accelerated rates of cobalt oxide deposition at elevated temperatures, and it was proposed that this was caused by a more crystalline oxide layer, as identified by XRD analysis. High temperature has been reported to be beneficial for Cl_2 selectivity versus O_2 [44], which in combination with a reduced activity coefficient of H^+ and higher transport of generated acid, may have favoured anode scaling, through higher local pH on the anode surface.

Anode potentials recorded during electrolysis at the different temperatures are depicted in Fig. 4.20. It is apparent that in this series of experiments, the second potential peak was more clearly defined compared to when the electrolyte pH was varied, see Fig. 4.7. The rise in potential after the first peak may be related to a decreasing participation of the DSA® in producing Cl_2, as the cobalt oxide film was growing thicker. The reason for the different potential behaviour for different series is not known. However, small variations between the anode disks could be a plausible explanation.

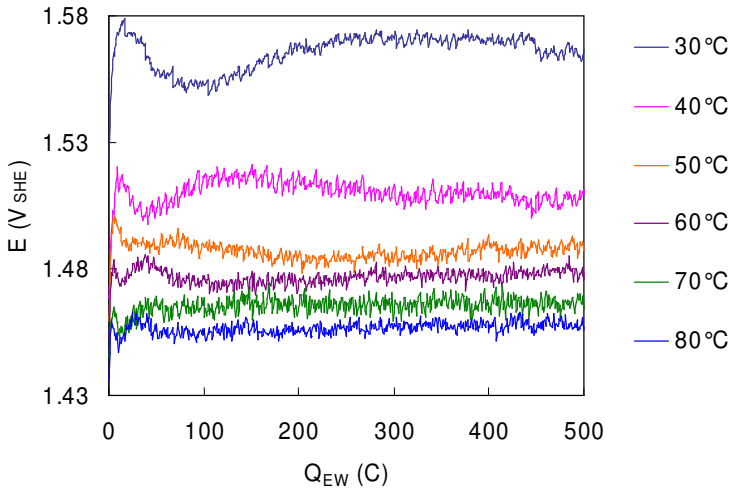

Figure 4.20 *Anode potential vs. charge applied during electrowinning at different temperatures.*

For most of the experiments carried out in this work, a rapid stabilization of the anode potential was associated with a high rate of anode scaling.

The cobalt electrodeposited at 30 and 40°C was severely warped and had partly detached from the titanium cathode, due to tensile stresses in the metal. Increased temperature resulted in a change in appearance from dark to light grey, and at 70 and 80°C it became harder to strip the cobalt from the titanium. The falling trend in CE_{Co} for temperatures above 60°C, see Fig. 4.18 b), was probably related to lower Co^{2+} activity and enhanced transport of H^+ ions and dissolved Cl_2 towards the cathode, although the concentration of the latter is reduced with increasing temperature [125]. Higher transport rates of H^+ will increase the limiting current of hydrogen evolution, which is partly diffusion controlled (see section 4.2.1.8). When using a stationary cathode and a cobalt anode (i.e. no Cl_2 release), Kongstein [65] measured a 1 % decrease in CE_{Co} from 60 to 80°C, despite the fact that pH was adjusted at room temperature.

4.2.1.7 Effects of current density

To compare the electrochemical kinetics of anodic cobalt oxide deposition versus chlorine evolution, current densities in the range 10 – 3170 A/m^2 were tested (based on geometric electrode areas, which were identical for the anode and the cathode). 500 coulombs of electric charge were applied in each experiment, giving electrolysis durations varying from 8.4 minutes to more than 44 hours. The remaining parameters were kept at the standard conditions given in Table 4.2.

The influence of current density on CE_{CoOOH}, E_{avg} and CE_{Co} is illustrated in Fig. 4.21. From Fig. 4.21 a) it can be seen that CE_{CoOOH} was very low at 10 and 11 A/m^2. An increase in current density to 18 A/m^2 resulted in a step in CE_{CoOOH} to 0.21 %. CE_{CoOOH} remained constant at this level up to 100 A/m^2, from where it started to decrease on further increase in current density. At 3170 A/m^2, CE_{CoOOH} was reduced to 0.05 %. The anode potential became more fluctuating and increased continuously with increasing current density, from 1.35 V (vs. SHE) at 10 A/m^2 to 1.53 V at 3170 A/m^2. Fig. 4.21 b) shows that CE_{Co} was improved from 32 to 95 % when the current density was increased from 10 to 1000 A/m^2, whereas at 3170 A/m^2 it dropped to 80 %.

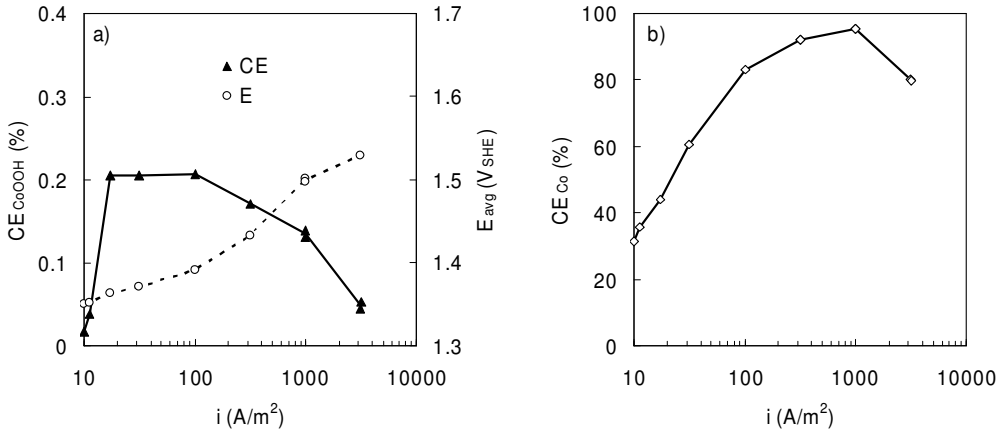

Figure 4.21 *Effects of current density on the cobalt electrowinning process. a) Anode scaling rate and anode potential, and b) Cathodic cobalt current yield.*

In a standard $CoCl_2$ electrolyte at pH 1.6 and 60°C, the estimated reversible potential for CoOOH deposition, using thermodynamic data given by Benson et al. [7], was a few millivolts higher than the value for Cl_2 evolution. This indicates that it may be possible to produce Cl_2 from this electrolyte without any parallel anode scaling, at very low overpotentials. The recorded anode potential at the lowest current density tested was, however, 30 mV higher than E^{rev} for CoOOH. The low CE_{CoOOH} obtained may, therefore, be related to the need for a certain overpotential for CoOOH to nucleate on the foreign DSA® substrate. Using cyclic voltammetry, Sasaki et al. [159] demonstrated a nucleation overpotential of at least 200 mV for CoOOH deposition on platinum, from a 0.02 M cobalt acetate solution at pH 6 and 50°C.

It was observed that more electric charge had to be applied to stabilize the anode potential at low current densities, see Fig. 4.22. At 10 A/m^2, E_a increased gradually with time and no peak could be seen, i.e., steady state conditions were not established even after almost two days of electrolysis. The subsequent potential scan did not show any clear reduction wave, which indicates that the anode was still almost free from cobalt precipitate. On the other hand, at 11 A/m^2 a peak in E_a appeared after 460 C, and a reduction peak was easily identified by potential sweep. In a preliminary experiment at 10 A/m^2 using another anode disk, the peak appeared already after ~150 C of electrolysis, and appreciable amounts of scale were then produced.

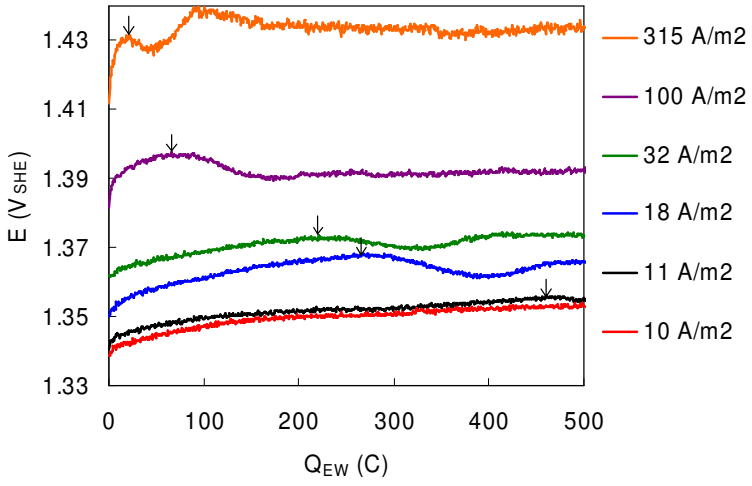

Figure 4.22 *Anode potential vs. charge applied during electrowinning at different current densities. The positions of the first potential peaks are marked by arrows.*

As pointed out earlier, the initial rise in anode potential was probably generated as chloride concentration gradients and gas bubbles were developing in cracks and pores of the DSA® coating. When a certain potential was reached, stable cobalt oxide nuclei were formed on the anode surface, and the subsequent growth of a CoOOH film increased the active electrode area for Cl_2 evolution, causing depolarization. It may, however, be possible that the amount of scale varied when the potential peak was reached, depending on the growth mode of cobalt oxide (2- vs. 3-dimensional) and the degree of precipitation in pores of the DSA®. Nevertheless, if the time from the start of electrolysis to the first potential peak included only the induction period and the formation of a monolayer of CoOOH, the rate of anode scaling should not be regarded as constant with time at low current densities. A recalculation of CE_{CoOOH}, assuming that cobalt oxide was produced only after the potential peak was passed, gave an almost linear decline in CE_{CoOOH} against the logarithm of current density. It should be mentioned that when CoOOH was deposited from a 0.01 M cobalt acetate solution (pH 6, room temperature) at 0.95 V vs. Ag/AgCl, Matsumoto et al. [75] obtained a much lower current efficiency during the initial electrolysis. CE_{CoOOH} increased from 20 % at 0.001 C of electric charge to about 60 % for 0.007 C and above.

Based on the CE_{CoOOH} data given in Fig. 4.21 a), the average partial current density of CoOOH deposition, i_{CoOOH}, was estimated. From the results illustrated in Fig. 4.23 it is apparent that the anode scaling reaction was activation controlled up to at least 1000 A/m^2 of total current density. However, a further increase to 3170 A/m^2 resulted in only a small increase in i_{CoOOH}, which indicates a change in the reaction scheme. When the current density is increased, more O_2 evolution will be produced within a certain time period, decreasing the local pH on the anode surface. Moreover, if the limiting current density of Cl_2 evolution was exceeded at the highest current density, even more acid may have been produced, suppressing anode scaling. In addition, the vigorous gas release may have caused more of the anode deposit to peel off during electrolysis. On the other hand, from occasional filtration of the electrolyte after electrolysis, more black flakes were in fact identified in bulk solution at low current densities, but this may also be due to a less soluble precipitate.

The falling trend in CE_{CoOOH} with increasing current density demonstrates that the rate of anode scaling increased less than the rate of Cl_2 evolution. Since both reactions were activation controlled, this indicates that the Tafel slope for CoOOH deposition was higher than for the generation of Cl_2. As a consequence of the method used for IR compensation (at zero faradaic current, see section 3.1.4), the blocking effect of gas bubbles was not taken into account, resulting in too high potentials at high current densities. Therefore, to get a rough estimate of the Tafel slope for CoOOH deposition, b_{CoOOH}, the anode potentials were adjusted so that b_{Cl2} became 45 mV/dec, based on literature data for Cl_2 evolution on cobalt oxides (40 mV/dec at 25°C, see section 1.5.2). From the Tafel plot in Fig. 4.24 it can be seen that the measured potentials followed this Tafel slope up to 100 A/m^2. The adjusted E_a values were then used to construct the Tafel plot for the anode scaling reaction. In order to reduce the disturbing effect of long induction periods at low current densities, adjusted values were used for i_{CoOOH}, assuming that the anodic cobalt oxide deposition was not initiated until the first potential peak was reached.

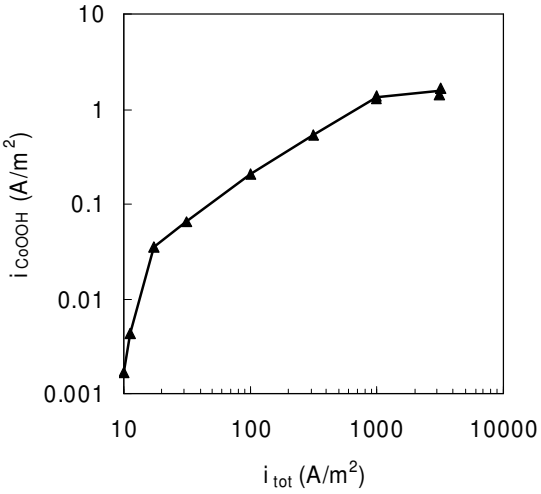

Figure 4.23 *Partial current density of CoOOH deposition vs. total current density.*

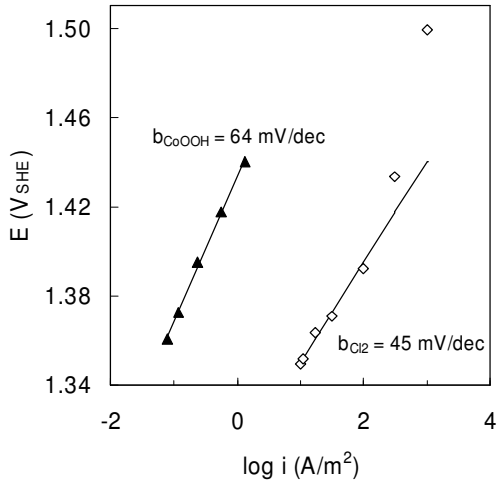

Figure 4.24 *Tafel plots of CoOOH deposition (full symbols) and Cl_2 evolution (open symbols).*

As shown in Fig. 4.24, a linear relationship was obtained for the electrodeposition of CoOOH in the range 18 – 1000 A/m^2 of total current density, giving a Tafel slope of 64 mV/dec. In addition to the uncertainties in the estimated anode potentials, it should be noted that the true electrode area was

probably not constant, due to variations in e.g., film thickness, porosity and morphology. It is also believed that the local pH on the anode surface was a function of current density.

Chen and Noufi [56] prepared Co(III) oxide films potentiostatically onto a graphite rotating disk electrode from a 0.05 M cobalt acetate / 0.5 M sodium acetate solution at room temperature. They also obtained a decrease in current efficiency for the cobalt deposition, from 93 % at 0.8 V_{SCE} to 63 % at 1.1 V_{SCE}, explained by a higher degree of O_2 evolution at the higher potentials. To minimize the extent of anodic growth of CoOOH versus the rate of Cl_2 production, operating at high current density seems to be beneficial, as long as the current density required to completely avoid scaling is too low to be of practical relevance.

For cobalt oxide films formed at low current densities, the current response measured during the following cathodic potential scan was found to change. It was observed that the negative current peak was shifted to less positive potentials, and that the peak height decreased. This trend is illustrated in Fig. 4.25, where voltammograms obtained for the films prepared at 18, 32 and 100 A/m^2 are shown. The amount of anode deposit was the same in these tests (CE_{CoOOH} = 0.21 %). Slower dissolution of films produced at low current densities indicates a more stable form of cobalt oxide. The increased stability may be related to a more compact morphology or to changes in structure, caused by the lower deposition potentials and longer deposition times (ageing). After potential sweeps, more brown precipitate was also observed on the DSA® surface. It was also found that the anodic current at the onset of potential sweeps was lower on films produced at low current densities, which indicates that these films were less active for Cl_2 evolution. Finally, the shoulder on the anodic side of the reduction peak for the films prepared at 18 and 32 A/m^2 was probably due solely to chlorine, which indicates that the reduction of this form of cobalt oxide started at a lower potential than Cl_2 reduction.

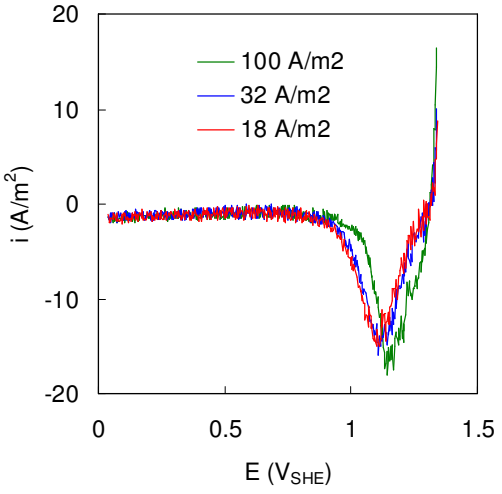

Figure 4.25 *Voltammograms of the cathodic dissolution of cobalt oxide films deposited at different current densities. Linear scans at -1 mV/s sweep rate in standard $CoCl_2$ electrolyte at pH 1.6 and 60°C.*

The strong improvement in CE_{Co} with increasing current density shown in Fig. 4.21 b) is related to the difference in thermodynamics and electrochemical kinetics between cobalt electrodeposition and hydrogen evolution. In Fig. 4.26, partial current densities of the cobalt deposition and the sum of cathodic side reactions (mainly H_2 evolution and Cl_2 reduction) are compared. The side reactions were predominant at low current densities, because these reactions are preferred thermodynamically. When the current density was increased, the rate of the side reactions increased only slightly due to slow kinetics and diffusion limitations, while the cobalt metal growth increased more steeply. At the highest current density of 3170 A/m^2, decomposition of water molecules into H_2 and OH^- ions may become feasible. However, experiments carried out by Kongstein [65] showed that even higher current densities must be applied for this reaction to proceed. Using a cobalt anode, he obtained CE_{Co} of 90 % at 3000 A/m^2, 10 % higher than what was measured at 3170 A/m^2 in the present work (see Fig. 4.21 b)), which suggests that more intensive Cl_2 reduction was involved here.

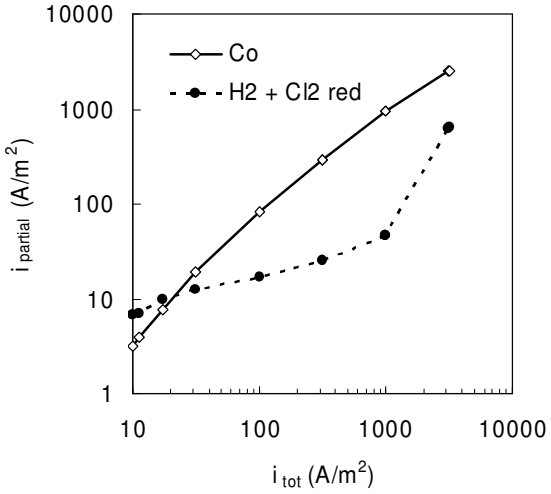

Figure 4.26 *Calculated partial current densities for cobalt metal deposition and the sum of cathodic side reactions (hydrogen evolution and chlorine reduction) vs. total current density.*

Cobalt produced at 10 and 11 A/m^2 had a light grey and shiny appearance, and the thin metal disks were nonuniform so that they did not cover the entire titanium substrate. Increased current density resulted in a gradual conversion to dark and dull electrodeposits. Even at 3170 A/m^2, smooth and coherent cobalt metal was obtained.

4.2.1.8 Effects of agitation

In a preliminary set of experiments, mixing of the electrolyte was investigated by varying the rotation speed of the magnet at the bottom of the cell from 0 to 700 rpm. Here, potential scans were performed in the same electrolyte as used in the former galvanostatic electrolysis. As a consequence, dissolved chlorine was then reduced on the working electrode along with cobalt oxide, resulting in too high values of CE_{CoOOH}. Despite this shortcoming, the most important results from these experiments are reported, since they gave some useful information about the actual system.

As shown in Fig. 4.27 a), CE_{CoOOH} and E_{avg} were nearly independent of stirring rate, except when the stirrer was turned off completely, which caused a slight decrease in CE_{CoOOH}. The behaviour of E_a versus the amount of

electric charge applied seemed not to be affected by the degree of agitation. CE_{Co} decreased with increasing stirring rate, see Fig. 4.27 b).

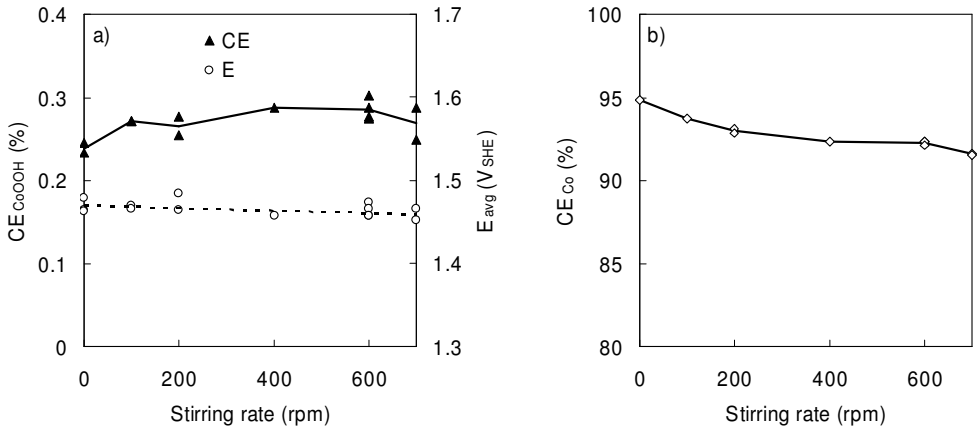

Figure 4.27 *Effects of agitation on the cobalt electrowinning process. a) Anode scaling rate and anode potential, and b) Cathodic cobalt current yield. Note that in these experiments potential scans were performed in a Cl_2-containing electrolyte.*

The fact that the agitation intensity did not have any significant influence on the rate of anode scaling at standard conditions is another indication of an activation controlled process, although gas bubbles formed always create some turbulence in the electrolyte during electrolysis. At 0 rpm, a small reduction wave was also observed during the second potential sweep, which suggests that there was still CoOOH present when the first sweep was completed. This in combination with a lower pH on the anode surface may explain the small decrease in CE_{CoOOH} at no stirring.

As opposed to electrolysis, stirring rate had a profound effect on the cathodic dissolution of the cobalt oxide film during potential sweeps, see Fig. 4.28. From the figure it can be seen that no stirring resulted in a very broad reduction wave, indicating slow CoOOH dissolution. When the stirring rate was increased, the reduction peak became deeper and sharper. The voltammograms did not change for stirring rates above 400 rpm.

Inhibited dissolution of CoOOH at low agitation levels was related to depletion of H^+ ions close to the surface of the working electrode, since no gas bubbles were generated during potential sweeps. Above 400 rpm,

CoOOH dissolution characteristics were dominated by the surface reaction and not diffusion. A higher cathodic current at low potentials, observed for high stirring rates, indicates more intensive Cl_2 reduction. In addition, the current was then found to fluctuate more.

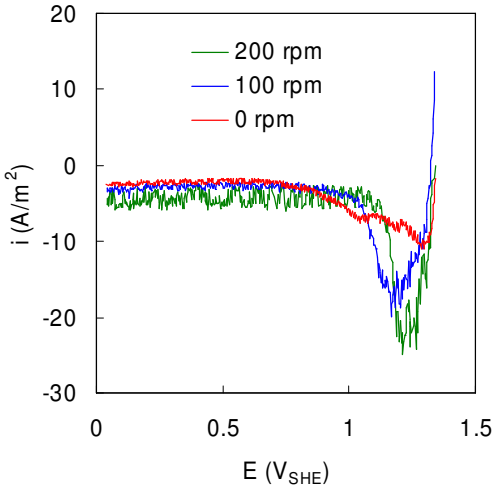

Figure 4.28 *Voltammograms of the cathodic dissolution of cobalt oxide films at different stirring rates. Linear scans at -1 mV/s sweep rate in Cl_2-containing $CoCl_2$ electrolyte at pH 1.6 and 60°C.*

The negative trend in cathodic current efficiency for cobalt with increasing stirring rate (Fig. 4.27 b)) is ascribed to enhanced transport of H^+ ions and dissolved Cl_2 to the cathode during electrolysis. Separate tests with a soluble cobalt metal anode instead of the Cl_2-producing DSA® showed the same trend, demonstrating the accelerating effect of forced convection on the rate of hydrogen evolution. By using a rotating disk electrode, Kongstein [65] showed that the H_2 evolution reaction during cobalt electrodeposition was controlled by both diffusion and electron transfer (mixed control). The degree of Cl_2 reduction is also dependent on the concentration of dissolved Cl_2 in the bulk solution, which may change with stirring rate. The cobalt metal produced at 0 rpm was somewhat darker, and a few white pits with vertical streaks were present on its surface.

Summary

When cobalt metal is produced by electrowinning from chloride solutions, a black substance precipitates on the DSA® anodes. This material, which contained ~60 % Co, was collected from anodes in the Xstrata Nikkelverk cobalt tankhouse and identified as α-CoOOH (heterogenite 3R). XRD analysis on thick films of cobalt oxide prepared in the laboratory indicated the same type of structure, but less crystalline.

Effects of key operating parameters on the cobalt electrowinning process were investigated by galvanostatic electrolysis in a three-electrode test cell. From SEM images it was apparent that the cobalt oxide film was growing all over the DSA® surface, although cracks were present and some flakes had peeled off. In most tests, one or two peaks were observed for the anode potential before it stabilized, and it is believed that these peaks represented the nucleation and growth of cobalt oxide in the time before the available electrode area for chlorine evolution became constant. Accordingly, freshly prepared cobalt oxide was a good electrocatalyst for chlorine evolution, and its electrical conductivity must have been relatively high. The growth of cobalt oxide seemed to take place at constant rates at conditions favouring this reaction. The electric charge applied for CoOOH deposition at the first potential peak was calculated to ~1 mC/cm^2, which is twice the quantity needed to form a monolayer of CoOOH on platinum [56]. However, at low pH or low current densities, the first potential peak appeared late compared to the total amount of cobalt oxide formed, which suggests slower initial rates of scaling on the clean DSA® surface compared to after it had been covered by cobalt oxide.

The anodic deposition of cobalt oxide was found to be highly dependent on several of the parameters investigated. At pH below 1 no anode deposit was detected, whereas at pH 2 precipitation occurred in the bulk solution as well as on the DSA®. Accelerated rates of anode scaling with increasing temperature and increasing current density, along with only minor influence of electrolyte stirring, demonstrated that the cobalt oxide formation was activation controlled. The Tafel slope for cobalt oxide formation was estimated to be 64 mV/dec at 60°C compared to 45 mV/dec for chlorine evolution, i.e. operating at high current densities was found advantageous in order to minimize the production of CoOOH versus Cl_2. Sulphate ions were present in the scale, and they were found to inhibit the growth of cobalt oxide, probably through adsorption. Finally, an insight into ionic activity

coefficients was essential in order to understand some of the trends observed for both the anodic and the cathodic reactions taking place in the electrowinning of cobalt.

4.2.2 Influence of anode material

Titanium electrodes coated with mixed oxides of various compositions supplied by Permascand AB were characterized and tested as anodes for cobalt electrowinning. Results from cobalt electrolysis experiments with either pure titanium metal without any noble metal oxide coating or graphite as anode material are also reported. Furthermore, effects of the thermal decomposition temperature were evaluated for Ru-Ir-Ti and Ir-Ta oxide coatings of fixed nominal composition. Details for the anode materials studied in the laboratory are summarized in Table 3.2.

The electrode characterization involved physico-chemical methods (scanning electron microscopy (SEM), x-ray diffraction (XRD)) and cyclic voltammetry (CV) in sulphuric acid. The experimental details are given in section 3.1.3.2. Galvanostatic electrolysis of cobalt was carried out at standard conditions (Table 4.2) from aqueous cobalt chloride electrolyte (for composition, see Table 3.1, March 2004), and the extent of cobalt oxide deposition on the various anode materials was determined by the chemical route (section 3.1.4).

4.2.2.1 Effects of anode composition

SEM examination

SEM micrographs of mixed oxide electrodes having different compositions are shown in Fig. 4.29 (all micrographs in this chapter have magnification 10 000×). The regular ternary oxide coating depicted in Fig. 4.29 a), Ti/RuO_2-IrO_2-TiO_2 (Ru:Ir molar ratio 2:1), had a compact surface morphology with crystallites of size ~500 nm. Some of these crystallites appeared as well developed pyramidal particles typical for the tetragonal rutile structure [160], and the element distribution from EDS analysis indicated that they were enriched with noble metals, mostly Ru but also Ir. Takasu et al. [161] prepared Ru-Ir-Ti oxide coatings on titanium by dipping in organic coating solution followed by heat treatment at 450°C. They also

obtained highly grown Ti-deficient crystallites (~200 nm) having the same characteristic planes, and separated by apparently flat areas composed of ultrafine Ti-rich particles being from 5 to 20 nm.

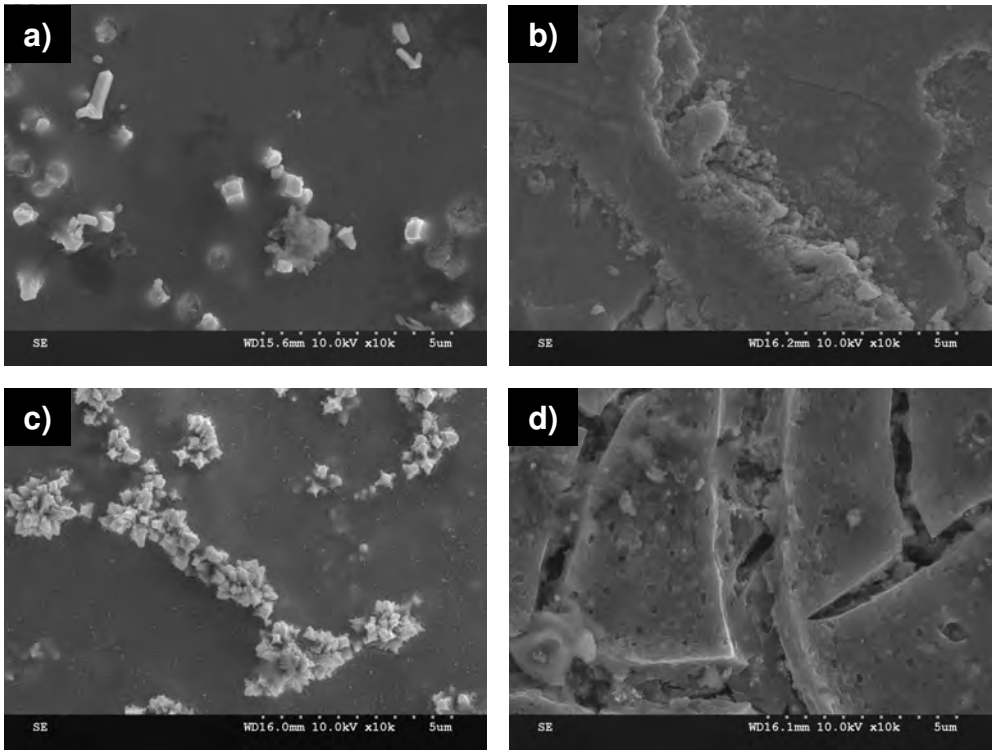

Figure 4.29 *SEM micrographs of the surface of mixed oxide electrodes. a) Reg, b) Reg* (used), c) Ir-Ru-Ti, d) Ru-Ti coatings.*

Originally, the Reg* electrode shown in Fig. 4.29 b) had a coating of regular composition (Ru-Ir-Ti, Ru:Ir molar ratio 2:1). However, after being exposed to various testing by Kongstein [65], of which the details are not known, its morphology was severely modified. Parts of the outer layer had peeled off so that the next layer of the coating emerged. This second layer consisted of fine particles enriched with ruthenium. It should be noted that SEM examination of regular electrodes after several experiments of cobalt electrolysis did not show any sign of surface modification. De Battisti et al. [162] performed depth profiling of Ru-Ti mixed oxides by means of Rutherford backscattering spectrometry and x-ray photoelectron spectroscopy with argon ion sputtering. Their results indicated the

occurrence of surface segregation of titanium, and the local ruthenium concentration was much lower at the surface compared to deeper into the coating. Kameyama et al. [163] also observed a surface content of RuO_2 that was lower than the nominal composition for Ti/RuO_2-IrO_2-TiO_2 electrodes, although the internal surface of pores and cracks was somewhat enriched with RuO_2.

Another version of the oxide coating containing ruthenium, iridium and titanium is shown in Fig. 4.29 c). Due to a Ru:Ir molar ratio of 1:1 compared to 2:1 in the regular coating, it was denoted as the Ir-Ru-Ti coating. From the micrograph it can be seen that the surface was heterogeneous, having chains of noble metal rich agglomerates of crystals distributed on a compact structure with few cracks. The crystals were smaller than those present in the regular coating.

The classic DSA® anode with layers of RuO_2-TiO_2 mixed oxide (30 mole-% Ru) supported on titanium was also studied (Fig. 4.29 d)). A typical "cracked mud" structure was demonstrated for this electrode. The cracks are believed to be generated from the thermal shock in the baking process, due to the difference in thermal expansion coefficient between the base metal and the coating [164]. Fine almost pure RuO_x crystallites were observed in the cracks, whereas the smooth islands surrounded by the cracks were dominated by TiO_x. Some of the cracks were quite deep and seemed to go through several of the individual layers of the coating.

XRD analysis

The mineralogical composition of the Ti-supported mixed oxide coatings and their degree of crystallinity were investigated by XRD. As illustrated in Fig. 4.30, the diffractograms are dominated by signals due to the underlying titanium substrate, along with common peaks of the tetragonal rutile structure, suggesting the presence of a solid solution of RuO_2, IrO_2 (if present) and TiO_2. Moreover, a shoulder appeared on the right side of the main rutile peaks at 2θ ~27.7 degrees, which may be attributed to noble metal rich crystals observed on the electrode surfaces by SEM (peak angles of pure phases: TiO_2 27.6, RuO_2 and IrO_2 28.1 degrees).

XRD results reported by Kameyama et al. [163] indicated that Ru-Ir-Ti oxide mixtures formed a three-component solid solution with rutile-type

structure. Due to almost identical structural parameters of RuO_2 and rutile TiO_2, these two components normally form films of solid solutions, which may coexist with the pure components [165]. Using transmission electron microscopy, Roginskaya and Morozova [36] found that Ru-Ti oxide layers prepared from aqueous chloride solutions were actually made up of nanometer-sized clusters of pure Ru and Ti oxide linked by chloride ions, aqua- and hydroxogroups.

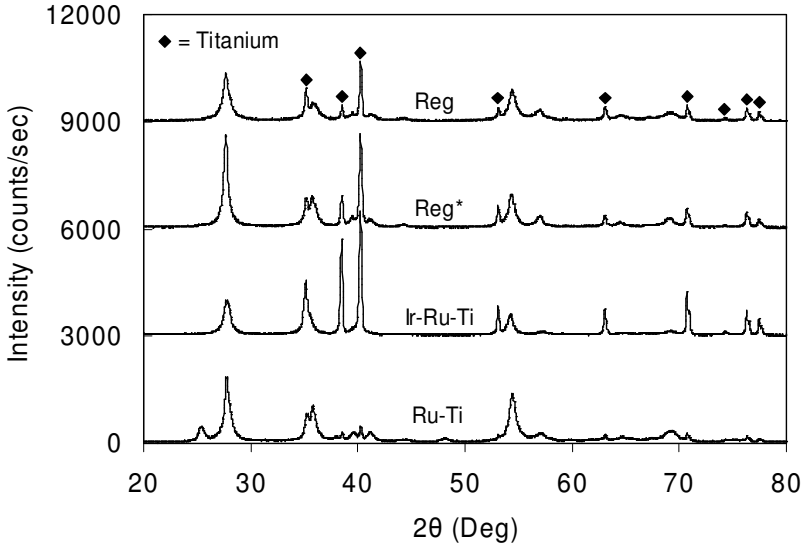

Figure 4.30 *XRD diagrams of mixed oxide electrodes. The peaks due to the titanium substrate are marked in the upper diagram (♦).*

From Fig. 4.30 it can be seen that the diffraction pattern of the worn Reg* electrode was more clearly defined than the unused Reg electrode. The Ir-Ru-Ti electrode showed small rutile peaks and sharp titanium peaks, in accordance with the low catalyst loading compared to the other electrodes. The rutile peak at ~35.8 degrees was also shifted towards lower peak angles and thus became part of the Ti signal, probably due to the higher iridium content in this coating. The Ru-Ti electrode gave well defined rutile peaks, while the lines corresponding to the titanium base had low intensities, suggesting a relatively high loading. Furthermore, the anatase form of titanium oxide was detected in this coating, with diffraction peaks at ~25.6 and ~48.5 degrees. A separate phase of anatase, which is the stable form of titanium oxide at low temperature, is typical for Ru-Ti mixed oxide coatings with 30 mole-% or less Ru [45]. The low temperature formation of rutile

TiO_2 seems to be catalyzed by the presence of ruthenium in the mixture, and at lower RuO_2 contents the part of TiO_2 exceeding that in the solid solution is present as anatase [165].

Cyclic voltammetry

Cyclic voltammetry (CV) is a very useful technique for in situ electrochemical characterization of metallic oxide electrode materials. By sweeping the electrode potential at a constant rate between hydrogen and oxygen evolution in acid or base, the active sites on the electrode will undergo solid-state surface redox transitions accompanied by proton exchange with the solution [42]:

$$MeO_x(OH)_y + \delta\ H^+ + \delta\ e^- = MeO_{x-\delta}(OH)_{y+\delta} \qquad (4.3)$$

where Me represents elements that change their oxidation state during CV, like Ru and Ir. Integration of the resulting voltammetric curve gives the voltammetric charge q*, which is proportional to the electrochemical active surface area, e.g. the number of active sites. Oxides of the valve metals, like titanium and tantalum, do not contribute to q* except for double layer charging, since the redox mechanism described by equation 4.3 is not operating for these inert oxides.

The voltammetric behaviour of the various types of mixed oxide coated electrodes studied in this work was recorded between 0.4 and 1.4 V_{SHE} in 0.5 M sulphuric acid at sweep rate 20 mV/s. Voltammograms obtained in the second cycle are shown in Fig. 4.31, and the calculated total q* values (sum of anodic q^*_a and cathodic $|q^*_c|$) are presented in Table 4.3. The shape of the voltammograms was typical of ruthenium-containing oxides [166]; a background current was spread over the entire potential range, and broad peaks appeared at ~0.8 V_{SHE}, ascribed to the $+3 \leftrightarrow +4$ redox reaction of Ru and Ir. The q^*_a:$|q^*_c|$ charge ratio was close to unity for all electrodes, which reflects a reversible charging/discharging process [167]. Compared to the range of q* values found in the literature, the results for these electrodes indicate rather compact coatings.

The voltammetric profile of an unused regular electrode (Fig. 4.31 a)) and the worn regular electrode (Fig. 4.31 b)) were similar in shape, but the voltammetric charge of the latter was higher (30 vs. 21 mC/cm^2). This activ-

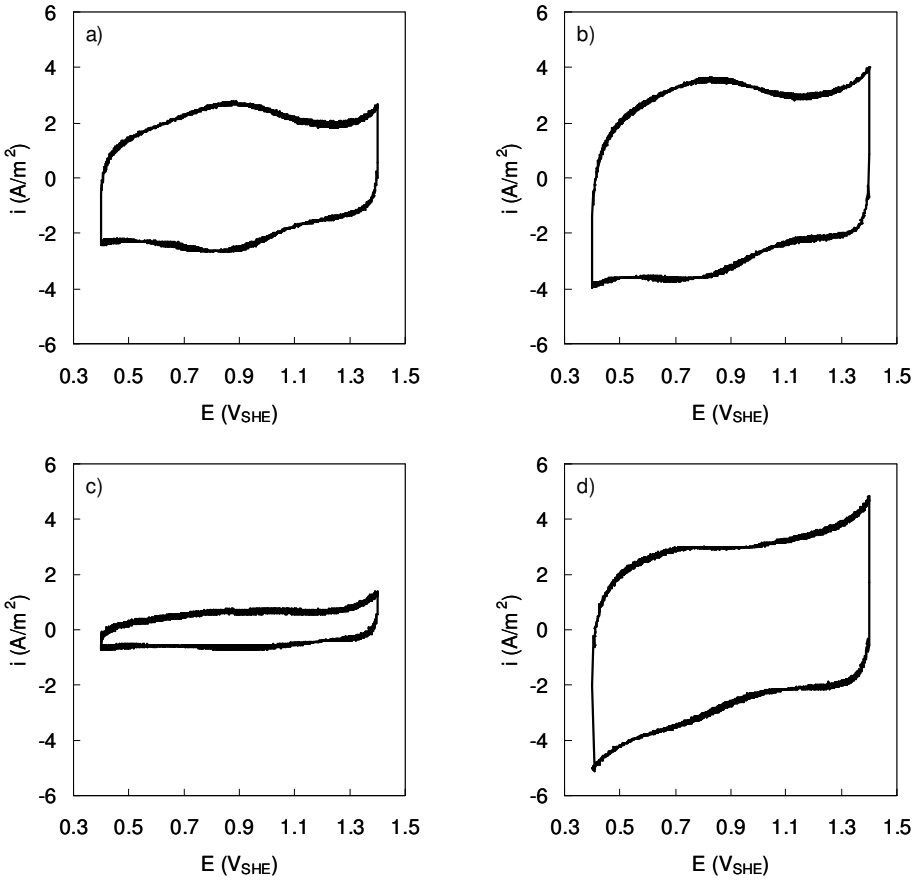

Figure 4.31 *Cyclic voltammograms of a) Reg, b) Reg*, c) Ir-Ru-Ti, d) Ru-Ti mixed oxide coatings in 0.5 M H_2SO_4. Scan rate 20 mV/s.*

ation of the worn electrode can be attributed to the partial detachment of the external coating layer as observed by SEM, resulting in Ru-rich fine particles in the second layer to become more involved in the redox reactions. A small q* of 6 mC/cm^2 was obtained for the Ir-Ru-Ti electrode (Fig. 4.31 c)), in agreement with the low intensities of the rutile peaks in XRD. The current peaks in CV were also less distinct and shifted to higher potentials for this coating (0.9-1 V_{SHE}), probably due to its higher iridium content. Kötz and Stucki [168] prepared Ru-Ir mixed oxides of varying Ru:Ir ratio by reactive sputtering, and they found a linear positive shift in both anodic and cathodic CV peak positions with increasing Ir content. The current response during CV with the Ru-Ti electrode (Fig. 4.31 d)) was higher than for the other unused electrodes (q* = 29 mC/cm^2), probably a result of the more cracked

surface. The relatively large cathodic current at low potentials in cathodic direction may be due to both hydrogen adsorption and further reduction of the oxide [169].

Galvanostatic electrolysis from cobalt chloride solution

In order to identify the different anode materials' abilities to generate cobalt oxide during cobalt electrowinning, galvanostatic electrolysis was performed at standard conditions from cobalt chloride solution. From the results summarized in Table 4.3 it is evident that for the titanium-based electrodes the current efficiency for CoOOH formation was approximately the same at ~0.2 %, except for the Reg* electrode which showed a current efficiency of only 2/3 of that value. On the other hand, graphite produced more than twice the amount of cobalt oxide formed on the other electrodes, even though its average anode potential was about 50 mV lower. Repetitive tests of a particular anode disk or another anode disk of the same anode material gave only minor differences in CoOOH formation. The small variation in cathodic current efficiency for cobalt indicates that the test conditions were similar.

Table 4.3 Performance of various anode materials in galvanostatic electrolysis from cobalt chloride solution. Voltammetric charges q* measured in sulphuric acid are also included.

Anode	q* (mC/cm^2)	E_{avg} (V_{SHE})	CE_{Co} (%)	CE_{CoOOH} (%)
Reg 1 [a]	21	1.48	94.7	0.18
Reg 2 [a]			94.9	0.18
Reg*	30	1.47	94.8	0.13
Reg* #2 [b]			95.0	0.12
Ir-Ru-Ti 1 [a]	6	1.48	94.7	0.19
Ir-Ru-Ti 2 [a]			95.0	0.21
Ru-Ti 1 [a]	29	1.47	94.8	0.20
Ru-Ti 1 #2 [b]			94.8	0.21
Ru-Ti 2 [a]			95.0	0.20
Ti	~0 [144]	1.46	94.9	0.20
Graphite 1 [a]	-	1.42	94.9	0.41
Graphite 2 [a]			94.9	0.47

[a] 1 and 2 indicate two different disks of the same anode material.

[b] #2 indicates a second test of the same anode disk.

When an electrode has become fully covered by cobalt oxide, the influence of the underlying anode material seems to be of less importance, since most of the reactions will then take place on the anode deposit. This view is supported by the fact that the steady-state anode potentials were similar for the different anode materials, see Fig. 4.32. In the first half of the experiment, the worn Reg* electrode operated at a lower potential than the regular electrode, and no potential peak was recorded. It is believed that the depolarization was caused by the high density of fine Ru-rich crystallites present on the Reg* electrode, which may facilitate chlorine evolution in preference to nucleation and growth of cobalt oxide. The Ru-Ti electrode exhibited a broader initial peak in potential compared to the regular electrode (see Figs. 4.32 a) and d)), which may be due to a larger number of active sites.

According to Figs. 4.32 e) and f), both the titanium and the graphite electrodes experienced high initial potentials. However, as electrolysis proceeded, the electrodes became activated by the increasing amount of cobalt oxide catalyst growing on the anode surface. For the titanium electrode this behaviour was surprising, since it was expected that it would passivate by the build-up of an insulating film of stoichiometric TiO_2 on the surface. Boggio et al. [170] studied Ti/Co_3O_4 electrodes prepared by thermal decomposition of $Co(NO_3)_2$, and a RuO_2 interlayer was introduced to avoid passivation in e.g. sodium chloride solution. They claimed that the porous Ti/Co_3O_4 electrodes prepared at low temperatures became passivated because Co_3O_4 was not able to protect the titanium support, since it does not form a solid solution with TiO_2. On the other hand, a thin film of electrodeposited cobalt oxide between the titanium base and the mixed metal oxide coating has been suggested as a means of increasing the service life of oxygen-evolving DSA®'s [171]. In this case the cobalt oxide works as a barrier layer, which prevents the diffusion of oxygen to the underlying substrate. It should also be mentioned that titanium anodes are used in the electrolytic production of battery-grade manganese dioxide. By operating at low current density (~100 A/m^2), low acid concentration (~50 g/l H_2SO_4) and high temperature (~100°C), a coherent compact layer of hydrous γ-MnO_2 is formed that retards passivation [49, 172].

The performance of titanium as an anode material was evaluated further by performing a couple of additional electrowinning tests in an alternative test cell equipped with larger electrodes (2 dm^2). When using gently ground titanium plates in cobalt chloride electrolyte, cobalt oxide was deposited

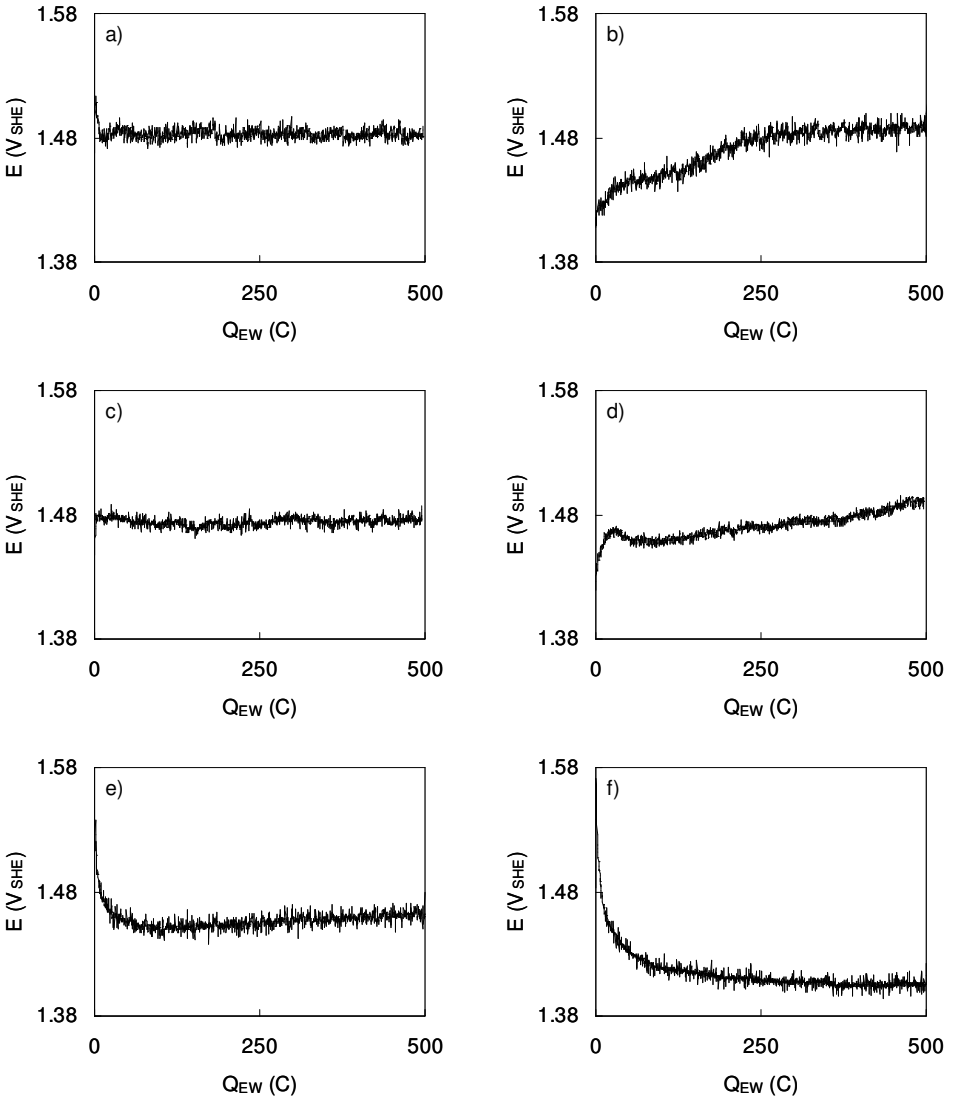

Figure 4.32 *Anode potential vs. total electric charge applied for different anode materials, during galvanostatic electrolysis from aqueous $CoCl_2$ solution. a) Reg, b) Reg*, c) Ir-Ru-Ti, d) Ru-Ti, e) titanium, f) graphite.*

evenly on the titanium surface, and chlorine gas was evolved at a stable cell voltage for the five hour duration of the test. Switching to untreated titanium, chlorine gas was still produced, but cobalt oxide was not covering the entire surface, which is an indication of uneven current distribution. In a third test,

titanium plates were heat-treated in air at 800°C for one hour to oxidize the titanium surface. Cobalt electrowinning using these plates as anodes resulted in an initial cell voltage of ~12 V, which dropped and stabilized at ~9 V. No appreciable amounts of chlorine seemed to be generated, and inspection of the anodes after the test revealed that they were severely attacked by pitting corrosion. Titanium had dissolved from the anodes and precipitated in the bulk electrolyte in the form of fine white particles.

These tests demonstrate that the form of cobalt oxide deposited anodically during cobalt electrowinning protects, at least in the short term, a titanium anode from becoming passivated. However, if a titanium oxide layer above a certain thickness is present on the surface already at the beginning of electrolysis, cobalt ions in solution are not capable of increasing the electrical conductivity of this insulating TiO_2 film to avoid the titanium from reaching its breakdown potential, after which the metal starts to dissolve. Passivation of non-pretreated titanium anodes during laboratory-scale cobalt electrowinning experiments has been reported in the literature [173]. From the results above, these titanium anodes could have been covered by a too thick oxide film initially, or titanium covered by cobalt oxide may be less resistant to passivation when producing oxygen from sulphate solution.

The reason why graphite produced more cobalt oxide than the other electrodes is not fully understood. Unimpregnated graphite is porous, and electrolyte may percolate through this type of material [174]. Moisture was actually observed on the back side of the graphite disks after testing, and increased levels of chloride were measured in the etching solution, which suggests contamination by cobalt chloride electrolyte. This part of the cobalt content was, however, excluded when calculating the amount of cobalt oxide formed. One explanation could be that the pores in the graphite were filled by cobalt electrolyte prior to electrolysis, which was then partly converted to cobalt oxide during the first phase of electrolysis when the anode potential was high. In addition, the low potential obtained as electrolysis proceeded suggests improved electrode conductivity or a highly porous anode deposit. A low local current density has been shown to facilitate cobalt oxide growth vs. chlorine evolution, as long as it is above a certain lower limit and the surface has been covered by cobalt oxide (see section 4.2.1.7). Finally, Vaaler [174] referred to studies where only 100 mg/l cobalt added to the anolyte or incorporated in the graphite anode resulted in 0.1 V reduction in anode potential in a chlor-alkali diaphragm cell. A 20 % decrease in anode

consumption rate was also claimed, while current efficiency for chlorine appeared to be somewhat reduced.

4.2.2.2 Effects of thermal decomposition temperature

At the 206th Meeting of The Electrochemical Society in Honolulu, October 2004, the author attended a presentation given by a Japanese group on the inhibition of lead dioxide formation on insoluble anodes for copper foil production [175]. By decreasing the thermal decomposition to below 400°C in the preparation of the Ti/IrO_2-Ta_2O_5 electrodes, a less crystalline structure was formed. The anodic deposition of PbO_2 was inhibited on these low-temperature anodes due to an increase in the PbO_2 nucleaction overpotential, caused by the mismatch between the amorphous coating and crystalline PbO_2.

Inspired by the interesting results obtained by the Japanese group, the author was able to convince people at Permascand AB that this concept should be tested in the electrowinning of cobalt. It was decided to study the effects of decomposition temperatures of 350, 400, 450 and 500°C for two different oxide compositions supported on titanium; i.e. the ternary Ru-Ir-Ti mixed oxide of regular composition (Ru:Ir molar ratio 2:1), and the binary Ir-Ta mixed oxide (70 mole-% Ir) like the Japanese group. After receiving the electrodes from Permascand, they were characterized and tested as anodes for cobalt electrowinning with the main focus on the deposition of cobalt oxide.

SEM examination

Figs. 4.33 and 4.34 show SEM micrographs of the Ru-Ir-Ti and the Ir-Ta electrodes prepared at different temperatures. The surface of the Ru-Ir-Ti oxide coating prepared at 500°C consisted of some cracked and some compact areas having irregular-shaped agglomerates enriched with noble metal oxides (Fig. 4.33 a)). Separate cracks that did not follow those in the external coating layer were observed in the underlying layer. EDS analysis indicated higher levels of noble metals within the cracks, and by using large magnification, a high density of small particles (< 100 nm) was detected. The microstructure differed considerably from the regular coating fired at similar temperature (Fig. 4.29 a)), which is explained by the different

techniques used for the application of coating solution (brushing vs. electrostatic spray) combined with post heat treatment only for the latter electrode.

Lower baking temperatures of 450 and 400℃ did not result in extensive modifications of the morphology, apart from an increased number of wider and deeper cracks (Figs. 4.33 b) and c)). Some parts of the 400℃ coating were covered by crystals (not shown). However, at 350℃ the Ru-Ir-Ti electrode had a more rounded-shaped appearance, and the islands separated by cracks were less smooth (Fig. 4.33 d)). No crystallites were detected on the surface, but segregation of ruthenium and iridium in the cracks was still indicated by EDS. This coating also contained 2-3 % of residual chlorine originating from the metal chloride precursors.

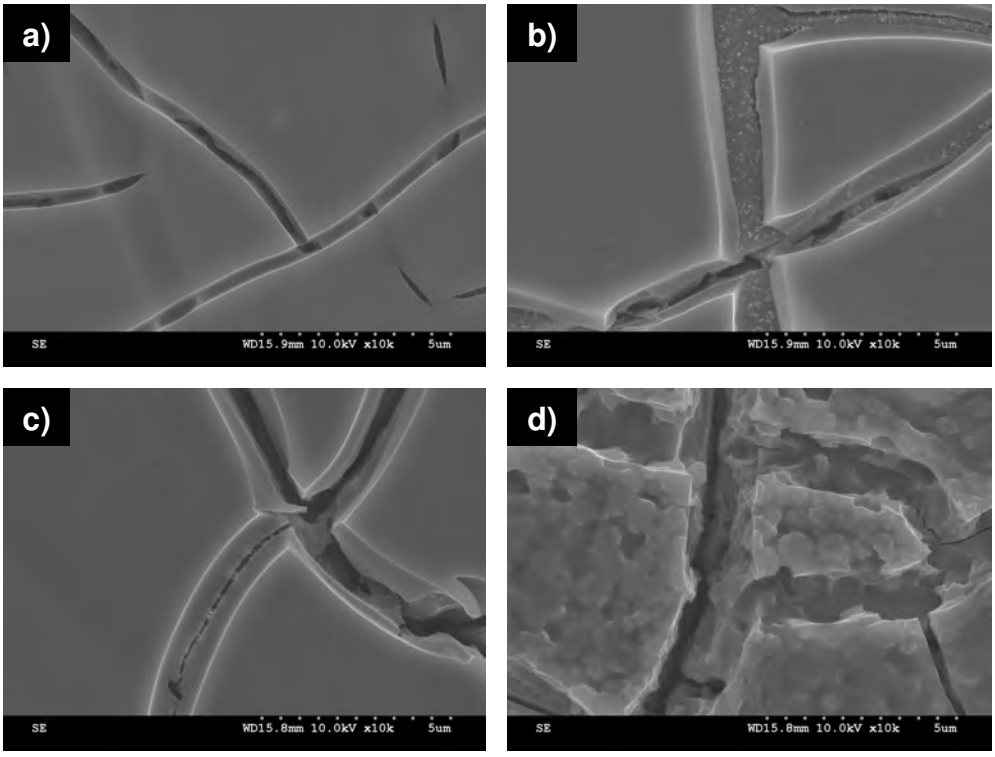

Figure 4.33 *SEM micrographs of Ru-Ir-Ti oxide coatings prepared at different decomposition temperatures. a) 500°C, b) 450°C, c) 400°C, d) 350°C.*

The Ir-Ta mixed oxide coatings thermally decomposed at 500 and 450°C were heterogeneous structures, consisting of agglomerates of IrO_2 needle crystallites distributed on a rather compact tantalum-rich surface, which contained some smaller cracks (Figs. 4.34 a) and b)). A SEM image of an almost identical surface morphology for the same type of coating on titanium has been reported earlier by Comninellis and Vercesi [176]. The crystallization is attributed to epitaxial growth of pure stoichiometric rutile IrO_2 on the isomorphous rutile TiO_2 sites, and a rough substrate in combination with an organic coating solution are required to generate these crystals [164].

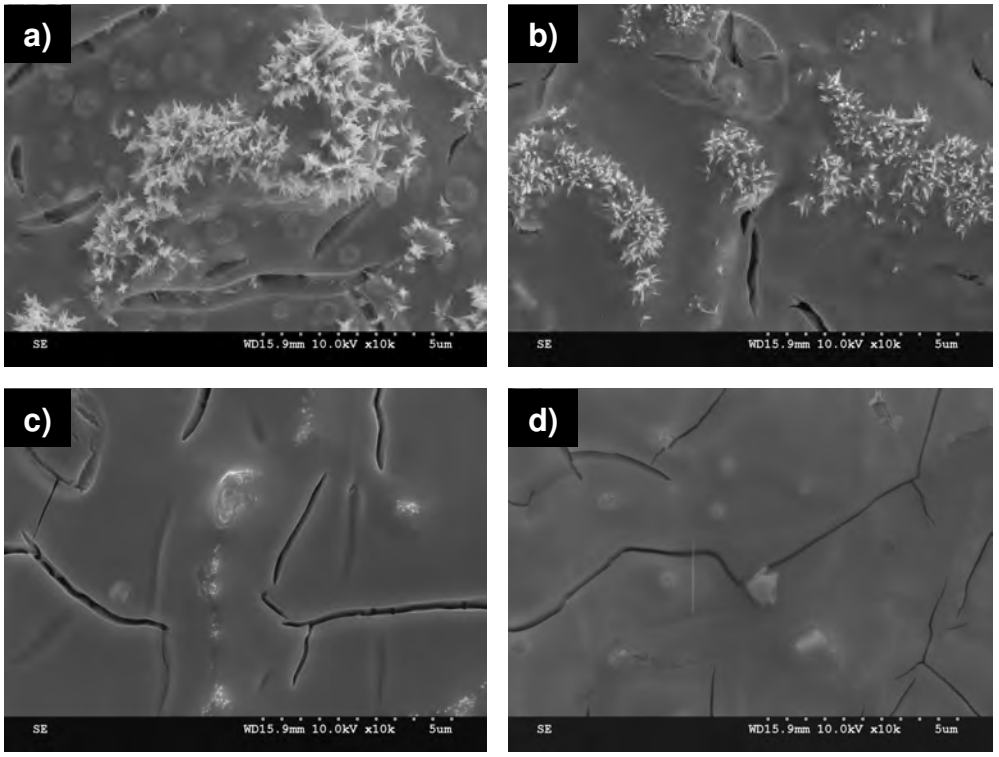

Figure 4.34 *SEM micrographs of Ir-Ta oxide coatings prepared at a) 500°C, b) 450°C, c) 400°C, d) 350°C.*

When fired at 400°C less crystal agglomerates were observed on the Ir-Ta electrode surface (Fig. 4.34 c)). At large magnification it was revealed that they were still made up of needle-like IrO_2 crystallites, though much smaller. Both open and closed cracks could be seen.

The lowest baking temperature of 350°C seemed to be too low for proper oxidation of the Ir-Ta type of coating, in accordance with Vercesi et al. [164]. No defined crystallites appeared (Fig. 4.34 d)), and high concentrations of chlorine and carbon were identified by EDS. During SEM investigation it was also difficult to focus due to problems with charging, which indicates low electrical conductivity of the poorly decomposed coating layer. The residual chlorine originated from the chloride precursors, while the source of the carbon is more unclear. It has, however, been reported that the precursors can form organometallic complexes with the organic solvent [38]. If the high levels of chlorine and organic material were accumulated in the coating layer during preparation, the higher catalyst loading given for this electrode in Table 3.2 may be too high, since it was based on weight increase measurements.

XRD analysis

Diffraction patterns of the Ru-Ir-Ti and the Ir-Ta electrodes prepared at different temperatures are given in Figs. 4.35 and 4.36 respectively. For both types of coating the rutile peaks became lower and broader with decreasing decomposition temperature, indicating reduced crystallinity. The diffractogram of the regular electrode was included in Fig. 4.35 for comparison. It is evident that the regular coating had a more ordered structure than the Ru-Ir-Ti coating calcined at 500°C, probably due to the different procedures used for coating application and annealing. This fact in combination with fewer coating layers may explain why some of the titanium oxide was separated into a second anatase phase in the Ru-Ir-Ti coatings but not in the regular coating. Small rutile peaks appeared for the Ru-Ir-Ti oxide mixture even at the lowest firing temperature of 350°C.

The Ir-Ta electrodes prepared at 500 and 450°C showed diffraction peaks from the titanium substrate and a pure IrO_2 rutile phase only. No tantalum peaks were detected, reflecting an amorphous structure of tantalum oxide. According to Vercesi et al. [164], higher temperatures (≥ 750°C) are needed to obtain crystalline Ta_2O_5, which does not form a solid solution with IrO_2. On the other hand, Roginskaya and Morozova [36] have found that up to three individual rutile phases may coexist in Ir-Ta mixed oxide coatings (IrO_2 and two solid solutions), the number of phases being dependent on the type of iridium precursor ($Ir(III)Cl_3$ or $H_2Ir(IV)Cl_6$).

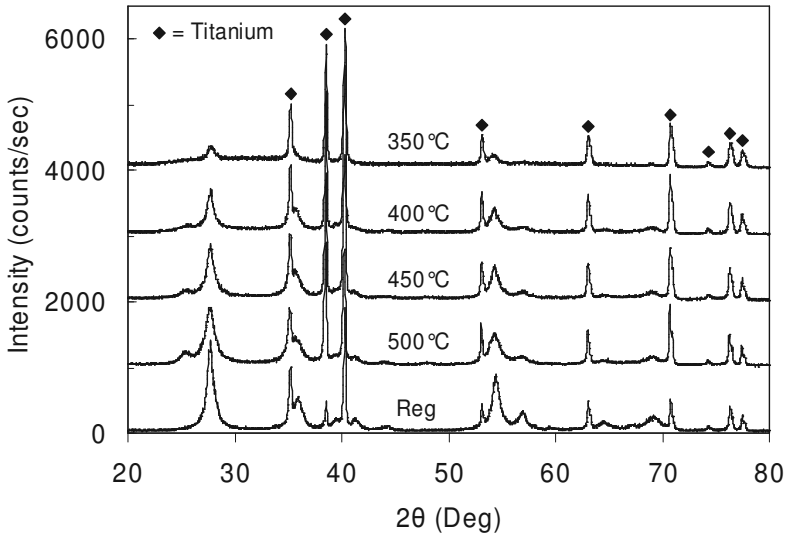

Figure 4.35 *XRD diagrams of the regular coating and Ru-Ir-Ti coatings prepared at different temperatures.*

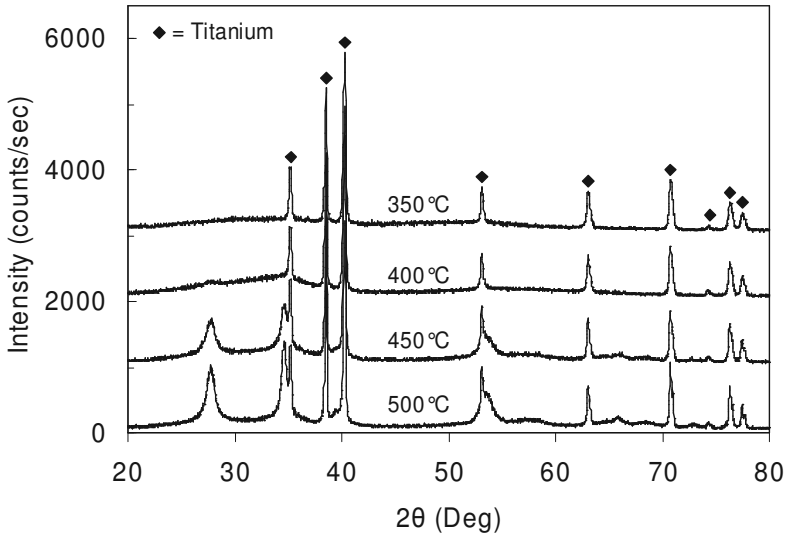

Figure 4.36 *XRD diagrams of Ir-Ta coatings prepared at different temperatures.*

When thermal decomposition was carried out at 400°C, the IrO_2 signals appeared as broad waves, while at 350°C only lines from the titanium base

were present. The absence of iridium peaks indicates an amorphous phase or incomplete decomposition of the coating solution at these low temperatures. It has been shown by thermogravimetric analysis that a higher temperature is required to oxidize $IrCl_3$ than $RuCl_3$ [177]. No rutile peaks were obtained in the XRD pattern of the Ir-Ta coating prepared at 350°C by Vercesi et al. [164] using the H_2IrCl_6 precursor, whereas Lodi et al. [40] produced a powder of crystalline rutile IrO_2 by decomposition of pure $IrCl_3$ at the same temperature. This shows how even minor changes in procedures can have profound effects on the degree of conversion of precursors into defined oxide structures at low temperatures.

Cyclic voltammetry

The effect of the thermal decomposition temperature on the electrochemical active surface area was investigated by cyclic voltammetry in sulphuric acid solution. Voltammograms of the Ru-Ir-Ti electrodes are shown in Fig. 4.37 a). Their shape resembled those recorded with the Reg and Reg* electrodes (Figs. 4.31 a) and b)), and the calculated voltammetric charge q* increased exponentially with decreasing baking temperature, from 27 mC/cm^2 at 500°C to 293 mC/cm^2 at 350°C. Such a trend in q* is typical for thermally decomposed conductive oxides, attributed to more extensive crystallization and sintering at high temperatures [178]. The increasing anodic current at

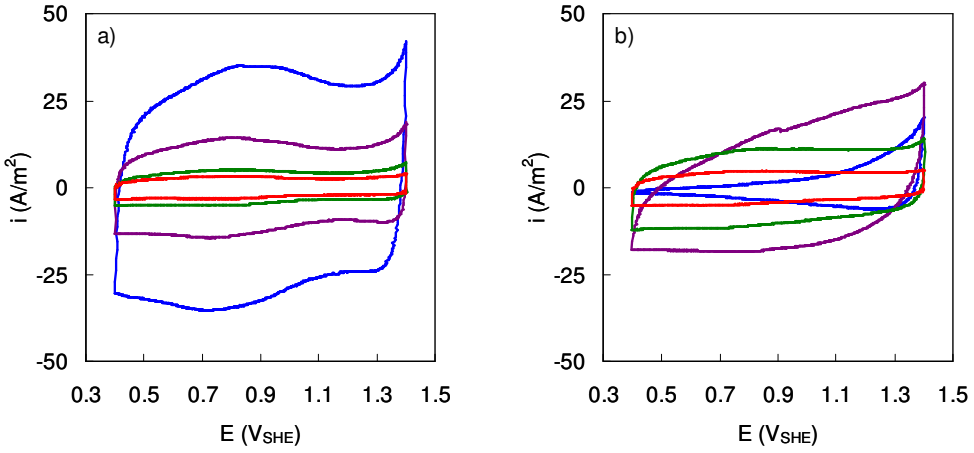

Figure 4.37 *Cyclic voltammograms of a) Ru-Ir-Ti and b) Ir-Ta mixed oxide electrodes prepared at different temperatures.*
Red curves: 500°C, green: 450°C, purple: 400°C, blue 350°C.

high potentials for the lower temperature Ru-Ir-Ti coatings was probably due to oxygen evolution [179], i.e. reduced preparation temperature resulted in improved electrocatalytic activity for this reaction.

As shown in Fig. 4.37 b), the voltammetric curves obtained with the Ir-Ta electrodes were featureless with no distinct current peaks, characteristic of ruthenium-free iridium oxide coatings [180]. When the firing temperature was reduced from 500 to 400°C, the voltammetric charge increased linearly from 41 to 153 mC/cm^2. However, a further lowering of the temperature to 350°C resulted in a drop in q* to 38 mC/cm^2. This fact together with the different shape of the voltammogram suggest an incomplete decomposition of the coating solution at 350°C, in line with the SEM examination.

Galvanostatic electrolysis from cobalt chloride solution

The Ti-supported mixed oxide electrodes prepared at different decomposition temperatures were evaluated as anodes for cobalt electrowinning by performing electrolysis experiments in the laboratory cell (Fig. 3.1) at standard conditions (Table 4.2). Key results are summarized in Table 4.4, and they show a remarkable decrease in the extent of anodic deposition of cobalt oxide for the majority of the electrodes. A current efficiency of 0.008 % represents only ~4 % of the amount of deposit produced on regular anodes at similar conditions. Moreover, the CE_{CoOOH} data in Table 4.4 are based exclusively on the cobalt content in the etching solutions, due to scatter in the chloride analyses at low concentrations. This means that some or all of the cobalt in the etching solutions could have been due to contamination by electrolyte trapped in cracks and pores of the coatings. Consequently, anode scaling was possibly totally inhibited on those electrodes in Table 4.4 reported with less than 0.01 % current efficiency.

The Ru-Ir-Ti electrode calcined at 500°C showed an increase in anode potential with electrolysis time, as opposed to the other electrodes, which operated at lower and more stable potentials. After electrolysis with the Ru-Ir-Ti mixed oxide electrodes, precipitates were seen only on the coating prepared at 500°C. For the Ir-Ta electrodes, a few small yellow-brown particles were observed at the centre of the 500°C coating, and some dark material was also formed on both of the 350°C anode disks tested. The other Ir-Ta electrodes appeared to be free of deposit. After cleaning of Ir-Ta 350°C

electrodes in etching solution, there was apparently no coating left on the exposed part of the electrodes. The fact that this coating was unstable is understandable from the incomplete oxidation of coating agents, as revealed by SEM and CV. Some of the other electrodes had become somewhat darker in colour after electrolysis and etching. According to X-ray fluorescence analysis, there were no traces of any remaining cobalt on the surface of these electrodes.

Table 4.4 Performance of Ru-Ir-Ti and Ir-Ta mixed oxide electrodes prepared at different temperatures, in galvanostatic electrolysis from cobalt chloride solution. Voltammetric charges are also included.

Coating	T_{decomp} (°C)	q* (mC/cm^2)	E_{avg} (V_{SHE})	E_{Co} (%)	E_{CoOOH} (%)
Ru-Ir-Ti	350°C	293	1.41	94.9	0.007
	400°C	119	1.42	94.7	0.007
	400°C #2 [a]			94.8	0.007
	450°C	43	1.42	94.8	0.008
	500°C 1 [b]	27	1.45	94.9	0.082
	500°C 2 [b]			94.8	0.086
Ir-Ta	350°C 1 [b]	38	1.43	94.9	0.021
	350°C 2 [b]			94.8	0.022
	400°C	153	1.44	94.8	0.007
	450°C 1 [b]	96	1.42	95.0	0.006
	450°C 2 [b]			94.8	0.006
	500°C 1 [b]	41	1.43	95.0	0.011
	500°C 2 [b]			94.8	0.008

[a] #2 indicates a second test of the same anode disk.

[b] 1 and 2 indicate two different unused disks of the same anode material.

Several factors may have played a role in the suppression of cobalt oxide deposition on mixed oxide electrodes prepared at reduced temperatures. The observed depolarization of chlorine evolution from increased active surface area should reduce the extent of Co^{2+} oxidation. Higher nucleation overpotentials of CoOOH on the less crystalline low-temperature coatings may also be involved. However, reduced rates of anode scaling were obtained even for coatings having highly grown crystallites distributed on the surface, e.g. the Ir-Ta 450°C electrode (Fig. 4.34 b)). It is believed that the degree of coating crystallinity will have less effect on the nucleation of

α-CoOOH with hexagonal structure than for instance PbO_2, which has the same tetragonal rutile structure as the coating. In addition, XRD analysis indicated a less ordered symmetry for thin films of cobalt oxide on DSA® (Fig. 4.2), suggesting that the coating crystallinity should have less influence on the nucleation process. On the other hand, a coating made up of smaller crystallites may retard the nucleation and growth of cobalt oxide to some extent, since the solubility of hydrous metal oxide nuclei increases with decreasing particle size, see section 2.1.1. Stable CoOOH nuclei were formed on the regular coating at lower potentials than recorded for any of the electrodes given in Table 4.4, but those experiments carried out at low current densities continued for much longer time, see section 4.2.1.7.

During etching a varying degree of gas evolution was observed on the surface of the different electrodes. The formation of bubbles stopped after a couple of seconds when the regular coating or the other compact coatings were cleaned, whereas the Ru-Ir-Ti and Ir-Ta electrodes characterized by high voltammetric charge continued to evolve gas for the whole etching period. The initial gas formation was due to reduction and dissolution of cobalt oxide by reaction with hydrogen peroxide present in the etching solution, while the continued gassing is attributed to catalytic decomposition of H_2O_2. Trasatti and Lodi [165] referred to studies where high temperature RuO_2 oxides were actually found inactive for H_2O_2 decomposition, related to low surface density of active sites.

The promising results obtained in the laboratory encouraged further long-term testing of full-scale electrodes prepared at reduced temperatures. Compared to regular anodes, the formation of cobalt oxide was moderately suppressed on coatings applied by brushing and then fired at low temperature, while the coatings applied by electrostatic spray produced similar amounts of scale as the regular anodes during one month of operation in the Xstrata Nikkelverk cobalt tankhouse. However, during the first day of operation the rate of cobalt oxide growth was suppressed on all types of low-temperature coatings tested. It was confirmed by XRD that the coatings applied by brushing were less crystalline than the coatings applied by electrostatic spray. Furthermore, increased levels of coating peeled off together with cobalt oxide during operation, and the low temperature coatings were also less stable in etching solution.

The long-term results confirm the importance of coating crystallinity with respect to nucleation and growth of cobalt oxide. When the anode surface

has been fully covered by a layer of anode scale, it also seems like the structure of the underlying mixed oxide coating has little influence on the deposition rate, since the anode is then probably working as a cobalt oxide anode, and cobalt oxide is growing on cobalt oxide. This means that over time total inhibition of CoOOH deposition is preferred to control anode scaling. Electrode geometry with areas of high local current density, variations in coating thickness, masking by impurities in the electrolyte or just long enough electrolysis duration to pass the long induction period are factors that may have initiated cobalt oxide deposition on the low-temperature coatings. Finally, the adhesion of the coating to the titanium substrate must be improved for such anodes to be of practical interest.

Summary

The extent of cobalt oxide deposition on alternative anode materials for cobalt electrowinning was investigated. Titanium-supported Ru-Ir-Ti and Ru-Ti oxide coatings prepared by electrolytic spray and decomposition at normal temperature (~500°C) produced similar amounts of cobalt oxide from cobalt chloride electrolyte. These coatings were heterogeneous with noble metal rich crystallites and a relatively low electrochemically active surface area. A worn Ru-Ir-Ti electrode, where parts of the external coating layer were absent, operated at a lower initial potential, and less cobalt oxide was formed. The second coating layer had a higher density of small ruthenium-rich particles.

Titanium and graphite showed high anode potentials in the beginning of electrolysis, but the build-up of cobalt oxide resulted in depolarization of chlorine evolution. The nature of the cobalt oxide deposited seemed to protect the underlying titanium from passivation. While the amount of cobalt oxide produced on titanium was similar to the regular Ru-Ir-Ti oxide coating, graphite produced more than twice as much cobalt oxide. Percolation of cobalt electrolyte through the graphite disk was observed, and it is believed that some of the cobalt oxide was generated inside this porous material.

Ru-Ir-Ti and Ir-Ta mixed oxide coatings of constant nominal composition were prepared by applying the coating solution by brushing and firing at different temperatures ranging from 350 to 500°C. The coatings became less crystalline and the active surface area increased when the temperature was

lowered, except for the Ir-Ta 350°C coating which was not completely converted into oxide. The formation of cobalt oxide was extensively suppressed on the low-temperature coatings, either due to their higher activity for chlorine evolution, or possibly increased nucleation overpotential for cobalt oxide, or a combination of both factors.

4.2.3 Addition of hydrogen peroxide to the electrolyte

4.2.3.1 Hydrogen peroxide in metal electrowinning

The use of hydrogen peroxide (H_2O_2) in the electrolyte has been suggested for the electrowinning of zinc from acidic sulphate solutions. According to Dominguez and Makwana [181], the addition of ~2 kg H_2O_2 per ton of zinc produced results in less manganese dioxide sludge being generated, improved current efficiency for zinc, lower levels of lead in the zinc product and decreased anode overpotential. By introducing between 0.9 and 3.57 g H_2O_2/h to 1 litre of 2 M sulphuric acid at 35°C containing 10 g/l Mn^{2+}, Nijjer [49] avoided build-up of MnO_2 deposit on a Ti/IrO_2-Ta_2O_5 electrode operated at 500 A/m^2 for 100 hours. Anode depolarization in the range of 500-700 mV was obtained. At the highest H_2O_2 addition, large sections of the coating fell off the electrode, and the electrolyte became yellow. The exfoliation of the coating was attributed to dissolution of the titanium substrate by H_2O_2 forming yellow titanium peroxide complexes. According to Schmets et al. [182], titanium and TiO_2 will corrode in acid solutions in the presence of H_2O_2 with the formation of orange pertitanyl ions TiO_2^{2+}.

To eliminate pitting of cathodes from adhering hydrogen bubbles, H_2O_2 in the electrolyte has also been suggested for nickel electrowinning [151]. It was supposed that H_2O_2 reacted with adsorbed hydrogen intermediates on the cathode surface forming water, although the true mechanism is not well understood [117].

Kongstein [65] studied the influence of H_2O_2 on the cobalt electrowinning process from chloride solutions. He used the same laboratory test cell as used in the present work, and the test conditions were similar, except for a lower current density (230 A/m^2) and less charge applied (~200 C). When 0.054 g/l H_2O_2 was added to the electrolyte prior to electrolysis, the quantity of cobalt oxide formed on the Ti/RuO_2-IrO_2-TiO_2 electrode dropped to less than half. After electrolysis with higher H_2O_2 concentrations of 0.17 and

0.22 g/l, no deposit was seen on the anode surface. Furthermore, a small decrease was observed in the anode potential with H_2O_2 in the electrolyte. No changes were detected in the plated cobalt metal or cathodic current efficiency when cobalt was deposited from an electrolyte containing 0.22 g/l H_2O_2 and using a soluble cobalt anode. From the experiments carried out by Kongstein [65], it was not possible to tell if H_2O_2 resulted in suppression of the cobalt oxide deposition reaction, or if cobalt oxide was redissolved by H_2O_2.

4.2.3.2 Chemistry of hydrogen peroxide

According to Pourbaix and de Zoubov [183], hydrogen peroxide has both oxidizing and reducing properties. It can act as an oxidizing agent with the formation of water:

$$H_2O_2 + 2\,H^+ + 2\,e^- = 2\,H_2O \qquad E° = 1.77\ V_{SHE} \tag{4.4}$$

or it can act as a reducing agent with the formation of oxygen:

$$H_2O_2 = O_2 + 2\,H^+ + 2\,e^- \qquad E° = 0.68\ V_{SHE} \tag{4.5}$$

From equations 4.4 and 4.5 it can be seen that H_2O_2 has a domain of double instability for standard electrode potentials between 0.68 and 1.77 V_{SHE}, where it can decompose into oxygen and water:

$$2\,H_2O_2 = O_2 + 2\,H_2O \tag{4.6}$$

The decomposition of H_2O_2 is catalyzed in the presence of transition metal ions, particularly at elevated temperatures. Cobalt has been shown to be a much more effective catalyst than nickel in the decomposition of peroxides [78].

Although H_2O_2 is a strong oxidizing agent it cannot be used efficiently to oxidize cobalt under acidic conditions [78]. Even at pH 6.5 only about 75 % conversion of the cobalt to CoOOH takes place. On the other hand, in more acidic solutions H_2O_2 becomes an effective reducing agent for Co(III), e.g. CoOOH:

$$2\,CoOOH + H_2O_2 + 4\,H^+ = 2\,Co^{2+} + O_2 + 4\,H_2O \tag{4.7}$$

In the present work, H_2O_2 was used as a reductant in the acidic etching solution to accelerate the dissolution of cobalt oxide deposits.

4.2.3.3 Electrolysis from cobalt chloride solutions containing hydrogen peroxide

The effects of H_2O_2 were investigated in the laboratory cell by performing two galvanostatic electrolysis experiments at the standard test conditions given in Table 4.2. In the first experiment, H_2O_2 corresponding to 0.26 g/l was added to the preheated electrolyte a couple of minutes before electrolysis was started. At the end of electrolysis, the electrodes were removed from the cell and immediately immersed in water. The quantity of cobalt oxide formed on the DSA® anode was then determined using the chemical route described in section 3.4. The second experiment was carried out in the same electrolyte after adding the same quantity of H_2O_2. However, in this test the anode stayed in the cell at open circuit potential (OCP) for 5 minutes after electrolysis.

The results in Table 4.5 show that the presence of H_2O_2 in the electrolyte suppressed the anodic cobalt oxide deposition, although some deposit was still produced. As shown in Fig. 4.38 a), the nucleation and growth of cobalt oxide appeared as a peak in the anode potential. This potential peak was broader with H_2O_2, which indicates reduced rates of cobalt oxide deposition.

Table 4.5 Summary of results from cobalt electrolysis experiments with and without H_2O_2 in the electrolyte.

H_2O_2 conc. (g/l)	Time at OCP (min)	ΔpH *	E_{avg} (V_{SHE})	CE_{Co} (%)	CE_{CoOOH} (%)
0	0	~0	1.48	95	0.18
0.26	0	-0.07	1.48	n.a.	0.07
> 0.26	5		1.49	90	0

* Change in electrolyte pH measured at room temperature. The result for the experiments with H_2O_2 represents the total change in pH from the start of the first experiment until the second experiment was finished.

When the anode was kept in the electrolyte at OCP after electrolysis, no cobalt oxide was detected. It was observed that the OCP was declining rapidly within the first minute before levelling out at ~0.8 V_{SHE} (Fig. 4.38

b)). The anode deposit was probably dissolved by remaining H_2O_2 according to equation 4.7, and the OCP was then controlled by the interaction between H_2O_2 and the DSA® noble metal oxides (equation 4.5), as opposed to the usual Co^{2+}/Co^{3+} and Cl^-/Cl_2 redox couples operating when no H_2O_2 was present.

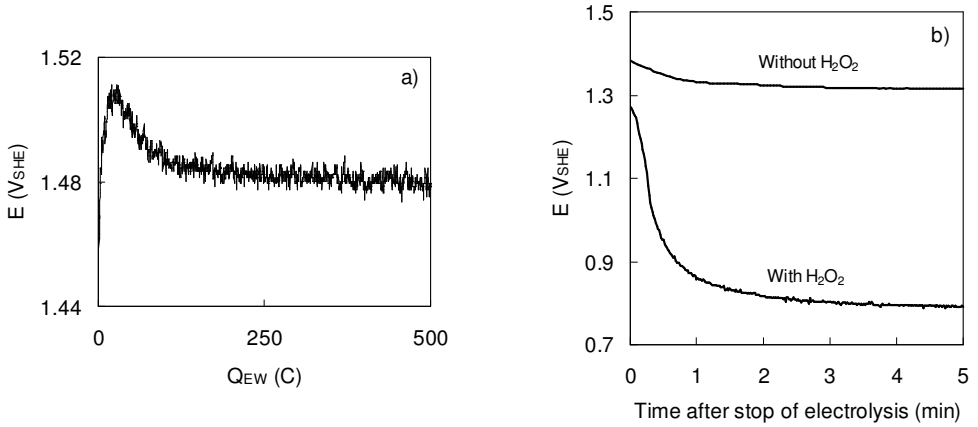

Figure 4.38 *a) Anode potential during electrolysis from $CoCl_2$ electrolyte containing H_2O_2 (second experiment). b) Open circuit potential after electrolysis in electrolyte with and without H_2O_2.*

The formation of chlorine was easily identified in the regular electrolysis experiments by its characteristic irritating smell. However, with H_2O_2 in the electrolyte there was no smell of chlorine. According to Valensi et al. [184], chlorine acts as an oxidation agent according to the following reaction:

$$H_2O_2 + Cl_2 = O_2 + 2\ HCl \qquad (4.8)$$

500 coulombs of electric charge can generate a maximum of 2.6 millimoles of Cl_2 (100 % CE), while the initial content of H_2O_2 in the 3 litres of electrolyte was 23 millimoles, i.e. a large excess of H_2O_2 versus Cl_2. If 2.6 millimoles of Cl_2 are decomposed quantitatively by H_2O_2, 5.2 millimoles of HCl will be generated. For two experiments this means a 3.5 mM increase in the HCl concentration of the electrolyte. An initial pH of 1.5 measured at room temperature, an H^+ activity coefficient of 1.9 in the electrolyte (Fig. 2.14) and 10 % cathodic consumption of the H^+ ions produced then gives a final estimated pH of 1.43 after two experiments. This represents exactly the same pH decrease as measured experimentally, suggesting that the chlorine evolved was decomposed by H_2O_2. The lower electrolyte pH with H_2O_2

should have contributed to the observed decrease in anode scaling, but the drop in CE_{CoOOH} was too large to be only a pH effect, see section 4.2.1.2.

In contrast to Kongstein [65], no depolarizing effect of H_2O_2 was observed for the anode process, which may be due to the higher current density used. Furthermore, the cathodic current yield of cobalt was negatively affected by the presence of H_2O_2 to a much higher extent than can be explained by the decreasing electrolyte pH. Lower levels of dissolved chlorine due to decomposition by H_2O_2 should in fact improve the current efficiency for cobalt. It is believed that the reduction in CE_{Co} was caused by cathodic decomposition of excess H_2O_2 according to equation 4.4. The high standard electrode potential of this reaction suggests that H_2O_2 should be reduced preferentially on the cathode rather than cobalt reduction and hydrogen evolution [117]. It is unclear why Kongstein [65] did not observe any effect of H_2O_2 on CE_{Co}.

H_2O_2 may seem as an ideal anode depolarizer based on its relatively low cost, availability and decomposition products compatible with the process. However, in a chloride-based electrowinning process where chlorine is the preferred anode product, the use of H_2O_2 cannot be recommended. The current yield of chlorine will deteriorate from the reaction with H_2O_2, and owing to the relative high solubility of chlorine in chloride solutions, only a small portion of the added H_2O_2 will reach the anode surface, resulting in almost no depolarization and minor dissolution of anode deposits during operation. Moreover, H_2O_2 in the catholyte may be decomposed on the cathodes, reducing metal current efficiency. The risk of accelerated degradation rates of the DSA®-type of anodes frequently used in chloride media is another obstacle related to the use of H_2O_2 in these processes.

The effects of H_2O_2 addition in the electrowinning of cobalt from chloride solution were also studied on a pilot scale, see section 4.3.2.5.

4.2.4 Advanced current supply

4.2.4.1 Periodically reversed current (PRC)

The cobalt oxide depositing on DSA® during cobalt electrowinning can be dissolved by cathodic polarization, as utilized in the electrochemical route for determination of the rate of anode scaling (section 3.4). By performing experiments with potential-controlled electrolysis, Kongstein [65] found that the current efficiency for CoOOH formation was reduced considerably if cathodic potential pulses were applied. The combination of long time at low cathodic potential, i.e. 20 % of the total time at 0.24 V_{SHE}, was found to be the most effective at the low frequency of 0.001 s^{-1}. When operating at these conditions, no deposit was observed on the DSA® surface at the end of the cathodic part of the pulse cycle.

In the present work, the influence of the frequency of periodic current reversal at 0.001, 0.01 and 0.1 s^{-1} was studied. To avoid hydrogen evolution and metal deposition on the DSA® during cathodic pulses, the electrode potential was controlled instead of the current. IR-corrected potentials of 1.48 and 0.8 V_{SHE} were applied for 85 and 15 % of the total time respectively. The duration of each experiment was 4000 seconds, and they were terminated at the end of a cathodic pulse. Otherwise, standard test conditions as listed in Table 4.2 were used, and CE_{CoOOH} was determined by the chemical route (section 3.4).

The results in Table 4.6 show that the extent of cobalt oxide deposition was reduced by operating in PRC mode. The lowest frequency tested resulted in less CoOOH being generated than at the intermediate frequency, reflecting the long time needed for CoOOH to dissolve. At the intermediate frequency, enough chlorine was probably available at the electrode for it to be preferentially reduced with respect to CoOOH in the shorter period of cathodic polarization. The highest frequency tested appeared to be the most efficient in suppressing anode scaling. Only a few small black particles were observed on the DSA® surface after this experiment, which indicates that the frequent potential pulsing was interrupting the nucleation and growth process of CoOOH.

Table 4.6 Anodic cobalt oxide deposition at different frequencies of PRC.

Frequency (s^{-1})	$t_{forward}$ (s)	$t_{reverse}$ (s)	Number of cycles	$i_{a,avg}$ (A/m^2)	CE_{CoOOH} (%)
0 *	1990	0	0	800	0.18
0.001	850	150	4	845	0.07
0.01	85	15	40	846	0.11
0.1	8.5	1.5	400	654	0.01

* Galvanostatic electrolysis at similar conditions.

From Table 4.6 it can be seen that higher anodic currents were recorded in those experiments where cobalt oxide was building up on the DSA®. This activation of the chlorine evolution reaction is also illustrated in Fig. 4.39, where current profiles for each of the PRC experiments are given. From these profiles it is evident that the anodic current showed an increasing trend with time at low and intermediate frequencies (Figs. 4.39 a) and b)), while it decreased rapidly and then stabilized at the highest frequency (Fig. 4.39 c)). The rise in anodic current after a cathodic pulse, as seen in Fig. 4.39 a), is believed to have been caused by reactivation of less accessible sites in the cobalt oxide film due to penetration of electrolyte into pores and along grain boundaries. During continued anodic polarization this inner surface area will, however, be gradually excluded as a result of concentration polarization and gas blocking, and the current then decreases before stabilizing. The increased active surface area from the growth of CoOOH also induced higher initial currents during cathodic polarization.

The cobalt metal deposited using PRC electrolysis was bent and was partly detached from the titanium electrode. Bent cobalt was also produced at slow pulsing by Kongstein [65], and the bending was attributed to internal stresses in the deposit.

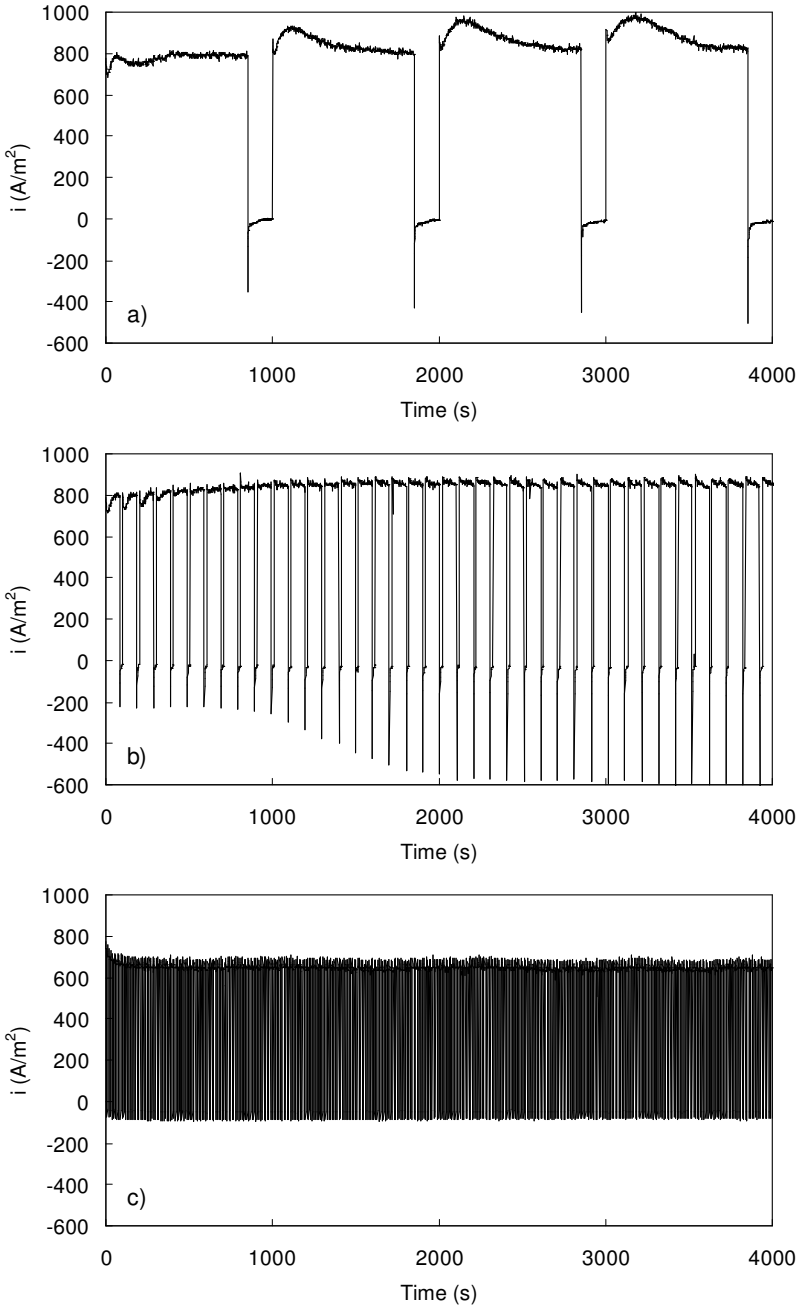

Figure 4.39 *Current response from potential-controlled PRC at different frequencies. a) 0.001, b) 0.01, c) 0.1* s^{-1}.

4.2.4.2 Stability of cobalt oxide deposits

To study the kinetics of chlorine evolution on DSA® anodes covered by cobalt oxide, steady state polarization curves were recorded in acidic sodium chloride solution [185]. However, these experiments were unsuccessful, since the electrodeposited cobalt oxide films were found to be unstable in such a medium (2 M NaCl, pH 1, 60°C). The dissolution rate was surprisingly high, and within a few minutes in the electrolyte at open circuit potential (OCP), there was apparently no cobalt deposit left on the anode surface. Higher pH in the NaCl solution (pH 1.5), increased film thickness and immediate anodic polarization failed to give acceptable stability of the cobalt oxide layer.

Based on the unexpected behaviour of the cobalt oxide films in NaCl solution, an investigation of the stability of cobalt oxide deposits in cobalt chloride electrolyte was carried out. Cobalt oxide films were deposited on DSA® by galvanostatic electrolysis at standard conditions (Table 4.2), and the electrodes were then kept in an electrolyte at OCP for various durations before being removed for the determination of remaining CoOOH. Two different types of DSA® were tested, the regular Ru-Ir-Ti coating and the Ru-Ti coating (Table 3.2). In most of the tests, when the electrolysis was accomplished, the electrode was transferred to a separate cobalt chloride electrolyte without dissolved chlorine, and the quantity of CoOOH was determined according to the chemical route (section 3.4). However, the stability of CoOOH in the same electrolyte as used for electrolysis was also studied for the regular electrode. For these and two additional tests in chlorine-free electrolyte, the electrochemical route was used to measure the amount of CoOOH.

The measured quantities of CoOOH on the DSA® anodes after different times at OCP are presented in Fig. 4.40 a). This figure shows that the freshly prepared cobalt oxide films were far from stable in standard cobalt chloride solution at 60°C and pH 1.6. A high initial dissolution rate of CoOOH was observed, and after 10 minutes at OCP more than 40 % was lost already. The dissolution rate then decreased with time. Furthermore, the film stability seemed to be similar on the two types of DSA®, and the presence of dissolved chlorine in the electrolyte reduced the extent of dissolution. The chemical and electrochemical routes gave similar results.

Fig. 4.40 b) shows 24-hour potential decay curves for CoOOH-covered regular DSA®'s in the electrolyte used for electrolysis and in a separate electrolyte without chlorine. A second test was performed in chlorine-free electrolyte. Here, the electrode was cleaned with deionized water after the electrolysis and then dried at room temperature before being immersed in cobalt chloride electrolyte. The three electrodes exhibited quite different decrease in OCP with time. No anode scale was detected on any of the electrodes after 24 hours at OCP.

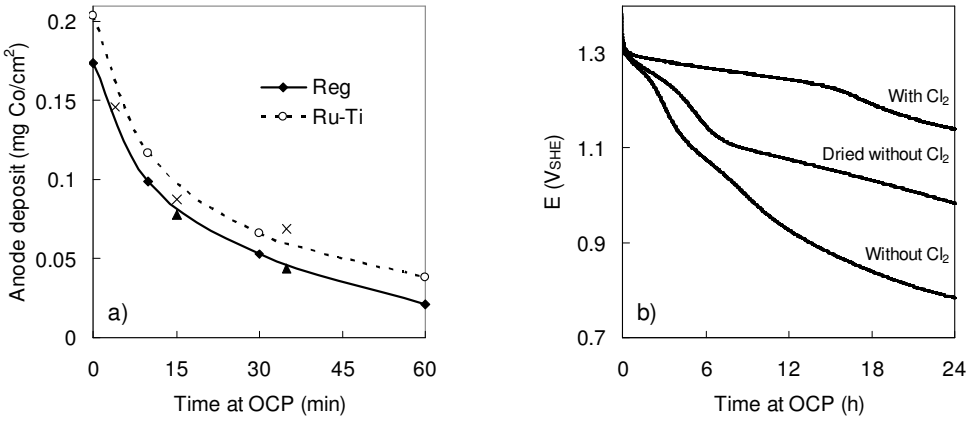

Figure 4.40 *Dissolution of cobalt oxide on DSA® at open circuit potential.*
a) Quantity of CoOOH vs. time at OCP for the regular and the Ru-Ti electrode. Results obtained for the regular electrode by the electrochemical route are also included; in a separate electrolyte (▲), and in the same electrolyte as used for electrolysis (×).
b) Potential decay curves for the regular electrode after electrolysis; in the same electrolyte as used for electrolysis (with Cl_2), or in a separate cobalt chloride electrolyte, either directly (without Cl_2) or after drying (dried without Cl_2).

Since it is known that the anode scale produced in the Xstrata Nikkelverk cobalt tankhouse is quite stable, the rapid dissolution of the cobalt oxide films, as observed in the laboratory, was very surprising. It can also be mentioned that in processes where cobalt is separated from nickel by means of chemical oxidation and precipitation, a reductant is added to the acidic leaching solutions in order to bring cobalt back into solution (see section

1.5.4). This indicates that the trivalent cobalt hydroxides produced are rather stable.

For the anode scale to dissolve, trivalent cobalt ions must be reduced to the divalent state, which in an aqueous cobalt chloride solution results in the oxidation of chloride ions to chlorine or the oxidation of water to oxygen:

$$2\ CoOOH + 6\ H^+ + 2\ Cl^- = 2\ Co^{2+} + Cl_2 + 4\ H_2O \qquad (4.9)$$

$$2\ CoOOH + 4\ H^+ = 2\ Co^{2+} + ½\ O_2 + 3\ H_2O \qquad (4.10)$$

According to the Pourbaix diagram of the Co-Cl-H_2O system given in Fig. 2.1, reactions 4.9 and 4.10 should be feasible at pH levels below 0.6 and 2.0 respectively. On the other hand, due to activity effects and the fact that the fresh cobalt oxide may exist in the form of less crystalline and hydrous metastable phases, equation 4.9 is believed to be the main dissolution reaction even at pH 1.6, since the formation of oxygen from water is normally very slow. Reaction 4.9 will be shifted to the left by the presence of dissolved chlorine in the electrolyte, which explains the reduced dissolution rates observed in the electrolyte used for electrolysis. The improved stability of the dried cobalt oxide film, as can be seen from the potential decay curves in Fig. 4.40 b), was probably related to dehydration so that it took some time for the electrolyte to penetrate the material.

Cobalt oxide may be less stable in the form of a thin and porous layer on a DSA® than being dispersed as free particles in the bulk electrolyte. If the noble metal oxides at the DSA® surface get into contact with the electrolyte, they may catalyze the chloride oxidation half cell reaction, thereby increasing the driving force for cobalt oxide dissolution. Matsuo et al. [186] have demonstrated that the reduction of PbO_2 films at OCP can be inhibited by using oxide coatings with low activity for oxygen evolution. When using Ir-Sn oxide coatings rich in Sn, showing a higher reversible potential for oxygen evolution than the reversible potential for PbO_2 reduction, no local galvanic cell could be established and PbO_2 was stabilized.

Metal hydroxides typically undergo phase transformation over time from amorphous metastable compounds to more stable crystalline structures [187]. Such an ageing effect was observed for cobalt oxide produced in the Xstrata Nikkelverk cobalt tankhouse. Relatively fresh anode scale from the bottom of an anode bag was not stable when suspended in chlorine-free

cobalt chloride electrolyte at 60°C and pH 1, whereas older precipitate taken from the anolyte manifold contained very little hydrated water and seemed to be almost completely insoluble under identical conditions. In addition, the dissolution of the deposit from the anode bag stopped after less than 24 hours when the electrolyte pH had increased to ~1.3. The slurry was then filtered and the solid material suspended in fresh electrolyte. Now much less anode scale was dissolved, which indicates some sort of stabilization. The accumulation of black particles in the laboratory cell also showed that the exfoliated cobalt oxide became less soluble (see section 4.2.1.1).

Another passivation phenomenon was sometimes observed when cathodic polarization was employed to dissolve cobalt oxide layers on DSA®. The black adherent films could then be converted to brown particles, which were loosely bonded to the electrode surface and more stable in the electrolyte. This process was facilitated by a rapid decrease in potential, large quantities of anode deposit, high pH and the presence of chlorine in the electrolyte. It is suggested that the formation of particles instead of complete dissolution can be explained by re-precipitation of another form of cobalt oxide, as a result of the increased local pH generated during the dissolution of the original film. Benson et al. [7] found that β-CoOOH could be converted to the more stable $CoHO_2$ phase if $Co(OH)_2$ was present in the oxide layer. $Co(OH)_2$ may have been formed on the DSA® due to high surface pH.

Titanium-supported cobalt oxide electrodes prepared by thermal decomposition of suitable precursors have been suggested for chlorine evolution from slightly acidic solutions [60]. However, these electrodes are not stable if the pH becomes too low. Tarasevich and Efremov [188] have reported that for pH levels below 2.5, the active layer is subjected to higher chemical wear because the electrode surface structure undergoes changes. When OCP was measured for Ti/Co_3O_4 in chloride solution at decreasing pH, Garavaglia et al. [153] obtained a break at about pH 5, which was ascribed to leaching of Co^{2+} from the surface at lower pH values. Da Silva et al. [61] showed that the cobalt oxide coating was unstable during potential cycling in a 5 M NaCl + 0.01 M HCl electrolyte. They suggested that trivalent Co_2O_3 formed by oxidation of Co_3O_4 during the anodic scan was reduced to soluble divalent CoO during the cathodic scan. In two other papers about the cobalt oxide electrode by the same authors [189, 190], results are reported on the characterization and investigation of the oxygen evolution reaction from acidic sulphate solution. They referred to experiments showing that the cobalt oxide electrode suffered from anodic

corrosion at high potentials in acid media (> 1.47 V_{RHE}). It was assumed that trivalent CoOOH is oxidized to unstable tetravalent CoO_2, which then decomposes into soluble CoO with the simultaneous liberation of O_2. About 1 % of the O_2 was produced through active dissolution of the cobalt oxide layer. Finally, it should be mentioned that thermally prepared cobalt oxide electrodes could be stabilized by introduction of small quantities of ruthenium. This stabilizing effect was attributed to a strong surface enrichment of this component [189].

4.2.4.3 Periodically interrupted current (PIC)

The lack of stability at OCP, as discovered for the cobalt oxide deposits, suggested that its rate of growth could be reduced by operating with current interruptions during electrowinning. The anode potential recorded in a test of periodically interrupted current (PIC) is displayed in Fig. 4.41. Galvanostatic electrolysis commenced with a clean regular DSA® using the standard conditions listed in Table 4.2. After applying 500 C of electric charge, the current was interrupted for 6 minutes before being switched on again. Electrolysis proceeded for an additional 500 C, and the electrode, now covered by cobalt oxide, was then removed from the cell, washed with deionized water and dried over night at ambient temperature. The next day the dried electrode was immersed in preheated electrolyte and kept at OCP for 30 minutes before electrolysis was resumed (Fig. 4.41 b)). Two portions of 1000 C were applied with an intermittent 10 minutes current interruption.

It is obvious from Fig. 4.41 that leaving the CoOOH-covered DSA® at OCP resulted in anode depolarization in the first period of subsequent electrolysis. A reduction in potential of up to 50 mV compared to the steady state level was obtained. This activation, similar to what observed during PRC electrolysis (see section 4.2.4.1), is also attributed to penetration of electrolyte into the cobalt oxide layer, increasing the active electrode surface area available for chlorine evolution. The same type of experiment was carried out in nickel solution (mixed chloride-sulphate) without anode scale formation. In this test the anode potential increased much faster after current interruption. The current efficiency for CoOOH formation was not measured in the PIC laboratory experiment, however, the concept of PIC electrolysis was studied further on pilot scale, see section 4.3.2.7.

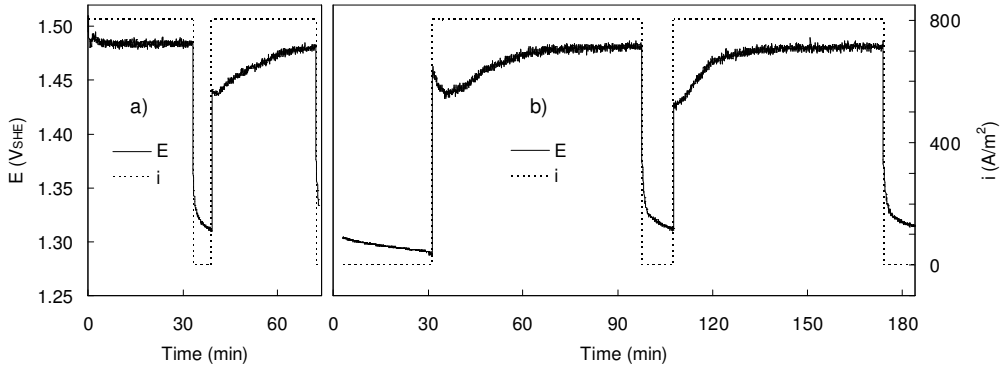

Figure 4.41 *Anode potential during galvanostatic electrolysis with current interruptions in $CoCl_2$ solution. a) Start with a clean DSA®, b) Continued electrolysis after drying of the DSA® covered by cobalt oxide.*

4.2.4.4 Short-circuiting of the cell

Compared to current interruption, the driving force for cobalt oxide reduction and dissolution can be increased considerably by just short-circuiting the cell after switching off the current. At unit activities and pH 1.5, the reversible potential difference between cobalt metal and CoOOH is close to 1.5 V. Hence, by connecting the anode to the cathode through an electrical conductor, cobalt oxide should be reduced and dissolved from the DSA® with simultaneous anodic dissolution of the cobalt cathode:

$$2\ CoOOH + Co^{\circ} + 6\ H^{+} = 3\ Co^{2+} + 4\ H_2O \qquad (4.11)$$

Following galvanostatic electrolysis at standard conditions (Table 4.2), the laboratory cell was short-circuited for 10 or 30 minutes, in either the same electrolyte as used for electrolysis (with chlorine), or in a separate cobalt chloride electrolyte without dissolved chlorine. 10 minutes of electric shorting resulted in some yellow-brown deposit on the DSA®, which may have been formed by reprecipitation caused by the abrupt drop in electrode potential, as shown in Fig. 4.42. Anode scale dissolution tests involving cathodic potential steps instead of sweeps demonstrated that if the dissolution process was forced to proceed too fast by a too large potential step, brown precipitates were generated. On the other hand, after 30 minutes of short-circuiting, the electrode surface was clean, i.e. the brown deposit

was also dissolved when exposed to very low potentials for a relatively long period of time.

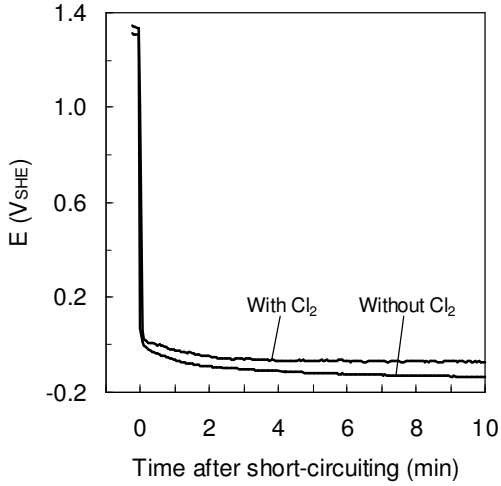

Figure 4.42 *Effect of short-circuiting on the potential of the DSA® anode; in the same electrolyte as used for electrolysis (with Cl_2), or in a separate cobalt chloride electrolyte (without Cl_2).*

When short-circuiting in chlorine-free electrolyte, no effect on the cobalt current yield was obtained, while in chlorine-containing electrolyte, CE_{Co} decreased by about 1 % in 30 minutes. The lower current efficiency in the latter solution can be explained by a higher shorting current owing to reduction of dissolved chlorine on the DSA®.

Short-circuiting of the cell after cobalt electrowinning was investigated further in the electrowinning pilot plant, see section 4.3.2.8.

4.2.4.5 Consequences of advanced current supply

The results reported in this chapter indicate that the build-up of cobalt oxide on DSA® in cobalt electrowinning can be reduced by frequent lowering of the anode potential, as obtained either by periodically reversed current, periodically interrupted current or short-circuiting. However, there are obviously quite a few negative consequences related to this kind of advanced current supply. On the cathode side, the current efficiency may deteriorate,

and internal stresses in the deposited metal causing cathode warping generate a range of operational problems. On the anode side, due to the high capacitance of DSA®-type anodes, high frequency PRC may result in loss of chlorine production, since a greater portion of the charge supplied will then be consumed by charging and discharging catalytic sites. Discontinuous operation has also been shown to enhance anode degradation; see below. Furthermore, the sophisticated rectifiers needed may be prohibitively expensive.

Several thermally prepared oxide electrodes are fairly stable towards cathodic polarization, and RuO_2 and IrO_2 coatings have in fact been proposed as potential cathode materials for electrolytic hydrogen production from acid solution [191]. However, when hydrogen is evolved, it may be absorbed by the electrode catalyst and the support, forming solid solutions of hydrogen in metal and metal hydrides [192]. This hydrogenization can result in change of lattice parameters, formation of microcracks, brittleness, metal bulging/rupture and pulverization. Morimitsu et al. [193] found that PRC drastically reduced the durability of Ti/IrO_2-Ta_2O_5 electrodes for oxygen evolution compared to continuous anodic electrolysis. The consumption of the catalytic layer was even higher than during continuous cathodic electrolysis, and they suggested that the high corrosion rate was induced by alternate preferential dissolution of tantalum and iridium during cathodic and anodic polarization respectively. Martelli et al. [47] carried out some tests showing that several polarity reversals in solutions containing foreign ions (Zn^{2+} in their case) can be very dangerous compared to H_2 evolution, because metals are deposited in the DSA® surface cracks during cathodic mode, and then dissolved again during anodic mode. This cycling results in coating damage due to mechanical weakening.

For Ti/RuO_2-TiO_2 electrodes it has been shown that the wear rate decreases steadily with time after the beginning of polarization in 5 M NaCl solution [44]. Enhancement in wear is also observed if the polarization is disconnected and then connected again. It was reported that periodic disconnections may shorten the life of the electrode by 20 – 50 %. During the initial period of chlor-alkali electrolysis, the coating dissolution rate is more than two orders of magnitude higher than the steady-state rate [45]. The steady-state dissolution rate is reached after about 100 hours, and the decrease in the rate of ruthenium dissolution is linked to adsorption phenomena of chloride ions. Mraz and Krysa [194] found that for a Ti/IrO_2-Ta_2O_5 anode, the steady-state rate of dissolution was reached after 600 – 700

hours, and it was 200 – 300 times lower than the initial dissolution rate. Interruption of electrolysis for more than 1 hour had a considerable influence on the iridium dissolution rate, since continuing electrolysis after interruption resulted in a rapid increase in Ir dissolution.

Summary

Addition of hydrogen peroxide to the electrolyte and various alternatives of advanced current supply were explored as potential methods to reduce the extent of anode scaling during cobalt electrowinning. The addition of 0.26 g/l H_2O_2 to the cobalt chloride electrolyte did not give rise to any noticeable depolarization of the anode process during standard galvanostatic electrolysis, and cobalt oxide was deposited on the DSA®. When the current was switched off, the open circuit potential of the anode was observed to decrease rapidly, and the cobalt oxide layer was dissolved. Furthermore, there was no indication of chlorine in the spent electrolyte, and from the measured drop in electrolyte pH it was estimated that the major part of the evolved chlorine was decomposed by excess H_2O_2. The cobalt current yield became lower with H_2O_2 in solution, presumably due to cathodic decomposition of H_2O_2.

Less cobalt oxide was produced when potential-controlled electrolysis with periodic current reversal was applied instead of continuous direct current. High frequency was found to be most effective, since the nucleation and growth of CoOOH was then probably severely interrupted. A low frequency was better than an intermediate frequency, indicating that the dissolution process of anode scale was slow. When a CoOOH-covered DSA® was polarized anodically following current reversal or interruption, the chlorine evolution reaction became depolarized before being stabilized at the previous level. This behaviour was attributed to penetration of electrolyte into pores in the cobalt oxide deposit, increasing the active electrode surface area. Internal stresses in the cobalt metal deposited by PRC electrolysis resulted in bending and partial detachment from the titanium cathode.

The anodic films of freshly prepared cobalt oxide on DSA® were not stable at open circuit potential in standard cobalt chloride electrolyte at 60°C and pH 1.6. A high initial dissolution rate was obtained, and after 10 minutes stop of electrolysis more than 40 % of the cobalt oxide had already dissolved. After 24 hours the DSA® was clean. The CoOOH dissolution was

suppressed by the presence of dissolved chlorine in the electrolyte. Solubility tests of industrial anode scale indicated an ageing process where the cobalt deposits were stabilized over time.

Short-circuiting of the cell after cobalt electrolysis was found to accelerate the dissolution of cobalt oxide from the DSA®. When short-circuited for 10 minutes, some yellow-brown deposit was observed on the electrode surface, while after 30 minutes the DSA® was clean. It was suggested that the yellow-brown deposit was generated by reprecipitation due to the rapid drop in potential experienced by the DSA® when short-circuited.

4.2.5 Evaluation of experimental techniques

4.2.5.1 Comparison of the two alternative routes for determination of the extent of anode scaling during cobalt electrowinning

To be sure that there was no significant drift in test conditions and procedures over time, a standard experiment was reproduced on a regular basis. In these experiments galvanostatic electrolysis of cobalt was carried out at the standard test conditions given in Table 4.2. From the results in Table 4.7 it can be seen that the measured current efficiency for anodic CoOOH deposition was dependent on the route applied for anode scale dissolution. Average values of 0.148 ± 0.005 and 0.173 ± 0.017 % were obtained for the electrochemical and the chemical routes respectively. The experimental errors were based on the standard deviations obtained from the samples of data in Table 4.7 and use of the Student's t distribution giving a 95 % confidence interval for the average values [195]. Determination of CE_{CoOOH} by measuring the anode weight increase was regarded as being inaccurate and, therefore, was not tested.

Table 4.7 Summary of experiments performed at standard conditions.

Time order	Route	DSA®		Electrolyte		E_{avg}	CE_{Co}	CE_{CoOOH}
		Disk no.	Exp. no.	Batch	Exp. no.	(V_{SHE})	(%)	(%)
1	El.chem	#1	52	Jan. 02	5	1.483	94.6	0.156
2	"	"	62	"	1	1.481	94.6	0.141
3	"	#2	4	"	10	1.477	95.3	0.148
4	"	"	7	"	1	1.477	94.9	0.149
5	"	#3	4	"	2	1.471	95.1	0.140
6	"	"	30	"	1	1.494	94.8	0.143
7	"	"	37	"	2	1.487	95.2	0.151
8	"	"	38	"	1	1.478	94.9	0.155
9	Chem	"	72	"	1	1.490	94.5	0.180
10	"	"	73	"	2	1.477	94.6	0.149
11	"	"	78	"	7	1.481	94.4	0.181
12	"	"	83	Mar. 04	1	1.483	94.7	0.176
13	"	#4	1	"	4	1.464	94.9	0.179

The larger error in CE_{CoOOH} for the chemical route was due to the lower number of experiments and the outlier in experiment no. 10. In this experiment, a higher chloride concentration was observed in the etching solution, indicating higher levels of entrained electrolyte. However, the difference was only 0.5 mg/l Cl, equivalent to the precision of the chloride analysis, but still it had a large effect on CE_{CoOOH} because of the low concentration. The blank etching solution contained between 2 and 4 mg/l Cl, and after etching it had increased by 0.5-1.5 mg/l in the standard experiments. Uncertainty in the chloride analysis was a major problem in the chemical route, especially when small quantities of anode scale were produced.

The series with different electrolyte pH was also reproduced by using the chemical route to compare with the results obtained by the electrochemical route (section 4.2.1.2). Fig. 4.43 shows the CE_{CoOOH} values measured by the two alternative routes. At high pH very good agreement was obtained, whereas at intermediate pH the chemical route gave systematically higher results for CE_{CoOOH} than the electrochemical route. The negative value for the chemical route at pH 0.9 was a result of 0.5 mg/l more chloride analysed in the etching solution than in the blank, even though it contained only 0.12 mg/l Co after etching.

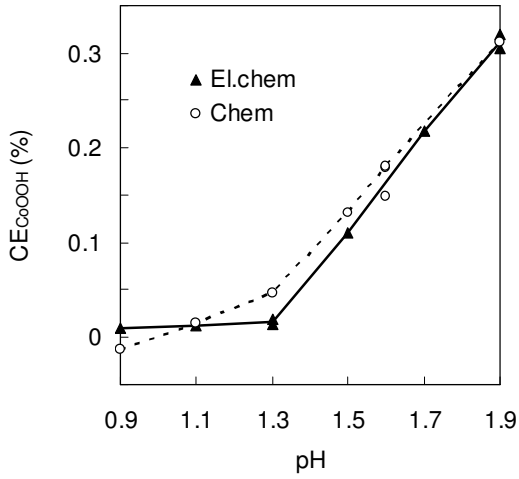

Figure 4.43 *Comparison at different solution pH of the electrochemical and the chemical route for determination of current efficicncy for anodic CoOOH deposition.*

The lower values of CE_{CoOOH} obtained by the electrochemical route can be explained by chemical dissolution of the unstable cobalt oxide deposit during the removal of the electrodes to the chlorine-free electrolyte and in the first part of the cathodic potential sweep, see section 4.2.4.2. The time from the end of electrolysis to the start of the potential sweep was normally between 4 and 5 minutes, and it is believed that the variation in this time period was the main contributor to the random error reported for the electrochemical route. The extent of the systematic error generated by cobalt oxide instability will depend on the amount of anode scale formed, the structure of the deposit and the electrolysis conditions in general (electrolyte composition, temperature etc.). However, the cobalt oxide was stabilized somewhat by the presence of dissolved chlorine, and the same type of electrolyte was always used for potential sweeps.

When calculating CE_{CoOOH} according to the chemical route, it was assumed that all the cobalt in the anode deposit was in the trivalent state (equation 3.3). The match between the two routes at pH 1.9 indicates that this was an acceptable assumption for freshly prepared cobalt oxide, since it was probably much more stable at lower acidity levels. Furthermore, the similar results obtained by the two routes when studying the stability of CoOOH on DSA® also support this view (see Fig. 4.40 – in these experiments the time

spent on the change of the electrolyte was included in the total time at open circuit potential).

4.2.5.2 Dissolution of anode deposit by cathodic potential sweeps

During anodic gas evolution the noble metal oxides in the DSA® coating are oxidized to higher valence states, and when polarized cathodically they will be reduced to lower valence states, see section 4.2.2.1. Therefore, the parallel reduction of the DSA® coating will increase the cathodic current measured during CoOOH dissolution by the electrochemical route. To subtract the contribution of the DSA® material, the potential sweep was repeated after polarizing the CoOOH-free anode at 1.34 V_{SHE} for one minute. The charge difference between the two sweeps was then used to calculate CE_{CoOOH} from equation 3.2. One minute of anodic polarization was probably sufficient to reoxidize most of the active sites. In any case, the influence of the regular coating must have been moderate due to its compact structure and low voltammetric charge q* (section 4.2.2). Half of the q* value obtained in sulphuric acid, equivalent to the cathodic part of the cyclic voltammogram (21 mC/cm^2 / 2 × 3.14 cm^2 = 33 mC), represents less than 5 % of the charge difference between the two potential sweeps in a typical standard experiment (740 mC). This rough estimate illustrates the minor contribution from the regular DSA® material, although its voltammetric charge will be somewhat different at lower sweep rates in cobalt chloride solution. When small amounts of CoOOH are deposited or if more porous DSA®'s are employed, the effect of the reduction of the catalytic coating will be more important.

Kongstein [65] found that cathodic dissolution of anode deposit was a slow process in cobalt chloride electrolyte. In the present work, the effect of sweep rate on the dissolution characteristics of cobalt oxide deposited at standard conditions was investigated. Linear voltammograms for sweep rates in the range 0.1 – 10 mV/s are shown in Fig. 4.44 a). The broadening of the CoOOH reduction wave with increasing sweep rate confirms the sluggishness of this reaction. Similar cathodic currents at low potentials were also recorded in the second potential sweeps on clean DSA®, suggesting that it was mainly due to the reduction of the noble metal oxides in the DSA® coating.

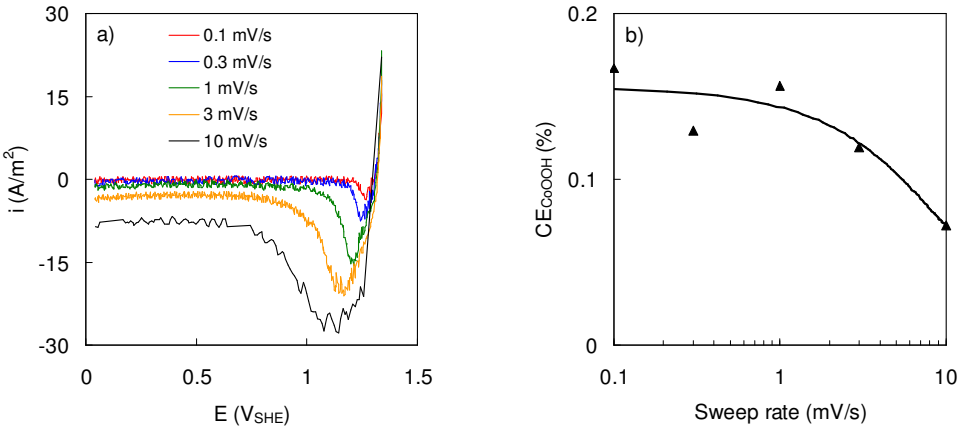

Figure 4.44 *Influence of sweep rate on the cathodic dissolution of cobalt oxide deposited at standard conditions. a) Voltammograms of linear potential sweeps from 1.34 to 0.04 V_{SHE} at different sweep rates. b) Calculated current efficiency for anodic CoOOH deposition vs. sweep rate.*

The current efficiency for anodic cobalt oxide deposition was calculated in the usual way from equation 3.2, and the results are presented in Fig. 4.44 b). It is assumed that the downward trend in CE_{CoOOH} at high sweep rates can be explained by reprecipitation of a more stable form of cobalt oxide (see section 4.2.4.2), which then inhibited the dissolution of the remaining anode scale. After three potential sweeps at 10 mV/s, the electrode was still covered by yellow-brown precipitate. By operating with a low sweep rate of 1 mV/s and a moderate electrolysis charge to avoid the build-up of very thick cobalt oxide films, all the deposited material was usually dissolved and no reprecipitation was observed.

4.2.5.3 Exfoliation of anode scale

Loss of anode deposit peeling off the DSA® during electrolysis, electrode handling or electrochemical dissolution was another systematic error which resulted in too low values of CE_{CoOOH} to be measured. Particles were detected at the bottom of the cell following a series of experiments, and SEM images of DSA®'s covered by thick layers of cobalt oxide showed that some deposit had fallen off the anode (see Fig. 4.5 f)). Since the anode deposit was not completely stable in the electrolyte, it was difficult to quantify the

magnitude of this error. On the other hand, results from the variation of the amount of electric charge applied indicated that if the electrolysis was terminated before the layer became too thick, flaking appeared to be of minor importance (see section 4.2.1.1).

4.2.5.4 Repeated use of the same electrolyte and electrode in consecutive experiments

Other factors like the time order, the electrolyte and the DSA® disk used appeared to be of secondary importance. The absence of any noticeable drift in the results suggests that the experimental procedures did not change over time and that the electrolyte was stable. At 100 % current efficiency, the concentration of cobalt and chloride in the electrolyte would decrease by only 0.05 and 0.06 g/l respectively, due to the large volume of electrolyte (3 litres) compared to the electric charge applied (500 C). Evaporation of water had in fact a larger but opposite effect on the electrolyte composition; the volume decreased by roughly 10 ml per experiment, corresponding to 0.18 g/l increase in cobalt concentration. The volume of electrolyte was checked and corrected by adding deionized water in between experiments. The pH of the electrolyte was also measured regularly, but usually no change was observed. The measurement of pH was discussed in detail in section 2.7.7.

Based on the fact that there might be slight differences between electrode samples having the same type of catalytic coating [156], it was decided to use the same anode disk in consecutive measurements. However, the results from the standard experiments showed that there was no significant difference between the regular anode disks tested. Furthermore, the use of the same anode disk in many experiments did not seem to affect the amount of anodic cobalt oxide generated at standard conditions, even though it is known that operation under harsh conditions, discontinuous current supply and cathodic polarization will accelerate the degradation of the DSA® coating. The stable operation of the anodes may be related to its reduced influence after being covered by cobalt oxide combined with a high coating durability, since the regular Ru-Ir-Ti mixed oxide electrodes were produced commercially and consisted of multi-layered coatings. It should, however, be mentioned that the behaviour of the anode potential was altered for DSA #3 after about 65 experiments. As illustrated in Fig. 4.45, the low and broad potential peak appearing in the first phase of cobalt electrolysis (Fig. 4.45 a)) then became higher and sharper (Fig. 4.45 b)). This may indicate that the

coating was partly deactivated, but this was not studied in more detail. The shape of the anode potential profiles before and after this modification was similar to those given in Figs. 4.45 a) and b) respectively. The reason for the abrupt change in potential behaviour is not known.

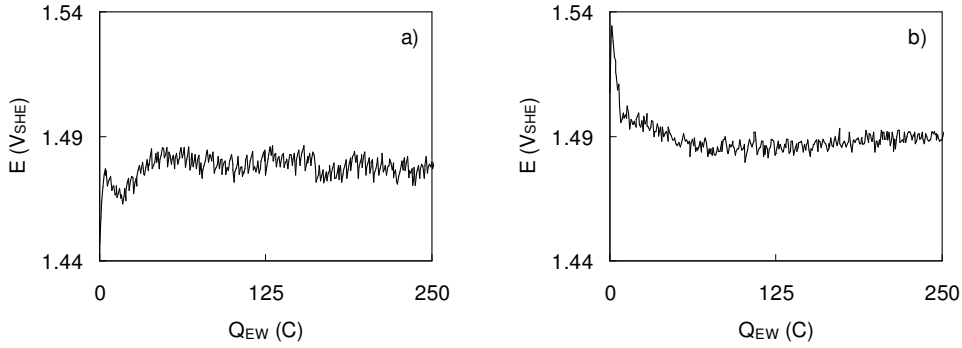

Figure 4.45 *Anode potentials recorded during the first half of galvanostatic electrolysis at standard conditions. a) Standard experiment no. 8, b) Standard experiment no. 9.*

4.2.5.5 Anode potential and anode design

As shown in Table 4.7, the recorded average anode potential differed by as much as 30 mV, although the majority of the standard experiments gave anode potentials at around 1.48 V_{SHE}. By plotting the IR-corrected anode potential as a function of the ohmic drop measured between the tip of the Luggin capillary and the DSA® surface at zero faradaic current, a positive correlation was revealed, see Fig. 4.46. Hence, small variations in the distance between the reference electrode and the working electrode were not completely compensated by the technique applied for IR correction. Moreover, owing to the additional resistance induced by the evolved gas bubbles, all potentials were more or less undercompensated (see section 4.2.1.7). The influence of the gas bubbles was, however, reduced by placing the Luggin capillary at the bottom of the DSA® where the concentration of bubbles was lower. To get accurate measurements of the anode potential, the IR-drop should be measured when the electrode is polarized and gas is produced, by using either electrochemical impedance spectroscopy or a current interruption technique.

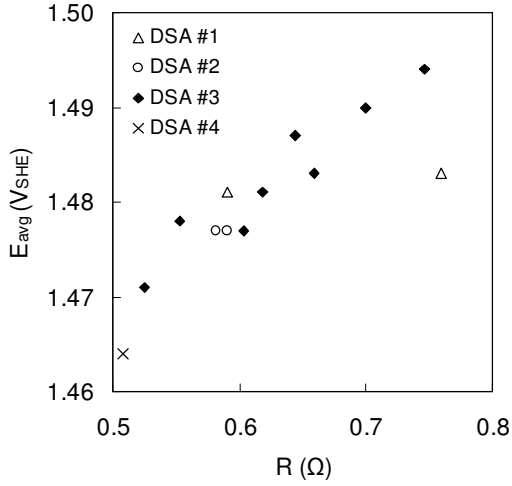

Figure 4.46 *IR-corrected average anode potential as a function of the measured ohmic drop in standard experiments.*

At high current densities massive bubble formation resulted in fluctuations in the measured anode potential. It was observed that large gas bubbles were accumulating along the periphery of the DSA®, and they seemed to adhere to the anode holder (details of the experimental setup are shown in Fig. 3.1). The design of the anode holder was very practical for testing different anode materials, but there were also a few shortcomings related to it. In addition to the adhering gas bubbles, contact problems were experienced between the back side of the anode disk and the copper conductor at high temperatures, which caused the PVDF material to expand. Furthermore, leakage of electrolyte into the anode holder took place in preliminary experiments, but this was later avoided by regular replacement of O-rings.

4.2.5.6 Cobalt metal electrodeposition

In the standard experiments the cathodic current efficiency for cobalt varied between 94.4 and 95.3 %; a difference equivalent to 1.3 mg of metal. The two alternative routes gave similar results for CE_{Co}, and no correlation was detected between CE_{Co} and CE_{CoOOH}. The variation in cobalt current yield was probably related to weighing error combined with small differences in cobalt ion activity, pH, convection and concentration of dissolved chlorine in the electrolyte.

Summary

Reproduction of cobalt electrolysis experiments at standard conditions gave anodic CoOOH current efficiencies of 0.148 ± 0.005 % for the electrochemical route and 0.173 ± 0.017 % for the chemical route. The lower amount of anode deposit obtained by the electrochemical route was explained by chemical dissolution in the time between electrolysis and cathodic potential sweeps. Imprecise analysis of the chloride content in etching solutions was the most important factor inducing experimental error in the chemical route. Other factors, such as the time order and the repeated use of the same electrolyte and electrode in several experiments appeared to be of less importance with respect to the extent of anode scaling.

4.3 Pilot scale experiments

The remaining part of this chapter is devoted to the work carried out in the Xstrata Nikkelverk electrowinning pilot plant described in section 3.2.1. The intention of the pilot testing was to investigate the cobalt electrowinning process with the use of similar size and design of electrodes and electrolytic cell as in the Xstrata Nikkelverk cobalt tankhouse. It was essential to find out how changes in the operating conditions affected the entire electrowinning process, e.g. the metal deposition, the composition of the anode gas and the energy consumption. However, the main focus was still the detrimental deposition of cobalt oxide on DSA® anodes.

Like in the laboratory scale experiments, key electrowinning parameters were studied one at a time, the other conditions being kept constant at the standard conditions given in Table 4.8. Regular rod anodes were employed in most of the experiments (section 3.2.2), and when calculated from the geometric surface area, the anodic current density was similar to the tests performed in the laboratory (800 A/m^2). Due to the much larger surface area of the cobalt cathodes, the standard cathodic current density was only a quarter of the anodic current density. The duration of a standard pilot experiment was 24 hours, which was more than 40 times longer than a typical lab experiment. Furthermore, the electrolyte pH was lower; pH 1 in the feed electrolyte compared to pH 1.5 in the standard laboratory electrolyte when measured at room temperature.

Table 4.8 Standard electrowinning conditions in the pilot experiments.

EW time (h)	pH [1]	Co [2] (g/l)	Temp. [2] (°C)	Current density [3] (A/m^2)	Anode suction (mm w.g. [4])	Inlet flow rate (m^3/h)
24	1.0	55	60	210	75	1.5

[1] pH in the inlet measured at room temperature.
[2] Inlet conditions.
[3] Cathodic current density.
[4] mm w.g. = millimetre water gauge.

The chlorine-saturated anolyte withdrawn from the anodes (900 mg/l dissolved Cl_2) was dechlorinated efficiently by introducing 1.6 Nm^3/h of air to each compartment at 750 rpm stirring rate (< 10 mg/l Cl_2 in the anolyte leaving the dechlorination facility). The experimental procedures for the pilot plant experiments are outlined in section 3.2.3.

4.3.1 Influence of key electrowinning parameters

Based on the laboratory study, which showed a large effect of electrolyte pH on the extent of anode scaling (section 4.2.1.2), particular attention was paid to monitoring the pH in the anode compartments when operating the electrowinning pilot plant. Cobalt current yield (CE_{Co}) and cell voltage were measured in order to determine the influence of process modifications on productivity and energy consumption. As opposed to the laboratory cell, the composition of the anode gas could also be measured for estimation of the selectivity between the anodic chlorine and oxygen evolution reactions.

4.3.1.1 Effects of electrowinning time

In the first set of experiments, the electrowinning time was varied between 14 and 95 hours to see if reproducible results were obtained with respect to time. This time only the worn Reg* rod anode was etched for determination of the current efficiency for anodic cobalt oxide deposition (CE_{CoOOH}). As shown in Table 4.9, scatter appeared in the results for CE_{CoOOH} and CE_{Co} due to small variations in the pH and temperature of the feed electrolyte. When the effect of pH was taken into account, the process seemed to be independent of time; see Fig. 4.48 where the CE_{CoOOH} values are plotted together with results obtained when studying the effects of pH.

Electrowinning for 24 hours was, therefore, regarded as being sufficient. These results clearly demonstrate the importance of proper pH control in this system, so that in the following experiments, the settings of parameters to be held constant were not adjusted within the series.

Table 4.9 Summary of results from the variation of electrowinning time.

EW time (h)	Time order	Inlet pH	Inlet temp. (°C)	Cell voltage (V)	Anode gas Cl_2 (%)	Anode gas O_2 (%)	CE_{Co} (%)	CE_{CoOOH} (%)
14	4	1.09	60	3.3	98	1	92.8	0.023
24	3	1.03	60	3.3	98	1	91.7	0.017
49	1	1.11	61	3.4	98	1	93.2	0.026
95	2	1.00	60	3.3	98	1	91.7	0.015

From Table 4.9 it can also be seen that the measured composition of the anode gas was stable at ~98 % chlorine, ~1 % oxygen and ~1 % nitrogen (due to dilution by air), i.e. selectivity was not affected by the thickness of the cobalt oxide layer. Furthermore, the cell voltage dropped by 0.1 V from the first to the second experiment. A somewhat higher cell voltage was usually observed when new thin cobalt starting sheets were introduced. As the weight of the cathodes was increasing, their alignment improved and the contact resistance became lower, thus reducing the cell voltage. The same cobalt cathodes were used in all four experiments.

Continuous measurements of the current and the anode potential were tested for the Reg* anode. The current was recorded by measuring the potential drop across a copper shunt mounted on the contact side of the anode hanger bar. Fig. 4.47 a) shows that the current was relatively stable, indicating steady current distribution between the electrodes in the cell. The porous tip of a glass capillary was placed close to a rod in the centre of the anode structure, and a KCl salt bridge was extended from the capillary through the top of the anode hood to a calomel reference electrode. The potential was measured between the reference electrode and a shielded titanium wire, which was welded to the anode surface next to the capillary tip to avoid the potential drop within the anode. As shown in Fig. 4.47 b), the recorded anode potential increased initially before stabilizing after about 2.5 hours of electrolysis. Contrary to the laboratory experiments, no potential peak appeared during the initial phase of electrolysis. These measurements were

abandoned due to frequent contact problems and the large and varying influence of solution IR drop.

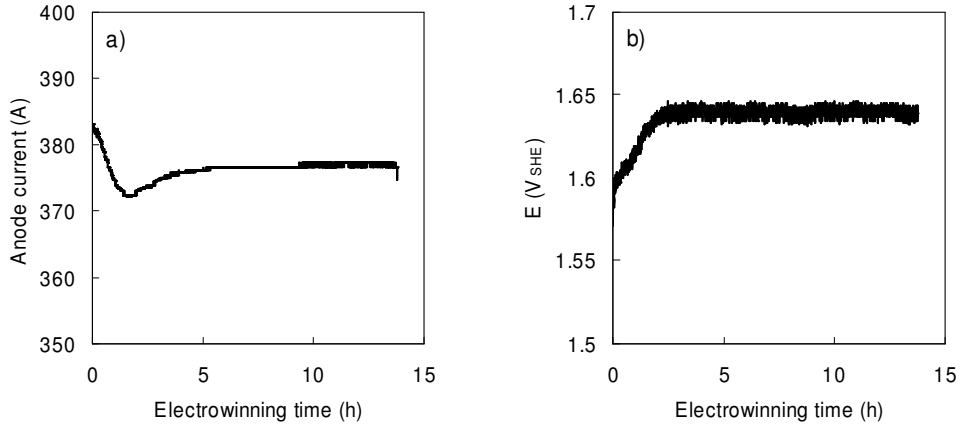

Figure 4.47 *a) Current and b) anode potential recorded for the Reg* anode in the 14-hour experiment.*

4.3.1.2 Effects of inlet pH

In the second series, the pH of the feed electrolyte was gradually decreased in an attempt to eliminate anode scaling, as achieved in the laboratory scale experiments (section 4.2.1.2). It was found that the catholyte pH had to be as low as 0.6 to completely avoid scaling (Fig. 4.48 a)), because the pH in the anode compartments did not decrease to the same extent. At standard electrowinning conditions, the pH in the anolyte was higher than in the catholyte, and this pH difference, denoted as ΔpH, increased when the catholyte pH was lowered, see Fig. 4.48 b). It is believed that the observed increase in ΔpH at low catholyte pH values was caused by a combination of less oxygen being formed on the anodes, thus generating less acid in the anode compartments, and a higher degree of proton migration out of the anode bags towards the cathodes. This view was supported by calculating anolyte pH values from the H^+ material balance for an anode compartment, as outlined in Appendix. From Fig. 4.48 b) it can be seen that a very good agreement was obtained between experimental and calculated ΔpH values.

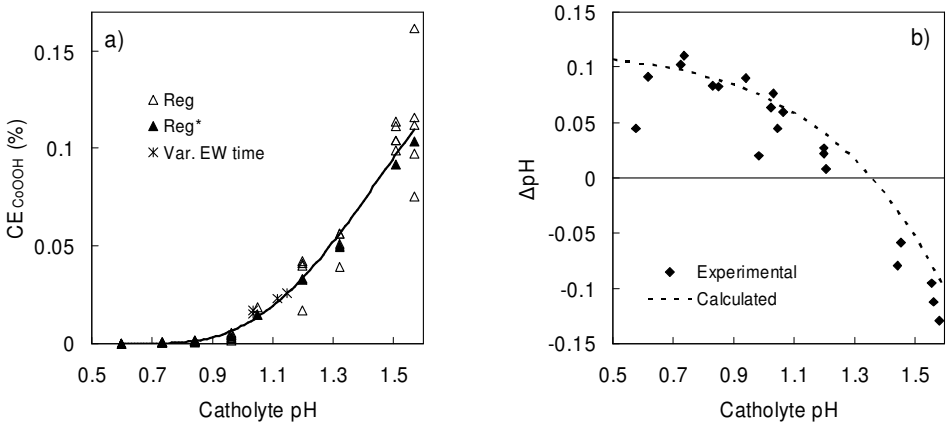

Figure 4.48 *Effect of catholyte pH on a) current efficiency for anodic cobalt oxide deposition and b) difference in pH between the anolyte and the catholyte. A set of CE_{CoOOH} values obtained at various electrowinning times are also shown.*

Increase in the electrolyte pH from the standard level at pH 1 gave accelerated rates of anodic cobalt oxide deposition, as illustrated in Fig. 4.48 a). All the anodes were etched, and the amount of CoOOH varied considerably. This was probably due to different conditions in each of the anode bags together with uncertainties in the experimental method, see section 4.3.3. The anode deposit seemed to adhere better to the worn Reg* anode than to the recoated Reg anodes, since for the latter, more scale was collected at the bottom of the bags. Moreover, there was no sign of any precipitation in the bulk solution. Compared to the lab work, similar trends were obtained for CE_{CoOOH} versus pH. However, the levels were somewhat lower in the pilot experiments, which may be explained by the difference in anode geometry and local current density.

When the pH of the catholyte exceeded ~1.3, ΔpH shifted from positive to negative (Fig. 4.48 b)). Increased rates of anodic O_2 and CoOOH formation generated more acid inside the anode compartments, and the lower acid concentration in the catholyte reduced the extent of H^+ transport by migration (see Appendix section A.3.1). At the highest pH tested, i.e. pH 1.6 in the catholyte, no HCl was added to the mixing tank to control acidity. In this case the acid balance for the pilot plant system gave an O_2 content of 2.5 % in the anode gas, in acceptable agreement with the experimental analysis (Appendix Fig. A.2 a)).

The current efficiency for cobalt dropped to 83 % when the catholyte pH was lowered from 1 to 0.6 (Fig. 4.49 a)). On the other hand, at pH 1.6, CE_{Co} improved to almost 96 %. The pH in the catholyte was higher than in the feed, and the difference increased from 0.01 at pH 0.6 to 0.05 at pH 1.6. Within the pH range tested, the cell voltage appeared to be independent of the electrolyte acidity (Fig. 4.49 b)).

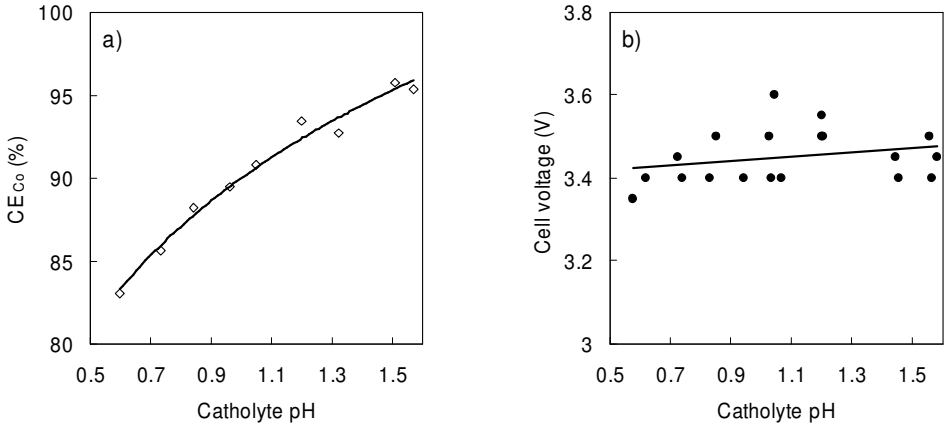

Figure 4.49 *Effect of catholyte pH on a) cathodic current efficiency for cobalt and b) cell voltage.*

Contrary to the other sets of experiments, the effects of pH were not studied in random order. Hence, it is believed that the high anolyte flows measured at high pH, see Appendix Fig. A.2 b), can be ascribed to a high permeability of the diaphragm and not the pH itself. This is further discussed in section 4.3.3.2.

4.3.1.3 Effects of cobalt chloride concentration

The concentration of cobalt was varied in the range 34 – 74 g/l, the chloride concentrations being 46 and 92 g/l respectively. Fig. 4.50 a) shows that the anode scaling was almost 5 times more intense at the highest concentration compared to the lowest concentration, even though the anolyte pH dropped close to 0.1 pH units (Fig. 4.50 b)), counteracting the rate of cobalt oxide deposition. This pH decrease is attributed to more cobalt and chloride ions being available for current transport across the diaphragm at higher concentrations, thereby reducing the extent of H^+ migration out of the anode

bags. The calculations of ΔpH presented in Appendix section A.3.2 demonstrate the much larger reduction in the proton migration term with increasing $CoCl_2$ concentration than the corresponding decrease in the anodic acid generation term. Cobalt and chloride concentrations were 1 – 2 g/l lower in the anolyte than in the catholyte, reflecting their contribution to current transport.

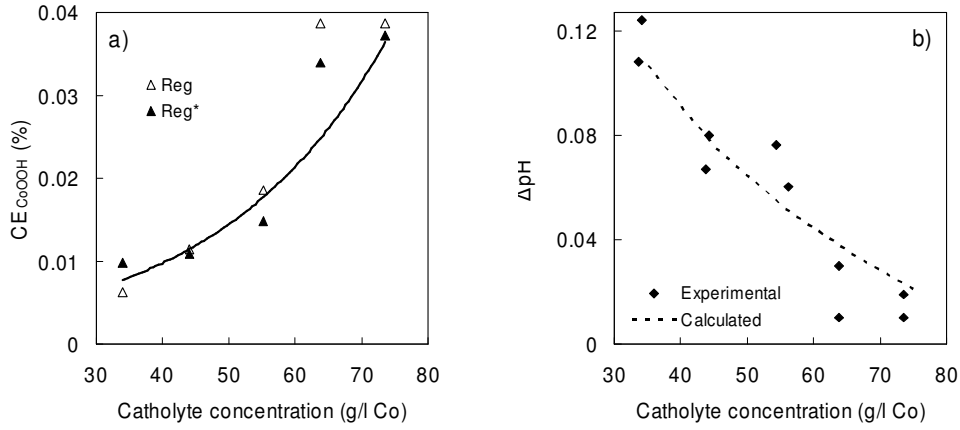

Figure 4.50 *Effect of catholyte cobalt chloride concentration on a) current efficiency for anodic cobalt oxide deposition and b) difference in pH between the anolyte and the catholyte.*

Owing to a pH ~0.05 higher than in the other experiments, a larger quantity of CoOOH was formed at 64 g/l Co. The higher pH can also explain the lower ΔpH values measured at this concentration. In the prevailing concentration range, CE_{CoOOH} was increased by ~0.0008 % per g/l increase in cobalt concentration compared to ~0.0032 % in the lab experiments. This large difference indicates that the cobalt oxide deposition reaction was more dependent on cobalt concentration at the higher electrolyte pH employed in the laboratory.

The cobalt chloride concentration also had a large effect on CE_{Co}, increasing from 83 % at 34 g/l Co to 95 % at 74 g/l Co (Fig. 4.51 a)). In the same concentration range, the cell voltage was reduced from 3.6 to 3.2 V (Fig. 4.51 b)). The depletion of cobalt and chloride ions was 1 – 2 g/l in the catholyte. From the negative influence of a lower concentration on both CE_{Co} and cell voltage, it seems to be more beneficial to control anode scaling

by pH. The ratio between the change in CE_{CoOOH} and the change in CE_{Co} was higher when varying the pH.

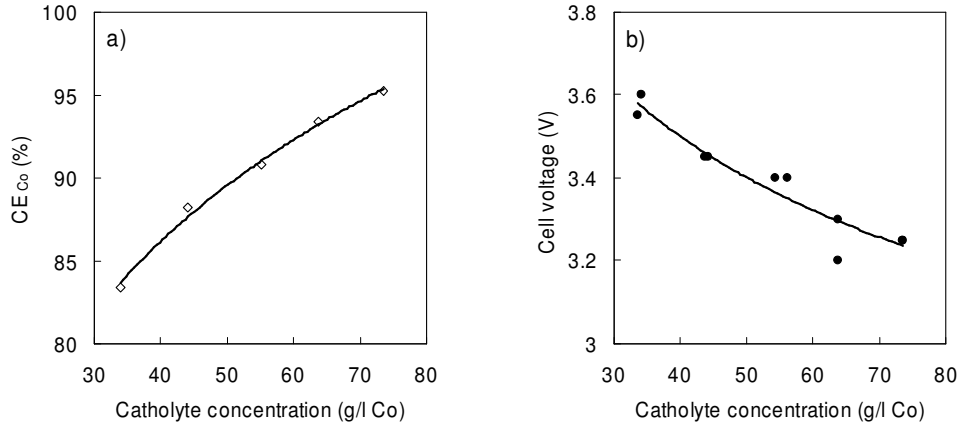

Figure 4.51 *Effect of catholyte cobalt chloride concentration on a) cathodic current efficiency for cobalt and b) cell voltage.*

4.3.1.4 Effects of temperature

As shown in Fig. 4.52 a), the anode scaling reaction was accelerated at elevated temperatures, almost four times more cobalt oxide being formed at 69°C compared to 50°C. A similar temperature dependence was observed at higher pH in the laboratory, see section 4.2.1.6. The pH in the anolyte compartments was higher than in the catholyte for all temperatures tested, in accordance with the calculated ΔpH values (Fig. 4.52 b)). The slightly reduced pH difference measured at higher temperatures may be due to a higher catholyte pH at the relevant temperature, since the electrolyte pH increases with temperature, see section 2.7.7 (pH was measured at room temperature in the pilot work).

Consequently, operating at low temperature would reduce the extent of scaling, but at the expense of both CE_{Co} and cell voltage, see Figs. 4.53 a) and b) respectively, thus increasing energy consumption from 3.1 kWh/kg Co at 69°C to 3.6 kWh/kg Co at 50°C. Higher levels of hydrogen and oxygen impurities absorbed in the cobalt cathodes is another negative effect of reduced temperature, lowering product quality. In contrast to the lab exp-

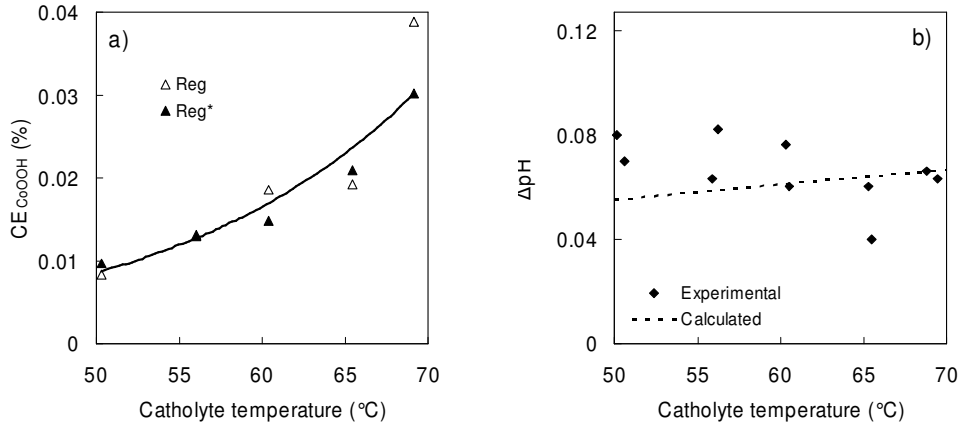

Figure 4.52 *Effect of catholyte temperature on a) current efficiency for anodic cobalt oxide deposition and b) difference in pH between the anolyte and the catholyte.*

eriments, where dissolved chlorine was reduced on the cathode, CE_{Co} increased monotonically with temperature in the pilot plant. The cobalt cathodes were replaced by new starting sheets before the experiment at 64°C, which increased the cell voltage.

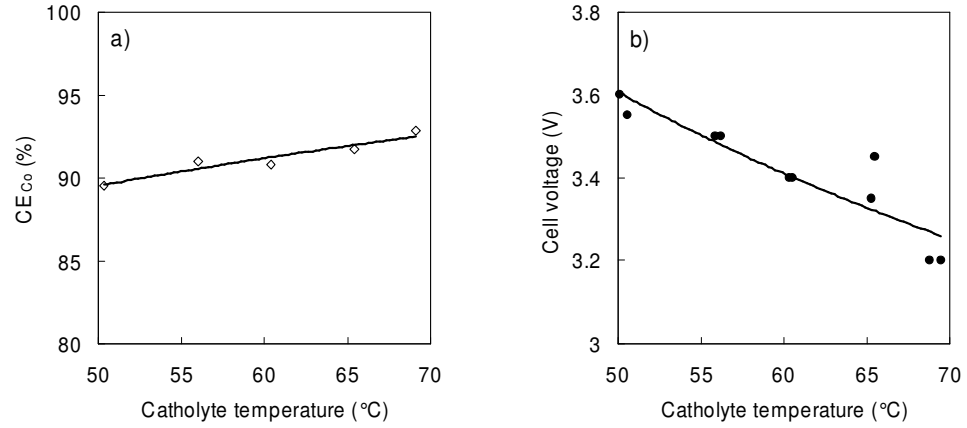

Figure 4.53 *Effect of catholyte temperature on a) cathodic current efficiency for cobalt and b) cell voltage.*

4.3.1.5 Effects of current density

The effects of current density on the cobalt electrowinning process were investigated by applying total cell currents ranging from 1000 to 3000 A, equivalent to 106 and 319 A/m^2 cathodic current density. The geometric surface area of the rod anodes was about four times lower than that of the cathodes, thus giving anodic current densities in the range 435 – 1311 A/m^2. Since the total charge supplied was about the same in each experiment (~50 kAh), electrowinning times varied between ~17 and ~46 hours.

Fig. 4.54 a) shows that the extent of anode scaling was only slightly increased at higher current densities, despite the observed increase in both anolyte pH (Fig. 4.54 b)) and temperature (see below). In four of the five experiments, the amount of CoOOH formed on the end anode placed next to the catholyte overflow was measured in addition to the Reg* anode. It can be seen from Fig. 4.54 a) that CE_{CoOOH} was higher on the end anode, which received just a little bit more than half the current compared to the Reg* anode. The same anode was used as end anode in all four experiments, and it should be mentioned that in the series involving different inlet pH values, this particular anode generated more cobalt oxide than the average value.

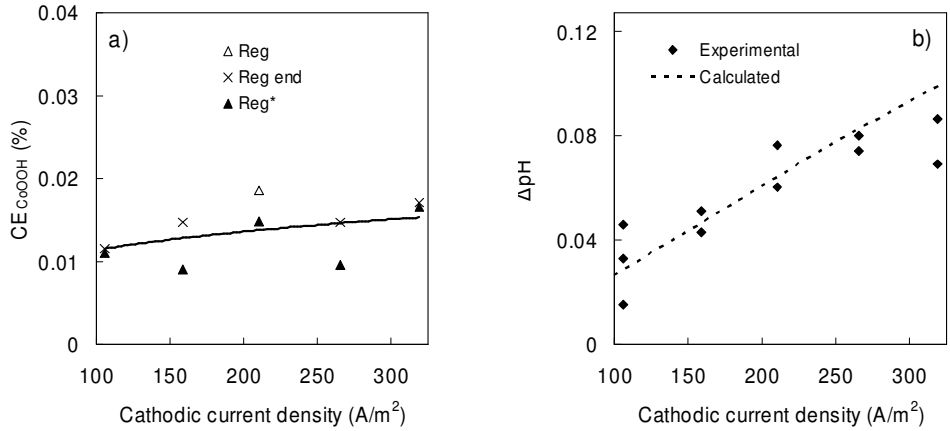

Figure 4.54 *Effect of cathodic current density on a) current efficiency for anodic cobalt oxide deposition and b) difference in pH between the anolyte and the catholyte.*

The larger pH difference between the anolyte and the catholyte is attributed to more H^+ ions being transported out of the anode bags to conduct the

higher currents. Furthermore, less oxygen was produced on the anodes when the current was raised, although a portion of the O_2 content given in Appendix Fig. A.5 a) came from air leakage at low current density. The ΔpH values were, however, suppressed by higher anolyte flows, see Appendix Fig. A.5 b). At higher currents, the gas bubble content of the electrolyte in the anode bags becomes more extensive, which increases the hydrostatic pressure difference across the diaphragm, leading to higher anolyte flows [20]. On the other hand, the increased rates of gas production resulted in a larger pressure drop from the manometer to the anode hoods.

High current densities were favourable with respect to CE_{Co}, improving from 89 % at 106 A/m^2 to 92 % at 319 A/m^2 (Fig. 4.55 a)). To increase the current from 1000 to 3000 A, additional energy had to be applied to the system, indicated by the almost linear increase in cell voltage from 2.6 to 4.2 V shown in Fig. 4.55 b). This extra energy input was converted into heat, reflected by the temperatures measured in the catholyte overflow, at 59°C and 63°C respectively. Heating of the electrode hanger bars was another consequence of higher current loads.

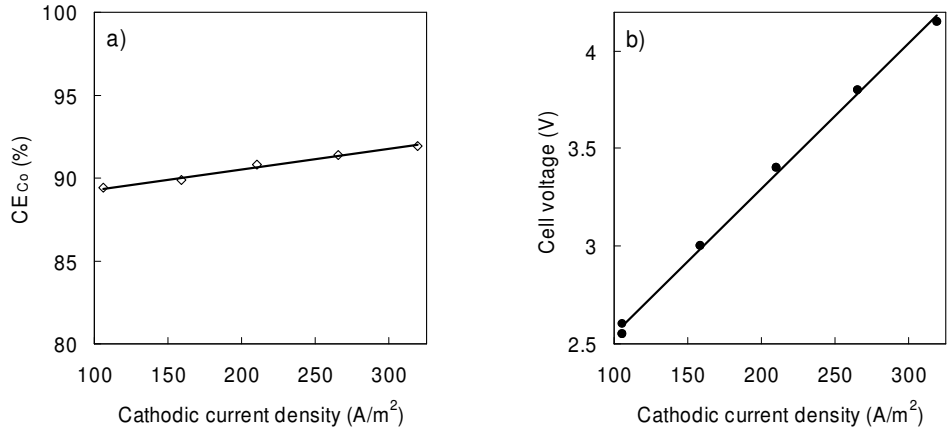

Figure 4.55 *Effect of cathodic current density on a) cathodic current efficiency for cobalt and b) cell voltage.*

4.3.2 Possible methods to suppress anode scaling

Based on the results obtained in the laboratory, it was decided to examine on a pilot scale some of the alternative methods to suppress anodic cobalt oxide deposition. Different anode geometries, various means of decreasing the pH in the anode compartments and advanced current supply were tested.

4.3.2.1 Effects of anode design

The various anode designs illustrated in Fig. 3.6 were tested at the standard electrowinning conditions listed in Table 4.8. From Fig. 4.56 a) it is evident that the quantity of deposited cobalt oxide increased with increasing anodic current density, calculated from the geometric surface area. In addition, the end anodes, operating at approximately half current, gave lower CE_{CoOOH} values than the other anodes in the cell that was separated by a cathode on either side. When new box anodes were employed, having the largest surface area of the five different substrates tested, almost no CoOOH was detected on the two end anodes. To see if the anode scaling was completely inhibited at slightly higher acidity, an additional test was performed with box anodes at pH 0.9 in the feed electrolyte. Less CoOOH was generated, but scaling was not avoided, including the end anodes. After the recoated ESA anodes were tested, the pH conditions were found to be nearly 0.1 pH units higher than in the other experiments reported in Fig. 4.56 a). When compared with

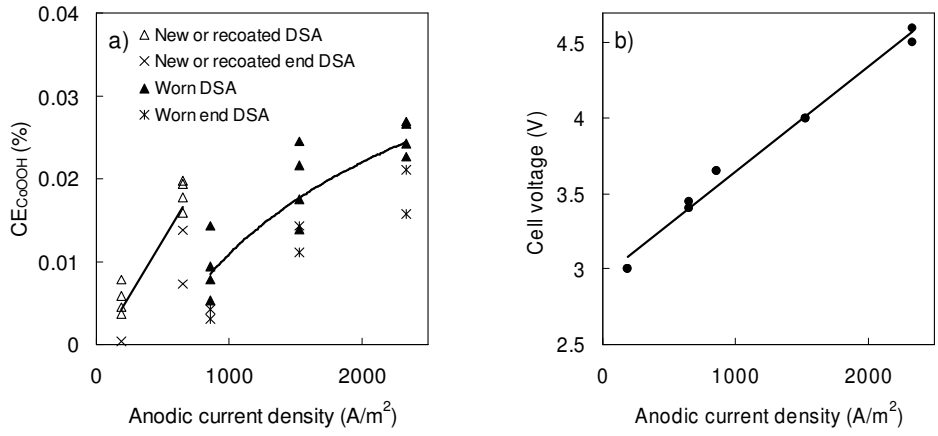

Figure 4.56 *Effect of anodic current density on a) current efficiency for anodic cobalt oxide deposition and b) cell voltage.*

results obtained with regular rod anodes at equivalent conditions, the larger area ESA anodes seemed to generate less anode deposit.

Before rods were removed from the group of 6 worn regular anodes in order to increase the local current density, these anodes were first tested without any modifications. Although the thickness of the catalytic coatings was within acceptable limits, an uneven current distribution appeared between the electrodes, and the cell voltage was 0.3 V higher than usual under the prevailing conditions. Moreover, CE_{CoOOH} was significantly reduced compared to recoated regular anodes, and very little deposit was flaking off these anodes during electrolysis. The lower rate of anode scaling on the worn anodes together with improved adherence to the anode surface might have been due to a more cracked catalytic layer enriched with ruthenium, similar to what observed for the worn Reg* electrode investigated in the laboratory cell, see section 4.2.2.1. When half of the vertical rods were cut off, anode scaling was more than doubled, and parts of the catalytic coating detached as a powder, which settled to the bottom of the anode bags. Removal of additional rods resulted in even higher CE_{CoOOH} values.

The measured cell voltage as a function of anodic current density is presented in Fig. 4.56 b). The energy efficient box anodes operated at close to 3 V, whereas with the anodes from which rods had been removed twice, the cell voltage was more than 4.5 V. As a consequence of the increased current density, the temperature of the catholyte was 62°C. A mirror image of the anode grid structure created by nodules had also developed on the surface of the cobalt cathodes, indicating that in this case the distance between the rods was too large for proper distribution of the current over the cathode surface. Despite the lack of uniform current distribution, CE_{Co} and the composition of the anode gas seemed to be only moderately affected by changes in the anode surface area.

When comparing the effect of current density on the anode scaling process observed in the pilot experiments with the laboratory results, it is obvious that a disagreement exists. The pilot results indicate that CE_{CoOOH} increases with increasing current density, whereas the laboratory work showed the opposite trend in the same current density range (see section 4.2.1.7). The reason for this discrepancy is unclear, as there may be several plausible explanations. The lab experiments were carried out at higher pH, ~1.5 when measured at room temperature, and the observed maximum in the CE_{CoOOH} vs. current density curve may be shifted to higher current densities when the

pH is decreased. More oxygen is evolved at higher pH, and the effect of current density on the change in local pH at the anode surface may be a function of electrolyte acidity. Furthermore, the influence of the induction period, i.e. the time from the start of electrolysis to the anode surface is covered by cobalt oxide, is probably more important at low pH. In the case of varying the anode surface area, the thickness of the cobalt oxide layer will be lower on the anodes having a high surface area, like the box anodes. Consequently, the contact area between the anode deposit and the electrolyte will be larger, facilitating dissolution of scale in the time period between electrowinning and etching. It should also be noticed that in additional tests not part of this work, box anodes were found to generate more cobalt oxide than regular rod anodes, at pH ~1.2 (1 month in operation) and pH ~1.5 (24 hours).

A group of worn rod anodes that were sandblasted were also tested as anodes for cobalt electrowinning at standard conditions. Analysis indicated that traces of noble metals were still present on the anode surface after sandblasting. These anodes exhibited excellent current distribution between the electrodes, and the cell voltage and the anode gas composition were both stable at normal levels. The quantity of CoOOH deposited was similar to coated anodes, CE_{CoOOH} varying from 0.012 to 0.026 % with the average value 0.016 % (all 6 anodes were etched). Very little deposit was observed at the bottom of the anode bags, indicating a relatively strong bonding to the anode structure.

4.3.2.2 Effects of anode suction

According to the proposed theory of H^+ ion migration described in Appendix, increased rates of anolyte flow should lower the pH inside the anode compartments as long as it is higher than the catholyte pH. When performing cobalt electrowinning in divided cells from sulphate solution, the acidity of the anolyte is much higher due to oxygen evolution only. Hence, the situation is opposite, and a low flow rate of electrolyte into the anode compartments has been recommended to attain a low anolyte pH, thereby suppressing the anodic deposition of cobalt oxide on the lead anodes [70].

The application of a higher suction from the anode hoods is one alternative way of increasing the anolyte flow. To elucidate the effects on the cobalt electrowinning process, anode suctions of 51, 76 and 104 millimetre water

gauge were applied in three individual experiments. As shown in Appendix Fig. A.6 b), the flow of anolyte increased linearly with suction within the range being studied, from 50 to 133 l/h,anode. A decline in anode scaling was obtained when the suction was increased (Fig. 4.57 a)), brought about by the lowering of ΔpH, which was in perfect agreement with the calculated values (Fig. 4.57 b)).

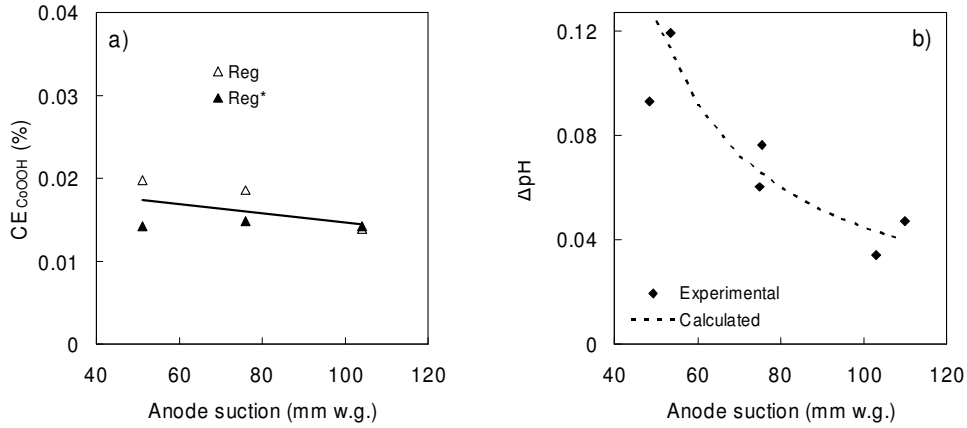

Figure 4.57 *Effect of anode suction on a) current efficiency for anodic cobalt oxide deposition and b) difference in pH between the anolyte and the catholyte.*

CE_{Co} and the cell voltage were only moderately affected by anode suction, see Figs. 4.58 a) and b). However, at the lowest applied suction, a faint smell of chlorine was recognized in the air surrounding the cell. In this case, the velocity of electrolyte flow through the diaphragm was not sufficiently high to completely avoid back-diffusion of chlorine. Chlorine in the catholyte will also be reduced on the cathodes, thus having a negative effect on CE_{Co}.

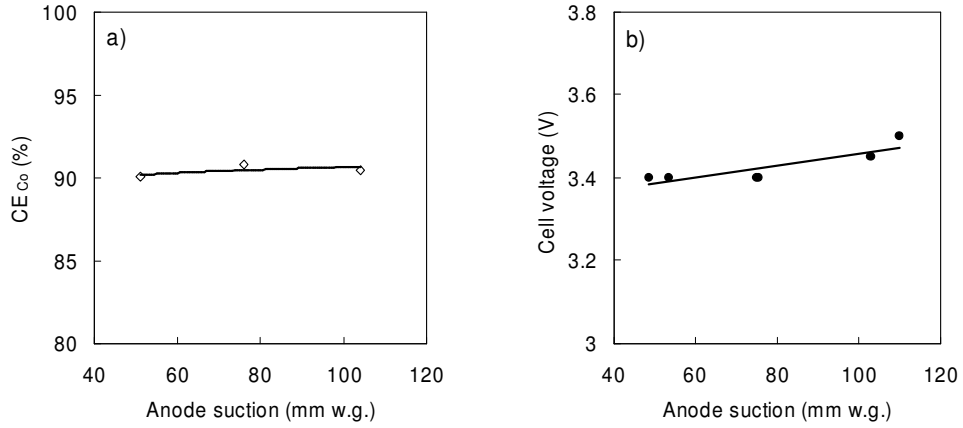

Figure 4.58 *Effect of anode suction on a) cathodic current efficiency for cobalt and b) cell voltage.*

4.3.2.3 Effects of inlet flow rate

Another means of increasing the anolyte flow rate is simply by pumping more feed electrolyte into the electrolytic cell. The higher catholyte level thus obtained imply that the distance the anolyte has to be lifted inside the hoods in order to reach the overflow duct will be reduced. Provided that the anode suction is maintained, a higher anolyte flow will then be achieved. In fact, a dual pH effect is associated with increased inlet flow rates. In addition to reduced ΔpH values between the anolyte and the catholyte, the shorter electrolyte residence time in the cell will lower the pH of the catholyte, which is normally higher than the inlet pH, owing to cathodic hydrogen evolution.

The effect of the flow rate of feed electrolyte was studied between 0.6 and 3.5 m^3/h, the other parameters being held at the standard conditions given in Table 4.8. Fig. 4.59 a) shows that the extent of anode scaling was reduced by one half when the inlet flow rate was increased from 0.6 to 3.5 m^3/h. The measured catholyte level differed by ~18 mm. Furthermore, the catholyte pH decreased by 0.05 pH units, and the anolyte flow rate increased from 68 to 113 l/h,anode (Appendix Fig. A.7 b)), both lowering the anolyte pH. The contributions of 0.05 pH units from the reduced catholyte pH and 0.03 pH units from the reduced ΔpH value (Fig. 4.59 b)) resulted in a reduction of the anolyte pH by 0.08 pH units.

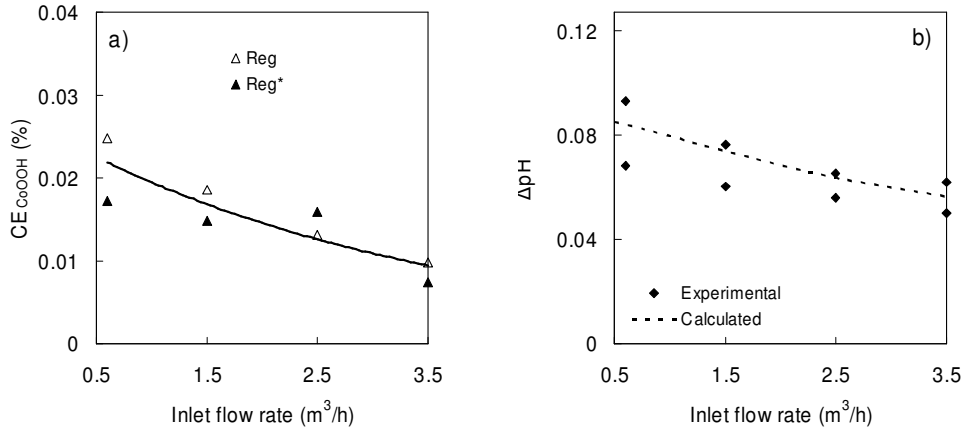

Figure 4.59 *Effect of inlet flow rate on a) current efficiency for anodic cobalt oxide deposition and b) difference in pH between the anolyte and the catholyte.*

As illustrated in Fig. 4.60 a), CE_{Co} declined somewhat at higher inlet flow rates due to the lower catholyte pH. The cell voltage was scarcely influenced by increasing inlet flow rate (Fig. 4.60 b)).

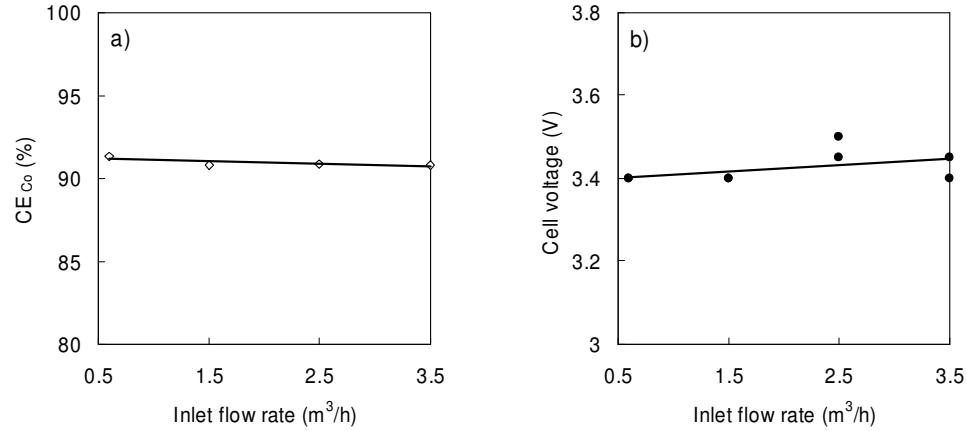

Figure 4.60 *Effect of inlet flow rate on a) cathodic current efficiency for cobalt and b) cell voltage.*

4.3.2.4 Hydrochloric acid addition to anode compartments

In the previous two sections it was demonstrated that the pH in the anode compartments can be modified by varying the anolyte flow rate. However, the effect was rather limited, and in order to achieve larger negative ΔpH values across the diaphragm, acid must either be generated inside or introduced directly into the anode bags. Results from pilot scale experiments involving the latter concept are reported below.

Concentrated HCl was pumped continuously into each of the six anode compartments via tubes going through the top of the hoods and ending close to the bottom of the bags. The results from the electrowinning of cobalt with HCl addition to the anodes are summarized in Table 4.10. In the first experiment, 0.6 l/h HCl was distributed between the anodes, the quantity being almost large enough to substitute the acid usually added to the mixing tank to keep the pH constant. The anolyte pH became lower than the catholyte pH, and CE_{CoOOH} dropped to less than one half relative to without HCl.

Table 4.10 Summary of results from the addition of HCl to the anode compartments.

HCl to anodes (l/h)	Catholyte pH	ΔpH Exp.	ΔpH Calc.	CE_{Co} (%)	CE_{CoOOH} Reg (%)	CE_{CoOOH} Reg* (%)
0.6	1.10	-0.06	-0.08	90.7	0.004	0.008
2.3	1.11	-0.30	-0.36	89.7	0.0014	0.0012
4.4	1.61	-0.95	-1.08	94.9	0.0005	0.0002

Since cobalt oxide deposits were still growing on the DSA® anodes, the HCl addition was increased to 2.3 l/h in the second experiment. In this case, the excess acid had to be neutralized in the mixing tank by pumping in slurry of basic cobalt carbonate in cobalt electrolyte produced in the Xstrata Nikkelverk cobalt refinery. The measured anolyte pH was now as low as 0.8, and only small amounts of anode scale were formed.

The possibility of operating at a lower catholyte acidity to increase cobalt current yield was also tested with simultaneous control of the anode scaling by acid addition to the anode compartments. By adding 4.4 l/h HCl to the anodes and then $CoCO_3$ to the mixing tank to raise the inlet pH to 1.6, a high

CE_{Co} of 95 % was obtained with only traces of CoOOH deposited on the anodes. Due to the high electrolyte flow rates into the anode bags, transport of H^+ ions to the cathode compartment was minimized, and high negative ΔpH values could be maintained across the diaphragm. However, both CE_{Co} and the calculated ΔpH values (Appendix section A.3.7) indicated that some of the added acid ended up in the catholyte. Most of the electrolyte is entering the lower parts of the anode compartments because the difference in hydrostatic pressure across the diaphragm increases with depth below the electrolyte surface [20]. Therefore, some of the acid might have diffused to the catholyte from the upper parts of the bags where the electrolyte velocity through the diaphragm is lower. Compared to the experiments performed at high acidity without HCl addition to the anodes, slightly higher CE_{CoOOH} values were obtained at similar anolyte pH. This may be explained by concentration gradients of protons within the anode bags, despite the mixing generated by gas bubble formation.

From a theoretical point of view, acidification of the anolyte by introducing HCl during cobalt electrowinning seems like a good idea, but there are some practical concerns associated with it. The large quantities of acid required will be challenging for the volume balance of the tankhouse, and neutralization of the electrolyte before it is returned to the electrowinning cells will add to the operating costs. Handling of strong acid in a myriad of small tubes is also a potential health hazard.

4.3.2.5 Hydrogen peroxide addition to the electrolyte

As described in section 4.2.3, H_2O_2 has been suggested as an additive to suppress anode scaling during electrowinning of cobalt. Two pilot scale experiments are reported, where H_2O_2 (35 %) was added either to the feed electrolyte or pumped directly into the anode compartments using the same equipment as used for HCl. The results presented in Tables 4.11 and 4.12 support the conclusions made from the work on H_2O_2 carried out in the laboratory cell. H_2O_2 was consumed both on the cobalt cathodes and by reaction with dissolved chlorine in the anode bags, leading to reduced CE_{Co} and acidified anolyte respectively. When H_2O_2 was added to the anodes, $CoCO_3$ slurry had to be used as neutralization agent in the mixing tank. A marked increase in the O_2 : Cl_2 ratio of the anode gas was another indication of the reaction between H_2O_2 and Cl_2, equation 4.8. The drop in anolyte pH

lowered the rate of cobalt oxide deposition, while the recorded cell voltage was not influenced by the H_2O_2 addition.

Table 4.11 Summary of results from the addition of H_2O_2 to the electrolyte.

H_2O_2 addition		Catholyte pH	Cell voltage	Anode gas		CE_{Co}	CE_{CoOOH}	
				Cl_2	O_2		Reg	Reg*
(l/h)			(V)	(%)	(%)	(%)	(%)	(%)
0.9	To inlet	1.12	3.6	88	10	82.7	0.016	0.012
1.2	To anodes	1.07	3.4	63	32	88.3	0.0010	0.0004

In order to further clarify the behaviour of H_2O_2 in the present system, a few simple calculations were made, see Appendix section A.3.8 and Table 4.12. When the calculated differences in pH between the anolyte and the catholyte were based on the measured oxygen content in the anode gas, assuming that all O_2 was formed by reaction with Cl_2, they agreed well with the measured ΔpH values. This fact suggests that most of the H_2O_2 had decomposed inside the anode bags, indicating a quite rapid reaction rate (mean residence time of anolyte in the bags typically < ½ h). However, lower redox potential in the dechlorinated anolyte demonstrated that some H_2O_2 was transported to the dechlorination facility, making the chlorine removal more efficient. Decomposition of H_2O_2 according to equation 4.6 also appears to be of minor importance, since acid is not formed by this reaction.

Table 4.12 Experimental and calculated differences in pH between the anolyte and the catholyte during H_2O_2 addition.

H_2O_2 addition		Measured	Calculated ΔpH	
(l/h)		ΔpH	Based on O_2	Based on H_2O_2
0.9	To inlet	-0.14	-0.10	-0.02
1.2	To anodes	-0.32	-0.34	-0.37

In the case where the ΔpH values were calculated from the rates of H_2O_2 addition, assuming complete conversion in the anode compartments by reaction with excess Cl_2, the measured anolyte pH was considerably lower than the calculated value when H_2O_2 was added to the inlet. It is believed that this can be attributed to build-up of H_2O_2 in the system due to incomplete decomposition at the cathodes. The concentration of H_2O_2 in the electrolyte sucked into the anode bags will, therefore, increase over time, which results in a lower anolyte pH. Higher CE_{CoOOH} values compared to results obtained at similar anolyte pH levels without H_2O_2 addition may be

explained by concentration gradients of protons in the anode compartments and continued decrease in pH during dechlorination (the pH was measured in the electrolyte leaving the dechlorination facility). The ~3 % decrease in CE_{Co} when H_2O_2 was added to the anodes is ascribed to diffusion of H^+ and H_2O_2 to the catholyte from the upper part of the anode bags, or H_2O_2 passing through the dechlorination step, thereby ending up in the feed solution.

4.3.2.6 Stability of anode deposit

Fresh cobalt oxide deposited anodically on DSA® anodes was found to dissolve in acidic cobalt chloride electrolyte at open circuit potential (OCP), see section 4.2.4.2. The stability of the anode deposit produced in the electrowinning pilot plant was also studied. Subsequent to electrowinning at the standard conditions in Table 4.8, the recoated rod anodes remained in the cell for 0.5, 1 and 1.5 hours at OCP before being removed and etched. For withdrawal of chlorine from the anodes, the same suction was applied after interruption of electrolysis, and the anolyte contained in the anode compartments was then replaced by Cl_2-free catholyte.

The amount of anode deposit is shown as a function of time at OCP in Fig. 4.61. It is obvious that CoOOH dissolved, although the rate of dissolution seemed to be reduced with time. A similar but more dramatic trend was observed in the laboratory, despite the higher electrolyte pH level (Fig. 4.40). The fact that the estimated thickness of the cobalt oxide film was almost one order of magnitude larger in the pilot plant experiment was probably one important factor with respect to its stability. In a preliminary test, where the anodes were left in the cell for three days after one day of electrolysis, no remaining cobalt oxide deposit was found, neither on the rods nor at the bottom of the bags.

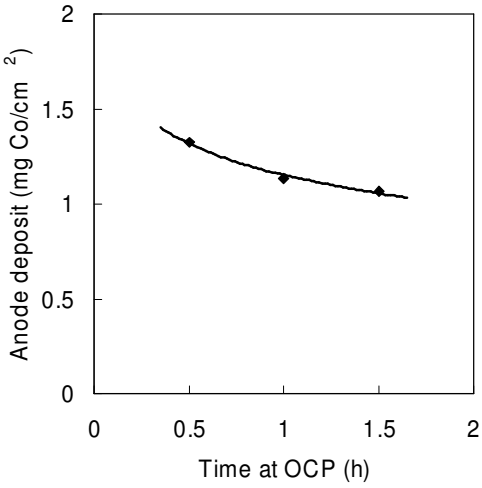

Figure 4.61 *Quantities of anode deposit measured for anodes kept at open circuit potential for different time periods after electrowinning at standard conditions.*

4.3.2.7 Periodically interrupted current (PIC)

Since the anode scale was not completely stable when the current was switched off and the pilot plant power supply could operate in PIC mode, it was decided to perform a set of cobalt electrowinning experiments involving this type of advanced current supply. The frequency was varied from 24 hours ($1.2 \cdot 10^{-5}$ s^{-1}) to 0.9 seconds, and the current on-time was set to 90 %. To counteract the negative effect of the off-time on productivity, the cathodic current density in the on period was increased by 10 % to 231 A/m^2. The electrowinning time was 24 hours except for the experiment with 24-hour frequency, which lasted for 72 hours. All experiments were terminated at the end of a current off period.

Fig. 4.62 a) shows that at the highest frequencies, PIC-type electrolysis did not have a large effect on CE_{CoOOH}. On the other hand, when the frequency was as low as 24 hours, the build-up of anode scale was reduced considerably. In this case, the current off-time of 2.4 hours was sufficiently long for most of the chlorine to be removed from the anode compartments. In addition, the anolyte pH decreased and became similar to the catholyte pH due to the absence of H^+ migration when the current was switched off. Both

lower redox potential in solution, i.e. less dissolved Cl_2, and lower pH will enhance the dissolution rate of cobalt oxide. As illustrated in Fig. 4.62 b), CE_{Co} was not dependent on the PIC frequency. The measured anode gas composition was ~98 % Cl_2 and ~1 % O_2 in all experiments.

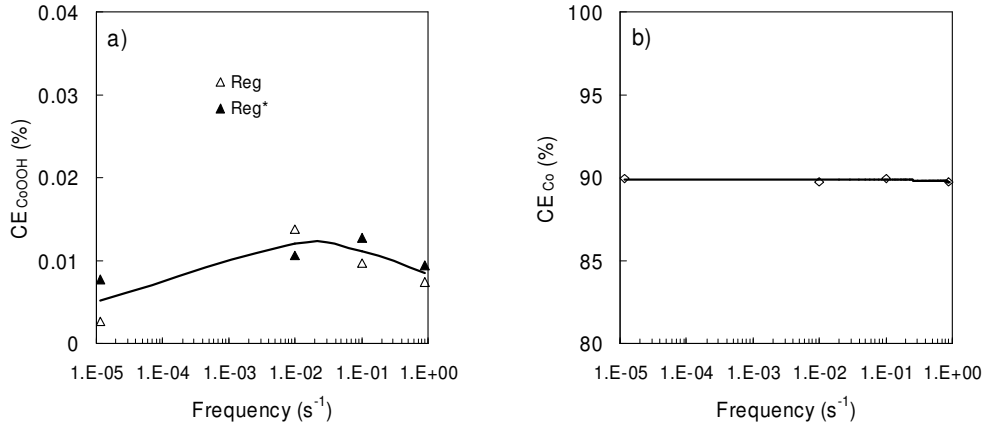

Figure 4.62 *Effect of PIC frequency on current efficiency for a) anodic cobalt oxide deposition and b) cathodic cobalt deposition.*

4.3.2.8 Short-circuiting of the electrowinning cell

In the laboratory part of the present work, it was found that the dissolution of cobalt oxide on DSA® was accelerated if the electrochemical cell was short-circuited subsequent to electrolysis, see section 4.2.4.4. To see if a similar effect could be obtained with full-size electrodes, the pilot electrowinning cell was short-circuited after 24 hours of standard cobalt electrowinning. Three aluminium cables (400 mm^2, 6 m) in parallel were bolted to the anode and the cathode bus bar respectively, and the opposite ends were connected to an air-driven switch made of copper. 30 seconds after interruption of electrolysis, the cell was short-circuited. The discharge current was recorded by measuring the potential drop across a shunt. Following 20 minutes of shorting, two of the anodes were removed from the cell and then etched for determination of the amount of remaining anode deposit.

The discharge current recorded during short-circuiting is presented in Fig. 4.63. Due to the high concentration of chlorine at the DSA® surface, the initial discharge current was very high. The first current recorded was 1170

A, representing almost 60 % of the total current load during electrowinning at standard conditions. However, it decreased rapidly with time, and after 1 minute it was less than 150 A. Just before anode removal, the shorting current had dropped further to only 18 A.

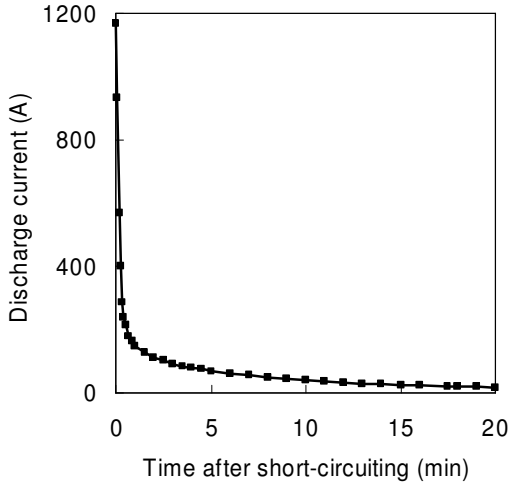

Figure 4.63 *Discharge current during short-circuiting of the electrowinning cell subsequent to electrolysis.*

As opposed to the laboratory results, short-circuiting of the pilot cell seemed to reduce the amount of cobalt scale only slightly. CE_{CoOOH} values of 0.004 and 0.009 % were obtained for the worn Reg* anode and the recoated Reg anode respectively, however, the average anolyte pH was as low as 1.09. The quantity of deposit at the bottom of the bags appeared to be larger than normal, and the short-circuiting will of course have only minor effect on CoOOH particles not in contact with the DSA® structure. Compared to the lab scale tests, the combination of higher concentration of dissolved chlorine and thicker cobalt oxide films was probably impeding the effective dissolution of anode scale when short-circuiting the pilot cell. The cathodic current efficiency for cobalt was ~2 % lower than without shorting, while the total electric charge based on the recorded discharge current represented only 0.04 % of the charge applied during electrowinning. The reason for the low CE_{Co} is not known.

4.3.3 Evaluation of experimental techniques

4.3.3.1 Determination of the extent of anodic cobalt oxide formation

It is evident that several of the shortcomings reported for the laboratory work were relevant for the pilot work as well, see section 4.2.5. The anodically deposited cobalt oxide was not stable in the electrolyte (Fig. 4.61), resulting in partial dissolution in the time period between electrowinning and anode removal. The anodes could not be lifted out of the cell before most of the toxic chlorine was withdrawn, but this time period was kept to a minimum. There was still some chlorine in the anodes when they were removed, and gas masks had to be used. The first anode was lifted out of the cell 15 – 20 minutes after electrolysis, and the operation took a couple of minutes per anode. To stabilize the anode deposit, the anodes were filled with water immediately after being removed from the cell. No clear trend was found between CE_{CoOOH} and the order of anode removal from the cell. If longer term experiments had been employed, more CoOOH would have been produced, reducing the influence of dissolution. However, the number of experiments would then have been lower, and the consequence of operational problems would have been larger. Different kinds of operational problems occurred from time to time, after which the experiment had to be stopped and then restarted with cleaned anodes.

The extent of cobalt oxide peeling off the anodes, which was included in CE_{CoOOH} for the pilot experiments, was dependent on the type of anode. Using worn rod anodes, sandblasted anodes and box anodes, there were only traces of deposit at the bottom of the bags after 24 hours of standard electrolysis, while using recoated rod anodes, roughly 15 % of the cobalt oxide was found in the bags. This material is no longer anodically protected, which means that at least some of it should dissolve. Furthermore, smaller particles detached from the anode surface may not settle, and will instead be transported out of the anode compartments along with the anolyte. To get an idea of the extent of this loss of CoOOH, a portion of the Cl_2-saturated anolyte in the manifold was filtrated continuously throughout one of the experiments. The material separated from the anolyte represented only about 1 % of the total amount of CoOOH produced.

The low concentration of cobalt and chloride ions in the etching solution was a major problem in the laboratory when determining CE_{CoOOH} by the chemical route, especially when small quantities of scale were formed. In a

typical pilot scale experiment, the cobalt concentration increased by 50 mg/l per anode compared to 6 mg/l in the lab. Due to the higher concentrations in the pilot experiments, the influence of the imprecise chloride analysis was lower.

4.3.3.2 Variation of electrolyte pH between anode compartments

In the majority of experiments, the CE_{CoOOH} was determined for two or more anodes, and the variation between the anodes was usually relatively large. During electrowinning at standard conditions, anolyte from each anode was sampled and cooled to room temperature for individual pH measurement. The results given in Table 4.13 show that the pH differed by as much as 0.06 pH units, which may explain why some anodes generated more cobalt oxide than others.

Table 4.13 Measured pH in electrolyte from individual anodes and the common dechlorinated anolyte.

Anode position in the cell	pH
1 (inlet)	1.06
2	1.12
3	1.06
4	1.06
5	1.12
6 (outlet)	1.09
After dechlor.	1.08

Several factors may have contributed to the difference in pH observed between the anode compartments, e.g. pH gradients in the catholyte and variations in anolyte flow rates, current distribution and O_2 : Cl_2 selectivity. Analysis of electrolyte sampled from different positions of the cathode compartment indicated that the catholyte had a very uniform composition, see Appendix, and no clear trend was found between CE_{CoOOH} and anode position.

Only the total anolyte flow was measured. However, it is believed that it could vary significantly between the anodes, owing to small differences in the distance from the catholyte level to the anolyte overflow ducts, the

negative pressure inside the hoods, the volume of the anode bags and the permeability of the diaphragms. The latter was found to be different in two tests carried out in January and March 2005, in which the anolyte flow rate was measured as a function of the applied suction. The results are illustrated in Fig. 4.64, and it is obvious that the permeability of the diaphragms was higher in January than in March. The experiments involving high pH values in the feed electrolyte were carried out in January 2005, and it is believed that the high anolyte flow rates observed in those experiments can be attributed to high diaphragm permeability (see section 4.3.1.2 and Appendix section A.3.1). For practical reasons, the anodes were equipped with new anode bags after etching. In order to reduce the noise in the results caused by variation in permeability, the same bags should have been used in many experiments, or alternatively, using cloth from the same roll only.

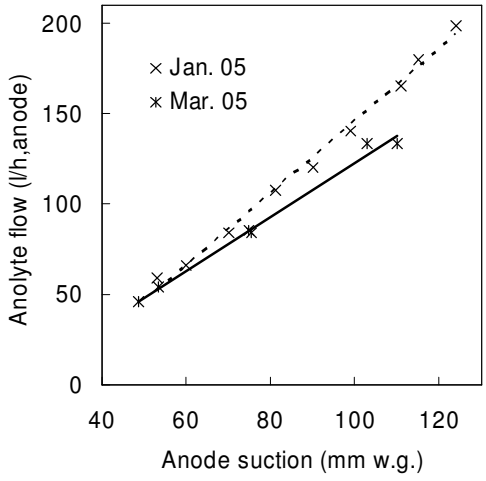

Figure 4.64 *Anolyte flow vs. anode suction measured during electrowinning at standard conditions in January and March 2005.*

The current distribution was normally good, the current being typically 200 – 230 A to each end anode and 370 – 410 A to each of the other anodes at standard conditions. It was also very stable during electrolysis. Whether differences existed in the selectivity between chlorine and oxygen evolution is not known, since only the composition of the mixed anode gas was measured. Cobalt oxide seemed to be formed preferentially on some anodes compared to others of the same type. To avoid uncertainties related to

individual differences between anodes, CE_{CoOOH} was determined for the same Reg* anode in all experiments where regular rod anodes were used.

4.3.3.3 Variations in operating conditions

For the experiments where the cobalt set point was equivalent to the standard value of 55 g/l (49 experiments), the chemical analysis of the sampled feed electrolyte varied from 53 to 59 g/l Co, with average value 55 g/l and standard deviation 1.4. The chloride content varied from 68 to 76 g/l, with average value 72 g/l and standard deviation 1.9. The sodium concentration was analysed in a few experiments, and it varied between 2 and 4 g/l. Once, concentrations of a range of elements were determined, and the composition was similar to the electrolytes used in the laboratory, see Table 3.1, with the exception of lower sulphate content (0.08 g/l). The electrolyte pH was a very critical factor in the investigated system. It was the most difficult parameter to control within acceptable limits, due to drifting of the pH electrode, small fluctuations in the temperature in the mixing tank etc.

The applied anode suction was adjusted manually as described in section 3.2.1. Therefore, when changes occurred in the operating conditions of the chlorine vacuum system in the nickel tankhouse, those were not compensated for, resulting in variations in the anode suction and thus the anolyte flow. In most of the experiments, the anode suction did not vary more than ± 5 mm water gauge.

The fact that several parameters could change simultaneously was another disadvantage related to the pilot work, which complicated the interpretation of the results. For example, when studying the effects of current density, the electrolyte temperature and the anolyte flow were also affected. This problem could have been reduced by adjusting the conditions in the mixing tank and the applied anode suction, but it would have taken some time to find the correct settings.

4.3.3.4 Analysis of anode gas composition

When measuring the composition of the anode gas with the Orsat apparatus, the gas was not dried prior to analysis. When saturated with water at 60°C, it

was calculated that the anode gas should contain approximately 20 % H_2O. Most of the water vapour was probably absorbed along with the chlorine gas, giving chlorine contents higher than the actual levels. On the other hand, the presence of typically ~1 % nitrogen in the anode gas indicated that parts of the measured oxygen concentration originated from dilution by air. Hence, both the Cl_2 and the O_2 contents measured were too high, suggesting that the O_2 : Cl_2 ratio was less affected. The extent of air dilution was increased at low currents and high anode suctions. In any case, it was difficult to determine the oxygen concentration accurately, due to its low concentration relative to that of chlorine. Absorption of the water content was tested in concentrated sulphuric acid, however, it was unsuccessful because some of the chlorine was co-absorbed.

4.3.3.5 Cobalt metal deposition

If dissolved chlorine is present in the catholyte, CE_{Co} will be negatively affected due to the reduction of chlorine on the cobalt cathodes. In a separate series of tests, the efficiency of anolyte dechlorination was examined under various conditions. By iodometric titration, the concentrations of chlorine in the anolyte leaving the dechlorination facility were found satisfactory with less than 10 mg/l Cl_2. At standard conditions, the chlorine content was approximately 1 mg/l in the dechlorinated anolyte.

In preliminary pilot experiments on the electrowinning of cobalt, titanium mother blanks were used as cathodes. Parts of the deposited cobalt sheets had a tendency to detach from the titanium surface due to internal stresses in the metal. As a consequence, some of the anode bags were ripped apart when the cathodes were harvested. In addition, inhibited metal deposition at the solution level was also experienced, probably related to the presence of organic material originating from the cobalt solvent extraction plant. These problems were overcome by using cathodes in the form of cobalt starting sheets.

Summary

The electrowinning of cobalt from chloride solution was investigated on a pilot scale, focusing on the undesirable deposition of cobalt oxide on DSA® anodes. In accordance with results obtained in laboratory scale experiments,

the anode scaling was found to be highly dependent on electrolyte pH. By operating at reduced pH levels, the anodic formation of cobalt oxide could be inhibited. The extent of scaling was also reduced by a decrease in cobalt concentration or temperature. However, these changes resulted in a drop in the cathodic current efficiency for cobalt and higher cell voltage, with adverse effect on productivity and energy consumption. The anode gas typically contained 98 % chlorine, 1 % oxygen and 1 % nitrogen, and the selectivity was not dependent on the thickness of the cobalt oxide film on DSA®.

At regular conditions, the pH in the anode compartments was higher than in the cathode compartment. This difference in pH was explained by little anodic oxygen evolution combined with hydrogen ions taking part in the current transport across the diaphragm, thus migrating out of the anode bags towards the cathodes. To support this view, the anolyte pH was estimated from the proton balance for an anode compartment, showing excellent agreement with the experimental results. As a consequence, the anolyte pH was decreased by increasing the rate of anolyte flow, suppressing the formation of cobalt oxide. When hydrochloric acid was added inside the anode bags, a large difference in pH was obtained between the anolyte and the catholyte. The cobalt current yield was then improved by increasing the pH of the feed electrolyte, with simultaneous inhibition of anode scaling. The build-up of anode scale was also reduced by periodically interrupted current at very low frequency, while the effect of cell short-circuiting was small.

The amount of cobalt oxide varied considerably between the anodes in the cell. This was partly due to different pH in each anode compartment, mainly caused by variation in anolyte flow rate. The degree at which cobalt oxide flaked off the anodes during electrowinning was dependent on the type of anode.

4.4 Suggestions for further work

- Examination of side reactions by experimental techniques is not an easy task. The measurements are often dominated by the main reaction, like chlorine evolution on DSA® in cobalt electrowinning from chloride solutions. The low current efficiency for anodic deposition of cobalt

oxide (CE_{CoOOH}) in acidic media may explain the lack of information about this process in the literature. Several studies have been published for neutral systems, where cobalt is stabilized in solution by complexing agents. However, the behaviour in acidic solutions having much higher concentrations of free cobalt ions is probably different, and a fundamental mechanistic study of cobalt oxide nucleation and growth on foreign substrates from such solutions is therefore desired. To suppress gas evolution, electrode materials like boron-doped diamond can be applied. Induction period and CE_{CoOOH} values may be readily obtained using an electrochemical quartz crystal microbalance. Nucleation overpotentials and reaction orders can be determined by anodic polarization at constant potential.

- Since stationary electrodes were employed in the present work, it is believed that the measured results were influenced by a lower pH at the DSA® surface than in the bulk solution, due to simultaneous oxygen evolution. This pH gradient can be effectively reduced by using a rotating disk electrode.

- The present work has demonstrated that the nucleation and initial growth of cobalt oxide are highly dependent on the anode material. A huge number of different mixed oxide coatings is available, and some of these should be tested for cobalt electrowinning. Coatings that favour oxygen evolution are of particular interest, due to the lower surface pH.

- Industrial electrolytes always contain trace amounts of impurities. Some of these may play a role in the deposition of cobalt oxide, e.g. Mn, Pb, Si and organic material. The influence of certain impurities should be investigated.

- Cobalt oxide films deposited on DSA® can be characterized by cyclic voltammetry in alkaline solution. In this way electrochemically active surface area, diffusion limitations in the film and the effect of the underlying DSA® can be studied vs. film thickness, conditions during deposition etc.

Chapter 5

CONCLUSIONS

Electrowinning of cobalt from chloride solutions was investigated in a laboratory cell and in a pilot cell equipped with electrodes of the same size and design as in the cobalt tankhouse at Xstrata Nikkelverk AS, Kristiansand, Norway. Most of the attention was paid to the undesirable deposition of cobalt oxide scale on dimensionally stable anodes (DSA®). The effects of key electrowinning parameters were studied, and alternative ways to suppress the extent of anode scaling were tested.

The black anode scale from industrial cells contained approximately 60 wt-% cobalt in dry form, and it was identified as alpha cobalt oxyhydroxide (α-CoOOH, heterogenite 3R). Fresh cobalt oxide films prepared in the laboratory appeared to be less crystalline than anode scale produced in the Xstrata Nikkelverk cobalt tankhouse. The anode deposit was growing all over the DSA® surface, and it was a good electrocatalyst for chlorine evolution. The anode gas measured in the pilot plant typically contained 98 % chlorine, 1 % oxygen and 1 % nitrogen.

The anodic deposition of cobalt oxide was accelerated at high pH, high cobalt chloride concentration and high temperature. Anode scaling was totally inhibited at lower pH, while at pH values higher than 2, cobalt oxide precipitated also in the bulk solution. The scaling reaction was found to be activation controlled, and the anodic current efficiency for CoOOH deposition was reduced when increasing the current density at higher pH. Sulphate ions were present in the anode deposit, and they were found to inhibit the growth of cobalt oxide.

DSA®-type anodes prepared at reduced decomposition temperatures had less crystalline coatings compared to commercial coatings, and the electrochemically active surface area was increased. These electrodes operated at lower anode potentials, and the extent of cobalt oxide formation was considerably suppressed. Cobalt oxide was also formed on graphite and pure titanium anodes, activating these anode materials for chlorine evolution. Due to the presence of the cobalt oxide film, the titanium electrode was not passivated.

In most of the pilot experiments, the pH in the anode compartments was higher than in the cathode compartment. This was explained by low rates of anodic oxygen evolution combined with migration of protons towards the cathodes. As a consequence, the anolyte pH was lowered by increasing the anolyte flow rate, resulting in less cobalt oxide being generated on the anodes.

The experimental results clearly demonstrated that several of the possible methods to suppress anode scaling had detrimental effect on other important parameters of the cobalt electrowinning process. Lower electrolyte pH, cobalt chloride concentration or temperature resulted in reduced cathodic current efficiency for cobalt and increased cell voltage, with adverse effect on productivity and energy consumption. The DSA® coatings prepared at reduced temperatures were shown to be less stable than the commercial coatings, giving shorter anode service life. Furthermore, hydrogen peroxide added to the electrolyte was consumed at the cathodes, and the anodic current efficiency for chlorine was negatively affected. The slow rate of cobalt oxide dissolution hindered effective use of advanced current supply, along with possible internal stresses in the cobalt metal deposit and accelerated degradation of the DSA® coating.

LIST OF SYMBOLS

Roman symbols and abbreviations

Symbol	Explanation	Unit
A	Constant in expression for mean activity coefficient developed by Debye and Hückel	$(mole/kg\ H_2O)^{-1/2}$
a	Ionic activity	
a_w	Water activity	
$a_{w,mix}$	Water activity in mixed solution	
a_w°	Water activity of pure solution with same ionic strength as the total ionic strength of the mixed solution	
$a_\pm$	Mean ionic activity	
å	Ion-size related parameter in expression for mean activity coefficient developed by Debye and Hückel	m
ads	Adsorbed on electrode surface	
B	Constant in expression for mean activity coefficient developed by Debye and Hückel	$(mole \cdot m^2/kg\ H_2O)^{-1/2}$
B	Constant specific to type of background chloride salt in expression for chloride activity given by Bjerrum	M^{-1}
b	Parameter extending the validity range of Debye and Hückel's expression for the mean activity coefficient	$(mole/kg\ H_2O)^{-1}$
b_{Cl2}	Tafel slope for chlorine evolution	mV/decade
C	Concentration	M or mg/l
C_{el}	Concentration in electrolyte	g/l
$C_\circ$	Initial concentration in etching solution	mg/l
CD	Current density	A/m^2
CE	Current efficiency = current yield	%
CoOOH	Cobalt oxyhydroxide	
CV	Cyclic voltammetry	
D	Diffusion coefficient	m^2/s
Deg	Degrees	
DRC	Democratic Republic of Congo	
DSA®	Dimensionally stable anode	
E	Potential	V
E_a	Anode potential	V
E_{avg}	Average anode potential	V
E_J	Liquid junction potential	V
E^{rev}	Reversible potential	V
E°	Standard potential	V
E'	Parameter for temperature compensation of pH measurement	V/°C
EDS	Energy dispersive spectroscopy	
emf	Electromotive force	V
EPDM	Ethylene propylene diene monomer	

Symbol	Explanation	Unit
ESA	Extended surface area	
F	Faraday constant (96487)	C/mole
F	Flow rate	l/h or l/(h · anode)
GRVE	Glass fibre reinforced vinyl ester	
h	Hydration number	
$h_\circ$	Hydration number at infinite dilution	
I	Ionic strength	mole/kg H_2O
I	Current	A or A/anode
i	Current density	A/m^2
I_{sweep}	Average current for potential sweep	A
I_{tot}	Total ionic strength of mixed solution	mole/kg H_2O
J	Flux of protons	mole/h
JCPDS	Joint Committee on Powder Diffraction Standards	
K	Equilibrium constant	
K_n	Stepwise stability constant	M^{-1}
LSV	Linear sweep voltammetry	
M	Atomic weight	g/mole
m	Molality	mole/kg H_2O
$m_\pm$	Mean molality	mole/kg H_2O
Me^{z+}	Metal ion	
mm w.g.	Millimetre water gauge	
mt	Metric tonne	
N_{anode}	Number of anodes	
NMR	Nuclear magnetic resonance spectroscopy	
NOK	Norwegian kroner	
OCP	Open circuit potential	V
org	Organic phase	
p.a.	Pro analysi	
PIC	Periodically interrupted current	
ppm	Parts per million	
PRC	Periodically reversed current	
PVDF	Polyvinylidene fluoride	
Q_{EW}	Electric charge applied during electrolysis	C
q*	Voltammetric charge	mC/cm^2
R	Universal gas constant (8.314)	J/(K · mole)
R	Ohmic drop	Ω
Reg	Regular anode	
Reg*	Worn regular anode	
rpm	Revolutions per minute	min^{-1}
S	Surface active site	
s	Sensitivity parameter correcting deviation from Nernstian behaviour of pH electrode	
SCE	Saturated calomel electrode	
SEM	Scanning electron microscopy	
SHE	Standard hydrogen electrode	

Symbol	Explanation	Unit
T	Temperature	K or °C
t	Duration of potential sweep	s
t	Transport number	
t_c	Cation transport number	
$t_{forward}$	Pulse time in forward direction	s
$t_{reverse}$	Pulse time in reverse direction	s
$t_{1/2}$	Half-life	days
U	Cell voltage	V
U	Parameter in Henderson equation	mole/(Ω · m^4)
u	Mobility	mole · m^2/(J · s)
V	Parameter in Henderson equation	mole/(Ω · m^4)
V	Volume of etching solution	ml
V_{O2}	Volume fraction of oxygen in anode gas	%
W	Parameter in expression for water activity in mixed solution	
W_{Co}	Mass of deposited cobalt metal	g
X	Cation ionic strength fraction in mixed solution	
X	Rate of proton formation	mole/h
XRD	X-ray diffraction analysis	
Y	Fractional molality in mixed solution	
z	Charge number	

Greek symbols

Symbol	Explanation	Unit
β	Slope in logarithmic plot of hydration number vs. water activity	
β_n	Cumulative stability constant	M^{-n}
Γ	Reduced activity coefficient	
Γ°	Reduced activity coefficient in pure solution of same ionic strength as the total ionic strength of the mixed solution	
γ	Activity coefficient	
$\gamma_\pm$	Mean activity coefficient	
ΔCo	Drop in cobalt concentration	g/l
$\Delta G°_f$	Standard Gibbs energy of formation	kJ/mole
ΔH	Enthalpy change for complex formation	kJ/mole
$\Delta H°_f$	Standard enthalpy of formation	kJ/mole
ΔHCl	Change in hydrochloric acid concentration	M
ΔpH	pH shift due to liquid junction potential	
ΔpH	pH difference between anolyte and catholyte	
λ	Equivalent conductivity	Ω^{-1} m^{-1}
υ	Stoichiometric coefficient	
ϕ	Osmotic coefficient	

REFERENCES

[1] *Co Facts*, The Cobalt Development Institute, 2007.

[2] *Cobalt News*, The Cobalt Development Institute, April 2008.

[3] *"Outlook for the Global Cobalt Market 2008"*, Cobalt News, The Cobalt Development Institute, January 2008.

[4] R.R. Moskalyk, A.M. Alfantazi, *"Review of Present Cobalt Recovery Practice"*, Minerals & Metallurgical Processing, **17**, 2000, 205-216.

[5] C.S. Simons, *"The Production of Nickel: Extractive Metallurgy – Past, Present, and Future",* Extractive Metallurgy of Nickel and Cobalt, The Metallurgical Society of AIME, 1988, 91-134.

[6] D.G.E. Kerfoot, P.D. Cordingley, *"The Acid Pressure Leach Process for Nickel and Cobalt Laterite. Part II: Rewiew of Operations at Fort Saskatchewan"*, Nickel-Cobalt '97 International Symposium. Vol. 1 Hydrometallurgy and Refining of Nickel and Cobalt, CIM, 1997, 355-370.

[7] P. Benson, G.W.D. Briggs, W.F.K. Wynne-Jones, *"The Cobalt Hydroxide Electrode – II. Electrochemical Behaviour"*, Electrochim. Acta, **9**, 1964, 281-288.

[8] J. Dille, J. Charlier, R. Winand, *"The Structure and Mechanical Properties of Thick Cobalt Electrodeposits"*, J. Materials Science, **32**, 1997, 2637-2646.

[9] C. Fenau, R. Breckpot, *"Optimalisation des Conditions d'electro-extraction du Cobalt"*, ATB Metallurgie, **9**, 1969, 115-125.

[10] J. Scoyer, R. Winand, *"Electrocrystallization of Cobalt from Acid Chloride Solution"*, Surf. Techn., **5**, 1977, 169-204.

[11] P. Louis, J. Dille, L. Hunga, T. Shungu, *"Electrodeposition of Malleable Cobalt"*, Extractive Metallurgy of Nickel and Cobalt, The Metallurgical Society of AIME, 1988, 505-515.

[12] O.E. Kongstein, G.M. Haarberg, J. Thonstad, *"Current Efficiency and Kinetics of Cobalt Electrodeposition in Acid Chloride Solutions. Part 1: The Influence of Current Density, pH and Temperature"*, J. Appl. Electrochem., **37**, 2007, 669-674.

[13] J.H. Huang, C. Kargl-Simard, A.M. Alfantazi, *"Electrowinning of Cobalt from a Sulphate-Chloride Solution"*, Can. Met. Quart., **43**, 2004, 163-172.

[14] K.C. Lenthall, A.W. Bryson, *"The Electrowinning of Cobalt from Sulphate Solutions"*, Aqueous Electrotechnologies: Progress in Theory and Practice, The Minerals, Metals & Materials Society, 1997, 305-320.

[15] S.C. Das, T. Subbaiah, *"Electrowinning of Cobalt. I. Winning from Pure Cobalt Sulphate Bath"*, Hydrometallurgy, **12**, 1984, 317-333.

[16] I.G. Sharma, P. Alex, A.C. Bidaye, A.K. Suri, *"Electrowinning of Cobalt from Sulphate Solutions"*, Hydrometallurgy, **80**, 2005, 132-138.

[17] D.J. MacKinnon, *"The Electrowinning of Metals from Aqueous Chloride"*, Hydrometallurgy: Research, Development and Plant Practice, The Metallurgical Society of AIME, 1983, 659-677.

[18] F.R. Archibald, *"The Kristiansand Nickel Refinery"*, J. Metals, **14**, 1962, 648-652.

[19] E.O. Stensholt, H. Zachariasen, J.H. Lund, *"Falconbridge Chlorine Leach Process"*, Trans. Inst. Min. Metall. C, **95**, 1986, C10-C16.

[20] F. Grøntoft, *"Electrowinning Metal from Chloride Solutions"*, US Pat. 4,155,821, 1979.

[21] D.G.E. Kerfoot, D.R. Weir, *"The Hydro and Electrometallurgy of Nickel and Cobalt"*, Extractive Metallurgy of Nickel and Cobalt, The Metallurgical Society of AIME, 1988, 241-267.

[22] A. Nidola, U. Nevosi, R.J. Ornelas, F. Zioni, *"Anode for Oxygen Evolution in Electrolytes Containing Manganese and Fluorides"*, US Pat. 6,103,093, 2000.

[23] L.R. Hougen, R. Parkinson, J. Saetre, G. Van Weert, *"Operating Experiences with a Pilot Plant for the Electrowinning of Nickel from All-Chloride Electrolyte"*, CIM Bull., **69**, 1977, 136-143.

[24] K. Twite, J.M. Dereydt, K. Mujinga, P. Louis, *"Industrial In-Pulp Co-Ni Alloy Electrowinning at the Gecamines Shituru Plant"*, JOM, **49** (12), 1997, 46-48 + 58.

[25] J. Aird, R.S. Celmer, A.V. May, *"New Cobalt Production from RMC's Chambishi Roast – Leach – Electrowin Process"*, Cobalt 80, 10th Annual Hydrometallurgical Meeting of CIM, 1980.

[26] R.G. Agnew, E. Krause, *"Electrolytic Cobalt Production at Inco"*, Minemetal '91, Vol. 1, 2nd International Symposium on Mining and Metallurgy, Havana, Cuba, Nov. 1991, 520-533.

[27] M. Fujimori, N. Ono, N. Tamura, T. Kohga, *"Electrowinning from Aqueous Chlorides in SSM's Nickel and Cobalt Refining Process"*, Chloride Electrometallurgy, The Metallurgical Society of AIME, 1982, 155-166.

[28] Y. Yuhua, M. Xianxuan, *"Operating Practice and Technical Developments in Nickel Refining and Cobalt Recovery at Jinchuan Non-Ferrous Metal Company"*, Electrometallurgical Plant Practice, Pergamon Press, New York, 1990, 253-268.

[29] G. Gravey, F. Peyron, *"A Frensh Producer of Cobalt: Metaux Speciaux S.A."*, International Conference on Cobalt: Metallurgy and Uses, Vol. 1, ATB Metallurgie, 1981, 79-84.

[30] S. Trasatti, *"Electrocatalysis: Understanding the Success of DSA®"*, Electrochim. Acta, **45**, 2000, 2377-2385.

[31] H.B. Beer, *"The Invention and Industrial Development of Metal Anodes"*, J. Electrochem. Soc., **127**, 1980, 303C-307C.

[32] H.B. Beer, *"Electrode and Coating therefor"*, US Pat. 3,632,498, 1972.

[33] H.B. Beer, *"Electrode having Platinum Metal Oxide thereon, and Method of Use thereof"*, US Pat. 3,711,385.

[34] G.P. Vercesi, J. Rolewicz, C. Comninellis, J. Hinden, *"Characterization of DSA-Type Oxygen Evolving Electrodes. Choice of Base Metal"*, Thermochim. Acta, **176**, 1991, 31-47.

[35] A. Nidola, *"Technological Impact of Metallic Oxides as Anodes"*, in S. Trasatti (ed.), *Electrodes of Conductive Metallic Oxides*, Part B, Elsevier, Amsterdam, 1981, 627-659.

[36] Y.E. Roginskaya, O.V. Morozova, *"The Role of Hydrated Oxides in Formation and Structure of DSA-Type Oxide Electrocatalysts"*, Electrochim. Acta, **40**, 1995, 817-822.

[37] O.R. Camara, S. Trasatti, *"Surface Electrochemical Properties of Ti/(RuO_2 + ZrO_2) Electrodes"*, Electrochim. Acta, **41**, 1996, 419-427.

[38] C. Comninellis, G.P. Vercesi, *"Problems in DSA® Coating Deposition by Thermal Decomposition"*, J. Appl. Electrochem., **21**, 1991, 136-142.

[39] L.M. Da Silva, D.V. Franco, L.A. De Faria, J.F.C. Boodts, *"Surface, Kinetics and Electrocatalytic Properties of Ti/(IrO_2 + Ta_2O_5) Electrodes, prepared using Controlled Cooling Rate, for Ozone Production"*, Electrochim. Acta, **49**, 2004, 3977-3988.

[40] G. Lodi, A. De Battisti, G. Bordin, C. De Asmundis, A. Benedetti, *"Microstructure and Electrical Properties of IrO_2 prepared by Thermal Decomposition of $IrCl_3 \cdot x\ H_2O$: Role played by the Conditions of Thermal Treatment"*, J. Electroanal. Chem., **277**, 1990, 139-150.

[41] S. Trasatti, *"Electrocatalysis in the Anodic Evolution of Oxygen and Chlorine"*, Electrochim. Acta, **29**, 1984, 1503-1512.

[42] S. Trasatti, *"Physical Electrochemistry of Ceramic Oxides"*, Electrochim. Acta, **36**, 1991, 225-241.

[43] S. Trasatti, *"Progress in the Understanding of the Mechanism of Chlorine Evolution at Oxide Electrodes"*, Electrochim. Acta, **32**, 1987, 369-382.

[44] S. Trasatti, G. Lodi, *"Oxygen and Chlorine Evolution at Conductive Metallic Oxide Anodes"*, in S. Trasatti (ed.), *Electrodes of Conductive Metallic Oxides*, Part B, Elsevier, Amsterdam, 1981, 521-626.

[45] J. Aromaa, *On the Corrosion of Ruthenium Oxide (RuO_2) Based Anodes in Chloride Solutions*, Dr.Sc. (Tech.) thesis, Helsinki University of Technology, 1994.

[46] C.G. Ferron, P.F. Duby, *"Iridium Oxide Coated Titanium as Anode in Copper Electrowinning"*, Performance of Electrodes for Industrial Electrochemical Processes, Proceedings Volume 89-10, The Electrochemical Society, Pennington, NJ, 1989, 259-277.

[47] G.N. Martelli, R. Ornelas, G. Faita, *"Deactivation Mechanisms of Oxygen Evolving Anodes at High Current Densities"*, Electrochim. Acta, **39**, 1994, 1551-1558.

[48] I.H. Warren, *"The Oxygen Electrode in Metal Electrowinning"*, Anodes for Electrowinning, The Metallurgical Society of AIME, Warrendale, Pennsylvania, 1984, 69-78.

[49] S. Nijjer, *Deposition and Reduction of Manganese Dioxide on Alternative Anode Materials in Zinc Electrowinning*, PhD thesis, Norwegian University of Science and Technology, 2000.

[50] M.S. Moats, K.L. Hardee, *"Inhibiting Unwanted Redox Reactions with Valve Metal Oxide Topcoats on Dimensionally Stable Anodes"*, Abstract #888, 209th Meeting of The Electrochemical Society, Denver, 2006.

[51] M.S. Moats, K.L. Hardee, C. Brown, *"Mesh-on-Lead Anodes for Copper Electrowinning"*, JOM, **55** (7), 2003, 46-48.

[52] W.K. Behl, J.E. Toni, *"Anodic Oxidation of Cobalt in Potassium Hydroxide Electrolytes"*, J. Electroanal. Chem., **31**, 1971, 63-75.

[53] L.D. Burke, M.E. Lyons, O.J. Murphy, *"Formation of Hydrous Oxide Films on Cobalt under Potential Cycling Conditions"*, J. Electroanal. Chem., **132**, 1982, 247-261.

[54] T.C. Liu, W.G. Pell, B.E Conway, *"Stages in the Development of Thick Oxide Films exhibiting Reversible Redox Behavior and Pseudocapacitance"*, Electrochim. Acta, **44**, 1999, 2829-2842.

[55] D. Tench, L.F. Warren, *"Electrodeposition of Conducting Transition Metal Oxide/Hydroxide Films from Aqueous Solution"*, J. Electrochem. Soc., **130**, 1983, 869-872.

[56] Y.W.D. Chen, R.M. Noufi, *"Electrodeposition of Nickel and Cobalt Oxides onto Platinum and Graphite Electrodes for Alkaline Water Electrolysis"*, J. Electrochem. Soc., **131**, 1984, 1447-1451.

[57] N. Spataru, C. Terashima, K. Tokuhiro, I. Sutanto, D.A. Tryk, S.M. Park, A. Fujishima, *"Electrochemical Behaviour of Cobalt Oxide Films Deposited at Conductive Diamond Electrodes"*, J. Electrochem. Soc., **150**, 2003, E337-E341.

[58] T. Pauporté, L. Mendoza, M. Cassir, M.C. Bernard, J. Chivot, *"Direct Low-Temperature Deposition of Crystallized CoOOH Films by Potentiostatic Electrolysis"*, J. Electrochem. Soc., **152**, 2005, C49-C53.

[59] C.C. Hu, T.Y. Hsu, *"Effects of Complex Agents on the Anodic Deposition and Electrochemical Characteristics of Cobalt Oxides"*, Electrochim. Acta, **53**, 2008, 2386-2395.

[60] R. Boggio, A. Carugati, G. Lodi, S. Trasatti, *"Mechanistic Study of Cl_2 Evolution at Ti-Supported Co_3O_4 Anodes"*, J. Appl. Electrochem., **15**, 1985, 335-349.

[61] L.M. da Silva, J.F.C. Boodts, L.A. de Faria, *"Chlorine Evolution Reaction at Ti/(RuO_2+Co_3O_4) Electrodes"*, J. Braz. Chem. Soc., **14**, 2003, 388-395.

[62] E.B. Castro, C.A. Gervasi, J.R. Vilche, *"Oxygen Evolution on Electrodeposited Cobalt Oxides"*, J. Appl. Electrochem., **28**, 1998, 835-841.

[63] L. Brossard, *"Oxygen Evolution in 30 % KOH at 70°C on Nickel Anodically Coated with $CoOOH/Co_3O_4$"*, J. Appl. Electrochem., **21**, 1991, 612-618.

[64] R.N. Singh, J.F. Koenig, G. Poillerat, P. Chartier, *"Electrochemical Studies on Protective Thin Co_3O_4 and $NiCo_2O_4$ Films prepared on Titanium by Spray Pyrolysis for Oxygen Evolution"*, J. Electrochem. Soc., **137**, 1990, 1408-1413.

[65] O.E. Kongstein, *Electrodeposition of Cobalt from Chloride Solutions*, PhD thesis, Norwegian University of Science and Technology, Trondheim, Norway, 2001.

[66] T.V. Galantseva, S.V. Kovalev, V.L. Kubasov, G. Vorob'ev, *"Optimum Conditions for the Operation of Ruthenium Dioxide-Titanium Dioxide Anodes in the Electrolysis of Cobalt Chloride"* (in Russian), Tsvetnye Metally, (3), 1990, 42-44.

[67] V.B. Spivakobskii, L.G. Trizna, T.M. Petrenko, *"Study on Conditions of Cobalt Ion Hydrolysis in Cobalt Chloride Solutions at Anode Surface"*, Tsvetnye Metally, (9), 1993, 27-29.

[68] B. Love, *"Nickel and Cobalt Electrowinning and Refining"*, Hydrometallurgy Short Course, Conference of Metallurgists 2003, Vancouver, Canada.

[69] R.G. Agnew, L.D. Kowal, D. Young, *"Process Optimization at Inco's Cobalt Refinery"*, Electrometallurgical Plant Practice, Pergamon Press, New York, 1990, 221-231.

[70] V.A. Ettel, E.A.P. Devuyst, J. Babjak, J. Ambrose, G.V. Glaum, *"Process for Recovering Cobalt Electrolytically"*, US Pat. 4,274,930, 1981.

[71] H. Leidheiser, A. Vértes, M.L. Varsányi, I. Czakó-Nagy, *"The Chemical State of Cobalt in Cobalt-Hardened Gold Electrodeposits"*, J. Electrochem. Soc., **126**, 1979, 391-394.

[72] G.R. Lakshminarayanan, E.S. Chen, J.C. Sadak, F.K. Sautter, *"Electrodeposition of Cobalt Using an Insoluble Anode"*, J. Electrochem. Soc., **123**, 1976, 1612-1616.

[73] E.S. Chen, J.C. Sadak, G.R. Lakshminarayanan, *"Method and Electrolyte for the Electrodeposition of Cobalt and Cobalt-Base Alloys in the Presence of an Insoluble Anode"*, US Pat. 4,111,760, 1978.

[74] Y. Matsumoto, H. Ohmura, T. Goto, *"Effect of Lanthanide Ions on the Electrodeposition of Cobalt and Manganese Oxides"*, J. Electroanal. Chem., **399**, 1995, 91-96.

[75] Y. Matsumoto, N. Bando, J. Hombo, T. Sasaki, *"Analysis of Hydration Number in Cobalt Oxyhydroxide Films using the Quartz Crystal Microbalance"*, J. Electroanal. Chem., **395**, 1995, 45-49.

[76] D.S. Flett, *"Chemistry of Nickel-Cobalt Separation"*, in Extractive Metallurgy of Nickel, ed. A.R. Burkin, Critical Reports on Applied Chemistry, Vol. 17, Wiley, Chichester, 1987, 76-97.

[77] M. Coussement, A. De Schepper, R. Standaert, *"Separation of Cobalt and Nickel in Acid Solutions"*, Hydrometallurgy: Research, Development and Plant Practice, The Metallurgical Society of AIME, 1983, 569-585.

[78] D.B. Mobbs, D. M. Mounsey, *"Use of Caro's Acid in the Separation of Nickel and Cobalt"*, Trans. Inst. Min. Metall, Sect. C, **90**, 1981, C103-C110.

[79] C. Nikolic, P.B. Queneau, W.G. Sherwood, C.B. Barlow, C.S. Simons, *"Nickel-Cobalt Separation by Ozonation"*, CIM Bull., **71**, 1978, 121-127.

[80] T. Robinson, J. Jenkins, S. Rasmussen, M. King, W.G. Davenport, *"Copper Electrowinning – 2003 World Tankhouse Operating Data"*, Copper Electrorefining and Electrowinning, The Canadian Institute of Mining, Metallurgy and Petroleum, 2003, 421-472.

[81] A.S. Gendron, V.A. Ettel, S. Abe, *"Effect of Cobalt Added to Electrolyte on Corrosion Rate of Pb-Sb Anodes in Copper Electrowinning"*, Can. Met. Quart., **14**, 1975, 59-61.

[82] O. Hyvärinen, *"The Effect of Silver and Cobalt on the Oxygen Evolution at Lead Anodes"*, Dr. thesis, Helsinki University of Technology, Finland, 1972.

[83] O.E. Kongstein, G.M. Haarberg, J. Thonstad, *"Current Efficiency and Kinetics of Cobalt Electrodeposition in Acid Chloride Solutions. Part 2: The Influence of Chloride and Sulphate Concentrations"*, J. Appl. Electrochem., **37**, 2007, 675-680.

[84] C.F. Baes, R.E. Mesmer, *The Hydrolysis of Cations*, John Wiley & Sons, New York, 1976.

[85] P.C. Kong, T.W. Swaddle, P. Bayliss, *"The Hydrothermal Chemistry of Some Common Transition Metal Compounds"*, Can. J. Chem., **49**, 1971, 2442-2446.

[86] O.M. Dotterud, *Versatic-prosessen for kobberkis*, PhD thesis, The Technical University of Norway, Trondheim, Norway, 1989.

[87] O.J. Kwok, R.G. Robins, *"Thermal Precipitation in Aqueous Solutions"*, International Symposium on Hydrometallurgy, The Metallurgical Society of AIME, Chicago, 1973, 1033-1080.

[88] M. Pourbaix, *Atlas of Electrochemical Equilibria in Aqueous Solutions*, Pergamon Press, Oxford, 1966.

[89] J.D. Hem, C.E. Roberson, C.J. Lind, *"Thermodynamic Stability of CoOOH and Its Coprecipitation with Manganese"*, Geochim. Cosmochim. Acta, **49**, 1985, 801-810.

[90] D.D. Wagman, W.H. Evans, V.B. Parker, I. Halow, S.M. Bailey, R.H. Schumm, *Selected Values of Chemical Thermodynamic Properties*, National Bureau of Standards, Tech. Note 270-4, Washington D.C., 1969.

[91] C. Mansour, T. Pauporté, A. Ringuedé, V. Albin, M. Cassir, *"Protective Coating for MCFC Cathode: Low Temperature Potentiostatic Deposition of CoOOH on Nickel in Aqueous Media Containing Glycine"*, J. Power Sources, **156**, 2006, 23-27.

[92] W.M. Latimer, *The Oxidation States of the Elements and Their Potentials in Aqueous Solutions*, Prentice-Hall, New York, 1938.

[93] M.W. Chase, *NIST-JANAF Thermochemical Tables*, Journal of Physical and Chemical Reference Data, Monograph 9, 4th ed., part 1, New York, 1998.

[94] J.H. Huang, C. Kargl-Simard, M. Oliazadeh, A.M. Alfantazi, *"pH-Controlled Precipitation of Cobalt and Molybdenum from Industrial Waste Effluents of a Cobalt Electrodeposition Process"*, Hydrometallurgy, **75**, 2004, 77-90.

[95] C. Mansour, S. Arroum, V. Albin, V. Lair, T. Pauporte, A. Ringuede, M. Cassir, *"Potentiostatic Deposition at Different Temperatures of Cobalt Oxide/Hydroxide Coatings on the Porous MCFC Cathode. Effect of Complexing Agents"*, poster, 7th International Symposium on Molten Salts Chemistry and Technology, Toulouse, France, Aug. 29 – Sep. 2, 2005.

[96] A.L. Rotinjan, L.M. Borisowa, R.W. Boldin, *"Das Redox-Standardpotensial von Co^{3+}/Co^{2+}"*, Electrochim. Acta, **19**, 1974, 43-46.

[97] A.J. Bard, R. Parsons, J. Jordan, *Standard Potentials in Aqueous Solution*, Marcel Dekker, New York, 1985.

[98] G. Davies and B. Warnqvist, *"Aspects of the Chemistry of Cobalt(III) in Aqueous Perchlorate Solution"*, Coord. Chem. Rev., **5**, 1970, 349-378.

[99] A.E. Martell, R.M. Smith, *Critical Stability Constants*, Plenum Press, New York, 1974-1989.

[100] G.W. Simmons, *"In Situ Studies of the Passivation of Cobalt by Emission Mössbauer Spectroscopy"*, Passivity of Metals, 4th International Symposium on Passivity, The Electrochemical Society, 1978.

[101] L.D. Burke, M.M. McCarthy, *"Modification of the Elctronic Transfer Properties of Co_3O_4 as Required for Its use in DSA-Type Anodes"*, J. Electrochem. Soc., **135**, 1988, 1175-1179.

[102] L.C. Schumacher, I.B. Holzhueter, *"Semiconducting and Electrocatalytic Properties of Sputtered Cobalt Oxide Films"*, Electrochim. Acta., **35**, 1990, 975-984.

[103] P. Rasiyah, A.C.C. Tseung, *"A Mechanistic Study of Oxygen Evolution on Li-Doped Co_3O_4"*, J. Electrochem. Soc., **130**, 1983, 365-368.

[104] C. Vu, K.N. Han, F. Lawson, *"Leaching Behaviour of Cobaltous and Cobalto-Cobaltic Oxides in Ammonia and in Acid Solutions"*, Hydrometallurgy, **6**, 1980, 75-87.

[105] P. Benson, G.W.D. Briggs, W.F.K. Wynne-Jones, *"The Cobalt Hydroxide Electrode – I. Structure and Phase Transitions of the Hydroxides"*, Electrochim. Acta, **9**, 1964, 275-280.

[106] Y.D. Kondrashev, N.N. Fedorova, Dokl. Akad. Nauk. SSSR, **94**, 1954, 229.

[107] G.G. Amatucci, J.M. Tarascon, D. Larcher, L.C. Klein, *"Synthesis of Electrochemically Active $LiCoO_2$ and $LiNiO_2$ at 100°C"*, Solid State Ionics, **84**, 1996, 169-180.

[108] G.W. Simmons, A. Vértes, M.L. Varsányi, H. Leidheiser, *"Emission Mössbauer Studies of Anodically Formed CoO_2"*, J. Electrochem. Soc., **126**, 1979, 187-189.

[109] G.G. Amatucci, J.M. Tarascon, L.C. Klein, *"CoO_2, The End Member of the Li_xCoO_2 Solid Solution"*, J. Electrochem. Soc., **143**, 1996, 1114-1123.

[110] R.A. Robinson, R.H. Stokes, *Electrolyte Solutions*, 2nd ed. (revised), Butterworths, London, 1965.

[111] P.W Atkins, *Physical Chemistry*, 5th ed., Oxford, 1994.

[112] V.M.M. Lobo, *Handbook of Electrolyte Solutions*, Part A, Elsevier, Amsterdam, 1989.

[113] J.J.C. Jansz, *"Estimation of Ionic Activities in Chloride Systems at Ambient and Elevated Temperatures"*, Hydrometallurgy, **11**, 1983, 13-31.

[114] G. Senanayake, D.M. Muir, *"Speciation and Reduction Potentials of Metal Ions in Concentrated Chloride and Sulfate Solutions Relevant to Processing Base Metal Sulfides"*, Metall. Trans. B, **19B**, 1988, 37-45.

[115] D.M. Muir, G. Senanayake, *"Principles and Applications of Strong Salt Solutions to Mineral Chemistry"*, Extraction Metallurgy '85, The Institution of Mining and Metallurgy, London, 1985, 65-91.

[116] K.C. Liddell, *"Ion Interaction Models for Co, Ni, Cu, Zn and Fe"*, Extractive Metallurgy of Copper, Nickel and Cobalt, Vol. 1, The Paul E. Queneau International Symposium, The Minerals, Metals & Materials Society, Denver, 1993, 757-786.

[117] J. Ji, *Fundamental Aspects of Nickel Electrowinning from Chloride Electrolytes*, PhD thesis, The University of British Columbia, Vancouver, Canada, 1994.

[118] T.M. Herrington, M.G. Roffey, D.P. Smith, *"Densities of Aqueous Electrolytes $MnCl_2$, $CoCl_2$, $NiCl_2$, $ZnCl_2$, and $CdCl_2$ from 25 to 72°C at 1 atm"*, J. Chem. Eng. Data, **31**, 1986, 221-225.

[119] E. Peters, *"Applications of Chloride Hydrometallurgy to Treatment of Sulphide Minerals"*, Chloride Hydrometallurgy, Benelux Metallurgie, Brussels, 1977, 1-37.

[120] C.L. Kusik, H.P. Meissner, *"Electrolyte Activity Coefficients in Inorganic Processing"*, AIChE Symposium Series, **74**, 1978, 14-20.

[121] H.S. Harned, B.B. Owen, *The Physical Chemistry of Electrolyte Solutions*, 2nd ed., Reinhold, New York, 1950.

[122] H.P. Meissner, C.L. Kusik, *"Activity Coefficients of Strong Electrolytes in Multicomponent Aqueous Solutions"*, AIChE J., **18**, 1972, 294-298.

[123] W.J. Hamer, Y.C. Wu, *"Osmotic Coefficients and Mean Activity Coefficients of Uni-univalent Electrolytes in Water at 25°C"*, J. Phys. Chem. Ref. Data, **1**, 1972, 1047-1099.

[124] W. Ostwald, *"Volumchemische und Optisch-Chemische Studien"*, J. Prakt. Chem., **18**, 1878, 328-371.

[125] A. Seidell, W.F. Linke, *Solubilities: Inorganic and Metal-Organic Compounds*, vol. 1, 4th ed., Am. Chem. Soc., Washington D.C., 1958.

[126] C.J. Downes, *"Thermodynamics of Mixed Electrolyte Solutions: The Systems H_2O-NaCl-$CoCl_2$ and H_2O-$CaCl_2$-$CoCl_2$ at 25°C"*, J. Solution Chem., **4**, 1975, 191-204.

[127] D.M. Muir, *"Basic Principles of Chloride Hydrometallurgy"*, Chloride Metallurgy 2002, CIM, Montreal, 2002, 759-777.

[128] C.H. Hamann, A. Hamnett, W. Vielstich, *Electrochemistry*, Wiley-VCH, Weinheim, 1998.

[129] G. Senanayake, *"Review of Theory and Pratice of Measuring Proton Activity and pH in Concentrated Chloride Solutions and Application to Oxide Leaching"*, Miner. Eng., **20**, 2007, 634-645.

[130] H. Galster, *pH Measurement*, VCH, Weinheim, 1991.

[131] B. Kaasa, *Prediction of pH, Mineral Precipitation and Multiphase Equilibria during Oil Recovery*, PhD thesis, Norwegian University of Science and Technology, Trondheim, Norway, 1998.

[132] J. Liddicoat, *A Review of Chloride Hydrometallurgy for Copper*, M.Sc. directed study, University of British Columbia, Vancouver, Canada.

[133] J.J.C. Jansz, *Chloride Hydrometallurgy for Pyritic Zinc-Lead Sulfide Ores: The Non-Oxidative Leaching Route*, PhD thesis, Delft University of Technology, Delft, The Netherlands, 1984.

[134] A.H. Zeltmann, N.A. Matwiyoff, L.O. Morgan, *"Nuclear Magnetic Resonance of Oxygen-17 and Chlorine-35 in Aqueous Hydrochloric Acid Solutions of Cobalt(II). I. Line Shifts and Relative Abundances of Solution Species"*, J. Phys. Chem., **72**, 1968, 121-127.

[135] J. Bjerrum, A.S. Halonin, L.H. Skibsted, *"Studies on Cobalt(II) Halide Complex Formation. I. A Spectrophotometric Study of the Chloro Cobalt(II) Complexes in Strong Aqueous Chloride Solutions"*, Acta Chem. Scand. A, **29**, 1975, 326-332.

[136] L.G. Sillén, A.E. Martell, *Stability Constants of Metal-Ion Complexes*, Special publication no. 17, The Chemical Society, 1964.

[137] L.G. Sillén, A.E. Martell, *Stability Constants of Metal-Ion Complexes*, Supplement no. 1, Special publication no. 25, The Chemical Society, 1971.

[138] E.A. Belousov, V.V. Bocharov, V.E. Mironov, *"The Composition and Stability of Cobalt(II) Chloride Complexes"*, Russ. J. Inorg. Chem., **17**, 1972, 1717-1719.

[139] L.H. Skibsted, J. Bjerrum, *"Studies on Cobalt(II) Halide Complex Formation. II. Cobalt(II) Chloride Complexes in 10 M Perchloric Acid Solution"*, Acta Chem. Scand. A, **32**, 1978, 429-434.

[140] R. Winand, *"Chloride Hydrometallurgy"*, Hydrometallurgy, **27**, 1991, 285-316.

[141] E. Wigstøl, K. Frøyland, *"Solvent Extraction in Nickel Metallurgy, The Falconbridge Matte Leach Process"*, Solvent Extraction in Metallurgical Processes, Technol. Inst. K.VIV, Antwerp, 1972, 62-72.

[142] M. Logeat, G. Mankowski, J. Molinier, M. Lenzi, *"Complete Separation of Copper from Cobalt by Solvent Extraction with Triisooctylamine"*, Hydrometallurgy, **9**, 1982, 105-113.

[143] A. Vaskelis, A. Jagminiene, I. Stankeviciene, *"Anodic Oxidation of Co(II) Complexes with Amines on a Rotating Au Electrode: Ligand Effects in Relation to the Application for Autocatalytic Metal Deposition"*, Electrochim. Acta, **51**, 2006, 2215-2220.

[144] I. Jacobsen, *"Electrode Kinetics for DSA in Chloride/Sulphate Solutions"*, MSc thesis (in Norwegian), Norwegian University of Science and Technology, 2004.

[145] M. Sjöberg, A. Ullman, K.A. Hugosson, M. Tenfält, M. Kroon, J.P. Saetre, T.H. Groesle, *"Clamping Device for Electrochemical Cell"*, US Pat. 6,471,835, 2002.

[146] W. Wei, W. Chen, D.G. Ivey, *"Anodic Electrodeposition of Nanocrystalline Coatings in the Mn-Co-O System"*, Chem. Mater., **19**, 2007, 2816-2822.

[147] M.A. Bouchat, J.J. Saquet, *"Electrolytic Cobalt in Katanga"*, J. Metals, **12**, 1960, 802-808.

[148] A.L. Monhemius, *"Precipitation Diagrams for Metal Hydroxides, Sulphides, Arsenates and Phosphates"*, Trans. Inst. Min. Metall. C, **86**, 1977, C202-C206.

[149] G. Soleng, *"Depolariserte anoder for elektrolytisk utfelling av metaller. Anodeprosesser under koboltelektrolyse"*, technical report, Norwegian University of Science and Technology, 2002.

[150] G.L. Silver, F.S. Martin, *"Method for Plating with Metal Oxides"*, US Pat. 5,340,605, 1994.

[151] B. Chen, Y. Shu, S. Xie, *"Study on the Inhibition of Gas Holes in Nickel Cathode by H_2O_2"* (in Chinese except for abstract and figures in English), J. Central-South Inst. Min. Metall., **20**, 1989, 317-323.

[152] J. Lu, D.B. Dreisinger, W.C. Cooper, *"Thermodynamics of the Aqueous Copper-Cyanide System"*, Hydrometallurgy, **66**, 2002, 23-36.

[153] R. Garavaglia, C.M. Mari, S. Trasatti, *"Physicochemical Characterization of Co_3O_4 Prepared by Thermal Decomposition. II: Response to Solution pH"*, Surf. Technol., **23**, 1984, 41-47.

[154] T. Ishikawa, R. Isa, K. Kandori, T. Nakayama, T. Tsubota, *"Influences of Metal Chlorides and Sulfates on the Formation of Beta-FeOOH Particles by Aerial Oxidation of $FeCl_2$ Solutions"*, J. Electrochem. Soc., **151**, 2004, B586-B594.

[155] T. Chen, *Physicochemical Properties of Nickel and Cobalt Sulphate Solutions of Hydrometallurgical Relevance*, PhD thesis, Murdoch University, Perth, Western Australia, 2003.

[156] L. Nylén, A. Cornell, *"Critical Anode Potential in the Chlorate Process"*, J. Electrochem. Soc., **153**, 2006, D14-D20.

[157] A.B. Velichenko, D.V. Girenko, S.V. Kovalyov, A.N. Gnatenko, R. Amadelli, F.I. Danilov, *"Lead Dioxide Electrodeposition and its Application: Influence of Fluoride and Iron Ions"*, J. Electroanal. Chem., **454**, 1998, 203-208.

[158] P.T. Davey, T.R. Scott, *"Removal of Iron from Leach Liquors by the "Goethite" Process"*, Hydrometallurgy, **2**, 1976, 25-33.

[159] T. Sasaki, Y. Matsumoto, J. Hombo, *"Effect of La^{3+} Ion on the Electrodeposition of Manganese and Cobalt Oxides"*, J. Electroanal. Chem., **371**, 1994, 241-249.

[160] J.W. Mullin, *Crystallization*, 4^{th} ed., Butterworth-Heinemann, Oxford, Great Britain, 2001.

[161] Y. Takasu, K. Kameyama, S. Onoue, M. Ueno, *"Surface Microstructure of Oxide-Coated Electrodes for Chlorine Evolution"*, Bull. Chem. Soc. Jpn., **67**, 1994, 1994-1997.

[162] A. de Battisti, G. Lodi, M. Cappadonia, G. Battaglin, R. Kötz, *"Influence of the Valve Metal Oxide on the Properties of Ruthenium Based Mixed Oxide Electrodes: II. RuO_2/TiO_2 Coatings"*, J. Electrochem. Soc., **136**, 1989, 2596-2598.

[163] K. Kameyama, K. Tsukada, K. Yahikozawa, Y. Takasu, *"Surface Characterization of RuO_2-IrO_2-TiO_2 Coated Titanium Electrodes"*, J. Electrochem. Soc., **141**, 1994, 643-647.

[164] G.P. Vercesi, J.Y Salamin, C. Comninellis, *"Morphological and Microstructural Study of the Ti/IrO_2-Ta_2O_5 Electrode: Effect of the Preparation Temperature"*, Electrochim. Acta, **36**, 1991, 991-998.

[165] S. Trasatti, G. Lodi, *"Properties of Conductive Transition Metal Oxides with Rutile-Type Structure"*, in S. Trasatti (ed.), *Electrodes of Conductive Metallic Oxides*, Part A, Elsevier, Amsterdam, 1980, 301-358.

[166] S. Ardizzone, G. Fregonata, S. Trasatti, *""Inner" and "Outer" Active Surface of RuO_2 Electrodes"*, Electrochim. Acta, **35**, 1990, 263-267.

[167] A. Marshall, *Electrocatalysts for the Oxygen Evolution Electrode in Water Electrolysers using Proton Exchange Membranes: Synthesis and Characterisation*, PhD thesis, Norwegian University of Science and Technology, Trondheim, 2005.

[168] R. Kötz, S. Stucki, *"Stabilization of RuO_2 by IrO_2 for Anodic Oxygen Evolution in Acid Media"*, Electrochim. Acta, **31**, 1986, 1311-1316.

[169] T.C. Wen, C.C. Hu, *"Hydrogen and Oxygen Evolutions on Ru-Ir Binary Oxides"*, J. Electrochem. Soc., **139**, 1992, 2158-2163.

[170] R. Boggio, A. Carugati, S. Trasatti, *"Electrochemical Surface Properties of Co_3O_4 Electrodes"*, J. Appl. Electrochem., **17**, 1987, 828-840.

[171] J.E. Bennett, K.J. O'Leary, *"Improvements in or Relating to Electrodes for Electrochemical Processes"*, GB Pat. 1 344 540, 1974.

[172] E. Preisler, J. Holzem, G. Mietens, G. Nolte, *"Process for the Preparation Electrolytic Manganese Dioxide"*, US Pat. 4,818,354, 1989.

[173] F. Thoumsin, *"Recherche d'un Procédé de Fabrication de Cobalt Electrolytique Marchand par Electroextraction. Problèmes poses – Mise au point par l'Union Minière du Procédé de Luilu"*, ATB Metallurgie, **9**, 1969, 33-42.

[174] L.E. Vaaler, *"Graphite-Electrolytic Anodes"*, Electrochem. Technol., **5**, 1967, 170-174.

[175] K. Matsumoto, M. Morimitsu, R. Otogawa, M. Matsunaga, *"Insoluble Anodes for Copper Foil Production (II): Inhibition of PbO_2 Formation"*, Abstract #1844, 206th Meeting of The Electrochemical Society, Honolulu, 2004.

[176] C. Comninellis, G.P. Vercesi, *"Characterization of DSA®-Type Oxygen Evolving Electrodes: Choice of a Coating"*, J. Appl. Electrochem., **21**, 1991, 335-345.

[177] A.E. Newkirk, D.W. McKee, *"Thermal Decomposition of Rhodium, Iridium, and Ruthenium Chlorides"*, J. Catalysis, **11**, 1968, 370-377.

[178] S. Trasatti, *"Oxide/Aqueous Solution Interfaces. Interplay of Surface Chemistry and Electrocatalysis"*, Mater. Chem. Phys., **16**, 1987, 157-174.

[179] C. Angelinetta, S. Trasatti, L.D. Atanasoska, Z.S. Minevski, R.T. Atanasoski, *"Effect of Preparation on the Surface and Electrocatalytic Properties of RuO_2 + IrO_2 Mixed Oxide Electrodes"*, Mater. Chem. Phys., **22**, 1989, 231-247.

[180] C. Angelinetta, S. Trasatti, L.D. Atanasoska, R.T. Atanasoski, *"Surface Properties of RuO_2 + IrO_2 Mixed Oxide Electrodes"*, J. Electroanal. Chem., **214**, 1986, 535-546.

[181] J.A. Gonzalez Dominguez, D. D. Makwana, *"Redox Control in the Electrodeposition of Metals"*, US Pat. 5,833,830, 1998.

[182] J. Schmets, J. Van Muylder, M. Pourbaix, *"Titanium"* in M. Pourbaix, *Atlas of Electrochemical Equilibria in Aqueous Solutions*, Pergamon Press, Oxford, 1966, 213-222.

[183] M. Pourbaix, N. de Zoubov, *"Hydrogen Peroxide"* in M. Pourbaix, *Atlas of Electrochemical Equilibria in Aqueous Solutions*, Pergamon Press, Oxford, 1966, 106-111.

[184] G. Valensi, E. Deltombe, N. de Zoubov, C. Vanleugenhaghe, M. Pourbaix, *"Chlorine"* in M. Pourbaix, *Atlas of Electrochemical Equilibria in Aqueous Solutions*, Pergamon Press, Oxford, 1966, 590-603.

[185] A.R. Pinheiro Pereira Moura, IAESTE trainee at Department of Materials Technology, NTNU, summer 2003. This work was supervised by the author.

[186] A. Matsuo, M. Morimitsu, R. Otogawa, M. Matsunaga, *"Insoluble Anodes for Copper Foil Production (I): Inhibition of Non-conductive $PbSO_4$ Film Formation"*, Abstract #110, 206th Meeting of The Electrochemical Society, Honolulu, 2004.

[187] G.P. Demopoulos, *"Aqueous Precipitation and Crystallization for the Production of Particulate Solids with Desired Properties"*, Hydrometallurgy Short Course, Conference of Metallurgists 2003, CIM, Vancouver, 2003.

[188] M.R. Tarasevich, B.N. Efremov. *"Properties of Spinel-type Oxide Electrodes"*, in S. Trasatti (ed.), *Electrodes of Conductive Metallic Oxides*, Part A, Elsevier, Amsterdam, 1980, 221-259.

[189] L.M. Da Silva, J.F.C. Boodts, L.A. De Faria, *"'In Situ' and 'Ex Situ' Characterization of the Surface Properties of the $RuO_2(x)$ + $Co_3O_4(1-x)$ System"*, Electrochim. Acta, **45**, 2000, 2719-2727.

[190] L.M. Da Silva, J.F.C. Boodts, L.A. De Faria, *"Oxygen Evolution at $RuO_2(x) + Co_3O_4(1-x)$ Electrodes from Acid Solution"*, Electrochim. Acta, **46**, 2001, 1369-1375.

[191] J.C.F. Boodts, G. Fregonara, S. Trasatti, *"Hydrogen Evolution on Oxide Cathodes"*, Performance of Electrodes for Industrial Electrochemical Processes, Proceedings Volume 89-10, The Electrochemical Society, Pennington, NJ, 1989, 135-145.

[192] N.V. Korovin, *"Electrocatalyst Deterioration due to Cathodic and Anodic Wear and Means for Retarding Electrocatalyst Deterioration"*, Electrochim. Acta, **39**, 1994, 1503-1508.

[193] M. Morimitsu, R. Otogawa, M. Matsunaga, *"Effects of Cathodizing on the Morphology and Composition of IrO_2-Ta_2O_5/Ti Anodes"*, Electrochim. Acta, **46**, 2000, 401-406.

[194] R. Mraz, J. Krysa, *"Long Service-Life IrO_2/Ta_2O_5 Electrodes for Electroflotation"*, J. Appl. Electrochem., **24**, 1994, 1262-1266.

[195] G.E.P. Box, W.G. Hunter, J.S. Hunter, *Statistics for Experimenters: An Introduction to Design, Data Analysis, and Model Building*, John Wiley & Sons, New York, 1978.

[196] J.S. Newman, *Electrochemical Systems*, 2nd ed., Prentice Hall, Englewood Cliffs, 1991.

APPENDIX

Estimation of electrolyte pH in anode compartments

Since the extent of anodic deposition of cobalt oxide during cobalt electrowinning was found to be highly dependent on electrolyte acidity, it was focused on how the various electrolysis parameters influenced the electrolyte pH in the anode compartments. In preliminary cobalt experiments performed in the electrowinning pilot plant, it was observed that the pH in the dechlorinated anolyte was somewhat higher than in the catholyte overflow. This was surprising, since in the nickel tankhouse the anolyte pH is considerably lower than the catholyte pH (pH ~2) [20]. Chlorination and subsequent nitrogen stripping of cobalt chloride electrolyte at pH 1 and 60°C did not result in any change in the measured pH, indicating negligible chlorine hydrolysis and stripping of HCl under these conditions. Anolyte sampled from the pilot plant manifold, saturated with chlorine, was also found to have the same pH as the substantially Cl_2-free electrolyte leaving the dechlorination facility.

Another hypothesis was that depletion of the catholyte in between the closely spaced electrodes could give an increased pH in the electrolyte sucked into the anode compartments. The catholyte was, therefore, sampled from different positions of the electrowinning cell during operation, and submitted to cobalt analysis and pH measurement. No significant concentration gradients were detected neither in the longitudinal nor vertical direction. Furthermore, the composition of the catholyte from the cell outlet and from within the cell was similar, indicating efficient electrolyte mixing.

It was then suggested that the increased pH in the anolyte versus the catholyte could be attributed to hydrogen ions taking part in the current transport across the diaphragm, thus migrating out of the anode bags towards the cathodes. To support this explanation, the anolyte pH was calculated from the proton material balance for an anode compartment at similar electrowinning conditions as studied experimentally. The assumptions and simplifications made, the equations used and the results from these calculations are outlined in the following paragraphs. The calculated differences in pH between the anolyte and the catholyte are compared graphically with the experimental measurements in section 4.3.

A.1 Assumptions and simplifications

In order to be able to estimate the electrolyte pH in the anode compartments, some assumptions and simplifications were necessary, which can be summarized as follows:

- The electrolyte was assumed to be an all-chloride solution containing Co^{2+}, Na^{+}, H^{+} and Cl^{-} ions dissolved in water. As shown in Table 3.1, the concentrations of other elements in the Xstrata Nikkelverk cobalt electrolyte are usually very low.

- Diffusion coefficients at infinite dilution and 25°C were used throughout. Transport numbers are normally only moderately affected by changes in concentration and temperature, since according to the Stokes-Einstein equation, the diffusion coefficients are modified to the same extent for each species [128].

- Except for the hydrogen ion, unit activity coefficients were employed. Furthermore, complete ion dissociation was assumed, and the calculations did not include any chloro complex formation. Fig. 2.17 shows that the cation transport number in aqueous $CoCl_2$ solution decreases only slightly with increasing concentration.

- It was further assumed that there were no concentration gradients in the electrolyte within the diaphragm, which means that it was supposed to have the same composition as the catholyte. The high linear velocity of electrolyte flow through the tightly woven diaphragm cloth, from the cathode compartment into the anode compartments, minimized the degree of back-diffusion. Hence, the concentration gradient of H^{+} was supposed to be located inside the anode bags, close to the diaphragm. When studying cobalt electrowinning from sulphate solution in a divided cell, Lenthall and Bryson [14] were able to inhibit back-diffusion of H^{+} ions by operating with a bulk flow through the diaphragm corresponding to 7.4 l/h,m^2 diaphragm area. This flow rate is several times lower than the anolyte flows in the present work, typically 50 l/h,m^2 diaphragm area.

- Due to the absence of any significant concentration gradients in the catholyte, its composition was regarded as uniform and identical to the catholyte overflow, which was sampled and analyzed in each test.

- The presence of water vapour was neglected in the anode gas. In any case, the oxygen analysis was rather rough owing to its low concentration compared to that of chlorine and the possible contamination by air.

- Any loss of water from the anode compartments and the dechlorination facility was ignored, so that the flow of anolyte was considered to be the same as the measured flow of dechlorinated anolyte.

- The two end anodes were regarded as one regular anode, i.e. the electrowinning cell was treated as if it contained 5 equal anodes. The end anodes received approximately half the current compared to the regular anodes having a cathode on either side, however, the flow of electrolyte into the end anodes was probably not that much reduced.

A.2 Equations used to estimate anolyte pH

The equations employed when calculating the material balance of protons, giving the electrolyte pH in the anode compartments, are explained below. Relevant fluxes J of H^+ and volumetric flows F are indicated in the principle drawing of the electrowinning cell depicted in Fig. A.1.

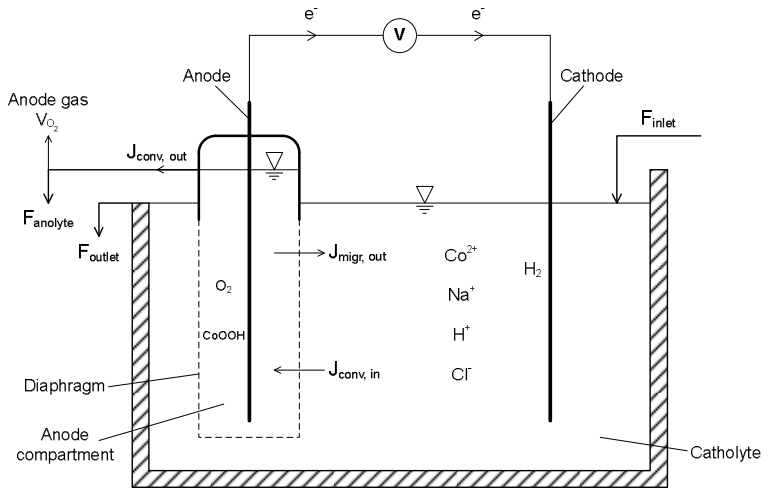

Figure A.1 *Principle drawing of the electrowinning cell with indicated transport of hydrogen ions.*

During cobalt electrowinning from cobalt chloride solution, hydrogen ions are transported through the aqueous electrolyte by migration, diffusion and convection. Since no concentration gradients were assumed for the electrolyte in the diaphragm, transport of H^+ between the cathode and anode compartments is restricted to convective transport into the anode bags, $J_{conv,in}$, along with H^+ migration in the opposite direction towards the cathodes, $J_{migr,out}$. Inside the anode compartments, acid is generated due to the anodic evolution of oxygen and CoOOH deposition on the anodes:

$$2\ H_2O = O_2 + 4\ H^+ + 4\ e^- \tag{A.1}$$

$$Co^{2+} + 2\ H_2O = CoOOH + 3\ H^+ + e^- \tag{A.2}$$

In addition to migration, protons may leave the anode compartments with the anolyte withdrawn from the anode hoods, $J_{conv,out}$. This gives the following material balance of H^+ for an anode compartment, where X_{O2} and X_{CoOOH} denote the rates of H^+ formation from oxygen evolution and anode scaling respectively:

$$J_{conv,\,out}\,(\text{moles } H^+/\text{h}) = J_{conv,\,in} - J_{migr,\,out} + X_{O_2} + X_{CoOOH} \tag{A.3}$$

The convective transport of H^+ into a single anode bag was calculated from:

$$J_{conv,\,in}\,(\text{moles } H^+/\text{h}) = c_{H^+,\,catholyte}\,F_{anolyte} \tag{A.4}$$

where $c_{H+,catholyte}$ is the concentration of H^+ in the catholyte and $F_{anolyte}$ the flow of anolyte per anode. $c_{H+,catholyte}$ was calculated from the pH measured at room temperature, and then adjusted by the activity coefficient of H^+, γ_{H+}:

$$c_{H^+,\,catholyte} = \frac{a_{H^+,\,catholyte}}{\gamma_{H^+}} = \frac{10^{-pH_{catholyte}}}{\gamma_{H^+}} \tag{A.5}$$

γ_{H+} was estimated by the addition of portions of hydrochloric acid to the cobalt chloride electrolyte and measuring the pH decrease, see section 2.7.7. A γ_{H+} value of 2 was used in all calculations, except when dealing with cobalt concentration deviating appreciably from 55 g/l, i.e. in the series involving variation of the $CoCl_2$ concentration.

The migration term in equation A.3, independent of the extent of convective flow, was obtained according to:

$$J_{migr,\,out}\,(\text{moles } H^+/h) = \frac{3600\,I}{F}\,t_{H^+} \qquad (A.6)$$

where I is the current per anode, i.e. 400 A, except for the experiments involving different current densities, F is the Faraday constant and t_{H+} is the transport number of the hydrogen ions.

The transport number t_i of component i, i.e. the fraction of the current carried by this component, can be defined as [128]:

$$t_i = \frac{z_i^{\,2}\,u_i\,c_i}{\sum_{i=1}^{N} z_i^{\,2}\,u_i\,c_i} = \frac{z_i^{\,2}\,D_i\,c_i}{\sum_{i=1}^{N} z_i^{\,2}\,D_i\,c_i} \qquad (A.7)$$

where z_i is the ionic charge and u_i the mobility of species i. The transition from mobility to diffusion coefficient D_i was done according to the Nernst-Einstein equation, which says that the diffusion coefficient is proportional to the mobility at constant temperature. The transport number of the hydrogen ion in the cobalt electrolyte was, therefore, calculated by the equation:

$$t_{H^+} = \frac{1^2 \cdot D_{H^+} c_{H^+}}{2^2 \cdot D_{Co^{2+}} c_{Co^{2+}} + 1^2 \cdot D_{Na^+} c_{Na^+} + 1^2 \cdot D_{H^+} c_{H^+} + 1^2 \cdot D_{Cl^-} c_{Cl^-}} \qquad (A.8)$$

The diffusion coefficients used to estimate the H^+ transport number are listed in Table A.1. Note the high value of D_{H+}, about one order of magnitude larger than for the other ions in the system, due to the unique Grotthuss proton hopping mechanism through water [128]. This means that even though the concentration of hydrogen ions is low, they may contribute considerably to the current transport.

Table A.1 Diffusion coefficients at infinite dilution in water at 25°C.

Ion	$D \cdot 10^9$ (m^2/s)
Co^{2+}	0.7318
Na^+	1.334
H^+	9.312
Cl^-	2.032

Data from Newman [196], except for Co^{2+}, which was taken from Robinson and Stokes [110].

Acid formation from the small amounts of oxygen liberated parallel to chlorine evolution was estimated by the equation:

$$X_{O_2}\,(\text{moles } H^+/\text{h}) = 4\frac{3600\,I}{4F}\cdot\frac{CE_{O_2}}{100} = \frac{3600\,I}{F}\cdot\frac{2\,V_{O_2}}{100+V_{O_2}} = \frac{7200\,I\,V_{O_2}}{\left(100+V_{O_2}\right)F} \quad (A.9)$$

where V_{O2} denotes the volume fraction of oxygen in the anode gas, as analyzed by using the Orsat apparatus (section 3.2.3). Acidification of the anolyte due to anode scaling was calculated from:

$$X_{CoOOH}\,(\text{moles } H^+/\text{h}) = 3\frac{3600\,I}{F}\cdot\frac{CE_{CoOOH}}{100} = \frac{108\,I\,CE_{CoOOH}}{F} \quad (A.10)$$

The average current efficiency for anodic CoOOH deposition, as obtained in each experiment, was employed in equation A.10.

After the convective flow of protons out of the anode compartment was calculated from equation A.3, the anolyte pH was derived by the relation:

$$pH_{anolyte} = -\log a_{H^+,\,anolyte} = -\log\left(\gamma_{H^+} c_{H^+,\,anolyte}\right) = -\log\left(\gamma_{H^+}\frac{J_{conv,\,out}}{F_{anolyte}}\right) \quad (A.11)$$

Finally, ΔpH was defined as the difference between the anolyte pH and the catholyte pH:

$$\Delta pH = pH_{anolyte} - pH_{catholyte} \quad (A.12)$$

A.3 Influence of electrowinning parameters on the estimated anolyte pH

In this section, results are presented from the calculations of anolyte pH at the various cobalt electrowinning conditions studied in the pilot plant. The measured oxygen content in the anode gas and the measured anolyte flow rates are also reported for each electrolysis parameter studied. In the case of HCl addition to the anode compartments and the addition of H_2O_2 to the electrolyte, the calculations were slightly modified, as outlined in the respective paragraphs.

A.3.1 Effect of catholyte pH

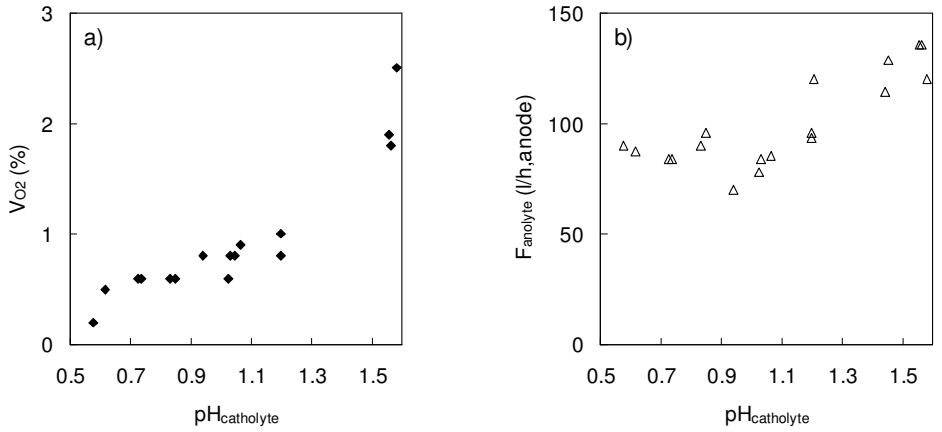

Figure A.2 *Effect of catholyte pH on a) oxygen content of the anode gas and b) anolyte flow rate.*

Range of values used in the calculations (pH 0.5 → 1.6 in the catholyte):

V_{O2}: 0.3 → 2.1 %
$F_{anolyte}$: 74 → 124 l/h,anode
CE_{CoOOH}: 0 → 0.12 %

Table A.2 Calculated proton material balance for a single anode compartment, and difference in pH between the anolyte and the catholyte, at various catholyte pH values.

$pH_{catholyte}$	t_{H+}	$J_{conv,in}$ (moles/h)	$J_{migr,out}$ (moles/h)	X_{O2} (moles/h)	X_{CoOOH} (moles/h)	$J_{conv,out}$ (moles/h)	ΔpH
0.5	0.18	11.7	2.6	0.09	0.000	9.1	0.11
0.6	0.15	9.7	2.2	0.11	0.000	7.7	0.10
0.7	0.12	8.1	1.8	0.13	0.000	6.5	0.10
0.8	0.10	6.8	1.5	0.16	0.000	5.5	0.09
0.9	0.08	5.6	1.2	0.19	0.001	4.6	0.08
1.0	0.06	4.7	1.0	0.22	0.004	4.0	0.07
1.1	0.05	3.9	0.8	0.26	0.009	3.4	0.06
1.2	0.04	3.2	0.6	0.31	0.015	3.0	0.04
1.3	0.03	2.7	0.5	0.37	0.023	2.6	0.02
1.4	0.03	2.3	0.4	0.44	0.033	2.3	-0.01
1.5	0.02	1.9	0.3	0.51	0.042	2.1	-0.05
1.6	0.02	1.6	0.3	0.61	0.052	2.0	-0.10

Constant in catholyte (g/l): Co 54, Na 2.3, Cl 70.

A.3.2 Effect of catholyte cobalt chloride concentration

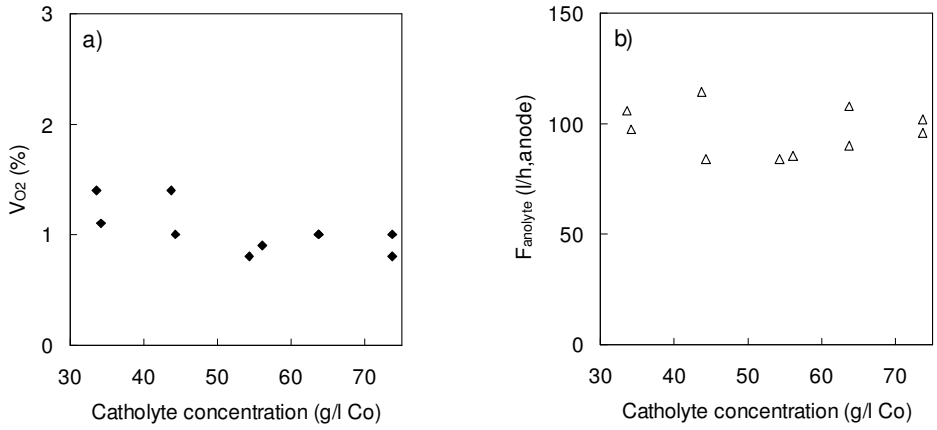

Figure A.3 *Effect of catholyte cobalt chloride concentration on a) oxygen content of the anode gas and b) anolyte flow rate.*

Range of values used in the calculations (35 → 75 g/l Co in the catholyte):

V_{O2}: 1.2 → 0.8 %
$F_{anolyte}$: 98 → 95 l/h,anode
CE_{CoOOH}: 0.008 → 0.045 %

Table A.3 Calculated proton material balance for a single anode compartment, and difference in pH between the anolyte and the catholyte, at various cobalt chloride concentrations in the catholyte.

$Co_{catholyte}$ (g/l)	γ_{H+} *	t_{H+}	$J_{conv,in}$ (moles/h)	$J_{migr,out}$ (moles/h)	X_{O2} (moles/h)	X_{CoOOH} (moles/h)	$J_{conv,out}$ (moles/h)	ΔpH
35	1.4	0.11	5.8	1.6	0.36	0.004	4.6	0.11
45	1.7	0.07	4.8	1.1	0.33	0.006	4.0	0.08
55	2.1	0.05	3.9	0.8	0.30	0.009	3.5	0.05
65	2.5	0.04	3.2	0.5	0.28	0.013	2.9	0.04
75	3.0	0.03	2.6	0.4	0.25	0.020	2.5	0.02

Constant in catholyte: pH 1.08, Na 2.9 g/l, Cl:Co ratio 1.3 (by weight).
* Estimated values for γ_{H+} at 25°C based on pH measurements in $CoCl_2$ electrolytes carried out by Kongstein [65] (Table C.1 p. 199).

A.3.3 Effect of catholyte temperature

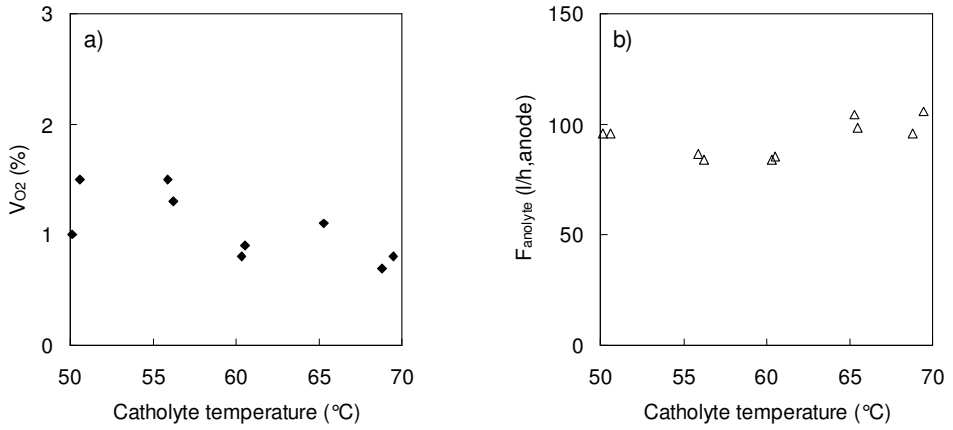

Figure A.4 *Effect of catholyte temperature on a) oxygen content of the anode gas and b) anolyte flow rate.*

Range of values used in the calculations (50 → 70°C in the catholyte):

V_{O2}: 1.3 → 0.8 %
$F_{anolyte}$: 88 → 99 l/h,anode
CE_{CoOOH}: 0.008 → 0.03 %

Table A.4 Calculated proton material balance for a single anode compartment, and difference in pH between the anolyte and the catholyte, at various catholyte temperatures.

$T_{catholyte}$ (°C)	t_{H+}	$J_{conv,in}$ (moles/h)	$J_{migr,out}$ (moles/h)	X_{O2} (moles/h)	X_{CoOOH} (moles/h)	$J_{conv,out}$ (moles/h)	ΔpH
50	0.06	3.9	0.9	0.40	0.004	3.5	0.05
55	0.06	4.0	0.9	0.35	0.005	3.5	0.06
60	0.06	4.2	0.9	0.31	0.007	3.6	0.06
65	0.06	4.3	0.9	0.27	0.010	3.7	0.06
70	0.06	4.4	0.9	0.23	0.013	3.8	0.07

Constant in catholyte: pH 1.05, Co 53 g/l, Na 2.4 g/l, Cl 69 g/l.

A.3.4 Effect of current density

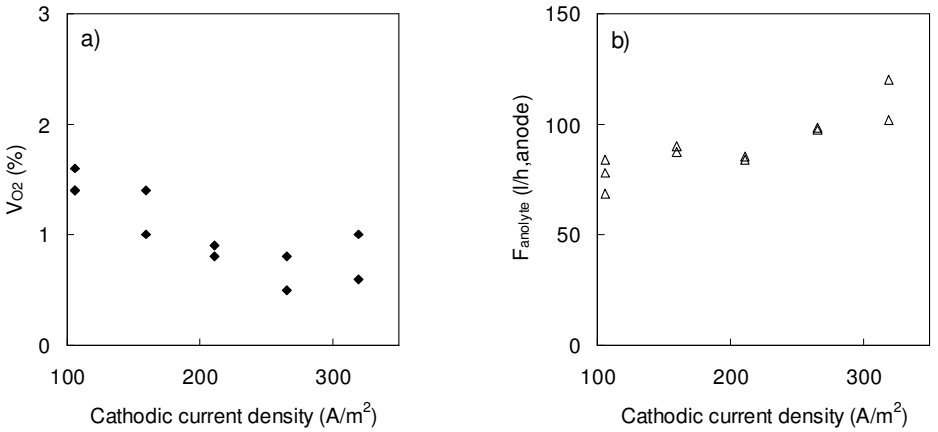

Figure A.5 *Effect of current density on a) oxygen content of the anode gas and b) anolyte flow rate.*

Range of values used in the calculations (current density 100 → 350 A/m^2):

V_{O2}: 1.4 → 0.6 %
$F_{anolyte}$: 76 → 110 l/h,anode
CE_{CoOOH}: 0.011 → 0.016 %

Table A.5 Calculated proton material balance for a single anode compartment, and difference in pH between the anolyte and the catholyte, at various current densities.

Cath. CD (A/m^2)	$pH_{catholyte}$	t_{H+}	$J_{conv,in}$ (moles/h)	$J_{migr,out}$ (moles/h)	X_{O2} (moles/h)	X_{CoOOH} (moles/h)	$J_{conv,out}$ (moles/h)	ΔpH
100	1.03	0.06	3.5	0.4	0.20	0.002	3.3	0.03
150	1.04	0.06	3.8	0.6	0.25	0.004	3.4	0.04
200	1.04	0.06	4.0	0.8	0.28	0.005	3.5	0.06
250	1.04	0.06	4.3	1.0	0.29	0.007	3.6	0.08
300	1.05	0.06	4.6	1.2	0.29	0.009	3.7	0.09
350	1.05	0.06	4.9	1.4	0.29	0.011	3.8	0.11

Constant in catholyte (g/l): Co 55, Na 2.7, Cl 72. The cathode area was 1.89 m^2.

A.3.5 Effect of anode suction

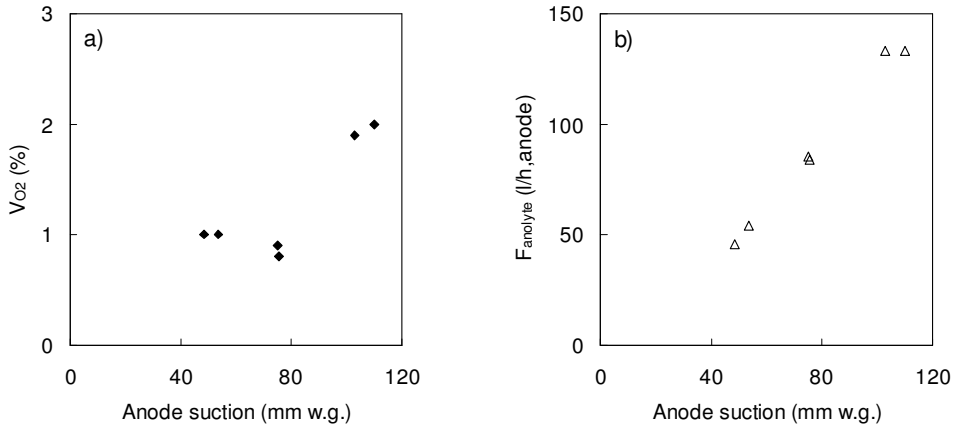

Figure A.6 *Effect of anode suction on a) oxygen content of the anode gas and b) anolyte flow rate.*

Range of values used in the calculations (anode suction 50 → 110 mm w.g.):

V_{O2}: 1 % The high O_2 content measured at high anode suction was caused by air leakage.
$F_{anolyte}$: 48 → 138 l/h,anode
CE_{CoOOH}: 0.018 → 0.013 %

Table A.6 Calculated proton material balance for a single anode compartment, and difference in pH between the anolyte and the catholyte, at various anode suction.

Suction (mm w.g.)	t_{H+}	$J_{conv,in}$ (moles/h)	$J_{migr,out}$ (moles/h)	X_{O2} (moles/h)	X_{CoOOH} (moles/h)	$J_{conv,out}$ (moles/h)	ΔpH
50	0.06	2.2	0.8	0.30	0.008	1.6	0.12
60	0.06	2.9	0.8	0.30	0.008	2.3	0.09
70	0.06	3.6	0.8	0.30	0.007	3.0	0.07
80	0.06	4.2	0.8	0.30	0.007	3.7	0.06
90	0.06	4.9	0.8	0.30	0.007	4.4	0.05
100	0.06	5.6	0.8	0.30	0.006	5.1	0.04
110	0.06	6.3	0.8	0.30	0.006	5.7	0.04

Constant in catholyte: pH 1.04, Co 55 g/l, Na 2.6 g/l, Cl 73 g/l.

A.3.6 Effect of inlet flow rate

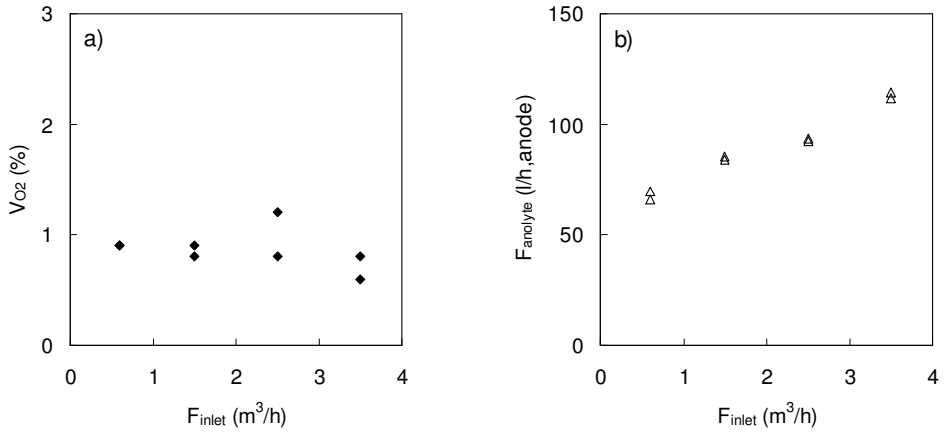

Figure A.7 *Effect of inlet flow rate on a) oxygen content of the anode gas and b) anolyte flow rate.*

Range of values used in the calculations (inlet flow rates 0.5 → 3.5 m^3/h):

V_{O2}: 0.9 → 0.8 %
$F_{anolyte}$: 67 → 111 l/h,anode
CE_{CoOOH}: 0.021 → 0.009 %

Table A.7 Calculated proton material balance for a single anode compartment, and difference in pH between the anolyte and the catholyte, at various inlet flow rates.

F_{inlet} (m^3/h)	$pH_{catholyte}$	t_{H+}	$J_{conv,in}$ (moles/h)	$J_{migr,out}$ (moles/h)	X_{O2} (moles/h)	X_{CoOOH} (moles/h)	$J_{conv,out}$ (moles/h)	ΔpH
0.5	1.08	0.05	2.8	0.8	0.28	0.010	2.3	0.08
1	1.05	0.06	3.3	0.8	0.27	0.009	2.8	0.08
1.5	1.04	0.06	3.7	0.9	0.26	0.008	3.2	0.07
2	1.03	0.06	4.1	0.9	0.26	0.007	3.5	0.07
2.5	1.03	0.06	4.5	0.9	0.25	0.006	3.9	0.06
3	1.03	0.06	4.9	0.9	0.24	0.005	4.2	0.06
3.5	1.03	0.06	5.2	0.9	0.23	0.004	4.6	0.06

Constant in catholyte (g/l): Co 56, Na 3, Cl 71.

A.3.7 Effect of hydrochloric acid addition

In the case where HCl was added to the anode compartments, the following term was included in the proton material balance (equation A.3):

$$J_{HCl}\,(\text{moles } H^+/h) = \frac{c_{HCl}F_{HCl}}{N_{anode}} = \frac{c_{HCl}F_{HCl}}{5} \qquad (A.13)$$

where c_{HCl} is the concentration of the added acid (405 g/l HCl), F_{HCl} the rate of total HCl addition (l/h) and N_{anode} is the number of anodes.

Table A.8 Data used in the calculations of anolyte pH at various HCl additions to the anode compartments.

F_{HCl} (l/h)	$pH_{catholyte}$	$Co_{catholyte}$ (g/l)	$Cl_{catholyte}$ (g/l)	V_{O2} (%)	CE_{CoOOH} (%)	$F_{anolyte}$ (l/h,anode)
0.6	1.10	52	67	1	0.006	100
2.3	1.11	52	67	1.5	0.001	96
4.4	1.61	53	69	4	0.0004	78

Constant in catholyte (g/l): Na 2.2.

Table A.9 Calculated proton material balance for a single anode compartment, and difference in pH between the anolyte and the catholyte, at various HCl additions to the anode compartments.

F_{HCl} (l/h)	t_{H+}	$J_{conv,in}$ (moles/h)	$J_{migr,out}$ (moles/h)	X_{O2} (moles/h)	X_{CoOOH} (moles/h)	$J_{HCl,in}$ (moles/h)	$J_{conv,out}$ (moles/h)	ΔpH
0.6	0.05	4.0	0.8	0.30	0.003	1.3	4.8	-0.08
2.3	0.05	3.7	0.8	0.44	0.001	5.1	8.5	-0.36
4.4	0.02	1.0	0.2	1.15	0.000	9.8	11.6	-1.08

A.3.8 Effect of hydrogen peroxide addition

Introduction of H_2O_2 to the anode compartments during cobalt electrowinning resulted in acid formation by reaction with chlorine:

$$Cl_2 + H_2O_2 = O_2 + 2\,HCl \qquad (A.14)$$

In the case of H_2O_2 addition, the anolyte pH was calculated in two alternative ways. The oxygen content of the anode gas was used in the first method, and it was assumed that all the oxygen measured was generated according to equation A.14. The X_{O2} term in equation A.3 was, therefore, replaced by:

$$X_{O_2,H_2O_2}\,(\text{moles } H^+/\text{h}) = 2\,\frac{3600\,I}{2F}\cdot\frac{V_{O_2}}{100} = \frac{36\,I\,V_{O_2}}{F} \qquad (A.15)$$

In the second method, all H_2O_2 entering the anode bags was assumed to be totally decomposed by the excess amount of chlorine present (anodic O_2 evolution was ignored here as well). Equations A.16 and A.17 were then used to calculate the generated acid when H_2O_2 was added to the inlet and directly to the anode compartments respectively:

$$X_{H_2O_2,\text{inlet}}\,(\text{moles } H^+/\text{h}) = \frac{2\,c_{H_2O_2}F_{H_2O_2}F_{\text{anolyte}}}{1000\,F_{\text{inlet}}} = \frac{c_{H_2O_2}F_{H_2O_2}F_{\text{anolyte}}}{500\,F_{\text{inlet}}} \qquad (A.16)$$

$$X_{H_2O_2,\text{anode}}\,(\text{moles } H^+/\text{h}) = 2\,\frac{c_{H_2O_2}F_{H_2O_2}}{N_{\text{anode}}} = \frac{2c_{H_2O_2}F_{H_2O_2}}{5} \qquad (A.17)$$

c_{H2O2} is the concentration of the H_2O_2 solution added (378 g/l H_2O_2), F_{H2O2} the total rate of H_2O_2 addition (l/h) and F_{inlet} is the inlet flow rate (m^3/h).

Table A.10 Data used in the calculations of anolyte pH at various H_2O_2 additions.

H_2O_2 addition (l/h)		$pH_{catholyte}$	$Co_{catholyte}$ (g/l)	$Cl_{catholyte}$ (g/l)	V_{O2} (%)	CE_{CoOOH} (%)	$F_{anolyte}$ (l/h,anode)
0.9	To inlet	1.12	52	69	10	0.014	67
1.2 *	To anodes	1.07	53	70	32	0.0007	77

Constant in catholyte (g/l): Na 2.
* The total quantity of H_2O_2 added to all the anodes.

Table A.11 Proton material balance for a single anode compartment, and difference in pH between the anolyte and the catholyte, at various H_2O_2 additions. The calculations were based on the measured oxygen content in the anode gas.

H_2O_2 (l/h)	t_{H+}	$J_{conv,in}$ (moles/h)	$J_{migr,out}$ (moles/h)	X_{CoOOH} (moles/h)	$X_{O2,H2O2}$ (moles/h)	$J_{conv,out}$ (moles/h)	ΔpH
0.9 [1]	0.05	2.5	0.8	0.006	1.4	3.2	-0.10
1.2 [2]	0.06	3.3	0.8	0.000	4.8	7.2	-0.34

[1] H_2O_2 addition to the inlet of the electrowinning cell.
[2] H_2O_2 addition to the anode compartments (total quantity for all the anodes).

Table A.12 Proton material balance for a single anode compartment, and difference in pH between the anolyte and the catholyte, at various H_2O_2 additions. The calculations were based on the quantity of H_2O_2 added.

H_2O_2 (l/h)	t_{H+}	$J_{conv,in}$ (moles/h)	$J_{migr,out}$ (moles/h)	X_{CoOOH} (moles/h)	X_{H2O2} (moles/h)	$J_{conv,out}$ (moles/h)	ΔpH
0.9 [1]	0.05	2.5	0.8	0.006	0.9	2.7	-0.02
1.2 [2]	0.06	3.3	0.8	0.000	5.3	7.8	-0.37

[1] H_2O_2 addition to the inlet of the electrowinning cell.
[2] H_2O_2 addition to the anode compartments (total quantity for all the anodes).